MULTI-SCALE INVESTIGATION OF TENSILE CREEP OF ULTRA-HIGH PERFORMANCE CONCRETE FOR BRIDGE APPLICATIONS

A Doctoral Thesis Dissertation
Presented to
The Academic Faculty

By

Victor Youssef Garas Yanni

In Partial Fulfillment of the Degree
Doctor of Philosophy in Civil Engineering
in the School of Civil and Environmental Engineering

Georgia Institute of Technology
December 2009

MULTI-SCALE INVESTIGATION OF TENSILE CREEP OF ULTRA-HIGH PERFORMANCE CONCRETE FOR BRIDGE APPLICATIONS

Committee Members:

Dr. Kimberly E. Kurtis, Co-advisor
School of Civil and Environmental Engineering
Georgia Institute of Technology

Dr. Lawrence F. Kahn, Co-advisor
School of Civil and Environmental Engineering
Georgia Institute of Technology

Dr. James S. Lai,
School of Civil and Environmental Engineering
Georgia Institute of Technology

Dr. Arun M. Gokhale,
School of Materials Science and Engineering
Georgia Institute of Technology

Dr. T. Russell Gentry,
College of Architecture
Georgia Institute of Technology

Date Approved: [September 24, 2009]

To:

Selvana My Parents Eriny

ACKNOWLEDGEMENTS

I would like to thank everyone who has made this Ph.D. experience such a unique opportunity for me to research and learn. I owe much appreciation and respect to my advisors, Dr. Kimberly Kurtis and Dr. Lawrence Kahn for their continuous guidance, generosity, support, and patience. Their insights and advice have been absolutely priceless. I am also grateful to the thesis committee members: Dr. James Lai, Dr. Arun Gokhale, and Dr. Russell Gentry for their time and support. I am also very grateful to Dr. Ken Gall for making the nanoindenter available for this research project.

This research was funded by the Georgia Department of Transportation (GDOT) research project No. 2043 Task Order No. 02-08. Mr. Vic Perry from Lafarge North America donated all the UHPC premix. BASF donated some of the chemical admixtures used in this study. Sika provided the high modulus epoxy used in the long-term study. The support provided by the sponsors is gratefully acknowledged. The opinions, conclusions, and recommendations presented herein are those of the author and do not necessarily represent the opinions and recommendations of the cooperating organizations.

I thank my fellow researchers Robert Moser, Kennan Crane, Amal Jayapalan, Dylan Fraser, Daniel Schuetz, Alex Crotty, Thibault Sauvage, Katherine Snedeker, Marcus Millard, Murat Engindeniz, Jonathan Hurff, Brett Holland, Reen Foley, Jun Chen, Ilker Kalkan, and John Bunyasaranand for their assistance, support, and time. I am also very grateful to Dr. Scott Kasprzak and Kathryn Smith for their help with nanoindentation. The continuous assistance of the Structural Engineering Research Laboratory Manger, Mr. Jeremy Mitchell, is greatly appreciated.

I could not have been here without the abundant support of my parents, my father Dr. Youssef Garas Yanni and my mother, Mrs. Madeleine Naguib, my brother Dr. Fady Garas, and my sister Mrs. Christine Garas. To all go my sincere love and deep appreciation.

Last but not least, my words are incapable of describing how much I love and appreciate my wife Selvana and my daughter Eriny. Their presence is my life gave it a new value and a true meaning. To both along with my parents I dedicate this thesis.

TABLE OF CONTENTS

LIST OF TABLES

LIST OF FIGURES

LIST OF SYMBOLS AND ABBREVIATIONS

v_{in}	Poisson's Ratio of The Diamond Berkovich Tip
v	Poisson's Ratio of the Indented Material
A	The Projected Area of the Elastic Contact
a/d	Shear-Span Effective Depth Ratio
ACI	American Concrete Institute
ASTM	American Society for Technology and Materials
ANOVA	Analysis of Varience
C_{cu}	Creep Coefficient
CSM	Continuous Stiffness Measurement Unit
DEF	Delayed Ettringite Formation
DEMEC gage	Detachable Mechanical Strain Gage
dP/dh	Initial Unloading Response of a Nanoindentation Tests
Ductal®	Ultra-High Performance Premix
E	Elastic Modulus of the Indented Material
E	The Apparent Activation Energy
E_{in}	Elastic Modulus of The Diamond Berkovich Tip
E_r	Reduced Modulus
$F'(t')$	Age-of-Concrete-at-Loading Multiplier
f_a	Actual Stress Applied for Tensile Creep Tests
f_c	Ultimate Compressive Strength
FHWA	Federal Highway Administration
f_t	Ultimate Tensile Strength
h	The Indentation Elastic Displacement
HPC	High Performance Concrete
HRWR	High-Range Water Reducer
HSC	High Strength Concrete
ITZ	Interfacial Transition Zone
L/h	Beam Span-to-Depth Ratio
LVDT	Linear Voltage Displacement Transducers
MDF	Macro-Defect Free

MSA	Maximum Size of Aggregate
P	The Indentation Load
P	Net Value of the Radial Compressive Pressure Exerted on a Fiber
PCA	The Portland Cement Association
PZT	Piezoelectric-Crystal Transducer
R	Initial Radius of the Curvature
R	Gas Constant, 8.3145 J/ G Mol/ ^{O}k (1.9859 Btu/ Lb Mol/ ^{O}r)
RH	Relative Humidity
RPC	Reactive Powder Concrete
SEM	Scanning Electron Microscopy
SIFCON	Slurry-Infiltrated Fibrous Concrete
SIMCON	Slurry Infiltrated Mat Concrete
T	Temperature During the Interval Δt_i (^{O}k)
t'	Age of Concrete at Loading (Days)
t_e	The Equivalent Age (Days)
T_s	Standard Temperature Taken As 23^{o}c (73^{o}f) In North America (296 ^{O}k)
UHPC	Ultra-High Performance Concrete
UHSC	Ultra-High Strength Concrete
u	Virtual Lateral Strains Occurring in the Matrix
u_m	Unrestrained Radial Shrinkage of the Matrix,
u_1	Lateral Deformation of the Matrix Resulting from Sustained Loads
u_f	Lateral Strain of the Fiber under Pressure P
V_{ay}	Interlock between Coarse Aggregate Particles
V_c	Concrete Shear Resistance
V_{cz}	Shear in the Compression Zone
V_d	Dowel Action of Reinforcement Bars
V_f	Fiber Content
V_u	External Factored Shear Force
X_1	Coefficient Linearly Dependant on σ
X_2	Coefficient Dependant on Insensitivity of the Shrinkage Process
α	Maturity Parameter Depending on the Type of Cement
Δt_i	Period of Time at Temperature T

δ_{cu}	Specific Creep
ε_{bc}	Strain of Loaded Concrete Prevented from Drying
ε_{bc}	Basic Creep Strain
ε_{c}	Total Creep Strain
ε_{cs}	Strain of Creep-Induced Shrinkage Dominating at the Beginning
ε_{dc}	Drying Creep Strain
ε_{fs}	Strain of Load-Free Concrete Exposed to Shrinkage
ε'_{fs}	Free Shrinkage Rate
ε_{sc}	Strain of Shrinkage-Induced Creep Dominating at the Later Stage
ε_{sh}	Free Shrinkage Strain
ε_{sw}	Swelling Strain
τ	Fiber-Matrix Shear Bond Shear Strength
μ	Coefficient of Friction between Steel Fibers and Cementitious Matrix
ε_{tot}	Total Time-Dependent Strain
σ	Stress Applied

SUMMARY

Ultra-high performance concrete (UHPC) is relatively a new generation of concretes optimized at the nano and micro-scales to provide superior mechanical and durability properties compared to conventional and high performance concretes. Improvements in UHPC are achieved through: limiting the water-to-cementitious materials ratio (i.e., w/cm $\leq$ 0.20), optimizing particle packing, eliminating coarse aggregate, using specialized materials, and implementing high temperature and high pressure curing regimes. In addition, and randomly dispersed and short fibers are typically added to enhance the material's tensile and flexural strength, ductility, and toughness.

There is a specific interest in using UHPC for precast prestressed bridge girders because it has the potential to reduce maintenance costs associated with steel and conventional concrete girders, replace functionally obsolete or structurally deficient steel girders without increasing the weight or the depth of the girder, and increase bridge durability to between 75 and 100 years. UHPC girder construction differs from that of conventional reinforced concrete in that UHPC may not need transverse reinforcement due to the high tensile and shear strengths of the material. Before bridge designers specify such girders without using shear reinforcement, the long-term tensile performance of the material must be characterized.

This multi-scale study provided new data and understanding of the long-term tensile performance of UHPC by assessing the effect of thermal treatment, fiber content, and stress level on the tensile creep in a large-scale study, and by characterizing the fiber-cementitious matrix interface at different curing regimes through nanoindentation and scanning electron microscopy (SEM) in a nano/micro-scale study.

Tensile creep of UHPC was more sensitive to investigated parameters than tensile strength. Thermal treatment decreased tensile creep by about 60% after 1 year. Results suggested the possibility of achieving satisfactory microstructural refinement at the same temperature input despite the maximum temperature applied. For the first time, the presence of a 10 μm (394 micro inch) wide porous fiber-cementitious matrix interface was demonstrated by nanoindentation and SEM for non-thermally treated UHPC only. Tensile creep at 90 days increased by 64% and 46% upon eliminating fibers for thermally and non-thermally treated UHPC, respectively. Increases in creep upon reducing the fiber content suggested that fibers carry part of the sustained load and thus reduce creep. Tensile creep strain was proportional to the stress applied up to 60% of the ultimate strength. No tensile creep failure occurred for a period of 1 year for pre-cracked UHPC under stress level of 40%. Also, no tensile creep failure occurred for a period of 90 days under stress level of 60%. Tensile creep failure occurred at stress levels of 70% and 80%. This study showed that fibers cannot be accounted for as shear reinforcement in lieu of stirrups unless micro-defect-free fiber-matrix interface is achieved.

CHAPTER 1
INTRODUCTION

1.1 Research Need

There is a specific interest in using Ultra-High Performance Concrete (UHPC) for precast prestressed concrete highway bridge girders because it has the potential to reduce maintenance costs associated with the typically steel and conventional concrete girders.

In 2006, about 26% of bridges in the US were classified as either structurally deficient, functionally obsolete, or both [Kirk and Mallett, 2007]. About 12% of bridges in that year, approximately 74,000, were classified as structurally deficient. In 2004, FHWA classified about 5% of Interstate bridges and 8% of bridges serving other purposes as structurally deficient.

$70.3 billion was spent on capital improvements to the nation's highways and bridges in 2004. Of that amount, $12.0 billion was spent on bridges. The expenditures on bridges are composed of $10.5 billion on the rehabilitation of existing bridges and $1.6 billion on the building of new bridges. In the light of this figures, the US Department of Transportation estimates that it would cost a total of $65.3 billion to fix all existing bridge deficiencies. The problem of bridge rehabilitation would continue to grow unless efforts are focused on building more durable bridges. One way of mitigating this problem is to use more durable construction materials compared to structural steel and normal concretes currently used. UHPC is a good example of on such durable material.

UHPC girder construction differs from that of conventional reinforced concrete in that the material may not need transverse reinforcement due to the higher tensile and shear strengths of the material. Before bridge designers specify such girders without using transverse shear

reinforcement, the long-term tensile performance of the material must be characterized and understood.

UHPC is a relatively new material that presents significant opportunities for improving the performance of prestressed bridge girders. However, with a new material there are new questions which must be resolved before it can be used in infrastructure construction.

1.2 Purpose and Objective

The overall purpose of this research is to assess the short and long-term properties of UHPC. Special attention is paid to tensile creep and shrinkage properties because of their influence on girder shear strength. The principle objective is to relate these properties to the long-term behavior of precast prestressed bridge girders made using UHPC.

This research was a multi-scale study that was designed to contribute to the fundamental understanding of the time-dependent, long-term tensile deformations of UHPC. The large-scale portion studied the tensile creep and shrinkage of nine different UHPC mixtures to assess the effect of mixture constituents and environmental and loading conditions on the performance. The micro/nano-scale study focused on characterizing the interfacial transition zone between reinforcing steel fibers and the bulk cementitious matrix for different curing conditions using scanning electron microscopy (SEM) and new nanoindentation testing scheme. There has been no previous research on long-term tensile properties of UHPC at these various scales conducted simultaneously. Combining results of different scales yielded new insights and understanding of the nature of the tensile creep problem of UHPC.

1.3 Definitions

High Performance Concrete (HPC) and Ultra-High Performance Concrete (UHPC): ACI Committee 116 [ACI Committee 116, 2000] as it defines HPC as "concrete meeting special combinations of performance and uniformity requirements that cannot always be achieved routinely using conventional constituent materials and normal mixing, placing, and curing practices; the requirements may involve enhancements of placement, compaction without segregation, long-term mechanical properties, early-age strength, volume stability, or service life in severe environments." However, in the absence of a standard definition of UHPC, the following general definition will be adopted: "UHPC is workable concrete with superior mechanical and durability properties compared to normal strength and high performance concretes" [Based on Mehta, 1999].

Creep: is the time-dependent increase in strain in hardened concrete subjected to sustained stress [3]. This includes basic creep occurring under no moisture loss to the environment and drying creep which is the additional creep due to moisture loss.

Shrinkage: is the decrease of hardened concrete volume with time. This is due to changes in the moisture content of the concrete and physico-chemical changes [ACI Committee 209, 2005]. This includes an autogenous portion that occurs under no moisture loss to the environment and a drying portion that considers moisture loss.

1.4 Dissertation Organization

The dissertation is organized as follows:

Chapter 2 summarizes the data found in the literature at the initiation of this study on the shear problem in beams, ultra-high performance concretes, and tensile and compressive creep of concrete.

Chapter 3 presents and analyzes the results of a preliminary short-term tensile creep study that was performed in order to assess the sensitivity of tensile creep and shrinkage of UHPC.

Chapter 4 introduces the research methodology and research program for the long-term study.

Chapter 5 mainly presents and analyzes the effect of curing conditions on the tensile creep of UHPC. This chapter reports also results from the large-scale and micro/nano-scale studies.

Chapter 6 presents and analyzes the effect of fiber reinforcement and stress level on the tensile creep of UHPC. This chapter contains results mainly from the large-scale

Chapter 7 is the final chapter that presents a summary of conclusions given throughout the dissertation and gives recommendations for future research efforts.

Each chapter contains its own reference section to improve the readability of the dissertation.

1.5 References

ACI Committee 116, "Cement and Concrete Terminology", *ACI Manual of Concrete Practice*, American Concrete Institute: Farmington Hills, MI. 2000, pp. 116R.1-116R.73.

ACI Committee 209, "Factors Affecting Shrinkage and Creep of Hardened Concrete", *ACI Manual of Concrete Practice*, American Concrete Institute: Farmington Hills, MI. 2005, pp. 209-1R-05.

Mehta, P.K., "Advancements in Concrete Technology", *Concrete International*, Vol. 21, No. 6, June 1999, pp. 69-76.

Robert S. Kirk, and William J. Mallett, "Report on: Highway Bridges: Conditions and the Federal/State Role", August 10, 2007, pp.1-18.

CHAPTER 2
LITERATURE REVIEW

2.1 Shear Behavior of Beams Made of Fiber-Reinforced Concrete

Reinforced concrete beams resist loads by means of internal moments and shears. Typically, a beam is designed first to contain the amount of reinforcement necessary for flexural resistance within the limits provided by design codes in order to ensure a ductile failure. Once this is done, a beam would then be designed for shear resistance. In a beam, the design for shear must ensure that the shear strength equals or exceeds the flexural strength at all points in order to avoid any shear failure which is frequently sudden and brittle [Anderson, 1957 and MacGregor and Wight, 2005].

In an uncracked simple span beam, the surfaces (stress trajectories) in which the principle tensile stresses act are plotted in Figure 2.1. The expected initial cracking pattern resembles the family of dashed lines shown, since concrete cracks when the principal tensile stresses exceed the tensile strength of the concrete. The cracking pattern in a test beam with longitudinal flexural reinforcement, but no shear reinforcement is shown in Figure 2.2 [Nawy, 2006] where two types of cracks can be seen, (a) flexural cracks which are the vertical cracks that start at the bottom of the beam where the flexural stresses are the largest, and (b) inclined cracks which form at the ends of the beam due to combined shear and flexure. These latter cracks are commonly referred to as inclined cracks, shear cracks, or diagonal tension cracks, and they develop at approximately an angle of 45^{o} to the normal at sections close to the support in non-prestressed beam. Such cracks must exist before a beam can fail in shear; and in order to prevent such cracks from opening, special transverse, shear reinforcement has to be provided. The main four functions of the shear reinforcement in flexural member are, (1) carrying a portion of external factored shear

force V_u, (V_s), (2) restricting growth of diagonal cracks, (3) holding longitudinal reinforcement in place to provide the dowel capacity, and (4) providing confinement to the concrete in the compression zone if the stirrups are closed and closely spaced (less than 100 mm (4-in)). However, in addition to the shear reinforcement, the other portion of the external shear forces, V_u, is resisted by the concrete itself (V_c) through the (1) dowel action of reinforcement bars (V_d), (2) shear in the compression zone (V_{cz}), and (3) interlock between coarse aggregate particles (V_{ay}). The distribution of internal shear stresses in a flexure member is shown in Figure 2.3. First, upon loading and before the development of any cracks, all shear stresses are carried by uncracked concrete. Upon the onset of flexural cracks and before inclined cracks start to develop, external shear is carried by V_{cz}, V_d, and V_{ay}. It is not until inclined cracks start to develop before shear reinforcement start carrying some of the shear forces. With inclined cracks getting wider, stirrups crossing an inclined crack yield and V_s remains constant for higher loads. Once stirrups yield, cracks open more rapidly and V_{ay} decreases due to the loss of interlock between coarse aggregates, forcing V_{cz} and V_d to increase until dowel splitting occurs and the compression zone crushes.

In reinforced concrete beams with span-to-depth ratio (L/h) greater than 5, flexural cracks at midspan generally occur before the principal tensile stresses at mid-height near the supports become critical. Once a flexural crack occurs, the tensile stress perpendicular to the crack in the concrete drops to zero, and major stress redistribution is necessary to maintain equilibrium. As a result, the onset of inclined cracking in a beam cannot be predicted from the principal stresses, unless shear cracking precedes flexural cracking.

A beam's shear span-to-depth ratio influences its failure mode (Figure 2.2). For any concrete beam without diagonal tension reinforcement, whether reinforced or prestressed or

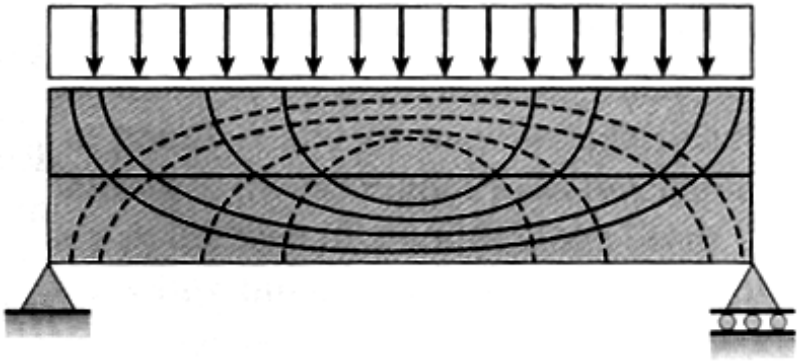

Figure 2.1: Principal stress trajectories for beams of rectangular cross sections [Gere, 2001]

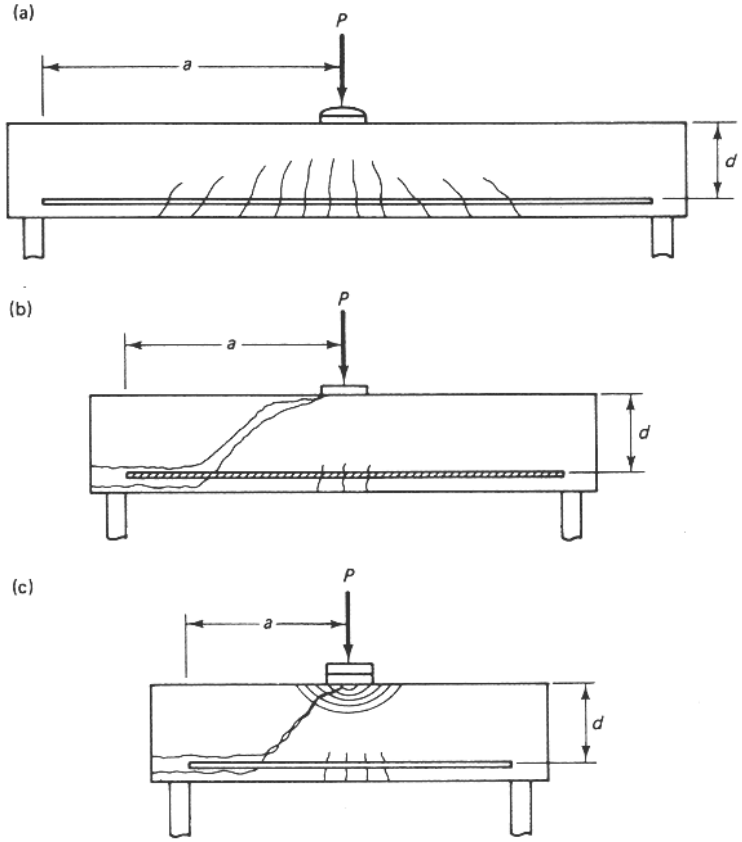

Figure 2.2: Failure patterns as a function of beam slenderness [Nawy, 2006]

both, the three major modes failure are (1) flexural failure, (2) diagonal tension failure, and (3) shear compression failure, among which the last two are considered to be brittle failure modes and should be completely avoided in design through providing the appropriate amount of shear reinforcement [Lim and Oh, 1999 and Nawy 2006].

Now, as a result of the absence of both the shear reinforcement (as per the manufacturers recommendation), and coarse aggregates (typical for UHPC matrices, will be discussed later); a significant portion of the shear cracks propagation resisting mechanism in an UHPC beam is missing (i.e. V_s and V_{ay}), this in turns dictates that the long-term diagonal tensile performance of the material is important and must be characterized before UHPC girders can be used in construction.

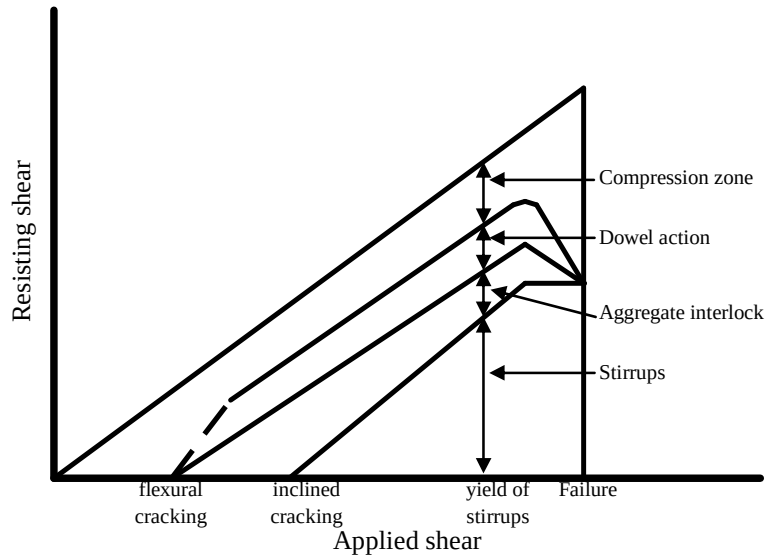

Figure 2.3: Distribution of internal shears in a beam with web reinforcement [MacGregor and Wight, 2005]

The effects of use of short steel fibers as shear reinforcement instead of conventional stirrups have been investigated for both reinforced and prestressed beams. beds Furlan and Hanai [1999] postulated that the elimination of conventional shear reinforcement (stirrups or bent bars)

can make the reinforcement simpler and may increase the productivity in long line precasting beds. Narayanan and Darwish [1987] conducted some 36 shear tests on simply supported rectangular prestressed and non-prestressed concrete beams, containing steel fibers (0.3x30 mm (0.012x1.18-in)) as web reinforcement with volumetric fiber fractions varying between 0.91% and 4.47%, variable shear-span effective depth ratio (a/d), and type and extent of prestressing. The results showed that the patterns of collapse were similar for both prestressed and non-prestressed concrete beams. For prestressed beams, fiber addition caused improvements in the ultimate shear capacity, and changed the brittle nature of a shear failure to be more ductile.

Imam et al. [1997] studied the incorporation of steel fibers in singly reinforced high strength concrete (HSC) beams without stirrups failing under the combined effect of flexure and shear. This study showed that inclusion of steel fibers in HSC beams without stirrups provided significant improvement of shear resistance and tended to increase the ultimate flexural capacity. It also showed that steel fibers can successfully replace the shear reinforcement, while the use of steel fibers as a complementary reinforcement of longitudinal bars had little effect.

Furlan and Hanai [1997 and 1999] studied the influence of prestressing and fibers on the shear behavior of thin-walled I-section beams with reduced shear reinforcement ratio. Nine concrete beams were built (six with prestressing forces) with three different mixtures: without fibers, with 0.2x2.3x25.4 mm (0.0079x0.091x1.0-in) steel fibers at 1% volume fraction, and with 0.05x42 mm (0.002x1.65-in) polypropylene fibers at 0.5% volume fraction. Shear reinforcement ratios varied from 0 to 0.225% (geometric ratio). This study showed that addition of steel fibers did not increase the compressive strength, but increased the tensile strength by 16% in some cases and also the shear strength except in the beams without shear reinforcement. More importantly, upon comparing fiber reinforced concrete beams to those with no fibers, the former

were characterized by: (1) smaller spacing between cracks, (2) slower development of cracks, (3) larger number of inclined cracks prior to collapse, (4) delayed appearance of inclined cracks and consequently the stirrups were tensioned later, and (5) more ductile failure. Thus steel fibers were suggested to be considered as equivalent shear reinforcement to stirrups. In this aspect, the advantages provided by steel and polypropylene fibers were similar, but because of the higher modulus of elasticity of steel fibers as compared to the polypropylene fibers, the strain in the stirrups in steel fiber beams was smaller. The potential for use steel fibers as shear reinforcement instead of stirrups was also confirmed in other research [Lim and Oh, 1999 and Cucchiara et al. 2004]. However, none of these studies have considered the effects of tensile creep on the long-term performance of flexural members with fibers substituting stirrups as shear reinforcement.

2.2 Ultra-High Performance Concrete (UHPC)

2.2.1 Definition

First, it is important to recognize that high strength concrete (HSC) is not necessarily high performance concrete (HPC) and also that ultra-high strength concrete (UHSC) is not necessarily ultra high performance concrete (UHPC).

ACI Committee 363 defines HSC as “concrete with a cylinder compressive strength that exceeds 41.4 MPa (6000 psi)”, while UHSC was defined by Shah and Weiss (1998) as “a concrete mixture with compressive strength greater than 22 ksi (150 MPa)”.

The term high-performance concrete (HPC) was first used for concrete mixtures with high strength, workability and durability [Mehta and Aitcin, 1990]. This definition, thus, recognizes high durability to be a major requirement in HPC beside high strength. As a result, HPC concrete mixtures ought to be designed for high dimensional stability in order to keep the structure free of cracks for a long period of time [Mehta, 1999].

As for UHPC, it was defined by Collepardi et al. [1997] as “an ultra high-strength and high-ductility concrete with advanced mechanical properties”., but when it comes to assessing the overall performance of concrete, previous definitions were broadened by the ACI Committee 116. ACI 116 defines High Performance Concrete (HPC) as "concrete meeting special combinations of performance and uniformity requirements that cannot always be achieved routinely using conventional constituent materials and normal mixing, placing, and curing practices; the requirements may involve enhancements of placement, compaction without segregation, long-term mechanical properties, early-age strength, volume stability, or service life in severe environments”. In addition, Goodspeed et al. [1996] went further and stated that HPC can be specified not only by the strength, but by any of the following: freeze-thaw durability, scaling resistance, abrasion resistance, chloride penetration, creep, shrinkage, and modulus of elasticity.

2.2.2 Principles of Developing UHPC

It is well known that the strength of brittle materials like concrete is related to the porosity of that material. As porosity decreases, an exponential increase in the strength is often observed [Mindess and Young, 1981]. The key for reducing the porosity and obtaining high strength is reducing the water-to-cement ratio and providing proper compaction [Powers and Brownyard, 1948] and for that reason water-reducing admixtures are used to alter attraction forces between the cement particles improving the fluidity of cementitious systems, better dispersing the cement particles, and reducing the size of voids [Dodson, 1990].

The main principles of development of UHPC matrices are improving the homogeneity, increasing the dry-compacted density, and enhancing the microstructure of regular concrete.

These have been achieved by either: 1- Modifying cement with a polymer (macro-defect free, MDF), or 2- Densification with addition of micro-fine particles [Shah and Weiss, 1998].

Macro-defect free (MDF) materials are made using cement, a water-soluble polymer (Such as PVA, typically less than 5%), and a low w/c (typically less than 0.2). Originally it was thought that the very high tensile strength of MDF (200 MPa (29,000 psi) approaching that of steel) was due to the reduction in pore size which occurs as a result of processing. However, recent work has shown that the significant increase in strength arises as a result of the cross-linking between cement and polymer [Poyola et al., 1990]. As a result, high shear mixing process is required for MDF mixtures to produce the mechano-chemical reaction between the mineral and polymer phases [McHugh and Tan, 1993].

Densification with micro-fine particles is based on the concept of particle packing and is the approach frequently used. As previously mentioned, superplasticizers allow the cement particles to pack more uniformly, reducing the porosity of conventional concrete, and thereby increasing strength. The particle-packing concept can be further utilized by adding submicron particles (e.g. silica fume) that fill remaining void space, resulting in a dense, strong material. If these particles are also pozzolanic, additional increase in strength may occur. In addition, the increased density of these materials reduces the connected porosity, decreasing the penetrability to water and corrosive agents and, thus, increasing long-term durability.

Graybeal [2005] it was stated that most of the UHPC matrices are generally composed of fine sand, between 150 and 600 μm (0.0059 and 0.0236-in), cement with an average diameter of approximately 15 μm (0.00059-in), crushed quartz with an average diameter of 10 μm (0.000394-in), and silica fume that has a diameter small enough to fill the interstitial voids between the cement and the crushed quartz particles. Depending on the time, temperature, and

particle size, quartz particles can react with alkaline solutions. Metamorphic quartz has been found to be alkali reactive, generally in the decreasing order of reactivity [Mehta and Monteiro, 2005].

Richard and Cheyrezy [1995], and Feylessoufi et al. [1997] stated that further improvements of the cementitious matrix could be achieved via thermal treatment as the reaction of silica fume is activated and the average size of pores is decreased through the application of thermal treatment. Porosimetric analyses with mercury intrusion conducted by Cheyrezy et al. [1995] showed zero porosity in confined RPC specimens cured between 150 ^{o}C (302 ^{o}F) and 200 ^{o}C (392 ^{o}F). Also, in a study by Collepardi et al. [1997] it was concluded that both shrinkage and swelling in RPC reduced upon applying steam curing. Similar trends were also observed by Richard and Cheyrezy [1995] where heat curing at 90 ^{o}C (194 ^{o}F) was applied. Also, Monosi et al. [2000] concluded from their study that high pressure steam curing at 160 ^{o}C (320 ^{o}F) causes further strength increase with respect to the RPC's that were steam-cured at 90 ^{o}C (194 ^{o}F).

In summary, ultra-high strength matrix could be achieved by (1) low water-to-binder ratio (typically below 0.2), and, using high dose of high-range water reducing agents (HRWR) typically based on polycarboxylate (PC) chemistry meeting the ASTM C 494 requirements for Type F high-range water reducing admixtures [Graybeal, 2005; Habel et al., 2007; and Ferron et al., 2007] as they provide better dispersion of cement particles due to the steric hindrance dispersion mechanism compared to other types of HRWR.), (2) large quantity of fine particles (typically silica fume), (3) aggregate containing only fine sand, and (4) thermal treatment (curing).

Now, as concrete is more homogenous, it would exhibit higher strength but becomes more brittle than normal strength concretes. Increased homogeneity can be observed by comparing a cross section of a typical HSC in comparison with UHSC (Figure 2.4). Unreacted cement and aggregate particles produce significant heterogenics in the standard high strength system, while the UHSC system is much more uniform at the same scale. Figure 2.5 provides insight into how the material performance changes with increased strength by showing the stress-strain failure envelope of conventional, high strength, and ultra-high strength concrete. It can be seen that an increase in compressive strength results in a material with high stiffness and ultimate failure strain. But on the other hand, concrete with higher strength exhibit a more sudden drop in load carrying capacity after the peak load is reached (post-peak) [Shah and Weiss, 1998]. This problem could be solved by incorporation of short fibers in the concrete mix.

Fiber reinforcement of cement-based matrices are known to (1) change the rheology or the flow characteristics of the material in the fresh state, (2) improve the tensile or flexural strength, (3) improve the impact resistance or toughness, (4) control cracking, and (5) alter the mode of failure by increasing post-cracking ductility. In most of the applications, fiber contents ranges from about 0.3 to 2.0% by volume. In the precast prestressed industry, an increase in tensile strength has a significant beneficial effect on the achievement of longer spans and the reduction of the amount of prestressing strands needed. However, fiber-reinforced concretes differ from conventional concretes in having lower coarse aggregates content (350 to 750 kg/m^3 (600 to 1250 lb/yd^3)), and a smaller size of coarse aggregate (10 mm (3/8-in) maximum size) [Lankard, 1975; Swamy and Barr, 1989; and Banthia et al. 1999].

In a study by Shah and Weiss [1998], fractured specimens of fiber-reinforced concrete showed that failure takes place primarily due to fiber pull-out or debonding and, unlike plain

concrete, a fiber reinforced concrete specimen does not fail immediately after initiation of the first crack. In explaining the toughening mechanism in fiber reinforced composites, Shah [1984] stated that the composite will carry increasing loads after the first cracking of the matrix if the pull-out resistance of the fibers at the first crack is greater than the load at first cracking. At the cracked section, the matrix does not resist any tension, and the fibers carry the entire load taken by the composite. With an increasing load on the composite, the fibers will tend to transfer the additional stress to the matrix through bond stresses. If these bond stresses do not exceed the bond strength, then there may be additional cracking in the matrix. This process of multiple cracking will continue until either fibers fail or the accumulated local debonding will lead to fiber pull-out.

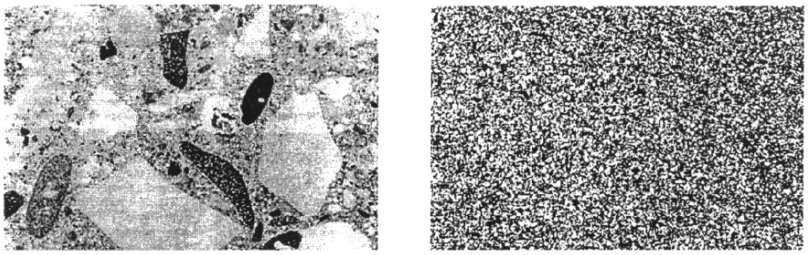

Figure 2.4: Comparison between conventional high performance concrete and reactive powder concrete at the same scale [Shah and Weiss, 1998]

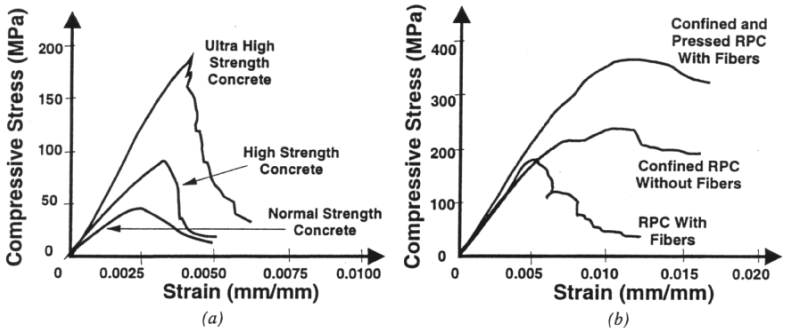

Figure 2.5: Stress-strain diagrams of concrete illustrating: increasing brittleness with increased strength (a) using external confinement; (b) using fiber reinforcement [Shah and Weiss, 1998]

Cracking in tension was further discussed in details by Rossi [2001]. Three different stages were defined from the beginning of loading until failure. In stage one, microcracks form

randomly throughout the entire volume of concrete. During stage two, the microcracks join together to form localized macrocracks which affect the mechanical behavior. In stage three, one or more macrocracks become wider and propagate causing the final failure. Similar scenario was also observed by Namaan and Homrich [1989]. However, different fibers may be more efficient than others in resisting crack propagation according to their relative size with respect to the crack they are bridging. Thus, having a large number of closely spaced fibers seems to be the most effective way to bridge microcracks formed in the mixture during stage one. This can be achieved by using short fibers (<5.08 mm (0.2 in)) with small diameters that allows the placement of a large number of fibers without the presence of workability problems. On the other hand, fibers used must be long enough (>20 mm (0.79 in)) to bridge macrocracks formed during stages two and three. However, the use of long fibers has been always associated with reduced workability and thus typically limited to a volume fraction of 3%. This workability problem can be overcome by: (1) the use of two different types of fibers in the mixture: short fibers bridging microcracks, and long fibers bridging macrocracks, and/or (2) the use of increased amounts of superplasticizers (HRWRs)

Several studies in the last few decades have focused on experimentally studying the influence of incorporating different types of short fibers on concrete performance. Hannant [1978] divided fibers used to reinforce concrete into two main groups, these with modulus lower than the cement matrix, such as cellulose, nylon and polypropylene and those with higher modulus such as asbestos, glass, steel, carbon, and Kevlar (aramid). The low modulus organic fibers are generally subject to relatively high creep which means that if they are used to support permanent high stresses in a cracked composite, considerable elongations or defections may occur over a period of time. Therefore, they are more likely to be used in situations where the

matrix is expected to be uncracked, but where transitory maximum loads are short-term such as handling stresses, impacts, or wind loads. Another problem with the low modulus fibers is that they generally have large values of Poisson's ratio and this, combined with their low modulus, means that if stretched along their axis, they contract diametrically much more than other fibers. This contraction leads to a high lateral tensile stress at the fiber-matrix interface which is likely to cause a short aligned fiber to debond and pull out. On the other hand, the high modulus short fibers may require mechanical bonding to avoid pull out unless the specific surface area in very large. For structural and nonstructural purposes, steel fiber are still the most commonly used of all the fibers, and are commonly produced with various cross-sections and may have bent ends to provide anchorage with the cementitious matrix [Mehta and Monteiro, 2005 and Bissonnette et al., 2007].

However, as only steel fibers are considered to be used in the proposed study, only the effect of incorporating short steel fibers on the tensile performance of concrete is discussed here.

Data from the tests by Krenchel [1974] on both plain and steel fiber-reinforced mortars showed that incorporation of 0.9 and 2% fiber by volume of concrete increased the flexural strength by approximately 15 and 30%, respectively. In addition, in both cases the elongation at rupture was 9 to 10 times that of the unreinforced mortar. In a study by Potrzebowski [1983], 2% volume fraction of steel fibers, 0.4 mm (0.016-in) in diameter and 40 mm (1.57-in) in length were used in concrete of 10 mm (0.40-in) maximum size of aggregate (MSA) to study the effect of fiber reinforcement on the splitting tensile strength. Results from this study showed that the splitting tensile strength increased with the increase of the amount of fibers passing the crack plane. Another study by Rossi et al. [1986] showed that incorporating round 1% volume fraction of 0.5x50 mm (0.020x2.0-in) steel fibers increased the load capacity by 200% when compared

to non-reinforced concrete. Kormeling and Reinhardt [1987] studied the effect of strain rate on mechanical properties of fiber-reinforced concrete in uniaxial tension. In this study, straight steel fibers, 0.4 mm (0.016-in) in diameter and 25 mm (1.0-in) in length were used at 1.5 and 3% volume fractions. The MSA was 8 mm (0.31-in). Results from this study showed that fracture energy of fiber-reinforced concrete was up to hundred times more than non-reinforced concrete. In a study by Naaman and Hormich [1989], the use of 12-14% volume fraction of hooked or deformed steel fibers, 0.5 mm (0.020-in) in diameter and 30 mm (1.18-in) in length in UHPC resulted in a multiple cracking pattern at low and intermediate load levels. However, failure still occurred through opening of a single large tensile crack. In addition, the tensile modulus of concretes with deformed fibers was substantially higher than that of concrete with hooked fibers. The difference between the behaviors of the two fibers was attributed mainly to the surface texture of deformed fibers which created at smaller strains a better matrix-to-fiber bond than hooked fibers [Bissonnette et al., 2007]. Krstulovic-Opara and Malak [1997] studied the effect of using high strength steel fibers on the tensile behavior of slurry infiltrated mat concrete (SIMCON). In this study stainless steel fibers with 0.334 mm (0.013-in) in equivalent diameter and 241.3 mm (9.5-in) in length were used at 2.16-5.39% volume fraction and direct tension tests were performed. Results from this study showed a monotonic increase in the tensile strength and toughness upon increasing the fiber content. The maximum tensile strength varied between 7 and 17 MPa (1015 and 2030 psi) for fiber volume fractions varying between 2.16 and 5.39%, respectively. In addition, the toughness values varied between 0.124 and 0.29 MPa (17.98 and 42.05 psi) for 2.16 and 5.39% fiber volume fractions, respectively. Also, the values of strength, strains at maximum stress, and energy absorption capacity reported in this study were respectively about one order, two orders, and three orders of magnitude larger than standard

unreinforced concrete. Similar observations were also reported previously by Hannant [1978]. Also, according to the ACI Committee 544, the total energy absorbed in fiber debonding as measured by the area under the load-deflection curve before complete separation of a beam might be about 10 to 40 times higher for fiber-reinforced concrete than for plain concrete.

The Portland Cement Association (PCA) investigated the changes in mix proportion upon incorporating 0.254 x 0.056 x 25.4 mm (0.01 x 0.022 x 1-in) steel fibers in fiber-reinforced concrete mixture designed for highways and airport pavements and overlays [Hanna, 1997]. Based on this study, a chart was also developed to determine the increase in the cement content and the decrease in aggregate proportions for the fiber additions in the range 0.5 to 2% by volume. Using this chart, the mix proportions in Table 2.1 showed how at a given water-to-cement ratio, the cement paste content had to be increased with a corresponding decrease in the proportion of aggregates to maintain adequate workability when 2% steel fibers were added to the plain concrete mixture. In addition, the maximum particle size of the matrix was also important because it affected the fiber distribution and the quantity of fibers which could be included in the composite, concrete which is intended to be used in conjunction with fibers should not have particles greater than 20 mm (0.787-in) and preferably not greater than 10 mm (0.394-in) otherwise uniform fiber distribution becomes difficult to achieve [Hannant, 1978].

On the other hand, in spite of the various improvements in concrete performance associated with incorporating steel fibers, recent studies have shown that using short steel fibers may have a negative effect on long-term tensile performance (tensile creep). This effect is discussed in detail later, but in general the effect was attributed to either the increase in the void ratio fraction upon incorporating fibers [Bissonnette and Pigeon, 1995] or to the hypothesis that

fibers are likely to act like course aggregate in a concrete mix, having a surrounding porous zone similar to the ITZ in the case of aggregates [Bissonnette et al., 2007].

Table 2.1: Comparison of mix proportions between Plain concrete and fiber-reinforced-concrete (lb/yd^3) [Hanna, 1997]

Material	Plain concrete kg/m^3 (lb/yd^3)	Fiber-reinforced concrete [a] kg/m^3 (lb/yd^3)
Cement	446 (752)	519 (875)
Water (water/cement ratio = 0.45)	200 (338)	234 (394)
Fine aggregate	853 (1440)	760 (1282)
Coarse aggregate	682 (1150)	607 (1024)
Steel fibers (2% by volume)	-	157 (265)

[a] The 14-day flexural strength 7.93 MPa (1150 psi) of the fiber-reinforced concrete was about 20% higher than that for plain concrete.

In summary, the main factors controlling the theoretical performance of a fiber-composite material are the physical properties of the fibers and the matrix and the strength of the bond between the two, some of which are hard to evaluate [Mehta and Monteiro, 2005].

2.3 Tensile Creep of Concrete

Findley et al. [1976] defined creep as the slow, continuous deformation of a material under constant load. Some materials like concrete exhibit an elastic action when rapidly loaded and then a slow and continuous increase of strains at a decreasing rate occurs. Upon unloading, initial elastic recovery was followed by a continuous decreasing strain. These materials are called "viscoelastic". Examples of viscoelastic materials are plastics, wood, natural and synthetic fibers, concrete, and metals at high temperatures.

In this section, a theoretical background of the phenomenon of tensile creep of concrete will be presented followed by a literature review of the tensile creep test setups, key results, and possible mechanisms that have been used to explain it.

Detailed discussion of the relatively well-established compressive creep phenomenon of concrete is presented in Appendix A for reference.

2.3.1 Theoretical Background

Creep of concrete usually occurs simultaneously with shrinkage. Although these two phenomena have been considered to be additive for many years; in fact, it is well known now that they are not, and that the principle of superposition cannot be applied [Kovler, 1999].

Pickett [1942] introduced the idea of ‘‘drying creep’’ to explain the observed excess of total creep at drying over basic creep (the component of concrete creep under conditions of no moisture movement to or from the ambient medium). In other words, the Pickett effect expresses the fact that, during simultaneous creep and shrinkage, the total time-dependent strain (ε_{tot}) is not equal to the sum of the separate strain of load-free concrete exposed to shrinkage (ε_{fs}) and that of loaded concrete prevented from drying (ε_{bc}), but ε_{tot} differs by an extra strain, called drying creep (ε_{dc}), as follows:

$$\varepsilon_{tot} = \varepsilon_{fs} + \varepsilon_{bc} + \varepsilon_{dc} \tag{2.1}$$

Due to the nonuniformity of the moisture distribution in a drying specimen (wet core in compression, and drying and shrinking surface in tension), the drying creep component was explained by many models by the so called microcracking effect [Pickett, 1942]. Due to the nonlinear inelastic behavior of creep in concrete caused by the tensile stresses, these microcracks cannot fully close when the moisture distribution approaches a uniform state. However, there can be no effect of microcracking for specimens under compression, and thus studying the Pickett effect under tension will be more helpful in solving the problem of microcracking in concrete skin at drying creep [Kovler, 1995].

Kovler [1995] investigated the problem of interdependence of creep and shrinkage under tension. Figure 2.6 shows that the nature of the basic creep is different than that of the total creep. Total creep increases monotonically with time, while the basic creep reaches an asymptotic value within few hours. In addition, and unlike the creep under compression, during the first 36-48 hours of the tensile creep test, the total tensile creep was less than the tensile basic creep. This means that the difference between the total and the basic creep (i.e. the drying creep, ε_{dc}) had a negative value initially, likely due to shrinkage which decreases with time and gradually transforms the ε_{dc} value to positive later. As a result, the negative ε_{dc} value at the initial stage of the test and the positive value later cannot be described by one term or one physical mechanism (i.e. creep or shrinkage) but rather combined mechanisms which are: (1) creep-induced shrinkage dominating at the beginning (ε_{cs}), and (2) shrinkage-induced creep, dominating at the later stage (ε_{sc}) [i.e. microcracking according to Bazant and Xi, 1994]. This approach can be represented by the following equation that reflects the interdependency between creep and shrinkage and can be used both in compression and tension:

$$\varepsilon_{dc} = \varepsilon_{cs} + \varepsilon_{sc} \tag{2.2}$$

According to Kovler [1995], the first term in Equation 2.2, (ε_{cs}), represents the additional shrinkage component of concrete that depends on creep. That is, the greater the basic creep of the material, the greater the creep-induced shrinkage. The sign of ε_{cs} will coincide with that of the free shrinkage. The second term in Equation 2.2, (ε_{sc}), represents the additional creep component of concrete that depends on shrinkage. That is, the greater the free shrinkage of the material, the greater the shrinkage-induced creep. The sign of ε_{sc} will coincide with that of the basic creep. In other words, Equation 2.2 implies that the deformations observed in drying creep result from

four mechanisms which are: (1) free shrinkage, (2) basic creep, (3) creep-induced shrinkage, and (4) shrinkage-induced creep.

Thus, Equation 2.2 can be rewritten in the following form:

$$\varepsilon_{dc} = \varepsilon_{sc} + \varepsilon_{cs} = \mu X_1 \varepsilon_{fs} + \mu X_2 \varepsilon_{bc} \quad (2.3)$$

Where X_1 and X_2 are positive coefficients that can be obtained by linear regression (as first approximation), and $\mu = 1$ for compression and $\mu = -1$ for tension.

The analysis of Equation 2.3 (Figure 2.7) showed that X_1 varies linearly with the stress applied, σ, unlike X_2. However, as both X_1 and X_2 depend on the stress applied, both ε_{cs}, ε_{sc} can also be considered stress-dependant and thus Equation 2.3 can be writing in the following form:

$$\varepsilon_{dc} = \varepsilon_{sc} + \varepsilon_{cs} = \mu X_1 \sigma \varepsilon_{fs} + \mu X_2(\varepsilon'_{fs})\varepsilon_{bc}(\sigma) \quad (2.4)$$

where ε'_{fs} is the free shrinkage rate, X_1 = coefficient linearly dependant on σ, and X_2 = coefficient dependant on insensitivity of the shrinkage process.

Kovler further investigated the phenomenon of tensile creep in concrete and presented the needed corrections to the previously suggested model (Equation 2.4) [Kovler, 1999]. This further investigation was motivated by: (1) the shortcomings found upon trying to apply the previously suggested model (Equation 2.4) to experimental work by Thelandersson [1988], (2) the observed mechanical behavior of drying concrete which was characterized by very insignificant hysteresis loops at loading and unloading cycles, constancy of elastic modulus, and growth of tensile strength (Figure 2.8) [Kovler, 1995], and most of all (3) the new experimental results that became available after the first study [Kovler, 1996].

Kovler [1999], suggested the existence of what is called the “abnormal” behavior of drying creep strain in the initial period of drying (1.5-2.0 days), when drying creep was contrary to the load direction (i.e. as shrinkage). This “abnormal” behavior was due to the fact that when

concrete elements are under simultaneous tensile loading and drying, these two factors produce deformations of opposite signs (i.e. expansion produced by tensile loading and contraction produced by drying), and thus the resulting drying creep strain will not necessarily coincide in direction with the load but will change with time (Figure 2.9) [Kovler, 1995, and Kovler, 1999].

This “abnormal” behavior was explained by attributing the excess basic creep strain over the total creep strain in the initial period to swelling (or reversible shrinkage) of the sealed concrete specimens if strains were considered from the moment of rewetting [Kovler, 1996]. Such a phenomenon was believed to be affected by three major factors: (1) capillary stress at RH > 40%, (2) disjoining pressure, (3) changes in surface free energy; in addition to (4) movement of interlayer water.

In this study, a simplified model was laid out to explain the dependency of the “abnormal” behavior or drying creep in the initial period (discussed above) on the vapor pressure in the capillaries (Figure 2.10). Initially, a loss in the free water in capillaries begins as the relative humidity drops below 100% of initial saturation level. The initial radius of the curvature R does not change until a spherical meniscus of a radius R is formed (Figure 2.10 (a)). This process of free water evaporation is not accompanied by any deformation (i.e. shrinkage).

Capillary water then continues to be removed only if the radius of the meniscus drops to a value, r, smaller than the initial radius R (Figure 2.10 (b)). This process of capillary water removal is accompanied by shrinkage in the material. When concrete is sealed after the initial drying period, the vapor pressure in the capillaries increases quickly, the radius of curvature of the meniscus increases and the level of liquid becomes flatter. As a result, the capillary surface tension is released and a swelling in the material occurs (Figure 2.10 (c)).

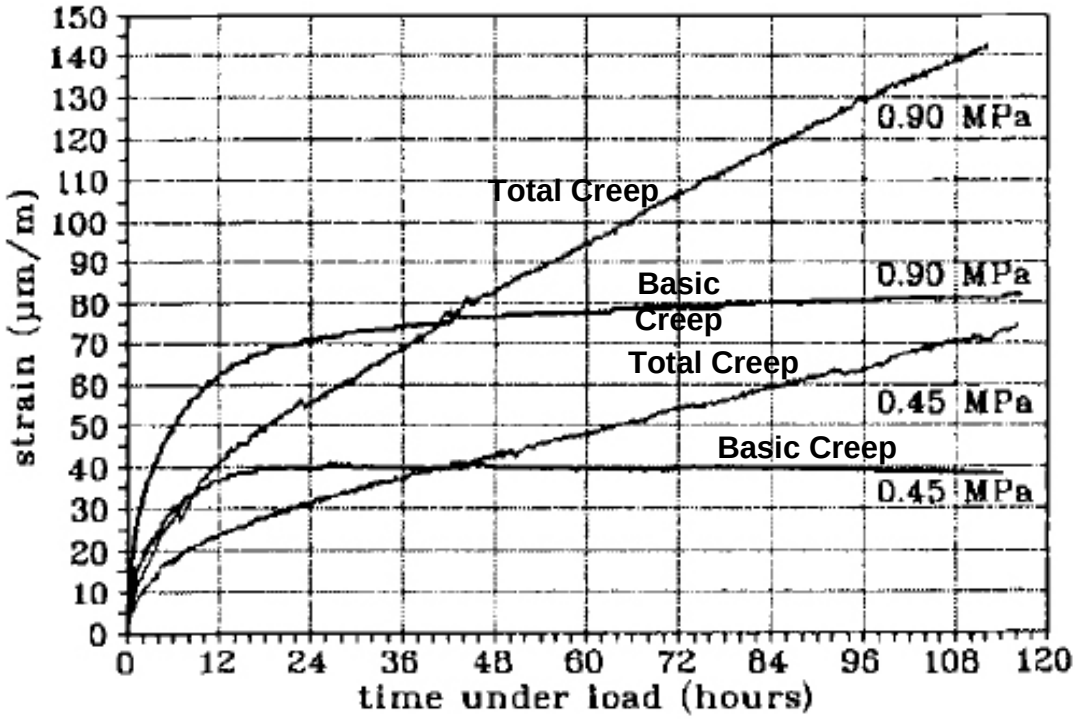

Figure 2.6: Typical curves of creep and basic creep strains for different tensile stresses applied [Kovler, 1995]

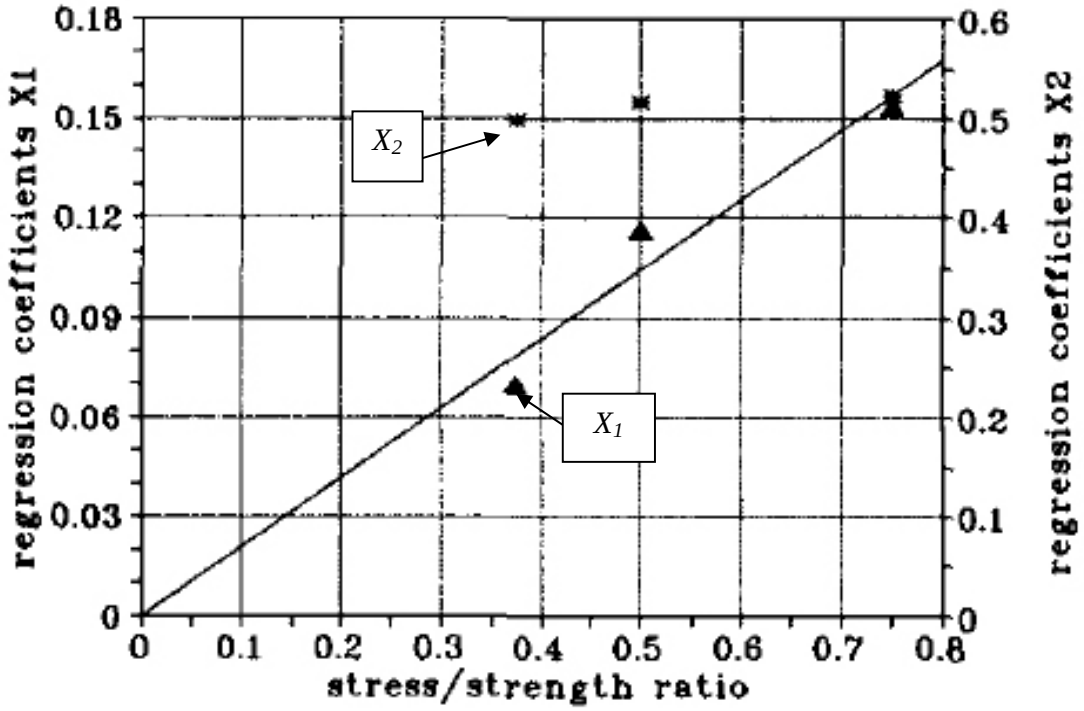

Figure 2.7: Regression coefficients X_1 and X_2 versus stress-strength ratio [Kovler, 1995]

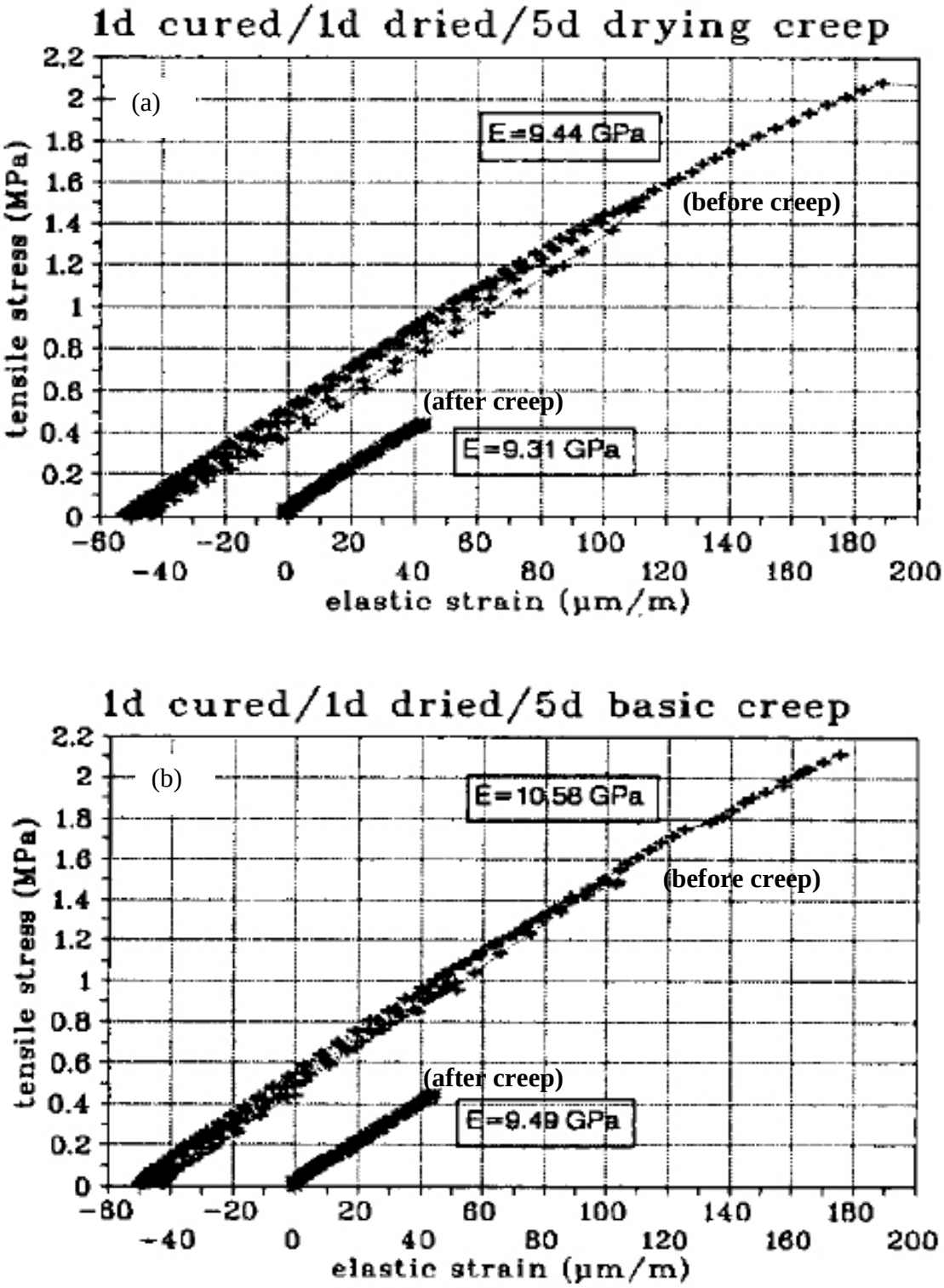

Figure 2.8: Stress-strain diagrams obtained before and after (a) basic creep test, and (b) drying creep test [Kovler, 1995]

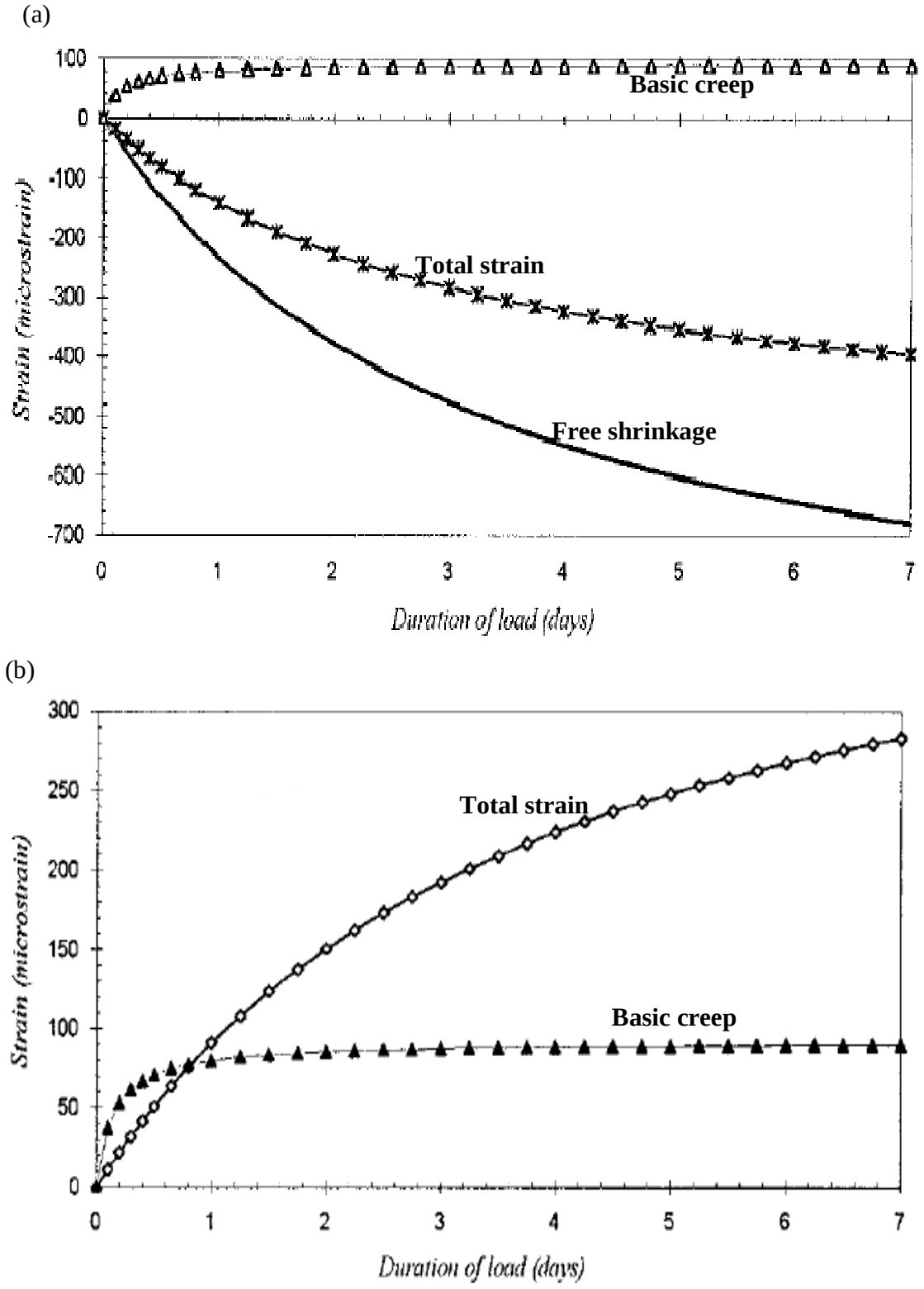

Figure 2.9: Results of tensile creep tests of concrete (a) all results, and (b) total and basic creep [Kovler, 1999]

It is here important to notice that the results that could be obtained from similar tests on

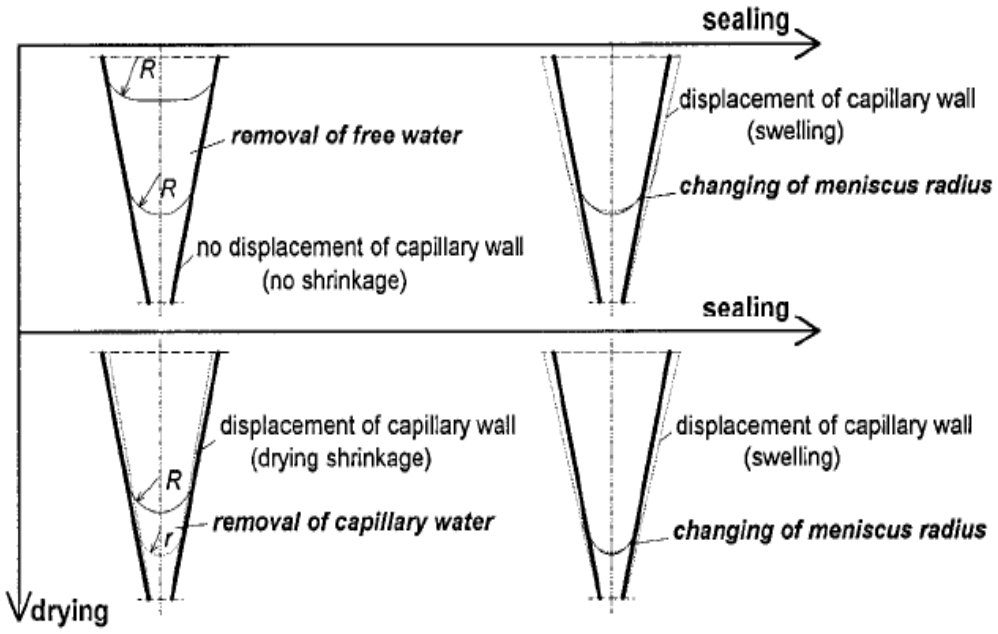

Figure 2.10: Simplified model of capillary water movement during evaporation and sealing, [Kovler, 1996]

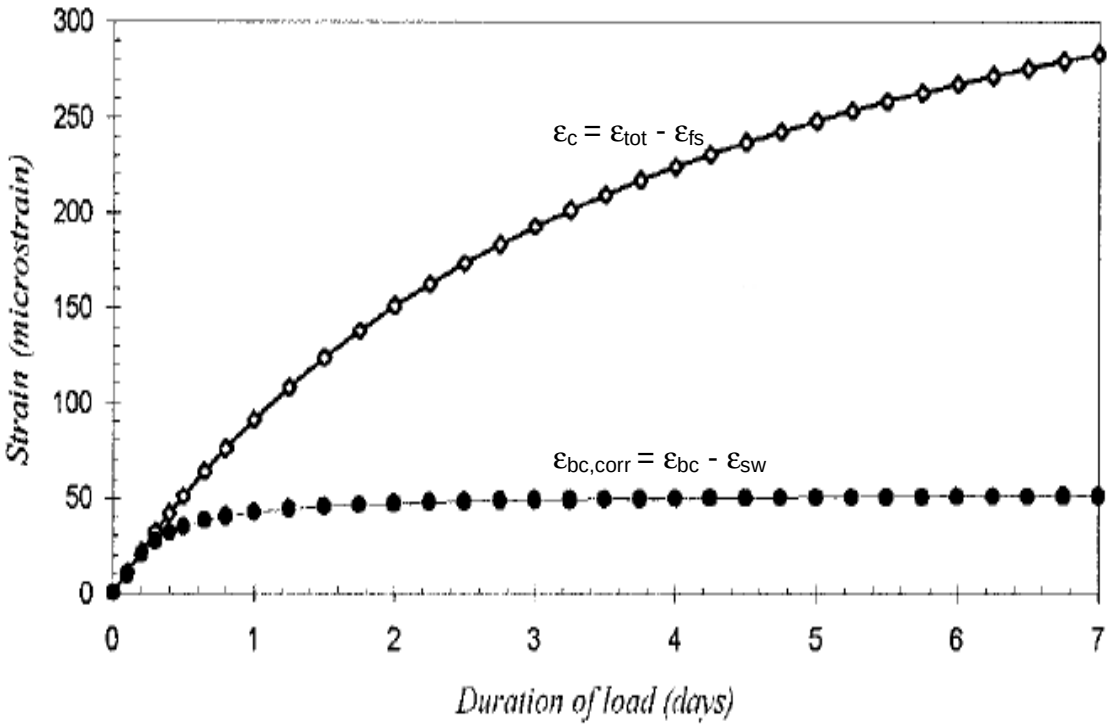

Figure 2.11: Total creep(ε_c), and corrected basic creep ($\varepsilon_{bc,corr}$) [Kovler, 1999]

The same concept can then be applied in case of concrete rewetting. According to this model, the deformations of sealed concrete should be looked at completely differently than concrete allowed to dry, as the vapor pressure within a sealed specimen is higher than an unsealed specimen.

To investigate this approach, Kovler [1999] measured deformations of load-free sealed concrete at water-to-cement ratio of 0.7 after some initial period of drying. The swelling deformations (ε_{sw}) observed did not exceed 40– 45 με and that the amount of swelling depended on both the duration of curing and the duration of drying before sealing. Upon considering swelling deformations in calculating drying creep, the following approximate relations were presented:

$$\varepsilon_{sh} = -t/(0.0010t + 0.0033) \quad (2.5a)$$

$$\varepsilon_{c} = t/(0.0023t + 0.0087) \quad (2.5b)$$

$$\varepsilon_{bc} = t/(0.0135t + 0.1636) \quad (2.5c)$$

$$\varepsilon_{sw} = t/(0.0285t + 0.0012) \quad (2.5d)$$

where ε_{sh}, ε_{c}, ε_{bc}, and ε_{sw} are free shrinkage, total creep, basic creep, and swelling strains respectively, and t is the time in days. The total tensile creep and the corrected basic creep are plotted in Figure 2.11, which is corrected version of Figure 2.10(b).

Based on these results, the corrected drying creep curve under tension coincided in direction with the tensile load applied from the very beginning of loading. It follows then that the drying creep of concrete under tension actually represents creep strain not shrinkage (as in the case of compression) [Bissonnette and Pigeon, 1995]. This means that the previously proposed two-mechanism model (Equation 2.4) cannot be valid, and that the mechanism of drying creep cannot be creep-induced shrinkage [Kovler, 1999]. The author hypothesizes that UHPC might be significantly different than what was obtained by Kovler [1999]. This is mainly due to the significant difference in the water-to-cement ratios between both the cases (i.e. typically less than 0.2 for UHPC and 0.7 in the previous study [Kovler, 1999]). This will likely reduce the

swelling deformation component in the case of UHPC, and hence, it would be of specific interest to verify applicability of this model to the tensile creep of UHPC.

2.3.2 Experimental Methods

2.3.2.1 Tension tests

2.3.2.1.1 Modulus of rupture test [ASTM C78 and ASTM C293]

The modulus of rupture test is and indirect tension test carried out under either the four-point loading configuration [ASTM C78] or the three-point loading configuration [ASTM C293] (Figure 2.12). However, in most cases, the former configuration is recommended as it creates a condition of pure bending at midspan.

The tensile strength determined by this method tends to overestimate the "true" tensile strength of the material due to the fact that a linear stress variation is assumed for the calculation of the flexural strength (Figure 2.13). Concrete presents a nonlinear stress-strain relation and additionally, the low span-to-depth ratio of the typical specimen indicates the presence of shear deformations. For these reasons the assumption of linear stress variation is not valid [Mehta and Monteiro, 2005]. Moreover, in a direct tension test, the total volume of the specimen is subjected to tensile stress, whereas in the flexural test, only a small portion near the bottom of the specimen is resisting high tensile stresses. This suggest that in a direct tension test the probability of finding the weakest part of the specimen is greater than in the modulus of rupture test.

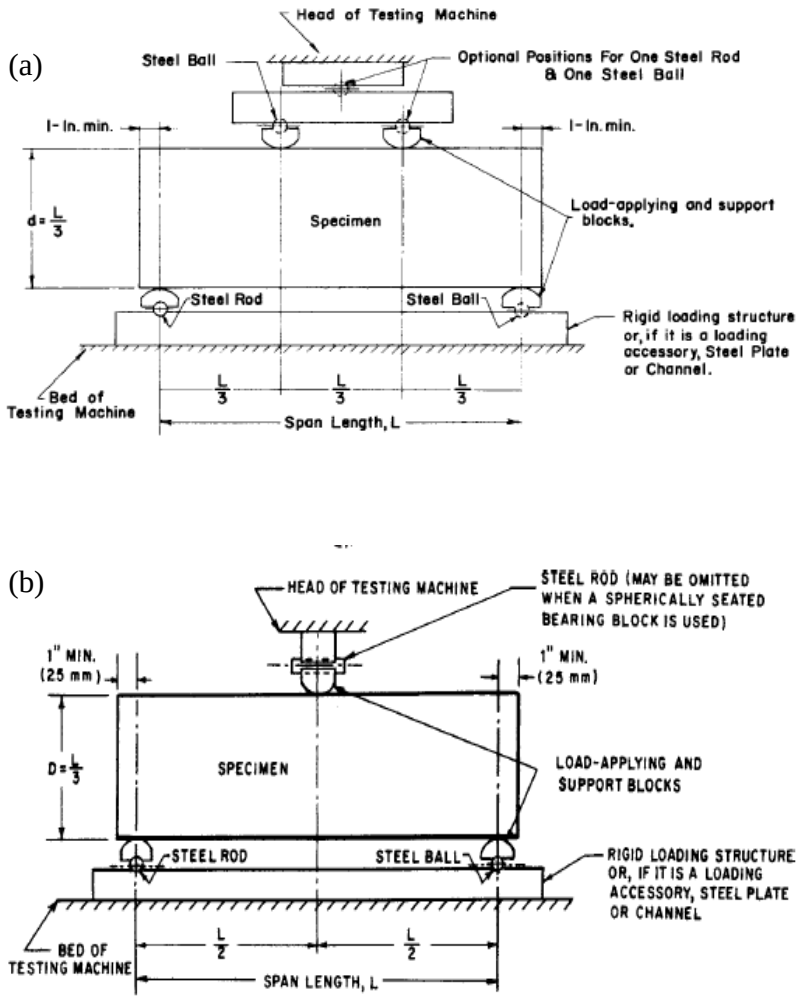

Figure 2.12: Modulus of rupture standardized test setups: (a) four-point bending [ASTM C78] and (b) three-point bending [ASTM C293]

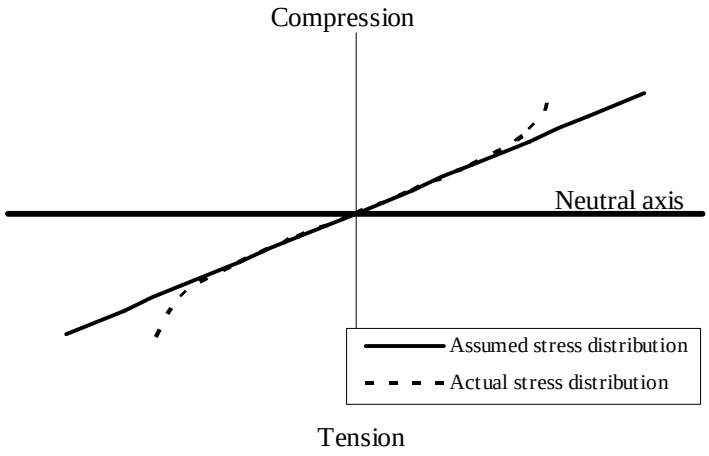

Figure 2.13: Stress distribution across the depth of the specimen in the modulus of rupture test [Mehta and Monteiro, 2005]

The modulus of rupture test is commonly used because of its simplicity and because cracking in beams under flexural loading is of concern and thus the test better represents the concrete property that is of interest for bridge girder applications. It is the author's opinion that the modulus of rupture cannot be taken as the tensile strength of the material and values obtained from this test cannot be used as basis for loading direct tensile creep specimens, where the "true" values are needed for real material characterization.

2.3.2.1.2 Splitting tensile test [ASTM C496]

In the splitting tensile test, a compressive force is applied perpendicularly to the longitudinal axis of the cylinder (Figure 2.14). This force creates an almost uniform tensile stress over the middle part of the vertical loading plane. However, high compressive stresses are generated close to the ends of the vertical plane as shown in Figure 2.14.b.

The tensile strength value calculated from the splitting tensile test is typically lower than the corresponding value determined from the modulus of rupture test, but it is higher than the result obtained from direct tensile testing [Graybeal, 2005]. This difference exists due to: (1) considering concrete a homogenous material, (2) neglecting the effect of the high compressive stresses generated at the ends of the vertical plane during the calculations; (3) neglecting lateral restraints provided by friction between the specimen and the thin plywood bearing strips. The effects increase the apparent value of tensile strength. Results obtained from this test should not be used in estimating the true tensile strength of the material.

The major difficulties for the design of a direct tensile strength test for concrete are associated with the stress concentrations and the secondary flexure and torsion induced to the concrete specimen through end-gripping. These additional stresses cause reduction in the measured tensile strength, and these stresses are difficult to determine practically for each test.

Generally, there are three major goals to be achieved in any direct tension test in order to obtain a good characterization of the material: (1) uniform tensile stress field in the failure area, (2) a single plane of cracking to clearly define the failure area of the specimen, and (3) stable failure in order to obtain the complete tensile response of the material. Each of the methodologies in the literature is strong in some aspects and weak in others. A brief description of some of the techniques found in the literature is presented in the following sections.

(a)

(b)

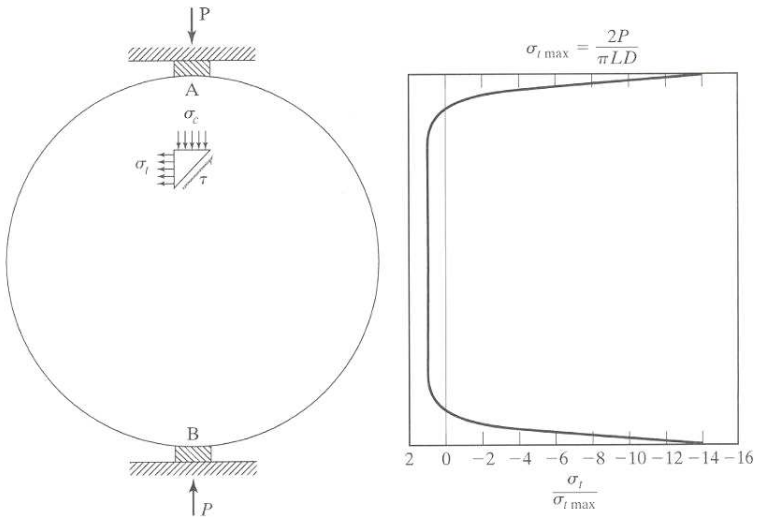

Figure 2.14: (a) Splitting tension test and (b) Stress distribution across loaded diameter in the splitting tensile test [Mehta and Monteiro, 2005]

2.3.2.1.3 Mortar briquette test [ASTM C190]

Specimen dimensions used for a standard mortar briquette test are shown in Figure 2.15. As this test was commonly used for the determination of the tensile strength of hydraulic cement mortars, the molds and equipment are usually available which is an advantage of the method. Another advantage of this technique is that the self-aligning grips shown in Figure 2.15 ensure an almost uniform tensile stress on the specimen across the 1-in. section [Graybeal, 2005].

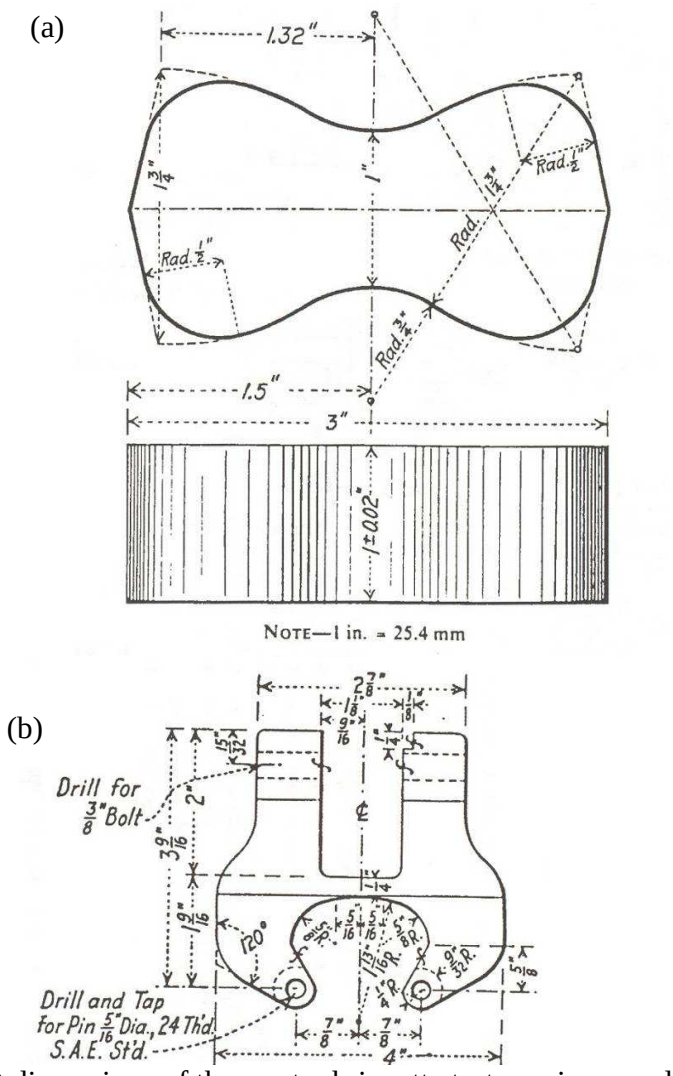

Figure 2.15: (a) dimensions of the mortar briquette test specimen and (b) clips for holding the mortar briquette test specimen [ASTM C190]

The small maximum size of the aggregate particles in UHPC allowed for the use of this type of specimens. However, the length of the discontinuous steel fibers, about 12 mm (½-in) became a problem as potential alteration of the desired random fiber orientation was reported due to the small cross-section at the neck in the middle portion of the specimen. This alteration in the fiber dispersion also resulted in a considerable scattering of the tensile strength results [Graybeal, 2005].

2.3.2.1.4 Todd's direct tension test [Todd, 1955]

In Todd's direct tension test, a steel bar with attached strain gages is installed through the center line of cylindrical concrete specimen (Figure 2.16). Uniaxial tension is applied to the steel bar until a tensile failure in the concrete is achieved. The stresses are transmitted to the concrete by bonding between the steel bar and the concrete.

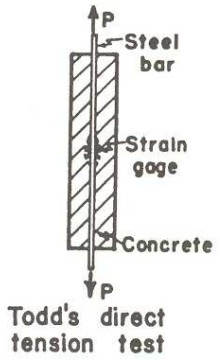

Figure 2.16: Configuration for Todd's direct tension test [Todd, 1955]

The final load carried by the 152.4 x 304.8 mm (6 x 12 in.) concrete cylinder is the difference between the total pulling load and the load in the bar calculated from the strain gage data. This methodology largely reduces the problem of load misalignment and stress concentrations due to gripping. However, the distribution of stresses along the concrete section is not uniform; higher stresses around the steel bar.

2.3.2.1.5 Unnotched cylinder

In the unnotched cylinder test, the top and bottom faces of concrete cylinders are pre-adhesively bonded to rigid steel loading plates or the loading heads of the test machine using high strength/high modulus epoxy prior to loading as done by Akita et al. [2003], Graybeal [2005], and as done by the author (Figure 2.17). In the case of UHPC, several problems have been reported and were encountered about using such cylinders, especially lack of control over the location of failure cracks. In addition, when multiple cracks are present, the observation of the tensile softening behavior was impossible or unreliable. Moreover, in a multi-crack pattern, overlapping of cracks is likely to occur and higher values of energy dissipation are obtained from the test. Multi-crack patterns represent the type of failure that is expected in a concrete structure especially when using UHPC. However, for material characterization, a very well defined single plane, as well as the most uniform stress distribution possible are desired. In addition, adhesive failure at the specimen ends often occurs in this test especially at high stress values.

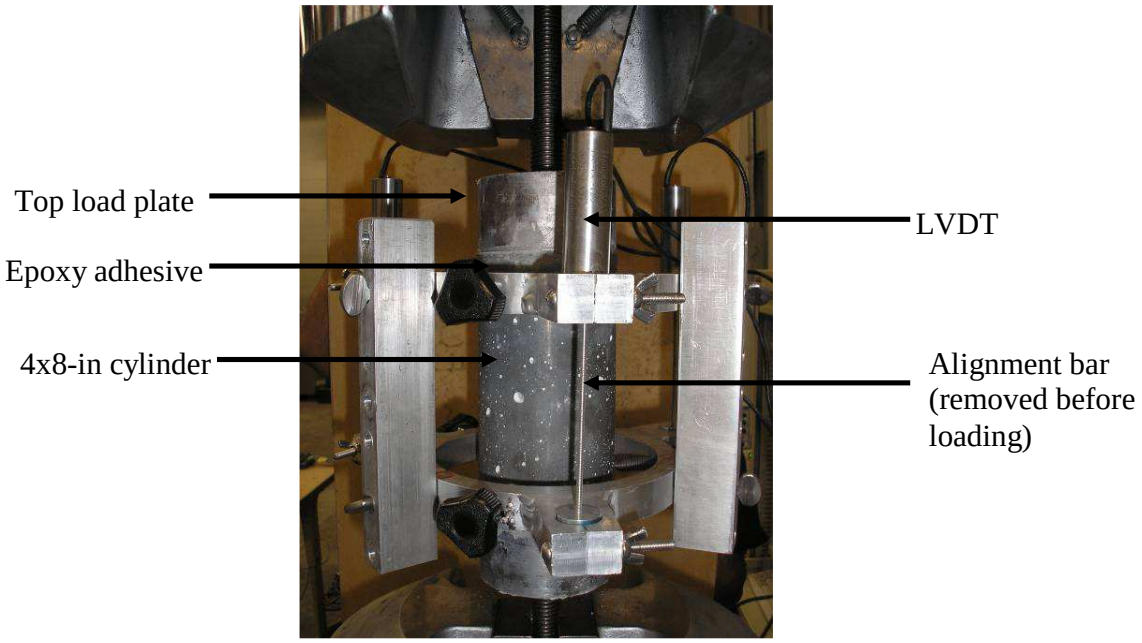

Figure 2.17: Unnotched direct tension test done at Georgia Tech

2.3.2.1.6 Unnotched rectangular prism specimen [Li et al., 1993]

Li et al. [1993] proposed a more complex methodology for the determination of the tensile properties of plain and fiber reinforced concretes in an attempt to obtain the post-peak tensile stress-strain response. In this method, tapered steel loading plates were epoxy-bonded to (330 x 127 x 28 mm (13 x 5 x 1.1-in) prismatic specimens to provide good loading alignment and to reduce the stress concentrations (Figure 2.18). Four linear voltage displacement transducers, LVDTs, each with a gage length of 70 mm (2.75-in) were mounted on the prism, spanning the entire test portion of the specimen. Each test was controlled by a C-Language program which was written in order to switch control rapidly to the LVDT recording the largest crack opening. It was found that controlling the test in this manner provided better results than the traditional approach of using the average deformation to control the test. Additionally, six piezoelectric-crystal transducers (PZT) were glued on the surface of the specimens to monitor the acoustic emission activity.

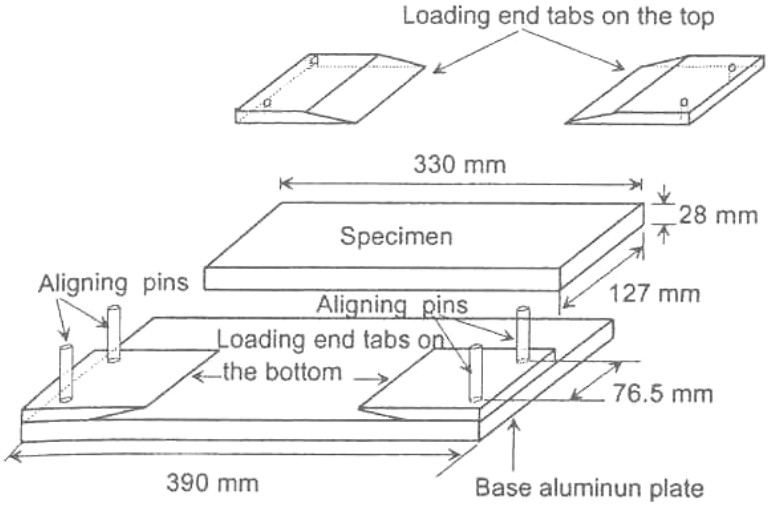

Figure 2.18: Procedure for gluing the steel loading plates to the specimen [Li et al., 1993]

The methodology used in this research program successfully achieved a stable failure, obtaining the complete tensile response of unnotched specimens. The stress concentrations and the predetermination of the plain of failure observed when notched specimens are used were avoided using this methodology. Moreover, at least for the information presented in the paper, the scattering in the results seemed to be reduced. On the other hand, this test set up was much more complicated than other tests and special software and equipment were needed.

2.3.2.1.7 Notched cylinders [RILEM TC 162-TDF]

The RILEM notched cylinder test differs from the cylinder test discussed in section *2.3.2.1.5* in that in this test a semi circular notch in created at mid-height of the 100 mm (4-in) diameter cylinder specimen prior to loading (Figure 2.19). The use of notched specimens prevents multi-crack patterns along the height of the specimen as found by Akita et al. [2003], Li. et. al. [1993], and the author (Figure 2.20). The main reason for using notched specimens is to predetermine the location of the major crack and facilitate the process of controlling the test by the deformation of the actual specimen. Doing this, a gradual and stable post-peak response can be more easily achieved. However, the presence of the notch creates a non-uniform distribution of stresses along the plane of failure. Moreover, the fact that the notch is cut with a diamond saw can produce scattering of the results due to the cut's inevitable difference in geometry (end sharpness) from one specimen to the other [Akita et al., 2003]. An alternative to cutting a notch is to cast the specimens with a notch in the form. In this manner, the notch geometry could be kept unchanged from one specimen to the other, and the scattering of the results resulting from post-cutting could be reduced. However, this alternative is not recommended because it could lead to non-uniform distribution of the fibers [Gettu and Barragan, 2003]. Another disadvantage of the use of notched specimens is related to the

predetermination of the crack location. This condition does not capture the variability of tensile strength through the specimen. Also, the tensile zone is not long enough to get an accurate tensile strain, so development of accurate stress-strain response is not possible.

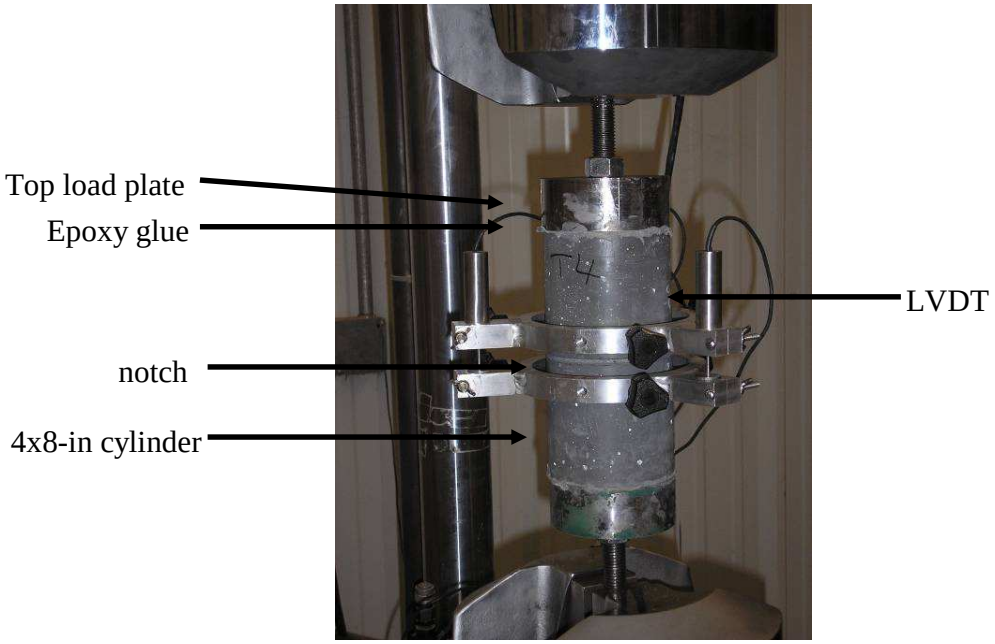

Figure 2.19: Direct tension test on notched specimen done at Georgia Tech

Figure 2.20: Fractured notched specimen (Georgia Tech)

2.3.2.1.8 Dog-bone test

Dog-bone specimens were used to determine the tensile properties of a fiber-reinforced UHPC mix named SIFCON by [Naaman and Homrich, 1989 and Naaman et al., 1991] (Figure 2.21). Test specimens were 457 mm (18 in.) long, and had a cross-sectional area of 75 x 38 mm (3 x 1.5-in) in the middle portion. The cross section at the ends of the specimens was 75 x 75 mm (3 x 3-in). The fibers were intentionally oriented along the longitudinal axis of the specimen in order to achieve the maximum tensile strength. Strains were measured using two linear variable differential transformers (LVDT) placed on opposite sides of the specimen.

The gage length was 150 mm (6 in). The load was applied using stroke control. During the ascending part of the stress-strain curve, the rate was 25.4 µm/sec (0.001 in./sec). Once the peak stress was achieved, a reduced rate of about 0.254 µm/sec (10^{-6} in./sec) was used in order to obtain a considerable portion of the post-peak response.

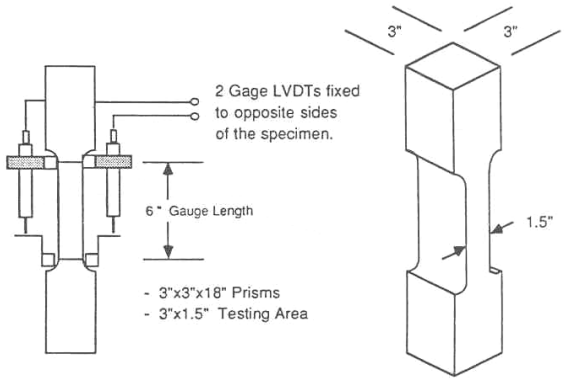

Figure 2.21: Tension Dog-bone specimens [Naaman and Hormich, 1989]

Results from this study showed that failure was initiated by the formation of small cracks evenly distributed along the portion having a constant reduced cross section. In fact, many of these cracks were caused by shrinkage before the load was applied. When the enlargement and opening of one of the small tensile cracks occurred, the peak tensile strength was achieved. The

post-peak behavior was characterized by the debonding of fibers at either side of a single, well defined crack. According to the researchers, the elongation measured in the ascending portion of the load-elongation curve can be translated into tensile strain. However, after the peak, the elongation principally represents a crack opening and cannot be directly used as strain.

In conclusion, based on the previously presented tension test methodologies, it is the author's opinion, that the dog-bone test configurations are the most accurate method to obtain the true tensile strength of UHPC. This conclusion is based on the following facts: (a) sections in a dog-bone test configuration are uniformly loaded, (b) tensile Young's modulus of elasticity and Poisson's ratio can be determined using dog-bone configuration, (c) the dog-bone specimen configuration offsets most of the problems related with adhesively bonding specimens' ends to loading plate or loading heads in constant cross section configurations, and (d) the use of a reduced cross section appears as a practical alternative to the use of notched specimens. In addition, and particularly for the present study, casting dog-bone specimens (i.e. from one side to the other along the longitudinal axis) is similar to casting prestressed bridge girders where fiber alignment occurs. Also, this casting method is similar to casting the tensile creep specimens.

2.3.2.2 Tensile creep tests

Very few studies have focused on studying the tensile creep behavior of concrete [Umehara et al., 1994; Gutsch and Rostasy, 1994; Kovler, 1994; Bissonnette and Pigeon, 1995; Kovler, 1995; Kovler et al. 1999; Kovler, 1999; Altoubat and Lange, 2001; and Tao and Wiezo, 2006] either because of the relative complexity of conducting tensile creep tests as compared to conducting standardized compressive creep tests, or because of a perception that the behavior of any concrete in tension can be completely ignored since most of the tensile stress are carried by

steel reinforcement provided. The latter has been justified because steel or other reinforcement is provided to resist tension after cracking; therefore tensile behavior is important.

Among those previously mentioned studies, only Bissonnette and Pigeon [1995] reported test results over more than a year, while all the other studies reported results for a maximum period of about 200 hours only. The use of short-duration tests is likely because of the complexity of the test setup used in these studies as it is discussed in the following section.

2.3.2.2.1 Jalal Vakili [1983 and 1984]

One of the first test setups used to characterize the tensile creep behavior of concretes was the one developed and used by Vakili [1983 and 1984] where an electro-hydraulic loading system was used for short term tensile creep tests on asphaltic concrete. No schematic diagram of the equipment was provided.

The time-dependent loads were controlled by the shape of a load-time curve mounted on the drum of a data track. A pair of LVDTs attached to the central portion of the specimen measured the vertical deformation. The specimen size was 100 mm (4-in) in diameter and 230 mm (9.0-in) in height. Specimens were bonded to aluminum end caps using a structural epoxy resin. A jig was used to ensure that the end caps were properly aligned and the adhesive was allowed to cure for 12 h before specimens were removed from the jig. Uniaxial tensile creep tests, were performed at 20°C. A constant stress was applied instantaneously to the specimen and the deformations were recorded for a period of 190 seconds. After unloading, each specimen was allowed to rest for 2 h and then the permanent deformation was recorded. The same setup also was used to observe the experimental recovery curve of asphaltic concrete where a tensile stress of 0.0307 MPa (4.45 psi) was applied to the specimen for 217 seconds. The load was then

removed and the deformations were recorded for an additional period of 418 seconds. In both of these studies, no additional information about the accuracy of measurements was provided.

2.3.2.2.2 Kovler [1994]

A general view of the experimental device developed by Kovler [1994] is shown in Figure 2.22. The device allows two dog bone specimens with a net cross section of 40 x 40 mm and a working length of 1,000 mm (1.57 x 1.57 x 39-in) to be mounted horizontally on the laboratory table, one for restrained shrinkage testing, and the other for free shrinkage testing.

The right end of each specimen is fixed. The displacements of the left movable grips were measured by a linearly variable displacement transducer (LVDT). Each displacement measurement cycle consisted of 256 measurements during 0.5 seconds, and the result was averaged and recorded. Such a procedure permitted very high accuracy and reproducibility of linear displacement measurements not less than ± 0.1 μm (0.0000039-in).

The stresses in the restrained specimen were measured by means of a load cell with an accuracy of ± 0.0003 MPa (0.0435 psi). The restrained specimen was loaded by a computer-controlled stepper motor according to a special program. The compensation cycle began when the absolute value of the total restrained specimen strain exceeded $5x10^{-6}$. Load was applied to recover the shrinkage strain. Two different rates of loading were chosen. In the initial period of fast evaporation and resultant drastic growth of shrinkage strain (period A), the loading rate was accepted to be 0.003 MPa s^{-1} (0.435 psi s^{-1}), and in the following stable stage (period B) 0.001 MPa s^{-1}(0.145 psi s^{-1})

The frequency of stress and strain measurements in these stages of the shrinkage process was chosen differently as well. The time interval between measurements in period A was taken as 180 seconds, and in period B it was 600 seconds. The duration of period A was 1-2 h.

Loading rates associated with shrinkage rates were chosen to exclude premature specimen failure. For the same purpose the grips were of a special shape, characterized by gradual widening of the internal part to eliminate any stress concentrations inside.

The possible physical eccentricity of the specimen, caused by non-uniform strain development in the net cross section, was checked and excluded. The movable grips were joined with spherical hinges. During the test the uniformity of progressive displacements of the grip was controlled on the left and right grip sides by means of two mechanical strain gages of accuracy ±1mm (±0.039-in): when the difference in their readings was more than 5 mm (0.20-in), the center of the hinge was moved horizontally by means of precise screws to the necessary direction. The measured value of the friction force did not exceed 20N (4.5 lb), and was therefore neglected at data analysis.

The uniaxial tensile loading apparatus developed in the Israel Institute of Technology (Figure 2.22) allowed performing two tests:

Restrained shrinkage test: in this test, one gripped end was fixed and the other was connected to a motor through universal joint. This system is a computer controlled closed loop one. When shrinkage occurs and its level is approaching a strain of 5x10-6, the motor automatically starts the motion to pull the specimen back to the initial position, to keep the length of the specimen constant at 1,000 mm (39.4-in). The load cell records the load induced in this motion.

Total strain (ε_{tot}) of a restrained shrinkage specimen consists of three strain components: elastic strain (ε_e), autogenous shrinkage strain (ε_{sh}) and creep strain (ε_{cr}). The total strain in the restrained shrinkage test is zero.

$$\varepsilon_{tot} = \varepsilon_e + \varepsilon_{sh} + \varepsilon_{cr} = 0 \qquad (2.6)$$

ε_{sh} is directly measured form the free autogenous shrinkage test. ε_e is calculated by the accumulation if the elastic strain increments in each cycle of the loading by the motor movement. The creep strain is obtained as the difference between free autogenous shrinkage strain of a free specimen and the cumulative strain of the restrained specimen (Figure 2.23 (a)).

Constant load creep test: this test is similar to conventional creep tests in compression. The cast concrete was also sealed, and twin specimens were cured for 24 hours. Thereafter, a tensile stress was applied to the movable grip. The closed loop computer-controlled system was programmed to move the grip to maintain the creep load constant. In this test, the measured total strain of the loaded specimen is the sum of the autogenous shrinkage strain and the creep strain

$$\varepsilon_{tot} = \varepsilon_{sh} + \varepsilon_{cr} \tag{2.7}$$

Thus, creep strain was obtained by subtracting free autogenous shrinkage strain from the measured strain of the loaded specimen (Figure 2.23 (b)).

It is important to develop a high accuracy method for displacement measurement for this kind of test because the absolute values of the deformations will be close to zero. This means that the total deformation of the specimen, equal to the sum of shrinkage and creep components, should be compensated by instantaneous deformations quite frequently during the test, in order to provide more gradual growth of tensile stress. If this condition is not met, larger and instantaneous compensations of deformation will be needed, and they may cause premature failure. Failure will occur when the tensile strength of the material is less than the value of the tensile stress induced in it at a given time. The physical eccentricity in the specimen caused by the non-uniformity in deformation distribution over the cross-section, or by stress concentration in the grips, can also lead to premature failure. Tensile test schemes are very sensitive to these factors [Kovler, 1994].

Thus, by means of a uniaxial restrained shrinkage test, simultaneously with a free shrinking companion specimen, it is quite possible to obtain a variety of mechanical characteristics of early age concrete in uniaxial tension.

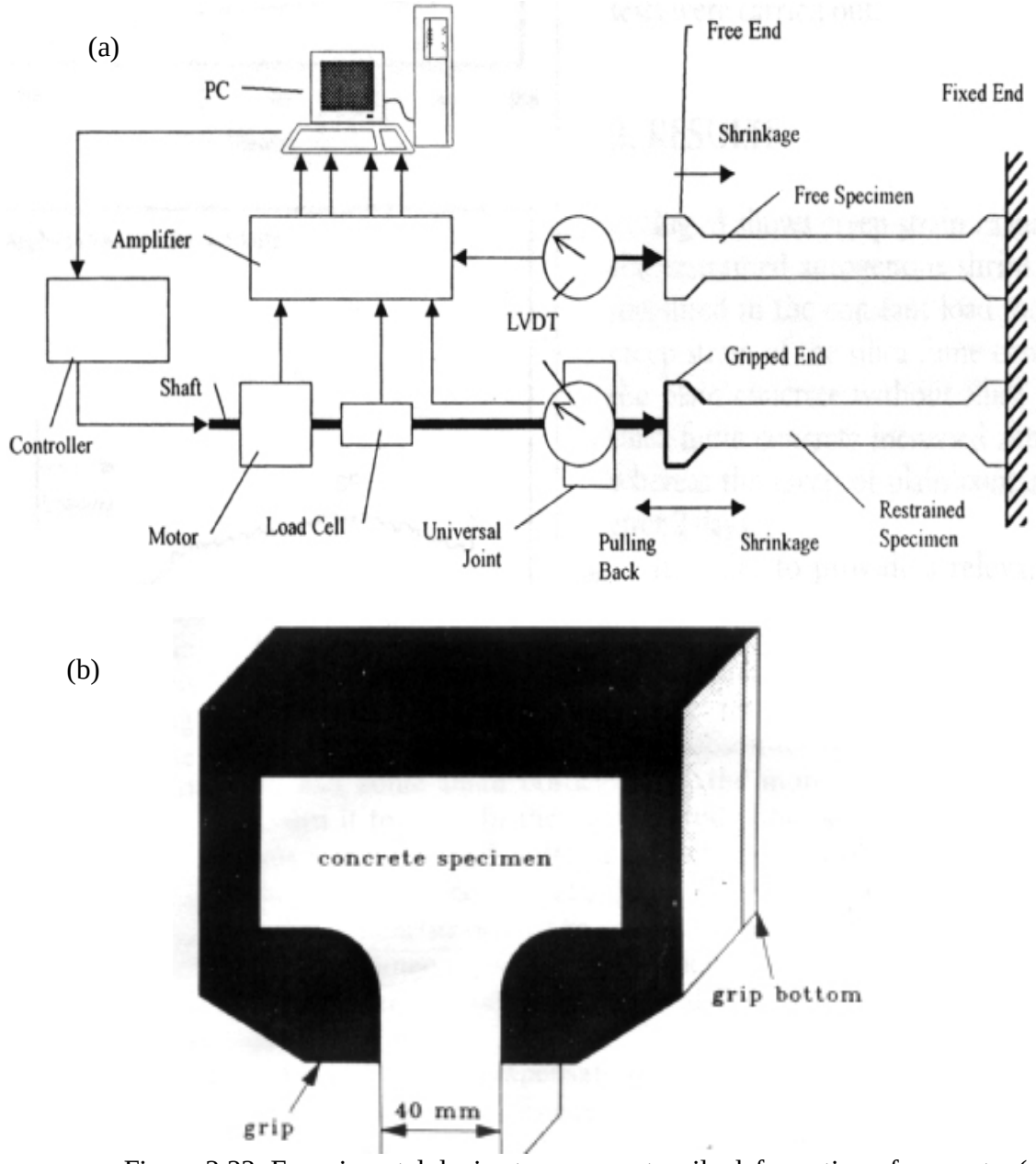

Figure 2.22: Experimental device to measure tensile deformation of concrete, (a) schematic description of the restrained shrinkage testing, and (b) specimen grip [Kovler, 1994]

Kovler [1994] designed this apparatus to meet the following requirements: (1) high accuracy measurement of linear displacement, (2) complete automation of the experiment, both in data registration and in governing the specimen loading, and (3) exclusion of any premature specimen failure, which may happen due to irregularity of loading, large load steps, or eccentricity of the specimen and stress concentration in the grips.

However, no information was given about the method of calculating the friction between the specimens and the table. Also, the literature reviewed where the same or very similar setups was used [Kovler 1994, 1995; Kovler and Bentur, 1999; Kovler, 1999; Salah and Lange, 2001; and Tao and Weizu, 2006] showed that this setup was only used for short-term creep tests with a maximum duration of 7 days. Such short duration tests may have been conducted because of the limited number of specimens that could be tested at a given time the high cost of the apparatus, and the space inefficiency related to the apparatus.

According to ASTM C 512 “Standard Test Method for Creep of Concrete in Compression”, no fewer than two specimens should be tested for creep and another two for shrinkage from a given batch under each test condition. The author believes that achieving that with this setup would be impractical for long-term tests because of the space restrictions.

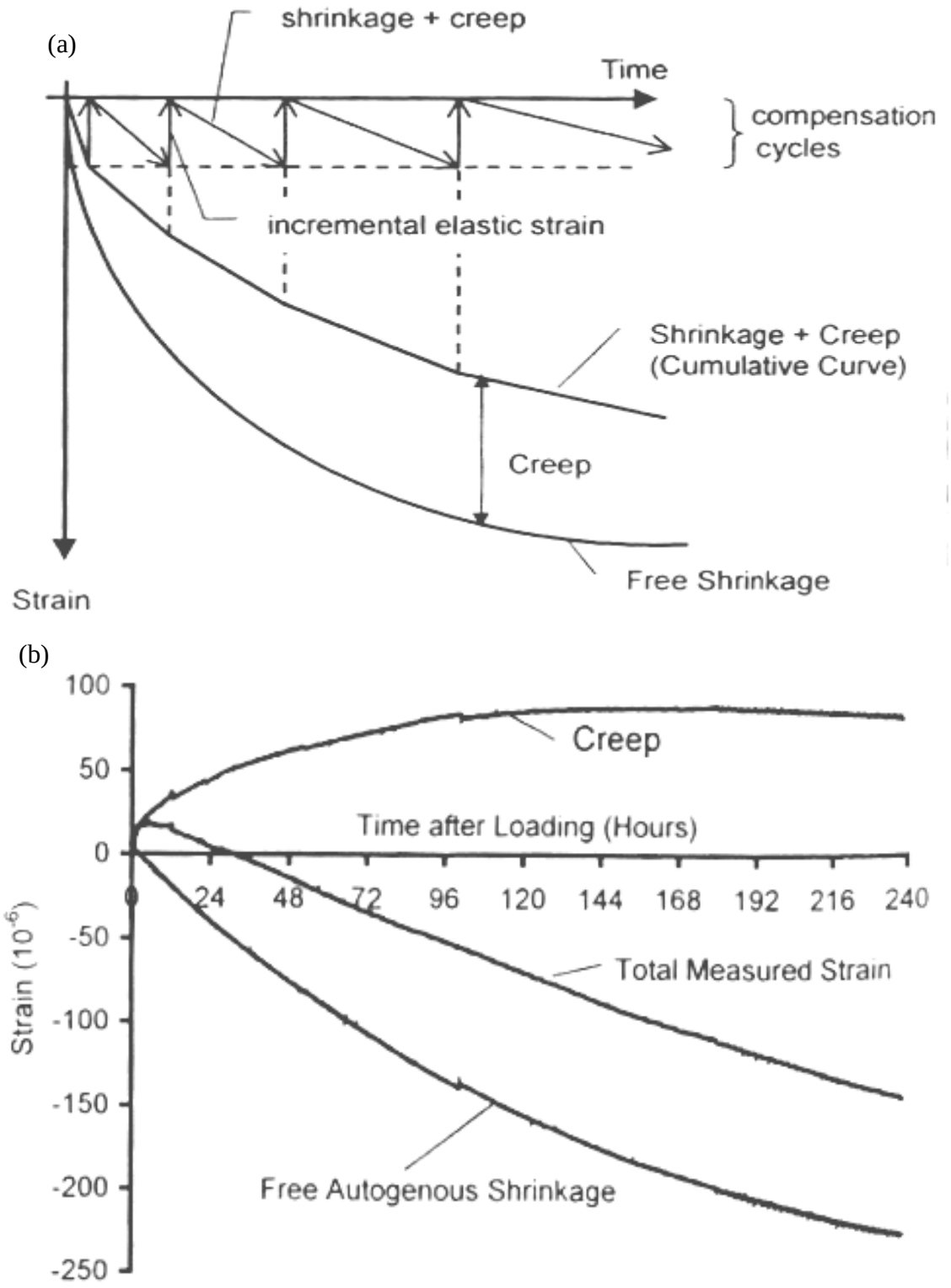

Figure 2:23: Creep strain calculated from the data of (a) restrained autogenous shrinkage tests, and (b) constant load creep tests [Kovler et al., 1999]

2.3.2.2.3 Bissonnette and Pigeon [1995]

Figure 2.24 shows the dead-load lever arm device (4:1) that was built at Universite Laval [1995] to study the tensile creep at early ages of ordinary, silica fume and fiber reinforced concrete. This device allowed 12 concrete specimens to be tested for creep at the same time. The load was applied to the prismatic specimens 50x50x700 mm (2.0 x 2.0 x 27.6-in) through precision-made steel plates anchored at the ends of the specimens with threaded rods, these plates were placed and aligned in the PVC molds prior to casting. At both ends of the specimens, the load is transmitted through a hinge (Figure 2.24). The test setup was placed in a temperature and relative humidity controlled room (23±2^{o}C and 50±5% R.H.).

The strain measurement device, similar to those used to determine the static modulus of elasticity of concrete, is also shown in Figure 2.24. Two frames were attached to the concrete specimens, 508 mm (20-in) apart (gage length). The upper frame was fixed, and the lower one was hinged, rotating around the rear rod (hinged at both ends) as the specimen deforms. The frames were attached to the specimens by means of brass plugs embedded in the concrete at the time of casting. For the rear and front rods, a special grade of stainless steel was used to avoid differential thermal strains between the measurement device and the concrete specimen. The thermal expansion coefficient of this steel 9.9x l0^{-6}/^{o}C (5.5x l0^{-6}/^{o}F) is close to the usual values for concrete 6-to-12x 10^{-6} /^{o}C (3.33-to-6.67x 10^{-6} /^{o}F). The dial gage was mounted on a lever arm (4:l), which means that the deformation that was measured represented four times the real deformation. The precision of this device is ±1 μm/m. Its performance was assessed through comparative shrinkage tests. The free shrinkage of three concrete specimens cast from the same batch was measured during 2 months with this device, and a standard extensometer was used to

measure the free shrinkage of three other specimens of the same batch. The results showed very good agreement.

According to ASTM C 512 “Standard Test Method for Creep of Concrete in Compression”, a creep loading frame should be capable of applying and maintaining the required stress on the specimen, despite any change in the dimension of the specimen. This setup as described before, in fact adequately satisfies this requirement as well as other test requirements like load centricity with the specimens.

It is the author’s opinion that as the loading capacity of this system was limited to 225 kg (500 lb.), and as maintaining a typical stress/strength ratio of 0.4 for ultra-high strength concretes with specimens of the same size requires a load of approximately 1,500 kg (3,300 lb), applying this system to UHPC becomes practically unfeasible.

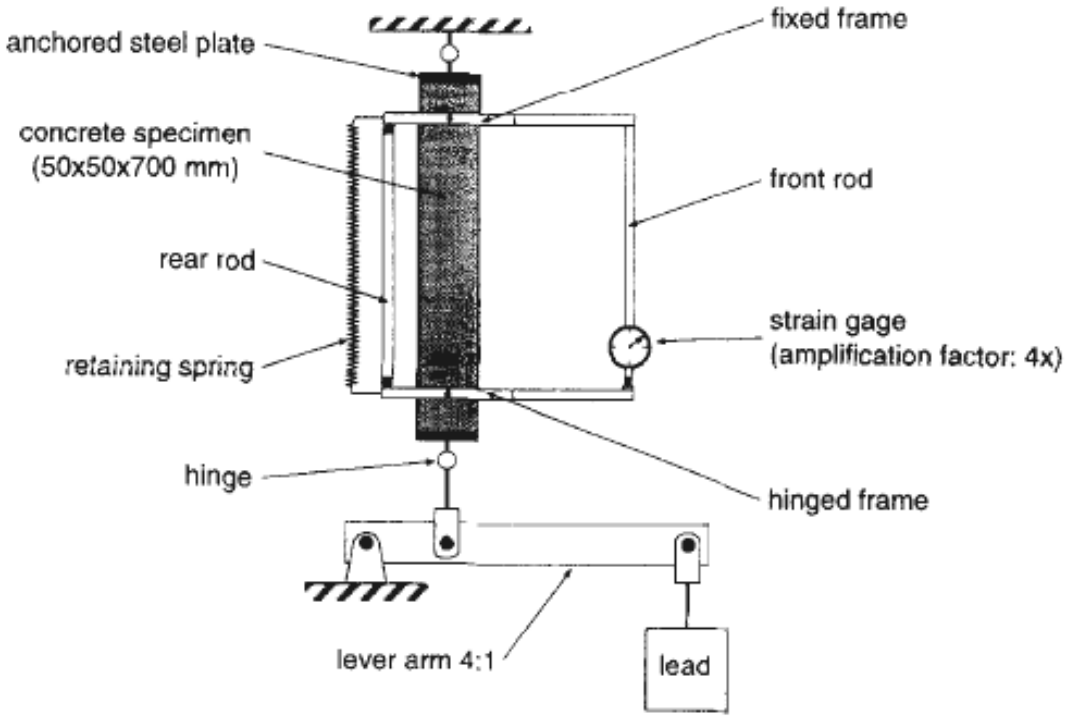

Figure 2.24: Creep test apparatus and strain measurement device [Bissonnette and Pigeon, 1995]

2.3.2.2.4 Bissonnette [1996]

Attempts were made in order to achieve higher loads by modifying the previously discussed setup by Bissonnette and Pigeon [1995].

First Modification:

Figure 2.25 shows the first of these attempts where a water tank was used as the sustained load in order to control the loading rate, and a system of pulleys was utilized to achieve an amplification factor of 48 (loading capacity of 3,600 kg (7,900 lb)) instead of 225 kg (500 lb) as in the previous setup. The prismatic specimens measured 70 x 70 x 400 mm (2.76 x 2.76 x 15.75-in). The major problem associated with this setup was the frictional losses created in the system of pulleys. These losses resulted in inconsistent loads delivered from the loading system to the specimens. Sometimes these losses decreased the load measured at the load cell at the bottom of the specimens to about 50% of the theoretical applied load.

Second Modification:

Previous problems were overcome in the modified setup shown in Figure 2.26. The setup allowed 18 specimens for creep and another 18 specimens for shrinkage to be tested at the same time. Figure 2.26 shows a detailed description of the setup:

Loading frame: The device was made of six independent loading units, each of them having a capacity of three specimens in series mounted on a rigid steel frame (Figure 2.26). The load, generated by a pneumatic jack and amplified with a 6:1 lever arm, was transmitted to the specimen series through hinged rods. Each loading unit is controlled individually with a pressure regulator and the actual load imposed to the specimens is measured with a load-cell inserted between the lower specimen of the series and the lever arm. As air is a compressible fluid, air

pressure was recommended to be checked once a day during the first week of the test and then twice a week after.

Load transfer plate: Load transfer plates consisting of 25 mm (1.0-in) thick steel discs with a diameter of 75 mm (3.0-in) were installed at each end of the specimens during casting. The discs were anchored into the concrete with 6 threaded steel rods (d = 4.8 mm (0.189-in); 10-24 NC) having different lengths (80, 105 and 130 mm (3.15, 4.13, 5.12-in)) so as to avoid the creation of a weak plane. For the companion specimens, the configuration is similar, except for the discs that were made from plastic.

Specimen size: The specimens were cylinders having a diameter of 75 mm (3.0-in) and a length of 460 mm (18.11-in).

Extensometer: The extensometer used is shown in Figure 2.27. The extensometers used are resistive strain gage mounted on half-rings which work like a conventional load cell. The monolithic aluminum half-rings (D = 160 mm (6.30-in)) are composed of two stiff legs (w = 30 mm (1.18-in); t = 6.3 mm (0.25-in)) connected through a flexible part (l = 30 mm (1.18-in); w = 15 mm (0.59-in); t = 2.7 mm (0.0465-in)) instrumented with four resistive strain gages in full-bridge configuration. The bridge potential difference is linearly proportional to the diametrical displacement of the half-ring (k = 5 V/m).

The extensometers are installed on the specimens by means of two aluminum plugs glued with an epoxy binder on the concrete surface. With an axial adjustment screw located on one of the two plugs, the extensometers are lightly tightened in place. The relative precision of this device is ±1×10-6 (absolute precision of ±0.2 µm (0.0000079-in) with a gage length of 210 mm (8.27-in)).

Procedure: Immediately before loading the creep specimens, the tensile strength of concrete was determined in accordance with ASTM Method C496, “Splitting Tensile Strength of Cylindrical Concrete Specimens”. After determining the tensile strength, three creep specimens and three companion shrinkage specimens were taken out of the conditioning room and installed on the testing apparatus. The creep specimens were assembled in the loading unit, and a pair of half-ring extensometers was installed, adjusted and zeroed on all specimens. Then, the creep specimens were loaded up to a specified fraction of the tensile strength on a shelf within the loading frame, the companion specimens were put upright to avoid any restraint.

Strain reading sequence − Readings were recorded automatically throughout the experiment with a data acquisition system. During the loading process, data were recorded at a rate of 1 Hz (1 s-1). After the specified load was reached, the recording sequence evolved as follows: $0 < t < 1$ hour, one reading every 5 minutes, $1 \leq t < 6$ hours, one reading every 15 minutes, $6 \leq t < 24$ hours, one reading every hour, and $t \geq 24$ hours, one reading every four hours.

The author believes that among the previously discussed test setups, this setup seems to be the most suitable for UHPC applications due to high load capacity as well as the ability of gradual application of loads and real time acquisition of loads and deformations. However, a simpler strain measurement technique may be desired.

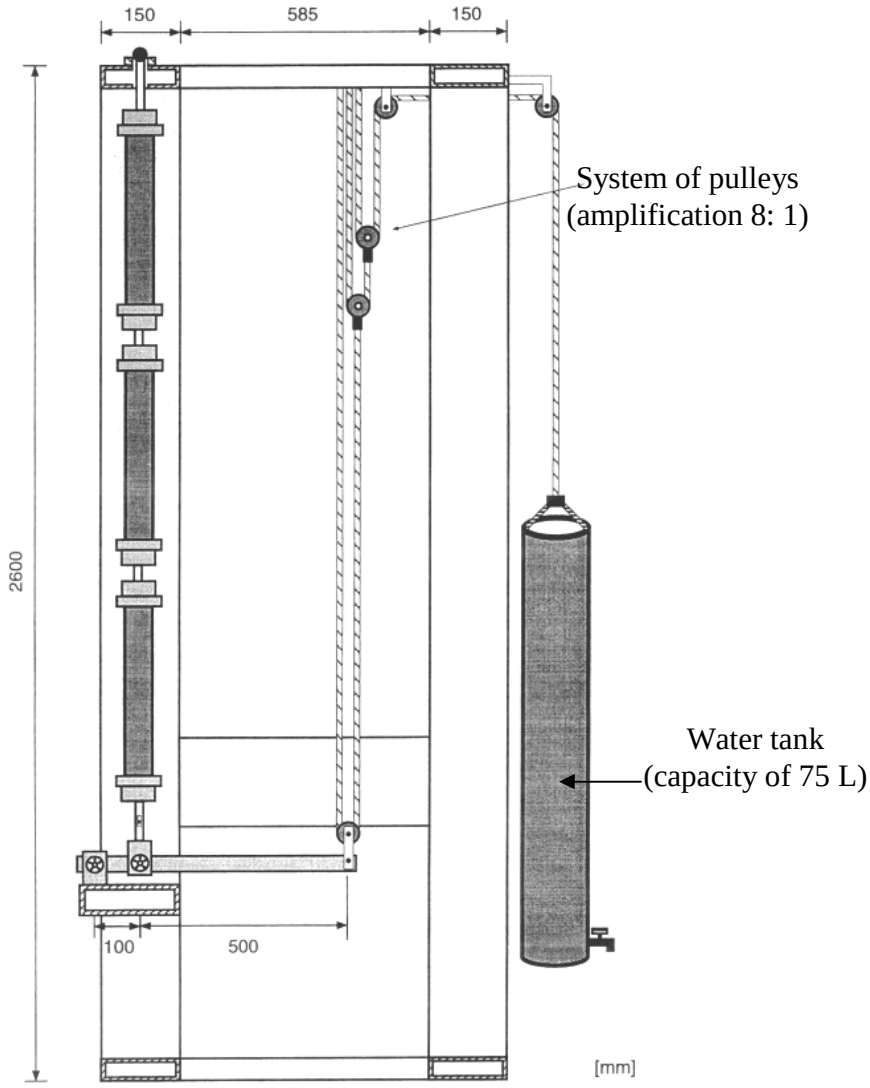

Figure 2.25: Initial modification setup where a water tank and a system of pulleys were used for loading, dimensions are in (mm)

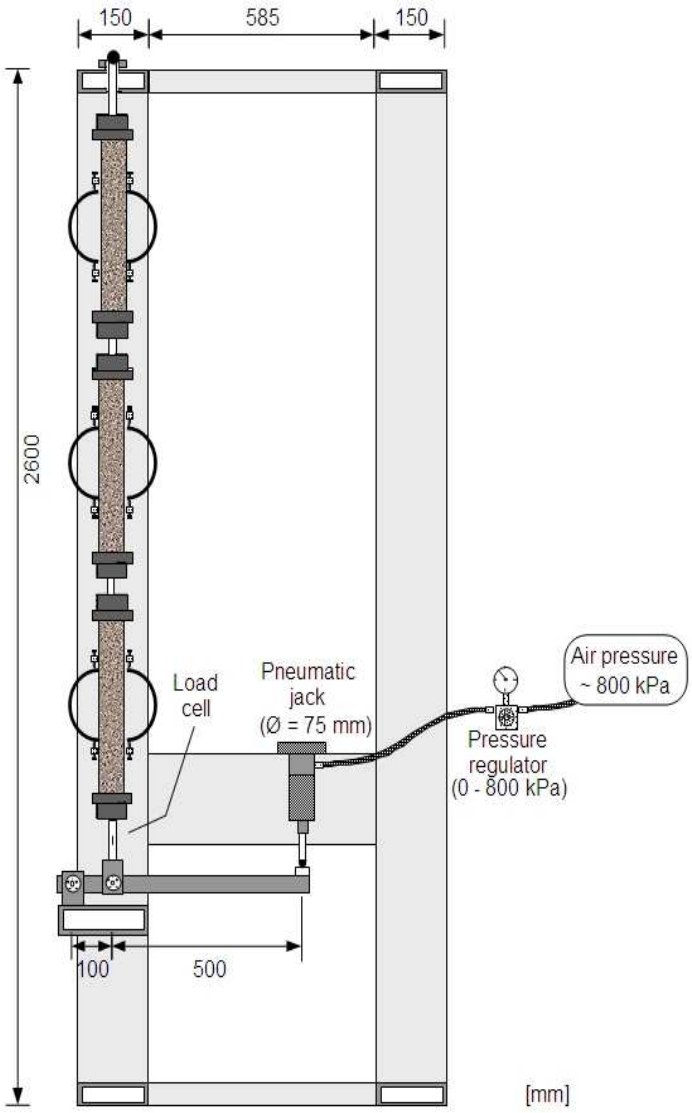

Figure 2.26: Tensile creep apparatus loading unit

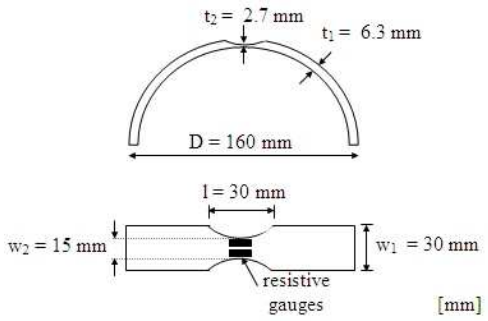

Figure 2.27: Tensile creep strain gage

2.3.3 Key Experimental Results

Bissonnette and Pigeon [1995] have emphasized the importance of studying tensile creep of concrete. They state that the only two strain components that can counteract any shrinkage-induced strains in a partially or fully restrained concrete member are the elastic tension strain and the tensile creep strain. The elastic tension strain capacity in the case of concrete is very small (i.e. 100 to 200 microstrain) and the tensile creep strain is not negligible, particularly when concrete is allowed to dry under load. In this study, six concrete mixes that varied in w/cm, silica fume content, curing period, and fiber content were investigated (Table 2.2). The applied stress was 0.77 MPa (112 psi), and 1MPa (145 psi) for specimens loaded after 1day and 7 days respectively. The results of the tensile creep tests showed that among the parameters tested (w/cm, cementitious materials characteristics, age of loading, and use of fibers), both w/cm and age of loading had the most significant effect of the tensile creep behavior (Table 2.3). However, the increase in tensile creep noticed upon incorporating silica fume and steel fibers in concrete mixes is of specific importance in the case of UHPC as it typically contains both. In this study, no explanation was provided in this study to the effect of incorporating silica fume, but it was later attributed to the smooth and spherical shape of silica fume particles that may facilitate deformation at early age before they react [Kovler et al., 1999]. On the other hand, the increase in creep measured for mixes incorporating steel fibers was attributed to the higher air content measured for these mixes (i.e. 8.8% and 3.0% for mixes with micro and macro fibers respectively). These results need to be further investigated especially in the case of UHPC used in prestressed structural members subjected to high loadings at early ages. While not examining UHPC, but rather a “microcrete”, a study by Kovler [1999] measured tensile creep over 5 days.

The material used in this study was ordinary portland cement concrete with crushed dolomite gravel with maximum particle size of 7mm (0.276 in)

Table 2.2: Testing program [Bissonnette and Pigeon, 1995]

Mix	Composition						Testing		
	w/cm		Cementitious Materials		Steel fibers		Age of loading		Sealed or unsealed
	0.55	0.35	Cement Type I	Silica fume (7% by weight)	Macro (0.63 in long)	Micro (0.12 in long)	1d	7d	
1	√		√				√	√	both
2		√	√				√	√	unsealed
3	√			√			√	√	unsealed
4		√		√			√	√	unsealed
5	√		√		√			√	unsealed
6	√		√			√		√	unsealed

Table 2.3: Tensile creep results [Bissonnette and Pigeon, 1995]

Mix	Sealed or unsealed	Age of loading	Specific total tensile creep μm/μm/MPa (μm/μm/ksi) @ age of 40 days	Summary of the Results
1	Unsealed RH= 50%	1 day	149 (1,030)	• The specific total creep increased upon increased upon increasing the w/cm (mixes 1 & 2; 3 &4) • The specific total creep decreased upon delaying loading from 1 day to 7 days (all mixes) • The specific total creep increased upon replacing 7% of the cement mass with silica fume (mixes 1 & 3; 2 & 4)
		7 days	100 (690)	
2		1 day	100 (690)	
		7 days	59 (410)	
3		1 day	165 (1,140)	
		7 days	131 (900)	
4		1 day	165 (1,140)	
		7 days	69 (480)	
1	unsealed RH= 50%	1 day	149 (1,030)	• The specific total creep decreased upon sealing specimens despite of the age of loading
	sealed	1 day	15 (100)	
	unsealed RH= 50%	7 days	100 (690)	
	sealed	7 days	41 (280)	
1	unsealed RH= 50%	7 days	100 (690)	• The specific total creep increased upon incorporating steel fibers in the mix, it also increased upon decreasing the size of fibers due to the increased void ratio that resulted from incorporating fibers.
5			150 (1,035)	
6			190 (1,311)	

used as coarse aggregate, quartz sand of fineness modulus of 1.76 used as fine aggregate, and a water-to-cement ratio of 0.7. The typical compressive strength was 30 MPa (4,350 psi). One day old concrete was exposed to drying in a hot climate simulator that had temperature of 29 to 31^{o}C (84.2 to 87.8 ^{o}F) and a relative humidity of 32 to 38% and RH. The tensile strength after one day was 1.20 MPa (174 psi). The applied tensile stress was between 0.45 MPa (65 psi) (0.375 stress/strength level) and 1.10 MPa (160 psi) (0.917 stress/strength level). Tensile strength test performed before and after the creep tests did not show any damage in the material, nor decrease but increase in the Young's tensile modulus of elasticity. It also showed an increase in the tensile strength with time despite the drying condition. These were all attributed to the continuous formation of hydration products while curing, especially with this high w/cm (i.e. w/cm = 0.7).

Altoubat and Lange [2001] studied tensile basic creep of concrete at early age (160 hours). In this study, mixes that varied mainly in their w/cm (0.4 and 0.5) and steel fiber content were investigated (Table 2.4). The constituent materials used were Type I cement, crushed lime stone with maximum size of 25.4 mm (1-in), and natural sand with fineness modulus of 2.2. Steel fibers with flared ends, 30.48 mm (1.2-in) long, and aspect ratio of 75 were used at 0.5% (volume fraction of the whole mixture). A moist curing technique was adopted where samples were covered with wet cloths throughout the test to suppress early-age autogenous shrinkage so that basic creep could be measured. This technique successfully suppressed the autogenous shrinkage as the measured relative humidity of the concrete under moist-cover condition was almost constant across the sample. This was also confirmed by zero shrinkage measured due to initial swelling [Kovler, 1996 and Altoubat and Lange, 2001]. The results summarized in Table 2.4 bring up two important problems that need further microstructural investigation. These are: (1) the effect of the w/cm on the tensile-creep behavior of concrete, as there is contradiction

between these results and the results reported previously in the literature [Bissonnette and Pigeon, 1995], (2) the effects of incorporating fibers in concrete on its tensile-creep behavior, and (3) whether drying is permitted or prevented. In addition, the same study showed that although the initial creep rate of plain concrete is higher than that of fiber-reinforced concrete, the creep function (solidification theory) of plain concrete stabilizes earlier than that of fiber-reinforced concrete, suggesting that steel fiber reinforcement provides stress relaxation for a longer period of time (Figure 2.28). However, this testing only lasted for a maximum of 160 hours, and thus there is a necessity for a more detailed and longer investigation to validate this concept over a longer period of time (i.e. more than 1 year).

Tao and Weizu [2006] studied the tensile basic creep of high strength concrete over a period of about 100 hours. In this study, concrete mixes with and without silica fume or fly ash were investigated. The water-to-cementitious ratio for all mixes was 0.35. The constituent materials used were Type I cement, crushed lime stone with maximum size of about 1 in, and natural river sand. For the silica fume binary blended mix, 6% of ordinary portland cement by weight in the control mix was replaced by silica fume, while for the fly ash binary blended mix, 30% of ordinary portland cement weight in the control mix was replaced by fly ash. Details about the specimens and the test setup were provided in Section 3.2.2.2. Results from this study again showed the silica fume concrete exhibited a greater tensile creep as compared to the control concrete, while the fly ash concrete showed the opposite (Figure 2.29). However, no explanation for these phenomena was provided.

Recently, Bissonnette et al. [2007] studied the effect of stress level, age of loading, fiber reinforcement, and the volume fraction of the cement paste on the tensile creep of concrete. In this study, tensile creep tests were carried out for a period up to 168 days. Tests were thus

performed at stress levels ranging from 0.20 to 0.50 of the short-term strength under drying conditions at 50% RH. Loading started at 7 or 28 days of age. Crimped or hooked steel fibers were used at 0.50 and 1.0% volume fraction. In addition, the cement paste of the matrix was 22%, 27%, and 32%. Results showed that fiber reinforcement did not have significant effect on drying shrinkage. On the other hand, as expected, tensile creep increased upon increasing the stress/strength ratio at loading and upon delaying the loading process (i.e. 7 vs. 28 days of age at loading). As for the effect of fiber reinforcement on tensile creep, using 0.50% volume fraction of hooked fibers resulted in an increase of about 30 to 35% in tensile creep when compared to the non-reinforced mixes, while the same dosage of crimped fibers lead to a reduction of 30 to 35%. However, doubling the dosage of crimped fibers resulted in increase in tensile creep. As a result, the authors suggested that an important part of the creep deformations could be taking place in the more porous paste-fiber interfacial areas. This means that the influence of fiber on tensile creep is a balance between their restraining effect and the viscoelastic properties of the surrounding cement paste. Results of the same study also showed a decrease in the tensile creep upon increasing the paste content, which is quite the opposite of what have been reported for years in the case of compressive creep. This result suggests that a significant part of tensile creep deformation could be taking place in the weak paste-aggregate interface.

However, according the author's knowledge, a microstructural study to confirm these recently proposed hypotheses has not been carried out yet and thus need further investigation.

2.3.4 Mechanisms

According to the author's knowledge, the study by Bissonnette et al. [2007] was the first comprehensive attempt to try explaining mechanisms of tensile creep of concrete.

Bissonnette et al. [2007] recognized three main mechanisms were by the authors; which are the water seepage, viscous shear, and microcracking. The assumptions of the seepage theory were consistent with the occurrence of basic creep in tension. Under tension, the gel porosity increases and tends to adsorb some of the free water from the larger capillary pores, which in turns result in expansion. However, the seepage theory was not able to explain the additional tensile creep that took place under drying conditions that was measured in the same study. However, the same study proposed that drying creep in tension can be explained by the viscous shear theory. That is, when concrete is loaded in

Table 2.4: Basic tensile creep results of moist-covered [Altoubat and Lange, 2001]

Mix	w/cm	Steel fibers (volume fraction)	Creep strain (μm/m) @ age of 100 hours	Summary of the Results
1	0.4	0	65	<u>Effect of fibers</u> • The incorporation of fibers in the wet condition decreased the initial basic creep as they controlled microcracking, and engaged more volume of the matrix in stress transfer. • Under drying conditions, these previously effects of using fibers are not evident likely because under these conditions, more surface microcracking occurs. This agrees with the results obtained by Bissonnette and Pigeon (1995). <u>Effect of w/cm</u> • The tensile basic creep increased upon decreasing the w/cm. This may suggest that the tensile creep behavior at early age is governed by different factors than in mature concrete. However, no mature concrete was investigated in this study. • Tensile creep in fiber-reinforced concrete seemed more sensitive to the w/cm
2	0.4	0.5	50	
3	0.5	0	36	
4	0.5	0.5	26	

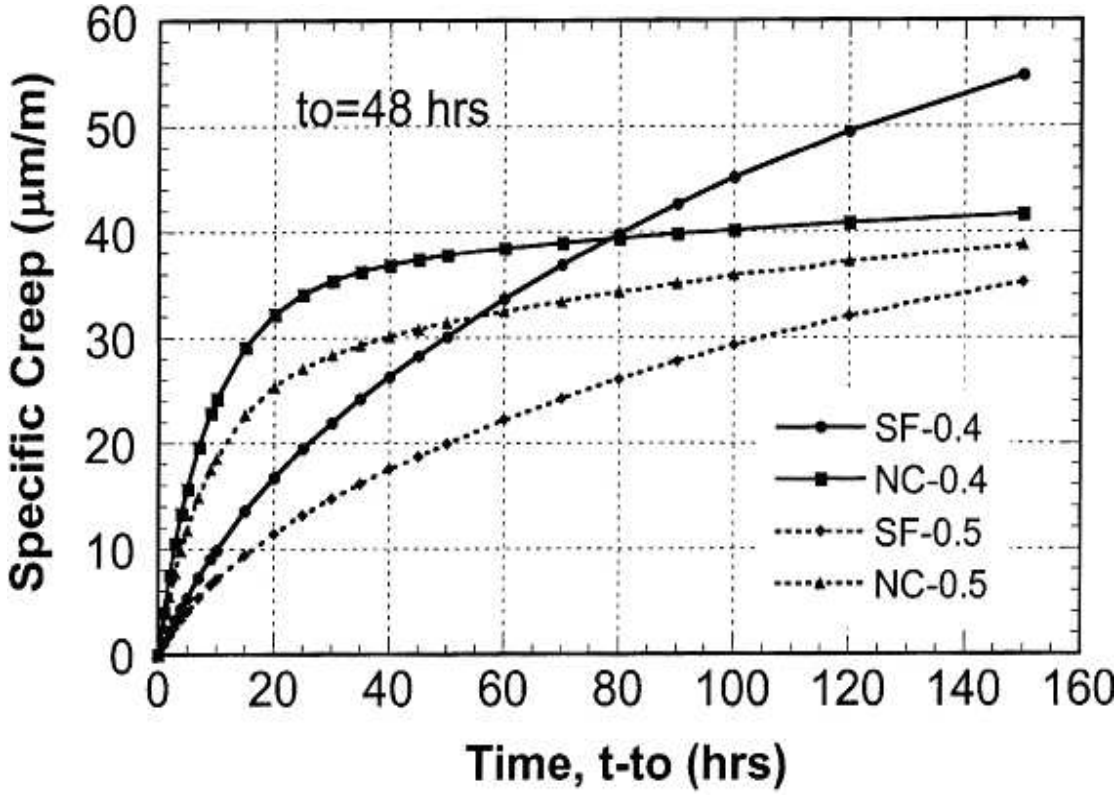

Figure 2.28: Effect of fiber reinforcement and w/cm on creep [Altoubat and Lange, 2001]

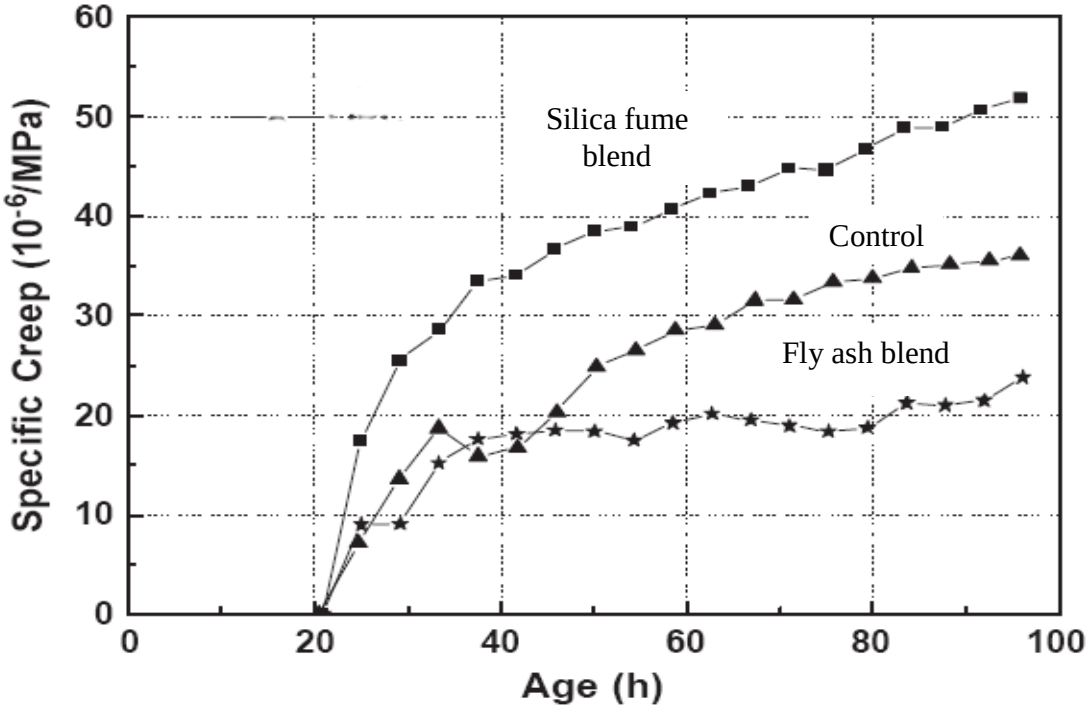

Figure 2.29: Specific total creep under isothermal conditions [Tao and Weizu, 2006]

tension and allowed to dry, the adsorbed water layers are disturbed by both the applied load (adsorption of water in the pores) and the water loss process. This simultaneous action increases shear between gel particles and thus facilitates the sliding or flow of gel particles one against the other and results in an overall increase in tensile creep. In addition, the effect of microcracking was investigated qualitatively by measuring the modulus of elasticity before and after creep. However, the results from this study did not show significant reduction in the modulus of elasticity after creep. This again emphasizes the need for a more detailed microstructural investigation in order to quantify the effect of microcracking on creep in tension.

2.4 References

ACI Committee 116, "Cement and Concrete Terminology", in ACI Manual of Concrete Practice. American Concrete Institute: Farmington Hills, MI. 2000, pp. 116R.1-116R.73.

ACI Committee 363, "State-of-the-Art Report on High-Strength Concrete: Chapter 1 - Introduction (Approved)". American Concrete Institute, 2005.

ACI Report 544.2R-78, ACI Journal and Proceedings, Vol. 75, No. 7, 1978, pp. 283-289.

Akita, H., Koide, H., Tomon, M., Sohn, D., “A practical method for uniaxial tension test of concrete”, Materials and Structures Vol. 36, No. 260, July 2003, pp. 365-371.

Altoubat, S. A., and Lange, D. A., “Tensile Basic Creep: Measurements and Behavior at Early Age”, ACI Materials Journal, Vol. 98, No. 5, September-October, 2001, pp. 386-393.

Anderson, B. G. “Rigid Frame Failures,” ACI Journal, Proceedings, Vol. 53, No. 7, January 1957, pp. 625-636.

ASTM C190, “Standard Test Method for Tensile Strength of Hydraulic Cement Mortars,” American Society for Testing and Materials Standard Practice C190, Philadelphia, Pennsylvania, 1990.

ASTM C293, “Standard Test Method for Flexural Strength of Concrete (Using Simple Beam With Center-Point Loading),” American Society for Testing and Materials Standard Practice C293, Philadelphia, Pennsylvania, 2008.

ASTM C496, “Standard Test Method for Splitting Tensile Strength of Cylindrical Concrete Specimens,” American Society for Testing and Materials Standard Practice C496, Philadelphia, Pennsylvania, 1990.

ASTM C512, “Standard Test Method for Creep of Concrete in Compression,” American Society for Testing and Materials Standard Practice C512, Philadelphia, Pennsylvania, 2002.

ASTM C78, “Standard Test Method for Flexural Strength of Concrete (Using Simple Beam with Third-Point Loading),” American Society for Testing and Materials Standard Practice C78, Philadelphia, Pennsylvania, 2008.

Banthia, N., MacDonald, C., and Tatnall, P., “Structural Applications of Fiber Reinforced Concrete”, ACI International SP 182, 1999.

Bažant, Z. P., and Xi, Y.,. “Drying Creep of Concrete: Constitutive Model and New Experiments Separating its Mechanisms.” Journal of Materials and Structures, Vol. 27, 1994, pp. 3–14.

Bissonnette, B., “Le Fluage en Traction: un Aspect Important de la Problematique des Reparations minces en Beton”, DSc Thesis in Civil Engineering, Université LAVAL, Québec, Canada, December 1996.

Bissonnette, B., and Pigeon, M., “Tensile Creep at Early Ages of Ordinary, Silica Fume and Fiber Reinforced Concretes”, Cement and Concrete Research, Vol. 25, N0. 5, 1995, pp. 1075-1085.

Bissonnette, B., Pigeon, M., and Vaysburd, A.M., “Tensile Creep of Concrete: Study of Its Sensitivity to Basic Parameters”, ACI Materials Journal, Vol. 104, N0. 4, 2007, pp. 360-368.

Cheyrezy, M., Maret, V., and Frouin, L., “Microstructural Analysis of RPC (Reactive Powder Concretes”, Cement and Concrete Research, Vol. 24, No. 7, October 1995, pp. 1491-1500.

Collepardi, S., Coppola, L., Troli, R., and Collepardi M., “Mechanical properties of modified Reactive powder Concrete”, ACI international Conference on “Superplasticizers and Other Chemical Admixtures in Concrete”, SP 173, October 1997.

Cucchiara, C., Mendola, L.L., and Papia, M., “Effectiveness of Stirrups and Steel Fibers as Shear Reinforcement”, Cement and Concrete Composites, Vol. 26, 2004, pp. 777-786.

Dodson, V. H., "Concrete Admixtures", Van Nostrand Reinhold, New York, 1990.

Ferron R.P., Gregori, A., Sun, Z., and Shah, S. P. “Rheological Method to Evaluate Structural Buildup in Self-Consolidating Concrete Cement Pastes”, ACI Materials Journal, Vol. 104, No. 3, May-June 2007, pp. 242-250.

Feylessoufi, A., Crepin, M., Dion, P., Bergaya, F., Van Damme, H., and Richard, P., “Controlled Rate Thermal Treatment of Reactive Powder Concretes”, Advanced Cement Based materials, Vol. 6, No. 1, 1997, pp. 21-27.

Findley, W.N., J.S. Lai, and K. Onaran, “Creep and Relaxation of Nonlinear Viscoelastic Materials : With an Introduction to Linear Viscoelastic”: Dover, 1989.

Furlan, Sydney Jr., and Hanai, J.B., “Prestressed Fiber Reinforced Concrete Beams with Reduced Ratios of Shear Reinforced”, Cement and Concrete Composites, Vol. 21, 1999, pp. 213-221.

Furlan, Sydney Jr., and Hanai, J.B., “Shear Behaviour of Fiber Reinforced Concrete”, Cement and Concrete Composites, Vol. 19, 1997, pp. 359-366.

Gere, J.M., ‘Mechanics of Materials’, 5th Edition, Brooks/Cole, 2001.

Gettu, R., and Barragan, B.E., “Direct tension test and interpretation”, Rilem Proceedings (Pro 31) Test and Design Methods for Steel Fibre Reinforced Concrete – Background and Experiences -, 2003, pp. 15-30.

Goodspeed, C.H., S. Vanikar, and R.A. Cook, "High-performance concrete defined for highway structures". Concrete International, 18(2): 1996, pp. 62-67.

Graybeal, B. A., "Characterization of the Behavior of Ultra-High Performance Concrete", Ph.D. Thesis, University of Maryland, 2005.

Gutsch, A., Rostasy, F.S., "Young concrete under High Tensile Stresses, Creep, Relaxation and Cracking", in: R. Springenschmid (Ed.), Thermal Cracking in Concrete at Early Age, E & FN Spon, London, RILEM, 1994, pp.111 –118.

Habel, K., Denarié, E., and Brühwiler, E., "Experimental Investigation of Composite Ultra-High-Performance Fiber-Reinforced Concrete and Conventional Concrete Members", ACI Structures Journal, Vol. 104, No. 1, January-February 2007, pp. 93-101.

Hanna, N., Steel Fiber Reinforced Concrete Properties and Resurfacing Applications, Portland Cement Association, Skokie, Ill., Report RD049.01P, 1997.

Hannant, D. J., "Fibre Cements and Fibre Concretes", John Wiley & Sons, 1978.

Imam, M., Vandewalle, L., Mortelmans, F., and Van Gemert, D., "Shear Domain of Fibre-Reinforced High-Strength Concrete Beams", Engineering Structures, Vol. 19, No. 9, 1997, pp. 738-747.

Karihaloo, B.L., and De Vriese, K.M.B., " Short-Fibre Reinforced Reactive Powder Concrete", Proceedings of the Third International RILEM Workshop on "High Performance Fiber Reinforced Cement Composites (HPFRCC3)", Edited by H.W. Reinhardt and A.E. Naaman, Mainz, Germany, 1999, p.53.

Kormeling, H.A., and Reinhardt, H.W., "Strain rate Effects on Steel Fibre Concrete in Uniaxial Tension", The International Journal of Cement Composites and Lightweight Concrete, Vol. 9, No. 4, February 1987, pp. 197-204.

Kovler, K., "A New Look at the Problem of Drying Creep of Concrete under Tension", ASCE Journal of Materials in Civil Engineering, Vol. 11, No. 1, February, 1999, pp. 84-87.

Kovler, K., "Interdependence of Creep and Shrinkage for Concrete under Tension", ASCE Journal of Materials in Civil Engineering, Vol. 7, No. 2, May, 1995, pp. 96-101.

Kovler, K., "Testing System for Determining the Mechanical Behavior of Early Age Concrete under Restrained and Free Uniaxial Shrinkage", Journal of Materials and Structures, Vol. 27, 1994, pp. 324-330.

Kovler, K., "Why sealed Concrete Swells?", ACI Materials Journal, Vol. 93, No. 4, 1996, pp. 334-340.

Kovler, K., Igarashi, S., and Bentur, A., "Tensile Creep Behavior of High Strength Concretes at Early Age", Journal of Materials and Structures, Vol. 32, 1999, pp. 383-387.

Krenchel, H., Fiber Reinforced Concrete, ACI SP-44, 1974, pp. 45-77.

Krstulovic-Opara, N., and Malak, S. "Tensile Behavior of slurry Infiltrated Mat Concrete (SIMCON)", ACI Materials Journal, Vol. 94, No. 1, January-February 1997, pp. 39-46.

Lankard, D. R., "Fiber Concrete Applications", (Fibre Reinforced Cement and Concrete), The Construction Press LTD, England, 1975.

Lim, D.H., and Oh, B.H., " Experimental and Theoretical Investigation on the Shear of Steel Fibre Reinforced Beams", Engineering Structures, Vol. 21. 1999, pp. 937-944.

MacGregor, J.G., and Wight, J.K., "Reinforced Concrete, Mechanics and Design", 4th Edition, Prentice Hall, 2005.

McHugh, A.J., and Tan, S.R., " Mechano-Chemical Aspects of the Processing/property/Structure Interactions in Macro-Defect Free Cement", ACBM Journal, Vol. 1, October 1993, pp. 2-11.

Mehta, P.K. and Monteiro, P. J. M., "Concrete Microstructure, Properties, and Materials" 3rd ed: McGraw-Hill, 2005.

Mehta, P.K., "Advancements in Concrete Technology", Concrete International, Vol. 21, No. 6, June 1999, pp. 69-76.

Mehta, P.K., and Aïtcin, P.C., "Principles Underlying the Production of High-Performance Concrete," Cement, Concrete, and Aggregates, ASTM, Vol. 12, No. 2, 1990, pp. 70-78.

Mindess, S., and Young, J.F., "Concrete", Prentice-Hall Inc., Englewood Cliffs, New Jersey, 1981.

Monosi, S., Pignoloni, G., Collepardi, S., Troli, R., and Collepardi M., "Modified Reactive Powder Concrete with Artificial Aggregate", ACI International Conference on "Superplasticizers and Other Chemical Admixtures in Concrete", SP 175, October 2000.

Naaman, A.E., and Homrich, J.R. "Tensile Stress-Strain Properties of SIFCON", ACI Materials Journal, Vol. 86, No. 3, May-June 1989, pp. 244-251.

Naaman, A.E., and Otter, D., and Najm, H., "Elastic Modulus of SIFCON in Tension and Compression", ACI Materials Journal, Vol. 88, No. 6, November-December 1991, pp. 603-611.

Narayanan, R., and Darwish, I.Y.S., "Shear in Prestressed Concrete Beams Containing Steel Fibres", The International Journal of Cement Composites and Lightweight Concrete, Vol. 9, No. 2, May 1987, pp. 81-90.

Nawy, E.G., "Prestressed Concrete, A Fundamental Approach", 5th Edition, Prentice Hall, 2006.

Pickett, C., "The Effect of Change in Moisture-Content on the Creep of Concrete under a Sustained Load", ACI Journal, Vol. 38, 1942, pp. 333-356.

Potrzebowski, J., "The Splitting Test Applied to Steel Fibre Reinforced Concrete", The International Journal of Cement Composites and Lightweight Concrete, Vol. 5, No. 1, February 1983, pp. 49-53.

Powers, T. C., and Brownyard, T. L., "Studies on the Physical Properties of Hardened Portland Cement Paste", Bulletin 22 of the Portland Cement Association, Chicago, IL, March 1948.

Poyola, G., Kriven, W. M., and Young, J. F., " Providing Interfaces in Macro-Defect Free Cement", Cementing the Future, Vol. 12, No. 2, Summer 1990.

Richard, P., and Cheyrezy, M., "Reactive Powder Concretes with High Ductility and 200-800 MPa Compressive Strength", ACI International Conference on "Concrete Technology Past, Present and Future", SP 144, 1995.

Rilem TC 162-TDF: “Test and Design Methods fir Steel Fibre Reinforced Concrete, Uniaxial Tension Test for Fibre Reinforced Concrete”, Materials and Structures, Vol.34, 2001, pp. 3-6.

Rossi, P., “Ultra-High-Performance Fiber-Reinforced Concretes”, Concrete International, Vol. 23, 2001, pp. 46-52.

Rossi, P., Coussy, O., Boulay, C., Acker, P., and Malier, Y., “Comparison between Plain Concrete Toughness and Steel Fibre Reinforced Concrete Toughness”, Cement and Concrete Research, Vol. 16, 1986, pp. 303-313.

Shah, S. P. "Fiber Reinforced Concrete," Handbook of Structural Concrete, Editors F. K. Kong, R. H. Evans, E. Cohen, and F. Roll, McGraw-Hill Book Company, New York, 1984.

Shah, S. P., and Weiss, W. J., "Ultra High Strength Concrete; A Look to the Future" ACI Special Proceedings from the Paul Zia Symposium Atlanta, GA, Fall 1998.

Swamy. R. N., and Barr, B., “Fibre Reinforced Cements and Concretes: Recent Developments”, Elsevier Science Publishing Co., Inc, 1989.

Tao, Z., and Weizu, Q., “Tensile Creep due to Restraining Stresses in High-Strength Concrete at Early Ages”, Cement and Concrete Research, Vol. 36, 2006, pp. 584-591.

Thelandersson, S., Martensson, A., and Dahlblom, O., “Tension softening and cracking in drying concrete.” Journal of Materials and Structures, Vol. 21, No. 6, 1988, pp. 416–424.

Todd J.D. “The Determination of Tensile Stress-Strain Curves for Concrete”, Proceedings, Institution of civil Engineers, Vol.4, No.2, Part 1, London, March 1955, pp. 210-211.

Umehara, H., Uehara, T., Iisaka, T., and Sugiyama, A., “Effect of Creep in Concrete at Early Ages on Thermal Stress”, in: R. Springenschmid (Ed.), Thermal Cracking in Concrete at Early Age, E & FN Spon, London, RILEM, 1994, pp.79– 86.

Vakili, J., “An Experimental-Study of Asphalt Concrete Based on a Multiple-Integral Representation of Constitutive Equation of a Non-Linear Viscoelastic Solid”, Journal of Rheology, Vol. 27, 1983, pp. 211-222.

Vakili, J., “Creep Behavior of Asphalt–Concrete under Tension”, Journal of Rheology, Vol. 28, N0. 5, 1984, pp. 573-580.

CHAPTER 3
SHORT-TERM TENSILE CREEP AND SHRINKAGE OF UHPC

3.1 Introduction

The tensile creep, free shrinkage, and autogenous shrinkage deformations of ultra-high performance concrete (UHPC) were examined through short-term testing to assess the sensitivity of the material to stress level (stress-to-strength ratio), steel fiber reinforcement, and thermal treatment. In this preliminary study, the stress levels were 40% and 60%, fiber volume fractions were 0% and 2%. Curing conditions considered were ambient curing and thermal treatment at 90^{o}C (194^{o}F) prior to loading. The tensile creep behavior of UHPC was compared to the published reports on compressive creep of the same material in order to understand the underlying mechanisms of tensile creep in UHPC.

3.2 Research Significance

While some studies have examined tensile creep behavior in ordinary and high performance concrete [Umehara et al., 1994, Gutsch and Rostasy, 1994, Kovler, 1994, Bissonnette and Pigeon, 1995, Kovler, 1995, Kovler, 1999, Kovler, 1999, Altoubat, 2001, Tao and Weizu 2006, and Bissonnette et al., 2007], tensile creep in UHPC has not been characterized in the published literature. Therefore, the main objective of this research was to provide some preliminary data characterizing the tensile creep performance of UHPC and to define parameters to be investigated in a detailed, long-term investigation. This overall program is necessary to develop a fundamental understanding of the tensile creep phenomena in UHPC so that design criteria can be developed for specifying UHPC for highway bridge girders.

3.3 Experiment Methodology

3.3.1 Materials

The UHPC mixes investigated were prepared from the ultra-high performance premix, Ductal®, provided by Lafarge North America and ultra-high strength steel fibers, Dramix 13/0.20, provided by Bekaert. The UHPC premix consisted mainly of Portland cement, silica fume, crushed quartz, and sand. The high strength steel fibers were 0.20 mm (0.008-in) in diameter and 13.0 mm (0.51-in) in length (aspect ratio = 65), and had a tensile strength of between 690 and 1000 MPa (100,076 and 145,038 psi), according to the manufacturer. Commercially available high range water reducer (HRWR), Glenium 3030 NS, and accelerator, Rheocrete CNI, provided by BASF were also used. A typical UHPC mixture design is shown in Table 3.1.

Table 3.1: UHPC composition

Constituent	kg/m^3 (lb/ft^3)
UPHC Premix	2194 (137)
Water	109 (6.80)
HRWRA	31 (1.94)
Accelerator	30 (1.87)
Steel fibers[1]	156[1] (9.74)

[1] Dose recommended by the UHPC manufacturer (2% volume fraction)

3.3.2 Sample Matrix

Four different conditions, designed to examine the influence of varying the stress level at the time of loading, fiber content, and thermal treatment were considered (Table 3.2). The nomenclature used in this study was based on the type of UHPC used (i.e., Ductal® = D), fiber

volume fraction (i.e., 2% volume fraction = 2f), maximum treatment temperature reached while curing (i.e. 23°C or 90°C (73 °F or 194°F)), and the stress level maintained during the creep test (i.e. 40% means that the tensile stress level at the time of loading was 40%). For example, Mix "D-2f-90C-40" indicates that the premix was used with 2% steel fiber content, thermally treated at 90°C (194°F), and loaded at 40% of its tensile strength at the time of loading.

Table 3.2: Different UHPC mixes, curing and loading conditions

Mixture ID	Stress/strength at loading (%)	Curing temperature[1]	Fiber content
D-2f-90C-40	40	90°C (194°F)	2% by vol.
D-2f-23C-40	40	23°C (73°F)	2% by vol.
D-0f-90C-40	40	90°C (194°F)	No fibers
D-2f-90C-60	60	90°C (194°F)	2% by vol.

[1] All samples were cured at 100% RH

3.3.3 Mixing and Curing Methodology

All tensile creep and free shrinkage specimens were cast according to procedures recommended by the UHPC manufacturer. First, the dry premix was mixed in an 85-liter (3 ft^3) capacity high shear mixer (Erich Model R 08 W) at 30-35 rpm for two minutes to break apart any clumps that might exist in the dry mix. This mixing speed was maintained over the entire mixing process. Water and half of the HRWR mixed were then added slowly to the dry premix over a period of two minutes and allowed to mix with the dry premix for one minute. The other half of the HRWR was then added over a period of 30 seconds, and mixing continued for another minute. The accelerator was then added over one minute and mixing continued until the "turning point" was reached. The turning point is defined as the point at which the UHPC mix turns from clumps into a flowable, uniform paste. Finally, and once the turning point was reached, fibers were added over a two minutes period, and mixing continued for another one to two minutes

until good fiber dispersion was visually evident. Once mixing was finished, flow table tests similar to ASTM C230 [1998] were performed to assess the flowability of each mix and to decide whether vibration should be used while casting or not. Based on the flow table results and according to the mixing procedures recommended by the UHPC manufacturer, vibration was used to cast all specimens from all mixes.

After casting, all specimens were stored in a fog room at 23^{o}C (73^{o}F) and 100% RH for 48 hours prior to demolding. Upon demolding, specimens were either stored in a fog room at 23^{o}C (73^{o}F) and 100% RH (D-2f-23C-40) or placed in an environmental chamber for thermal treatment (mixes D-2f-90C-40, D-0f-90C-40, and D-0f-90C-60) at temperature of 90^{o}C (194^{o}F) and 100% RH for the next 48 hours. After initial curing or initial curing and thermal treatment, creep samples were wrapped in aluminum tape to minimize moisture loss during the following sample preparation period while shrinkage specimens were kept in the fog room for the same period before tests started at 7 days of age.

3.3.4 Test Methodology

3.3.4.1 Autogenous shrinkage test

Autogenous shrinkage was measured on three replicate samples according to the method described by Jensen (1995) using rigid corrugated polyethylene tubes capped on both ends to prevent any moisture loss to the environment. Linear deformation of these tubes was first measured at final setting using a digital comparator (Figure. 3.1). Autogenous shrinkage samples were kept in an environmental chamber at 20 °C and 50% relative humidity over the test period.

Figure 3.1: Autogenous shrinkage test setup

3.3.4.2 Tensile creep and free shrinkage

Tensile creep and free shrinkage deformations were measured on 100 x 380 mm (4 x 15-in) cylinders, two loaded cylinders for tensile creep and two un-loaded companion specimens for free shrinkage (Figure 3.2). Each cylinder was fitted with four sets of steel inserts located diametrically opposite on the surface of the specimen. Each set had a gauge length of 250 mm (10-in). For each creep specimen, two 38 mm (1.50 in) thick steel plates were affixed, one on the top and one on the bottom using high modulus, high strength epoxy and left to cure for ~36 hours under a pressure of 2.75 MPa (400 psi) (no rods were embedded in the concrete for affixing the plates to the specimens in this study). At an age of 7 days, creep samples were loaded at a constant rate of 0.0046 MPa/second (0.76 psi/second) until the desired load was reached. For each specimen, deformations were measured on each set of inserts using mechanical DEMEC gage with an accuracy of 0.00254 mm (0.0001-in). The tensile creep test setup is shown in Figure 3.2. Test conditions were kept at 23 ± 2 ^{o}C (73^{o}C) and 50 ± 3% RH for the whole testing period. Tensile creep and shrinkage deformations were measured initially at 1, 2, 4, 6, 12, 24 hours after loading. Subsequently, measurements were made daily for the rest of the 14-day testing period.

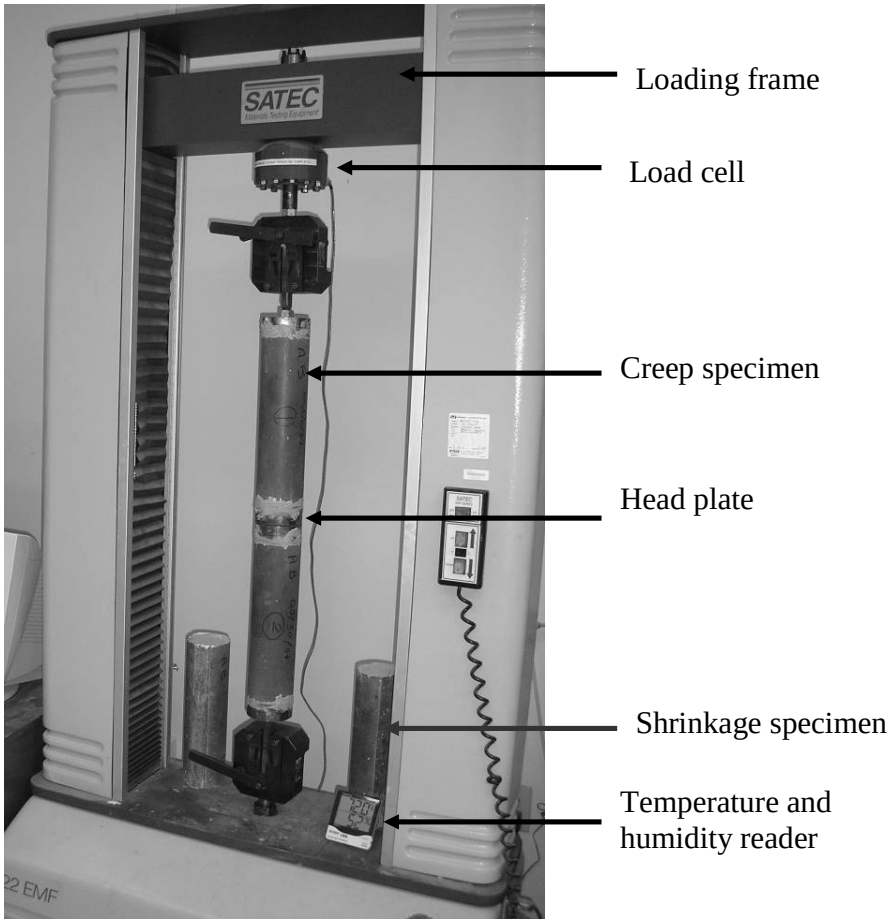

Figure 3.2: Short-term tensile creep test setup

3.4 Results and Discussion

Figures 3.3-3.5 show the measured autogenous shrinkage, free shrinkage and tensile creep for over 14 days where the influence of stress/strength, fiber reinforcement, and thermal treatment are examined. Only one of the mixes – the non-thermally treated mix (D-2f-23C-40), failed during this short-term tensile creep test; as a result, tensile creep data for this mix are only available up to 7 days.

Table 3.3 summarizes the average tensile strength at the time of loading, tensile creep coefficient and specific tensile creep at 7 and 14 days of loading, and the 7 and 14-day free

shrinkage strains for each sample type. It is worth noting that the 7-day tensile strength among the mixes did not vary considerably. The maximum difference in strength was about 8%, when comparing mixes D-2f-90C-40 and D-0f-90C-40 (Table 3.3). These results also show that eliminating fiber reinforcement has a slightly more pronounced effect on the reduction of 7-day tensile strength than eliminating thermal treatment.

3.4.1 Autogenous Shrinkage

First, results in Figure 3.3 show that 87% of the total autogenous shrinkage occurred during the thermal treatment. This is expected due to the accelerated rate of early hydration at higher temperature.

As for the effect of fibers, results in Figure 3.3 show that the use of 2% steel fibers by volume resulted in a 42% reduction in autogenous shrinkage at 14 days of age after batching. In addition, and by taking a closer look at Figure 3.3, it can be clearly seen that the effect of fibers in reducing autogenous shrinkage increased as the hydration of the cementitious paste progressed during the thermal treatment period. This result emphasizes that the properties of the fiber-matrix interface, which enhances, as hydration progresses, has a major influence on how efficiently the fibers can restrain deformations.

By comparing the drying shrinkage results shown in Figure 3.4 to the autogenous shrinkage shown in Figure 3.3, it can be seen that due to the low water-to-cementitious materials ratio used in the UHPC mixes (Table 3.1), autogenous shrinkage represented about 93% of the total shrinkage deformations for both mixes at age of 14 days after batching; autogenous shrinkage, then, must be considered when assessing performance of ultra-high performance concretes.

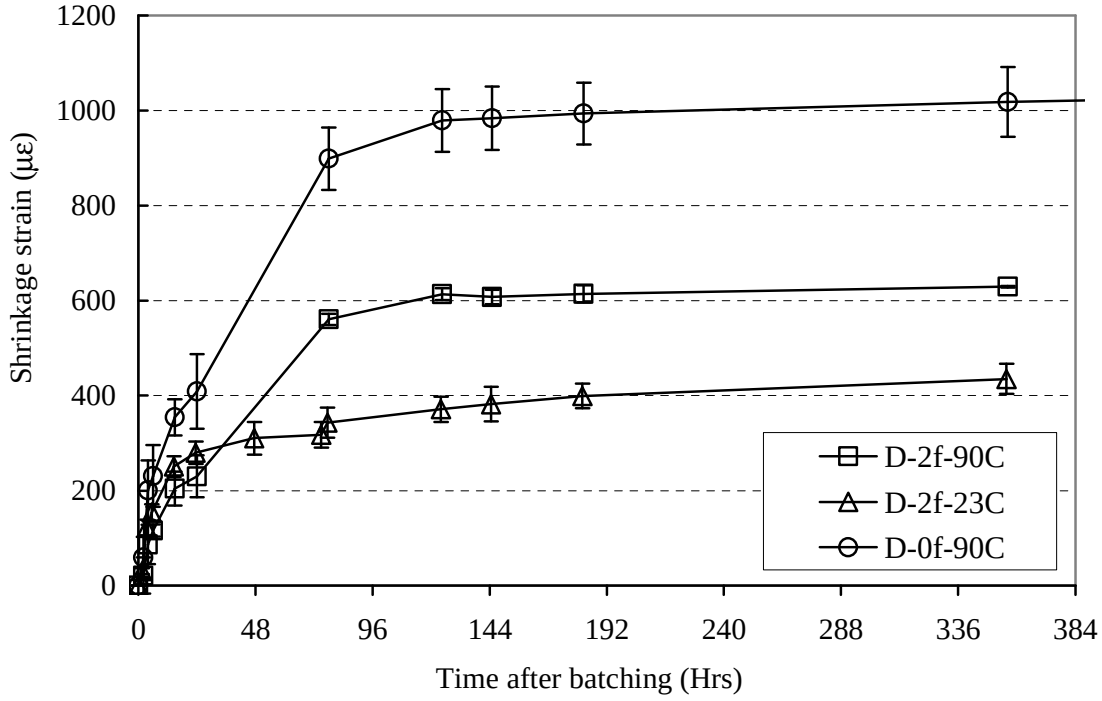

Figure 3.3: Autogenous shrinkage of different UHPC mixes

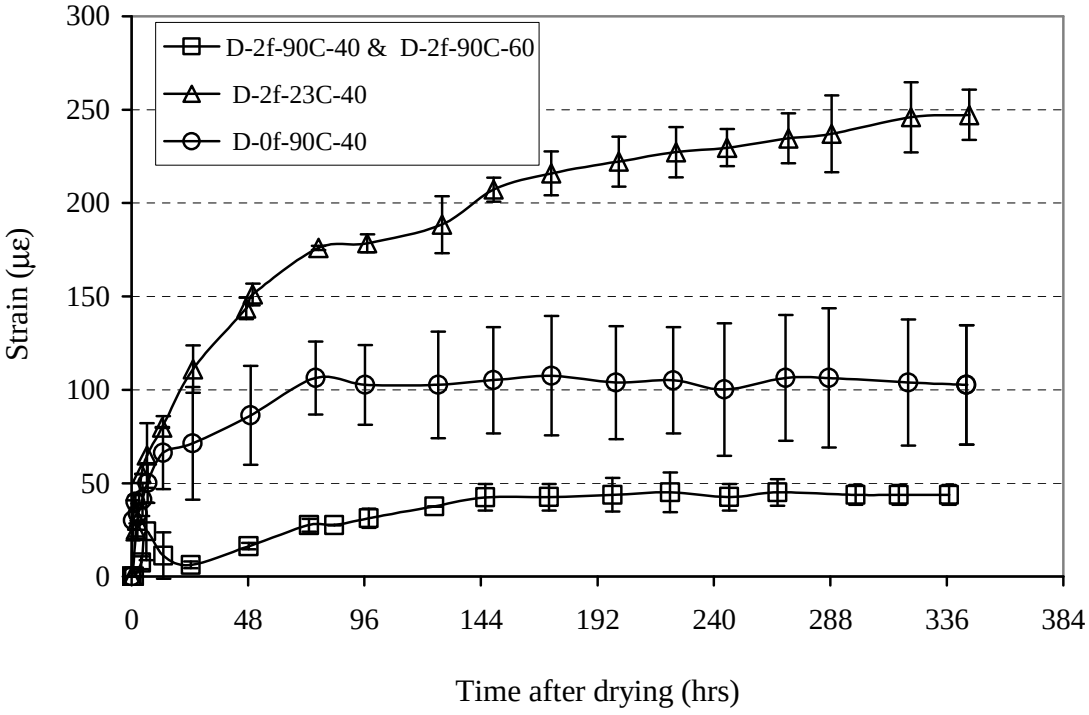

Figure 3.4: Free shrinkage of different UHPC mixes [drying started at 7 days of age]

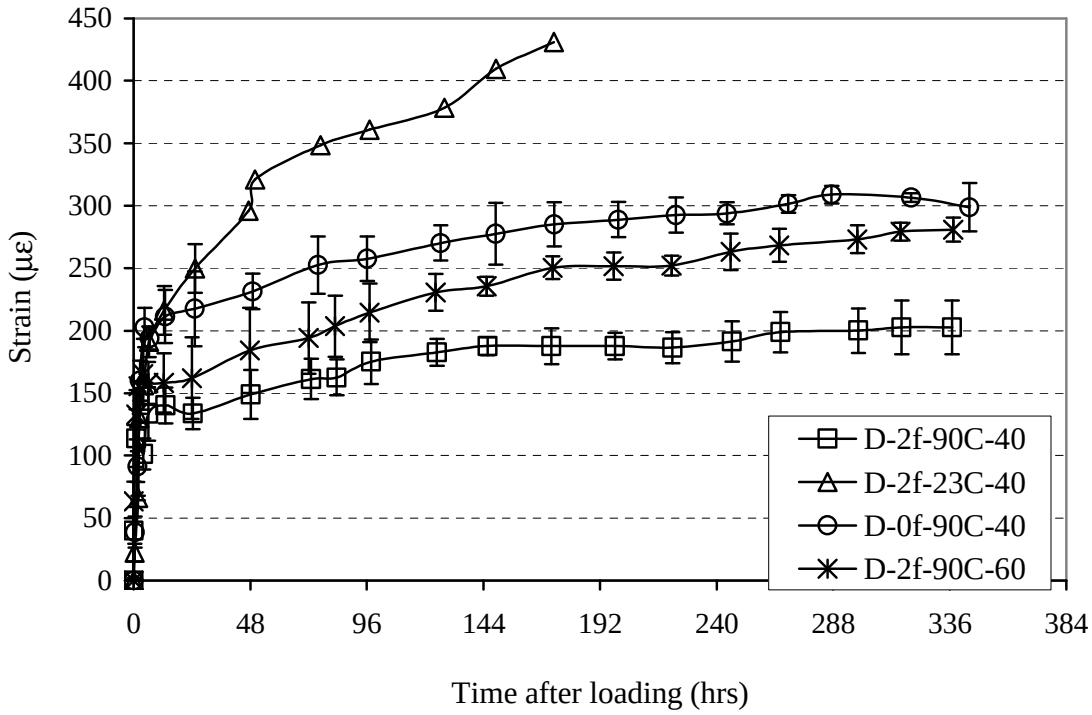

Figure 3.5: Tensile total creep of different UHPC mixes loaded at 7 days of age

Table 3.3: Summary of the results of the short-term study

Mixture	Tensile strength		Tensile creep coefficient		Specific tensile Creep in με/MPa (με/psi)		Free shrinkage strain (με)	
	Value MPa (psi)	SD MPa (psi)	7-day	14-day	7-day	14-day	7-day	14-day
D-2f-90C-40	6.50 (943)	0.29 (42)	0.65	0.78	28.44 (0.20)	34.22 (0.24)	43	44
D-2f-23C-40	6.09 (883)	0.40 (58)	2.38	N/A	124.66 (0.86)	N/A	216	247
D-0f-90C-40	6.04 (876)	0.30 (44)	0.78	0.87	51.78 (0.34)	57.44 (0.40)	108	103
D-2f-90C-60	6.50 (943)	0.29 (42)	0.89	1.12	30.2 (0.21)	38.00 (0.26)	43	44

3.4.2 Free Shrinkage

As shown in Figure 3.4 and Table 3.3, the incorporation of short steel fibers limited free shrinkage. Results at 14 days of drying show that the free shrinkage of mix D-0f-90C-40, with no

steel fibers, was about 135% more than that of mix D-2f-90C-40 in which 2% fibers by volume was incorporated. This suggests that the fibers offer some restraint to deformation, as would be expected when the fibers are well-dispersed in the matrix.

Figure 3.4 and Table 3.3 also show that after 14 days of drying, the free shrinkage of mix D-2f-23C-40 (i.e. where no thermal treatment was applied) was about six times that of the mix D-2f-90C-40 which was thermally treated at 90^{o}C (194^{o}F) for 48 hours. In addition, results in Figure 3.4 also show that mix D-2f-23C-40 continued to shrink for the whole testing period, while mix D-2f-90C-40 reached an asymptotic shrinkage strain value of about 45 με after about 6 days of drying. Similar results for UHPC were reported by Graybeal [2005], where specimens thermally treated at 90^{o}C (194^{o}F) for 48 hours did not show any measurable free shrinkage after thermal treatment, while air-cured specimens continued to shrink with time. Both microstructural refinement and consumption of most of the mix water due to the accelerated hydration associated with thermal treatment likely contribute to the reduced shrinkage in the thermally treated samples.

3.4.3 Tensile Creep

This section presents the effects of varying the stress level, incorporating short and randomly-dispersed high strength steel fibers in mix, and thermal treatment prior to loading on the tensile creep of UHPC. Results in Figure 3.5 show tensile creep increasing steadily with time for each of the four mix types examined. First, both the tensile creep coefficient and the specific tensile creep increased upon increasing the stress-strength ratios. However, both parameters decreased in the presence of steel fibers and with the application of thermal treatment prior to loading. The effect of steel fibers in this study is of particular importance since the creep behavior is contrary to published reports [Bissonnette and Pigeon, 1995, and Bissonnette et al.,

2007], which indicate an increase in tensile creep with fiber reinforcement in NSC and HPC. (This difference is discussed in further detail below.) Generally, these results show the tensile creep of UHPC to be lower than tensile creep results reported in the literature for normal strength and high performance concretes [Bissonnette and Pigeon, 1995, and Bissonnette et al., 2007]. However, the tensile creep measured here in UHPC is also significantly higher than the compressive creep previously reported by Graybeal [2005] for UHPC.

First, increasing the stress level from 40% (D-2f-90C-40) to 60% (D-2f-90C-60) increased the creep coefficient by 44% and increased the specific creep by 11% at 14 days of loading (Figure 3.5 and Table 3.3). These results in tension agree with the compression results of Graybeal [2005] who reported increasing compressive creep with increasing stress level for the same steel fiber reinforced UHPC material. Similar results have been also reported by Bissonnette et al. [2007] where the tensile creep of normal and high strength concretes have shown a dependence on the stress level.

As for the effect of steel fiber reinforcement, comparing the tensile creep results for mixes with (D-2f-90C-40) and without steel fibers (D-0f-90C-40) in Figure 3.5 and in Table 3.3 shows that the tensile creep coefficient decreased by 10% and the specific creep decreased by 40% with the addition of 2% fibers at 14 days. It is noted that the UHPC examined here was optimized based upon the use of 2% steel fibers by volume; hence, structure and performance were designed to be enhanced by the presence of fibers. These results, however, are opposite to those reported by Bissonnette and Pigeon [1995] and by Bissonnette et al. [2007] which investigated the influence of steel fiber reinforcement in normal and high strength concretes undergoing tensile creep. In both of these previous studies, an increase in tensile creep was typically associated with the use of steel fibers. The variation between the prior and current

results could be related to the differences in the material composition (e.g., particle packing, heterogeneity), material structure (e.g., lower strength, less microstructurally dense NSC vs. higher strength, lower micro/nano porosity UHPC), and processing (e.g., ordinary moist curing vs. thermal treatment). In particular, the application of thermal treatment to the fiber reinforced samples warrants further examination.

As previously noted, the application of thermal treatment was found to significantly affect tensile creep of UHPC. Thermally treating fiber reinforced UHPC at 90^{o}C (194^{o}F) for 48 hours prior to loading resulted in a 73% decrease in the creep coefficient and 77% decrease in specific creep when comparing the behavior of D-2f-23C-40 and D-2f-90C-40 at 7 days of loading (due to the premature failure of the D-2f-23C-40 mixture). It is proposed that this thermal treatment may result in refinement in the cementitious matrix nano- and microstructure, especially around the fibers. This proposed improvement in the structure and properties at the fiber/matrix interface may be viewed similarly – although occurring likely at the nanoscale in UHPC – to refinements by thermal curing at the microscale, interfacial transition zone (ITZ) around coarse aggregate [Mehta and Monteiro, 2005, and Bissonnette et al., 2007]. For non-thermal treated UHPC, the possibility of formation of water films around fibers during casting might have resulted in a higher local water-to-cementitious materials ratio. Mondal et al. [2008] monitored similar phenomenon around fine aggregates (1.18-2.36 mm (0.046-0.093-in) in size). The proposed porous interfacial zone around fibers might have been improved due to thermal treatment. Thermal treatment could have promoted further reaction of the cementitious paste, leading to a reduction in the porosity around fibers and minimization of the weakness in the fiber-matrix interfacial zone.

In addition, the D-2f-23C-40 specimens, which were not thermally treated, failed at the epoxy interface after one week of loading with the fracture occurring in the concrete. Substitute specimens were cast later but failed at the same location while loading. This failure may be related to the inadvertent introduction of defects into all the creep samples during the grinding of the specimen ends before applying the epoxy adhesive to attach the steel loading plates. Premature failure occurred only in the non-thermally treated samples and never in the various thermally treated samples. This behavior suggests that some self-healing of any defects induced during grinding may have occurred during thermal treatment where water was available at the surface to aid the self-healing process.

Tensile creep results for mix D-2f-90C-40 in the current study were compared to compressive creep results for steel fiber reinforced (2% by vol.) UHPC specimens thermally-treated at 90^{o}C (194^{o}F) and loaded at 40% of the compressive strength by the time of loading reported by Graybeal [2005]. At the age of 14 days of loading, this comparison shows that both the tensile creep coefficient and specific creep are about 12 times higher than the corresponding values during compressive creep. While the mechanisms of tensile creep behavior in UHPC have not been thoroughly examined, this significant difference in the magnitude and rate of development between compressive and tensile creep of UHPC, with the later being about an order of magnitude higher and faster at early age, suggests that tensile creep occurs phenomenologically quite differently than compressive creep in thermally treated, fiber reinforced UHPC. This may be, in part, due to the magnified effect of microcracking during tensile creep as compared to compressive creep, as well as the potential contributions of several other factors that are still to be investigated, including fiber restraint of compression creep, fiber/matrix debonding particularly during tensile creep, and deformation of the fiber

reinforcement. This observation is of significant importance as it emphasizes that tensile creep should be fundamentally and fully investigated prior to specifying this material for use where tensile capacity is of primary importance.

Finally, another important result of this study is that both thermal treatment and fiber reinforcement affected tensile creep more significantly than these factors affect early (7-day) tensile strength. That is, while the increase in the 7-day tensile strength was about 8% upon incorporating short steel fibers, the corresponding decrease in the tensile creep coefficient and the specific tensile creep at 14 days of loading was about 10% and 40% respectively. Also, while the increase in the 7-day tensile strength was about 7% upon applying thermal treatment, the corresponding decrease in the tensile creep coefficient and the specific tensile creep at 7 days of loading was about 73% and 77% respectively. The observed differences in the results between tensile creep and tensile strength emphasize the importance of conducting tensile creep testing to predict long-term tensile performance. It is proposed that, the more ability of cracks to coalesce and propagate during a tensile creep test rather than a tensile strength test may likely play an important role in describing the observed differences between the two sets of results.

3.5 Conclusions

Short-duration, 14-day tests were used to provide an initial understanding of the influence of varying the stress level at time of loading, incorporating short steel fibers, and thermal treatment on the tensile creep behavior of UHPC, with a complementary examination of drying shrinkage in these same mixtures. From this examination, the following observations can be made:

(1) While variations in 7-day tensile strength among the different conditions examined measured just a maximum of 8%, tensile creep behavior varied by up to ~70% when the influence of fiber reinforcement and curing conditions were compared. These results emphasize the

importance of conducting tensile creep testing rather than tensile strength tests to predict long-term tensile performance.

(2) Results from this study showed that 87% of the total autogenous shrinkage occurred during the thermal treatment due to accelerated rate of early hydration at higher temperature.

(3) The use of 2% steel fibers by volume resulted in a 42% reduction in autogenous shrinkage at 14 days of age after batching.

(4) The use of fibers and the application of thermal treatment decreased 14-day drying shrinkage.

(5) An increase from 40% to 60% in the tensile stress level at time of loading resulted in a 44% and 11% increase in the tensile creep coefficient and specific tensile creep after 14 days of loading.

(6) In contrast to tensile creep results provided literature for NSC and HPC, reinforcement with short straight steel fibers decreased the tensile creep of UHPC. It is proposed that this is, in part, due to the enhancements at the fiber/matrix interface during thermal treatment.

(7) Thermal treatment of UHPC at 90^{o}C (194^{o}F) for 48 hours decreased both the tensile creep coefficient and specific tensile creep at 7 days of loading by 73% and 77% when compared to companion concrete subjected to ordinary moist curing.

Overall, this research suggests that the combined effect of thermal treatment and incorporation of short steel fibers act to limit tensile creep and shrinkage in UHPC, with thermal treatment having the most pronounced effect. Furthermore, results from this study suggest that the tensile creep phenomenon in UHPC occurs differently than compressive creep in UHPC. This result emphasizes the importance of further study of the tensile creep behavior of UHPC, particularly for applications where satisfactory long-term tensile performance is required.

3.6 References

Altoubat, S. A., and Lange, D. A., "Tensile Basic Creep: Measurements and Behavior at Early Age", ACI Materials Journal, Vol. 98, No. 5, September-October, 2001, pp. 386-393.

ASTM C230. "Standard test method for flow table for use in tests of hydraulic Cement," American Society for Testing and Materials Standard Practice C230, Philadelphia, Pennsylvania, 1998.

Bissonnette, B., and Pigeon, M., "Tensile Creep at Early Ages of Ordinary, Silica Fume and Fiber Reinforced Concretes", Cement and Concrete Research, Vol. 25, N0. 5, 1995, pp. 1075-1085.

Bissonnette, B., Pigeon, M., and Vaysburd, A.M., "Tensile Creep of Concrete: Study of Its Sensitivity to Basic Parameters", ACI Materials Journal, Vol. 104, N0. 4, 2007, pp. 360-368.

Graybeal, B. A., "Characterization of the Behavior of Ultra-High Performance Concrete", Ph.D. Thesis, University of Maryland, 2005.

Gutsch, A., Rostasy, F.S., "Young concrete under High Tensile Stresses, Creep, Relaxation and Cracking", in: R. Springenschmid (Ed.), Thermal Cracking in Concrete at Early Age, E & FN Spon, London, RILEM, 1994, pp.111 –118.

Kovler, K., "A New Look at the Problem of Drying Creep of Concrete under Tension", ASCE Journal of Materials in Civil Engineering, Vol. 11, No. 1, February, 1999, pp. 84-87.

Kovler, K., "Interdependence of Creep and Shrinkage for Concrete under Tension", ASCE Journal of Materials in Civil Engineering, Vol. 7, No. 2, May, 1995, pp. 96-101.

Kovler, K., "Testing System for Determining the Mechanical Behavior of Early Age Concrete under Restrained and Free Uniaxial Shrinkage", Journal of Materials and Structures, Vol. 27, 1994, pp. 324-330.

Kovler, K., Igarashi, S., and Bentur, A., "Tensile Creep Behavior of High Strength Concretes at Early Age", Journal of Materials and Structures, Vol. 32, 1999, pp. 383-387.

Mehta, P.K. and Monteiro, P. J. M., "Concrete Microstructure, Properties, and Materials" 3rd ed: McGraw-Hill, 2005.

Mondal, P., Shah, S.P., and Marks, L.D., "Nanoscale Characterization of Cementitious Materials", ACI Materials Journal, Vol. 105, N0. 2, 2008, pp.174-179.

Tao, Z., and Weizu, Q., "Tensile Creep due to Restraining Stresses in High-Strength Concrete at Early Ages", Cement and Concrete Research, Vol. 36, 2006, pp. 584-591.

Umehara, H., Uehara, T., Iisaka, T., and Sugiyama, A., "Effect of Creep in Concrete at Early Ages on Thermal Stress", in: R. Springenschmid (Ed.), Thermal Cracking in Concrete at Early Age, E & FN Spon, London, RILEM, 1994, pp.79– 86.

CHAPTER 4
NEW TENSILE CREEP TEST SETUP AND RESEARCH PROGRAM

4.1 Research Objectives

Concrete made with very high performance cementitious matrix and short steel fibers (often called Ultra High Performance Concrete (UHPC) or reactive powder concrete (RPC)) is characterized by its very high strength and very low permeability, due to a material composition which optimizes the structure through consideration of particle packing (including the exclusion of coarse aggregate and fine particles larger than millimeter size) and reaction chemistry. The use of this type of material also presents new questions regarding performance that require further research.

For example, although some previous studies have suggested that the short steel fibers common in UHPC may serve as shear reinforcement instead of stirrups, the long-term inclined (shear) crack propagation and growth behavior in the absence of stirrups has not been investigated. This problem is of specific interest when bridge girders are made of such materials and long high performance service lives are required.

The overall purpose of this research is to assess the tensile creep and shrinkage properties of UHPC, and to relate these properties to the long-term behavior of precast prestressed bridge girders made using UHPC. Therefore, this multi-scale investigation has three main objectives:

1. The main objective of this study is to characterize the behavior and develop fundamental understanding of the tensile creep phenomenon in UHPC. This objective was dictated by the fact that no comprehensive study that focused on understanding tensile creep of concrete had been conducted and thus left this phenomenon poorly understood.

2. To characterize, by a parametric investigation, the effect of varying constituent materials, curing conditions, and stress levels on the tensile creep behavior of UHPC. It is of specific interest in this study to investigate the effect of steel fibers on the tensile creep behavior of UHPC. Also, as the curing environment plays an important rule in the refining the microstructure, different curing conditions are to be considered here in order to quantify their effect. The micro/nano scale part of this study which is based on scanning electron microscopy (SEM) and nanoindentation provides a clearer understanding of the tensile creep behavior of different UHPC investigated.
3. To finally assess the suitability and applicability of UHPC for use in bridge girders with 100 year service life.

4.2 Research Methodology

To meet the previously stated research objectives, which encompass both fundamental and practical understanding of the process and implications of tensile creep in UHPC, this research focuses on studying factors influencing tensile creep behavior of UHPC through: (1) a large scale study, and (2) micro/nano scale study. This includes bulk creep measurements of UHPC using 75x75x483 mm (3x3x19-in) specimens loaded for a period of 3-month to 1-year. In addition, nano/micro-scale characterization of the fiber-cementitious matrix interface using SEM and nanoindentation. Below are more details on the methodology used in each study.

4.2.1 Large scale Study

Figure 4.1 shows the large scale experimental program that investigated the effect of: (1) volume fraction of steel fiber reinforcement (without, 1%, and 2%, volume fraction), (2) curing regime 23^{o}C (73^{o}F) moist curing, 60^{o}C (140^{o}F), thermal treatment, and 90^{o}C (194^{o}F) thermal

treatment), and (3) stress/strength ratio at time of loading (0.40, 0.60, and 0.90) in addition to previously-cracked specimens loaded at stress/strength ratio of 0.40 on the tensile creep and shrinkage of UHPC. For all the mixes investigated, the creep and shrinkage was monitored before and after loading, at 2, 4, 6, and 24 hours, daily for a week, weekly for one month and then monthly for the rest of the testing period. In addition, direct tensile strength test, split tension test, compressive strength test, and modulus of elasticity test were performed on each mix prior to long-term loading.

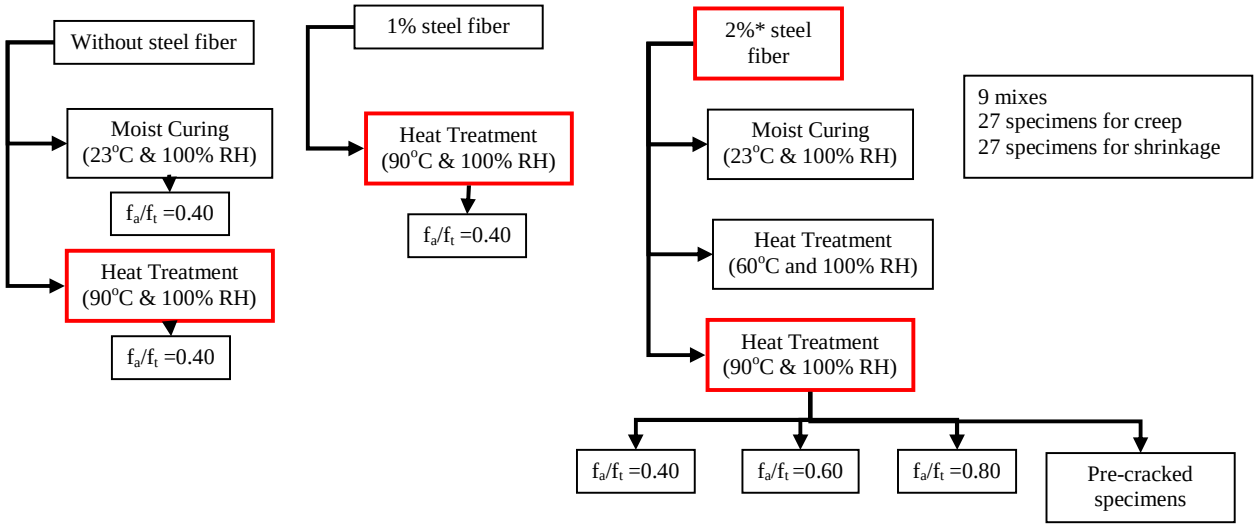

Figure 4.1: Research program for the large scale study

4.2.1.1 Tensile creep test

An experimental setup for tensile creep of concrete was developed based on a literature review previous setups. It was important in the design process to offset some of the disadvantages associated in the previous setups and to optimize the newly designed setup for use with any type of cement based materials.

Kovler [1994] developed an experimental device that allows testing two dog bone specimens with a net cross section of 40 x 40 mm and a working length of 1,000 mm (1.57 x 1.57 x 39-in) to be mounted horizontally on a laboratory table, one for restrained shrinkage testing, and the other for free shrinkage testing. However, no information was given about the method of calculating friction between the specimens and the table. Also, the literature reviewed where the same or very similar setups were used showed that this setup was only used for short-term creep tests with a maximum duration of 7 days [Kovler 1994, 1995; Kovler et al., 1999; Kovler, 1999; Altoubat and Lange, 2001; and Tao and Weizu, 2006]. Such short duration tests may have been conducted because of the limited number of specimens that could be tested at a given time or because of the high cost of the apparatus. In addition, according to ASTM C 512 "Standard Test Method for Creep of Concrete in Compression", no fewer than two specimens should be tested for creep and another two for shrinkage from a given batch under each test condition.

Bissonnette and Pigeon [1995] designed a tensile creep test setup that allowed testing one specimen per testing case. The load was applied to the prismatic specimens 50x50x700 mm (2.0 x 2.0 x 27.6-in) through precision-made steel plates anchored at the ends of the specimens with threaded rods placed and aligned in the PVC molds prior to casting. Bissonnette and Pigeon's test setup forms the foundation of developing the current setup. However, the design of their setup needed to be modified to increase the number of specimens tested per case. In addition, the loading capacity of the system needed to be increased to allow testing UHPC. The load capacity of the Bissonnette and Pigeon [1995] system was limited to 225 kg (500 lb.), and as maintaining a typical stress/strength ratio of 0.4 for UHPC specimens of the same size requires a load of

approximately 1,500 kg (3,300 lb), applying this system to UHPC becomes practically unfeasible.

Bissonnette [1996] attempted to achieve higher loads by modifying the previously discussed setup by Bissonnette and Pigeon [1995]. The first modification featured using a water tank as the sustained load in order to control the loading rate, and a system of pulleys was utilized to achieve an amplification factor of 48 (loading capacity of 3,600 kg (7,900 lb)) instead of 225 kg (500 lb). The major problem associated with the modification was the frictional losses created in the system of pulleys. These losses resulted in inconsistent loads delivered from the loading system to the specimens. Sometimes these losses decreased the load measured at the load cell at the bottom of the specimens to about 50% of the theoretically applied load [Bissonnette, 1996]. Bissonnette et al., [2007] made a second modification which featured six independent loading units, each of them having a capacity of three specimens in series mounted on a rigid steel frame. The load was generated by a pneumatic jack and amplified with a 6:1 lever arm. Tensile deformations were measured in this system using extensometers made of electrical resistance strain gages mounted on half-rings. This setup seemed to be the most suitable for UHPC applications due to high load capacity as well as the ability of gradual application of loads and real time acquisition of loads and deformations. However, a simpler strain measurement technique and one which eliminated electrical drift was desired. In addition, this system required regular and frequent adjustment of the air pressure to maintain the constant loads throughout the testing period.

Figure 4.2 shows the tensile creep testing frames designed and fabricated at the Georgia Institute of Technology to carry out the tensile creep tests of UHPC. This design was inspired by an original tension creep frame designed by Bissonnette and Pigeon (1995) with some

modifications. Specifically, these modifications include: (1) increasing the load capacity from 225 kg (500 lbs) to 6,800 kg (15,000 lbs) so that the frame can be used for testing higher-strength concretes, including UHPC, (2) increasing the number of specimens tested per case from one to three, (3) increasing the number of deformation readings from two to four for each specimen, and (4) increasing the dead load magnification factor from 4 to 10.

Each individual creep frame allows three 75x75x483 mm (3x3x19-in) UHPC concrete prisms to be tested for creep at the same time. Test conditions were kept at 23 ± 2 ^{o}C (73^{o}F) and 50 ± 3% RH throughout the testing period. More details of the tensile creep testing frames are provided below.

Loads: in this test setup, tensile loads were applied using 455x455x25 mm (18x18x1-in) plates weighting about 39-41 kg (85-90 lbs) each that were hung at the end of the dead load lever-arm via a metal ball knob that kept the threaded rod connecting the dead loads to the loading arm, always in a vertical position (Figure 4.3).

Dead load lever-arm: the dead load lever arm was designed with a magnification factor of 10:1. This high magnification factor was chosen to minimize the dead weights needed to apply high tensile stresses on the higher strength concrete prisms. The dead load lever arm was connected from one end to the dead loads via the metal ball knob and from the other end to the creep frame via a ball-bearing (pinned) connection (Figure 4.4). In between, the arm was also pin-connected to the test specimens to ensure concentric loading (Figure 4.4). During the test, the planar alignment of the dead load lever arm was guaranteed by providing rigid guides along each side of the dead load arm (Figure 4.5). Two track rollers were attached to each guide in order to eliminate friction between dead load lever-arm and the two guides.

Load cell: two 30 mm (1.2-in) electrical resistance strain gages were attached on two opposite sides of the eye-bolt connecting the top of the connected specimens to the tensile creep frame. These two strain gages were connected in a half bridge configuration and calibrated prior to loading. This allowed them to be used as a load cell to ensure the transfer of the target load to the specimens and to monitor the loads during the initial period of the creep test (Figure 4.6). The tensile creep load capacity of each frame is 6,800 kg (15,000 lbs) which is equivalent to 12.30 MPa (1,780 psi) tensile stress on a 75x75 mm (3x3-in) prism specimen. The moments due to possible eccentricity of loads were eliminated through the use two swivel connections, one at the top of the highest specimens and one at the bottom of the lowest specimen.

Load application: after dead loads were attached and prior to loading, a pallet jack was used to raise the dead loads to a position where the dead load lever-arm was in a horizontal position. At this point, the specimens-loading arm connection was tightened to keep the loading arm at an initial horizontal position before lowering the pallet jack (loading).

Specimens: three tensile creep 75x75x483 mm (3x3x19-in) concrete prism specimens connected in series and three companion free shrinkage specimens were used for each case. These dimensions were chosen to give each specimen: (1) an aspect ratio (height/width) of more than 3 which eliminates the St. Venant's effect and gives uniform stress in the middle part of the specimen and (2) width-to-fiber length ratio of 6 which produces more uniform tensile strength. The load was applied to specimens through 75x75x25 mm (3x3x1-in) steel end plates anchored with four tapered threaded bolts with an embedment length of 38 mm (1.5-in) for two rods and 50 mm (2.0-in) for the other two rods (Figure 4.7). This configuration was chosen after several trial designs to mitigate a stress concentration plane at the rods' ends. These end plates were placed and aligned in the steel prism molds prior to casting. High-strength/high modulus epoxy

was applied to the loading plates prior to pouring UHPC into the molds to strengthen the connection and to enhance the development of uniform stress field in the specimen. The tensile creep specimens were connected to each other through 25 mm (1.0-in) long threaded rods that connected the end plate of one specimen to the end plate of the adjacent specimen.

Deformation measurements: each specimen was fitted with four sets of steel inserts located on two opposite surfaces of the prism. Each set had a gauge length of 250 mm (10-in). Deformations were measured on each set of inserts using mechanical DEMEC gage with an accuracy of 10 microstrains (Figure 4.8).

4.2.1.2 Tensile strength test

Prior to performing the tensile creep test, it was necessary to measure the tensile strength as accurately as possible so that the applied stress/strength ratio could be controlled. Several tests, both direct and indirect, were investigated to find the most accurate tensile strength of the UHPC. Indirect tension tests mainly included the modulus of rupture tests [ASTM C 78 and ASTM C 293], modulus of rupture tests using prisms greater span length-to-depth ratios than the standard prisms, and the splitting tensile test [ASTM C 496]. These tests overestimated the true tensile strength of concrete and gave widely varying results. In the standard modulus of rupture test this overestimate is due to: (1) the fact that a linear stress variation is assumed for the calculation of the flexural strength, (2) the low span-to-depth ratio of the typical specimen indicates the presence of shear deformations which makes the assumption of linear stress variation not valid [Mehta and Monteiro, 2005], and (3) only the fact that only a small portion near the bottom of the specimen is resisting high tensile stresses in a flexural test. In the splitting tension test, the overestimation of true tensile strength is due to: (1) considering concrete a homogenous material, (2) neglecting the effect of the high compressive stresses generated at the

ends of the vertical plane during the calculations; (3) neglecting lateral restraints provided by friction between the specimen and the thin plywood bearing strips.

(a)

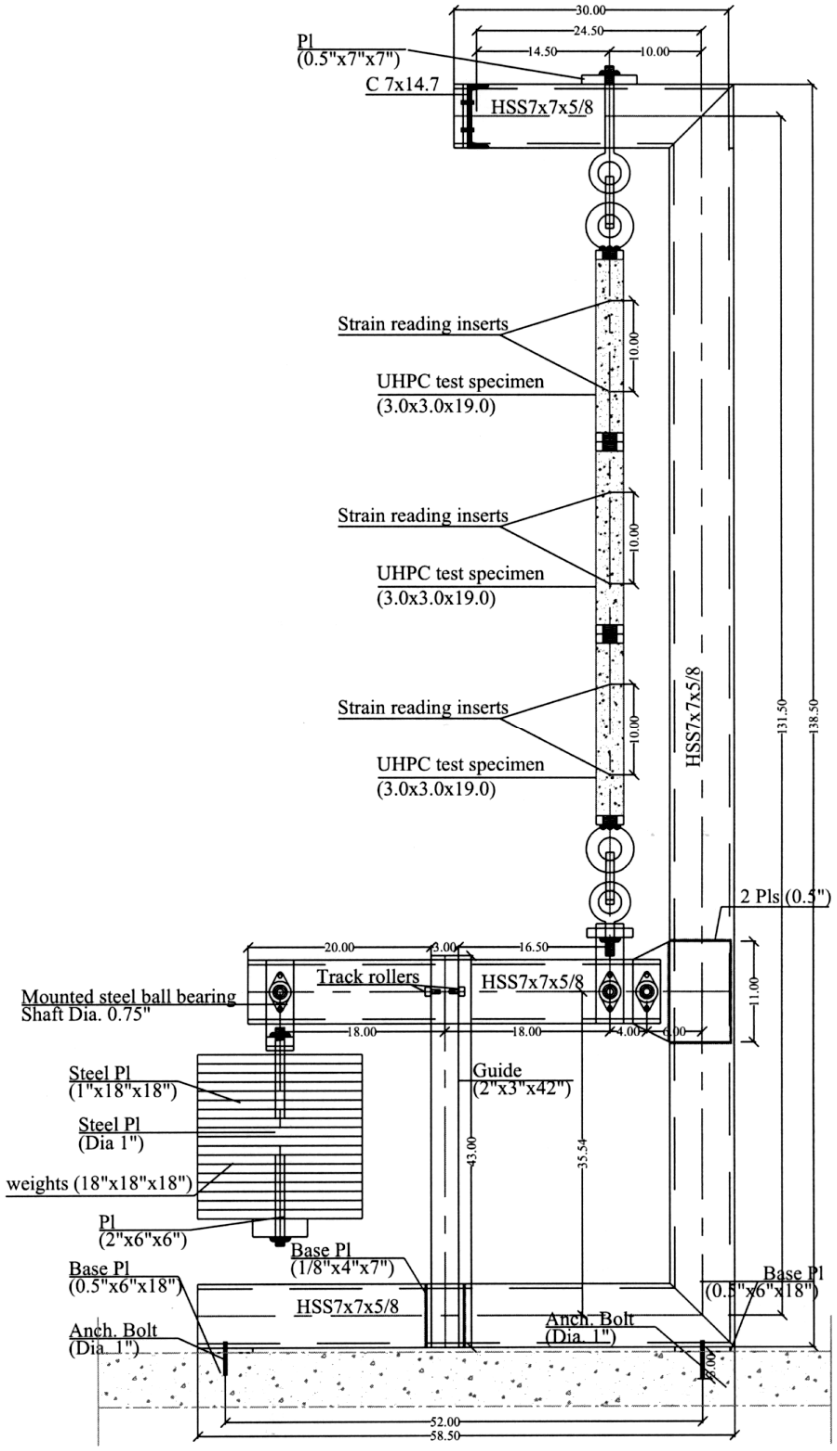

(b)

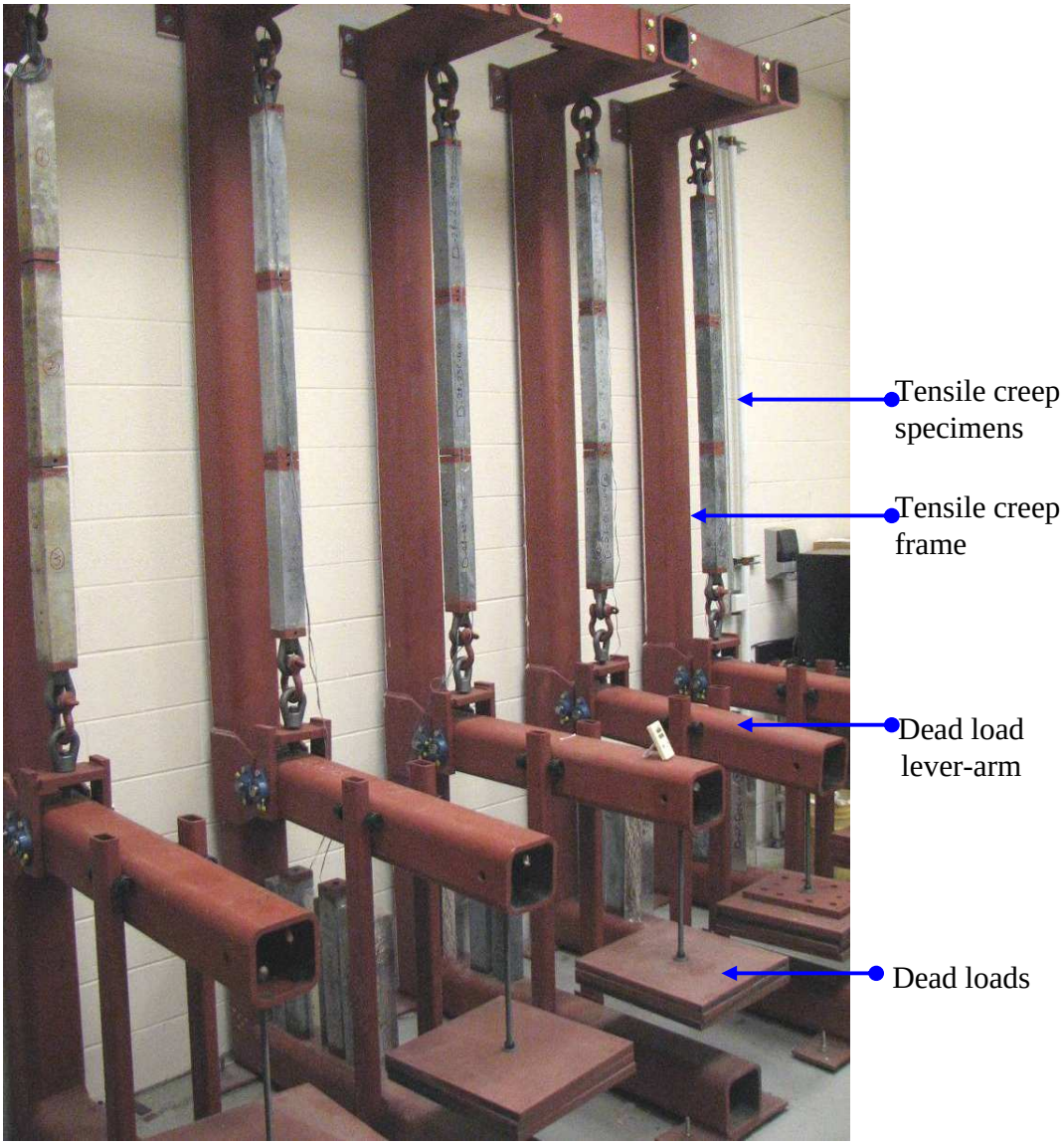

Figure 4.2: Tensile creep setup developed at Georgia Tech. (a) Schematic diagram of a typical tensile creep frame and (b) loaded specimens in tensile creep frames

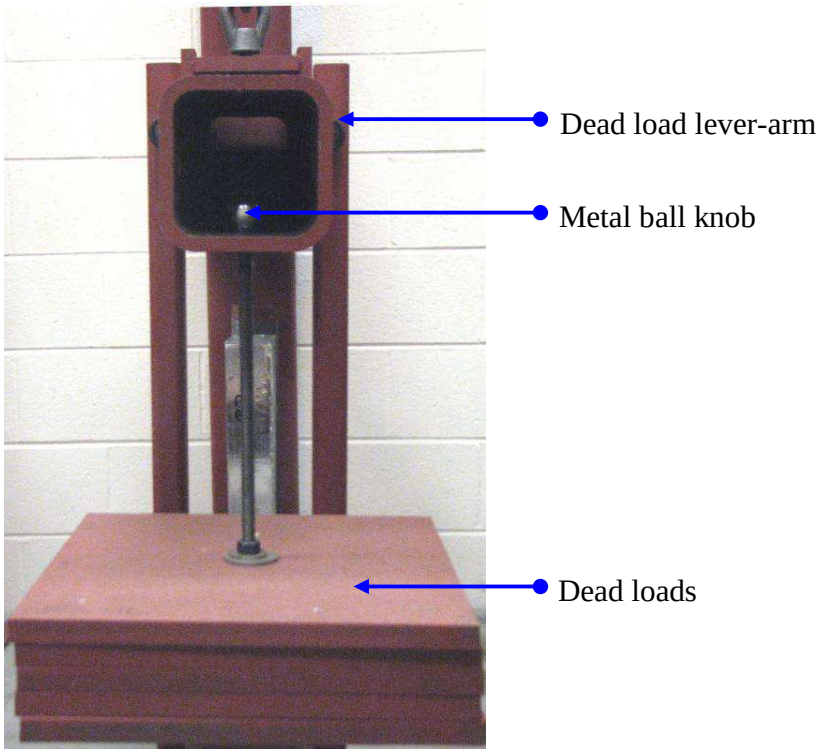

Figure 4.3: Tensile creep test setup: dead loads connection to the dead load lever-arm

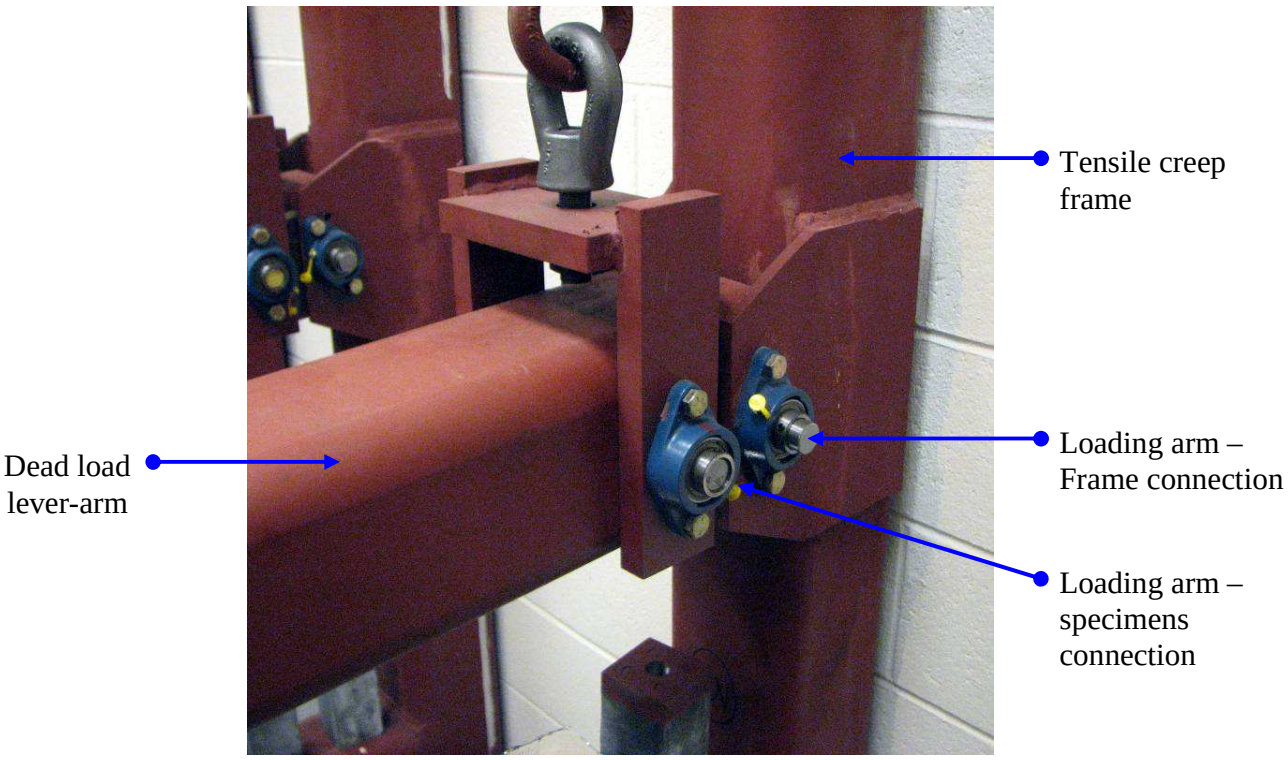

Figure 4.4: Tensile creep test setup: dead load lever-arm connections to frame and specimens

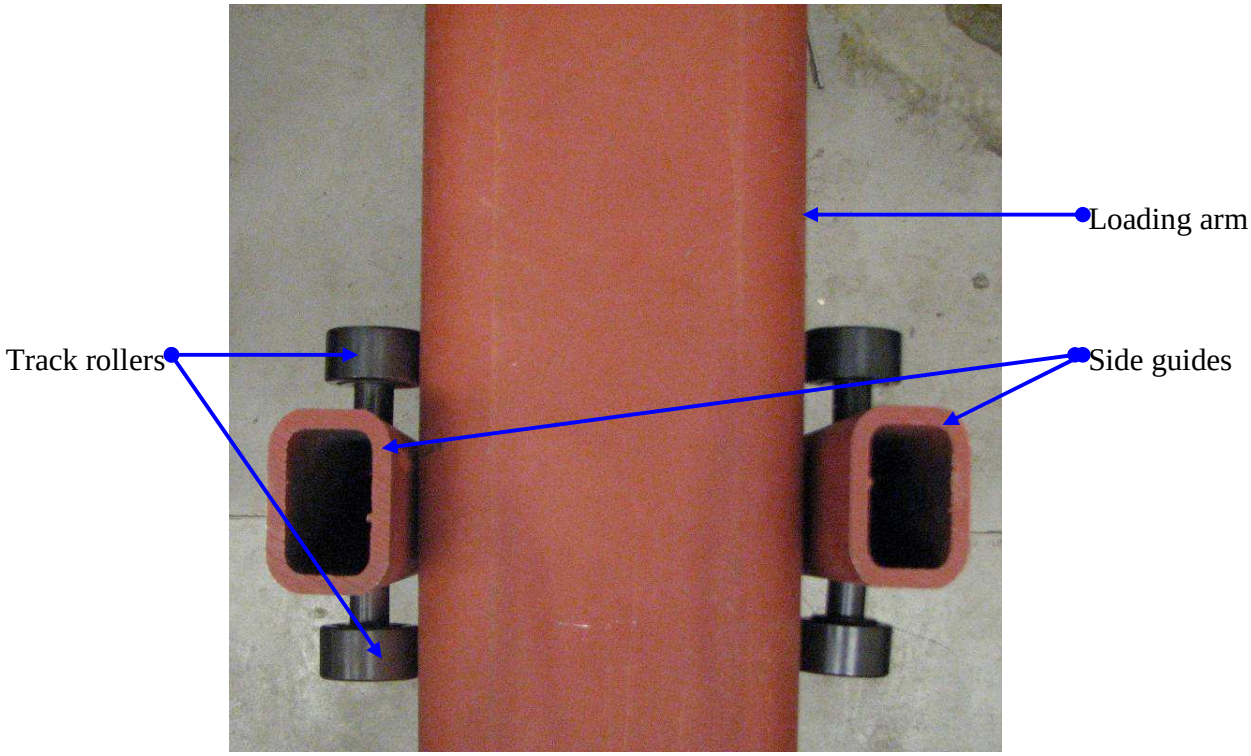

Figure 4.5: Tensile creep test setup: dead load lever-arm side guides

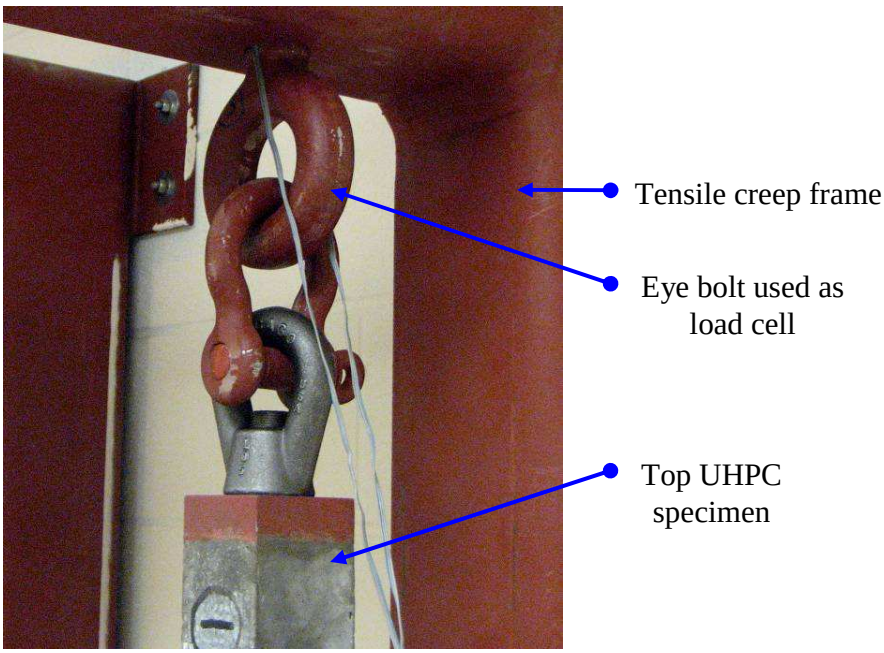

Figure 4.6: Tensile creep test setup: specimen-frame top connection and load cell

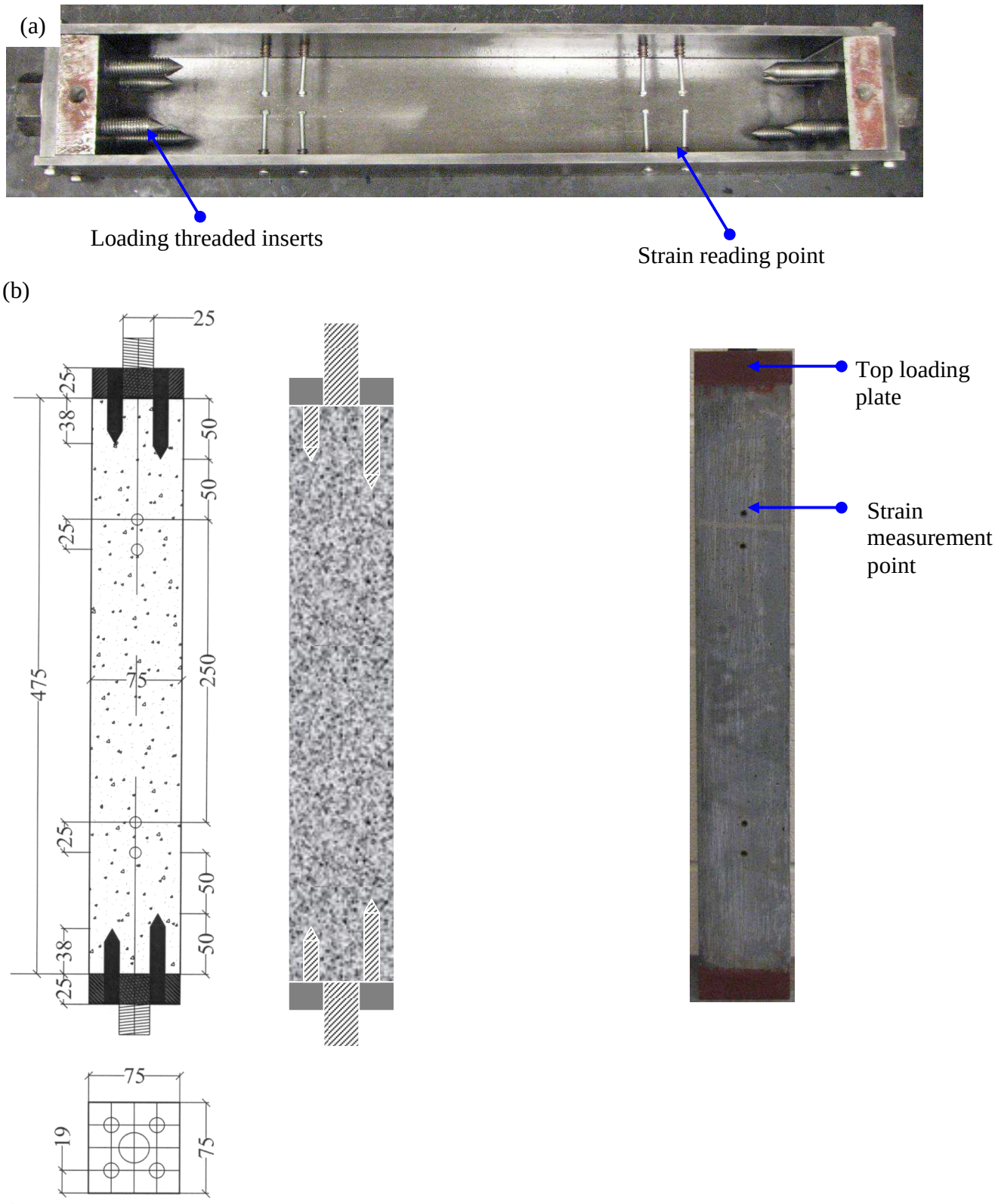

Figure 4.7: Tensile creep test specimen: (a) specimens mold and (b) specimen dimensions (mm)

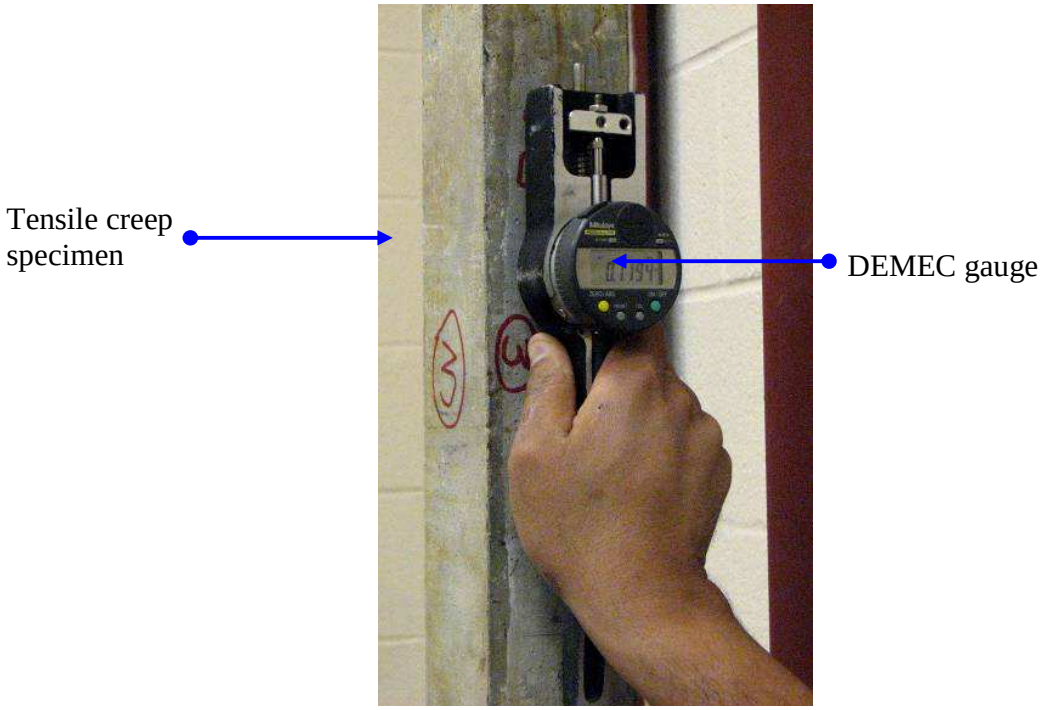

Figure 4.8: Tensile creep strain measurements using DEMEC gauge

On the other hand, there are major difficulties for the design of a direct tensile strength test for concrete because of problems associated with stress concentrations and possible secondary flexure and torsion induced in the concrete specimen through end-gripping.

One of the most commonly used direct tension tests is the Mortar briquette test [ASTM C 190]. The mortar briquette test while possessing some advantages like availability of molds and testing machines as well self-aligning grips is hard to apply to UHPC. The small cross section of the neck of the specimen in this test will result in potential alteration of the desired random fiber orientation. This alteration in the fiber dispersion resulted in a considerable scattering of the tensile strength results obtained for UHPC [Graybeal, 2005].

Another test is Todd's direct tension test [Todd, 1955]. In this test uniaxial tension is applied to a steel bar embedded in the middle of the specimen until a tensile failure in the concrete is achieved. Tensile stresses are transmitted to the concrete by bonding between the

steel bar and the concrete, thus creating a non uniform stress distribution along the concrete section with higher stresses around the steel bar.

Two other common direct tension tests are the notched and the unnotched cylinder tests. In these tests, the top and bottom faces of concrete cylinders are adhesively bonded to rigid steel loading plates or the loading heads of the test machine using high strength/high modulus epoxy [Akita et al., 2003; and Graybeal, 2005]. In the case of UHPC, several problems have been encountered with such cylinders, especially lack of control over the location of failure cracks and the failure at the epoxy interface. In addition, when multiple cracks are present, the observation of the tensile softening behavior was impossible or unreliable. Moreover, a major disadvantage of the notched cylinder test [RILEM TC 162-TDF] is the predetermination of the crack location. This condition does not capture the variability of tensile strength through the specimen. Also, the tensile zone is not long enough to get an accurate tensile strain, so development of accurate stress-strain response is not possible.

Based on the previously presented tension test methodologies, it was decided to develop a tensile strength test using a dog-bone type specimen. The dog-bone test configurations are the most accurate method to obtain the true tensile strength of UHPC, because: (1) sections in a dog-bone test configuration are uniformly loaded, (2) tensile Young's modulus of elasticity and Poisson's ratio can be determined using dog-bone configuration, (3) the dog-bone specimen configuration offsets most of the problems related with adhesively bonding specimens' ends to loading plates or loading heads in constant cross section configurations, and (4) the use of a reduced cross section appears as a practical alternative to the use of notched specimens. In addition, and particularly for the present study, casting dog-bone specimens (i.e. from one side to the other along the longitudinal axis) is similar to casting prestressed bridge girders where fiber

alignment occurs. Also, this casting method is similar to casting the tensile creep specimens; so the tension specimens replicate the stress behavior of the creep specimens.

Figures 4.9 and 4.10 show the direct tension test and the direct tension dog-bone specimen which is 235 mm (9.25-in) in length with a square cross section of 50x50 mm (2x2-in) in the middle section. Tensile loads were applied to specimens through 75x50x25 mm (3x2x1-in) steel plates anchored with two tapered threaded bolts with an embedment length of 38 mm (1.5-in). This configuration was chosen to mitigate stress concentrations. These end plates were placed and aligned in the steel molds prior to casting; high-strength/high modulus epoxy was applied to the loading plates prior to pouring UHPC in the molds to strengthen the connection and to enhance the development of uniform stress field in the specimen. Two 30 mm (1.2-in) long electrical resistance strain gages were attached on two opposite sides of the specimen These two strain gages were connected in a half bridge configuration in order to measure longitudinal strains during the tension test.

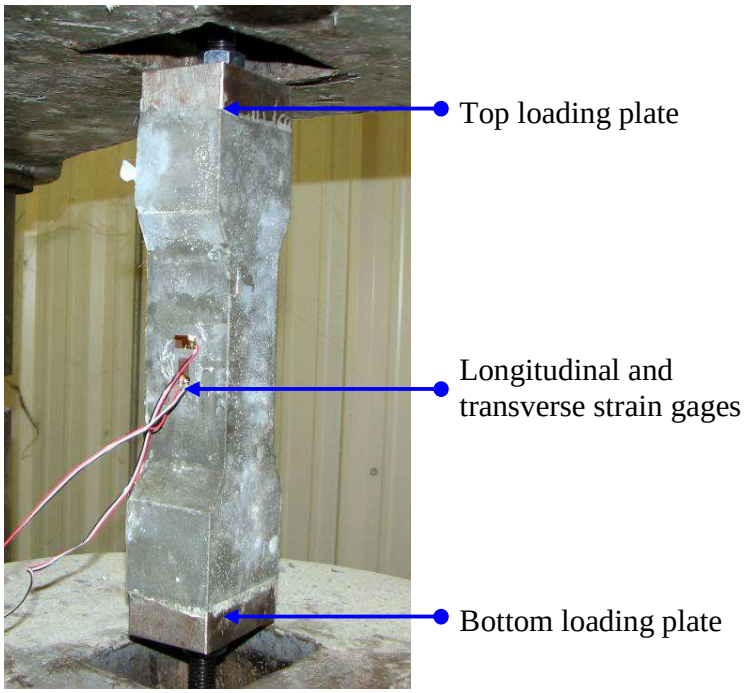

Figure 4.9: Direct tension test

(a)

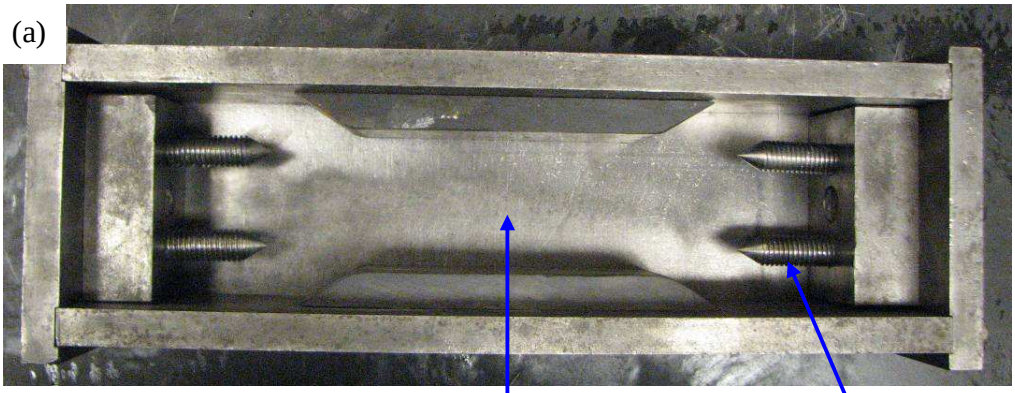

(b)

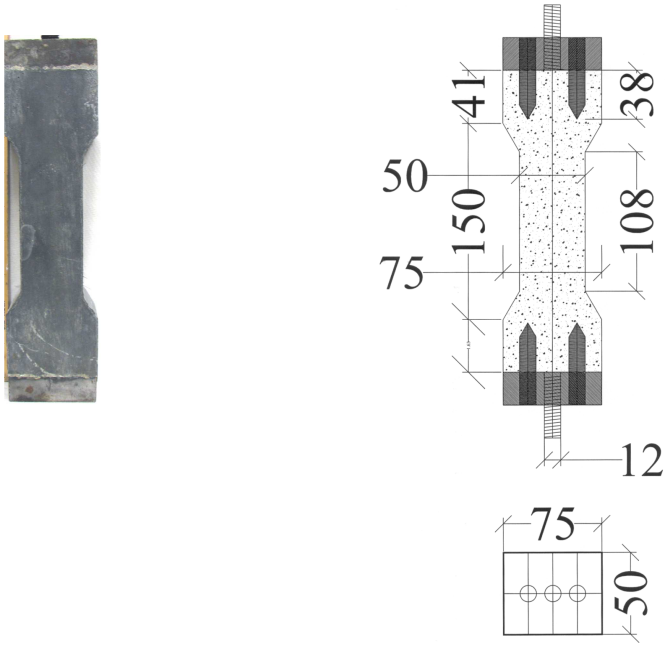

Figure 4.10: Tensile strength test specimen (a) mold and (b) dimensions (mm)

4.2.1.3 Split tension test

In the splitting tensile test, a compressive force is applied perpendicularly to the longitudinal axis of the cylinder (Figure 4.11.a). This force creates an almost uniform tensile stress over the middle part of the vertical loading plane (ASTM C 496). However, high

compressive stresses are generated close to the ends of the vertical plane as shown in Figure 4.11.b.

(a)

(b)

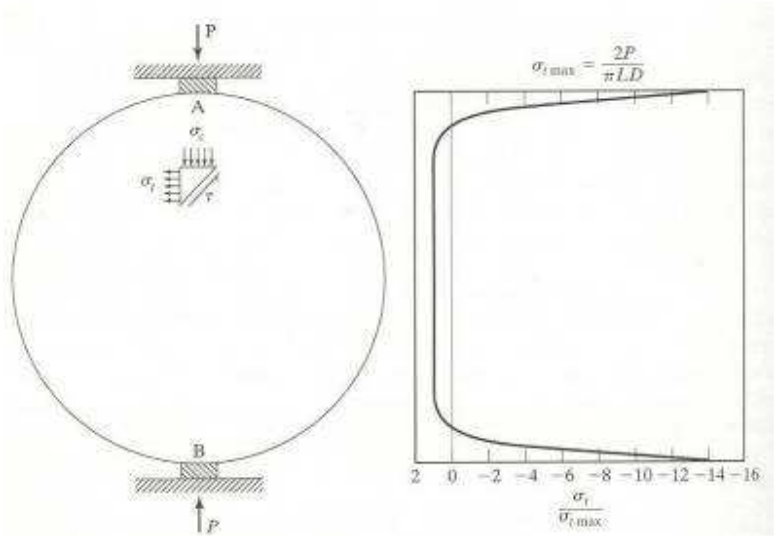

Figure 4.11: (a) Splitting tension test and (b) Stress distribution across loaded diameter in the splitting tensile test [Mehta and Monteiro, 2005]

The tensile strength value calculated from the splitting tensile test is typically lower than the corresponding value determined from the modulus of rupture test, but it is higher than the result obtained from direct tensile testing [Graybeal, 2005]. This difference exists due to: (1) considering concrete a homogenous material, (2) neglecting the effect of the high compressive

stresses generated at the ends of the vertical plane during the calculations; (3) neglecting lateral restraints provided by friction between the specimen and the thin plywood bearing strips. The effects increase the apparent value of tensile strength. Splitting tension tests were performed at the same times as compression strength tests using 75 x 150 mm (3x6-in) cylinders.

4.2.1.4 Compressive creep test

Compressive creep was measured on three 100x380 mm (4x15-in) cylinders under sustained load from each UHPC mixture according to ASTM C 512 specifications. Three additional non-loaded companion specimens were used to measure shrinkage. All specimens were cured and removed from their as mentioned before. The following tests were performed: (a) compressive strength, (b) modulus of elasticity, and (c) compressive creep and shrinkage. Compressive creep tests started at the same times as tensile creep tests. Figure 4.12 shows a picture of the creep frames used in this study. It is worth mentioning that the diameter of the cylinders used in this study was smaller than the standard from ASTM because the bearing capacity of some creep frames used was not enough for applying the required stress to 6x12-in (150x300 mm) UHPC cylinders recommended in ASTM C 512. Curing procedures were the same as for tensile creep.

The cylinders were instrumented with four sets of steel inserts located diametrically opposite on the surface of the specimen. Each set was a 10-in (254-mm) long gauge line for measuring deformation with a detachable mechanical gauge (DEMEC gauge) shown in Figure 4.13.

Figure 4.12: Compressive creep test setup

(a)

(b)

Figure 4.13: (a) compressive creep molds with strain reading inserts and (b) DEMEC reader and calibration bar used for creep and shrinkage

4.2.1.5 Compressive strength test

Compressive strength was determined by testing 100 x 200-mm (4 x 8-in) cylinders according to ASTM C 39. All compressive testing was performed in a SATEC MKIII 800 RD 3,558,580 kN (800 kip) capacity compression testing machine. Prior to testing the cylinders ends were ground to provide a smooth surface. A minimum of three specimens were tested from each batch for each measurement.

4.2.1.6 Modulus of elasticity test

The chord modulus of elasticity was measured using 100 x 200-mm (4 x 8-in) cylinders loaded in compression according to ASTM C 469. The tests were run in a SATEC Balwin 400 BTE 1,779,300 kN (400 kip) universal testing machine. Figure 4.14 shows the elastic modulus test. A minimum of three specimens were tested from each batch for each measurement.

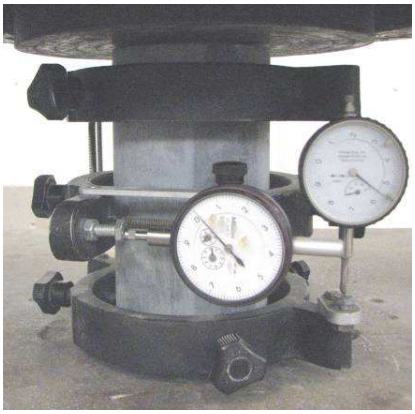

Figure 4.14: Modulus of elasticity test setup for UHPC

4.2.2 Micro/nano scale study

4.2.2.1 Nanoindentation and SEM samples

For characterization by nanoindentation and SEM, smaller scale UHPC samples were prepared using a paddle mixer following the same procedures described above, with the

exception of the method of fiber addition. These specimens were cast in 30 mm diameter cylinders with depth of ~12 mm (1/2-in) (Figure 4.15 a). After casting non-fiber reinforced UHPC into the molds, 16 steel fibers pre-fixed on a plastic sheet in a square configuration were pushed vertically into the middle 5 x 5 mm (0.2 x0.2-in) region of the specimen to create a 2% fiber volume fraction in this region similar to that of the creep specimens. Upon inserting the fibers, each specimen was vibrated for 30 seconds to ensure good compaction and bonding around the fibers. The arrangement of fibers in this manner was chosen to allow indentations in the radial direction of each fiber, Figure 4.15 b, and to ensure that the indentations performed at the fiber-cementitious matrix interface were not affected by underlying fibers (which if randomly dispersed could affect indentation measurements made in near-surface pastes).

After demolding, the smaller scale samples were, like the larger scale specimens, either stored in a fog room at 23^{o}C and 100% RH or placed in an environmental chamber for thermal treatment at temperature of 90^{o}C and 100% RH for the next 48 hours.

After curing or curing and thermal treatment, fast setting epoxy was poured on the top surface of the specimens to cover any fibers sticking out and also to provide more support to fibers during polishing.

Subsequently, they were polished in preparation for nanoindentation and SEM, generally following the procedures outlined by Mondal et al. [2008]. The bottom side of each specimen was successively dry-polished using paper discs of grits 116 μm (0.0046-in) (until the fibers were exposed), 34.2 μm (0.0013-in), 22.1 μm (0.0009-in), 14.5 μm (0.0006-in), 6.5 μm (0.0003-in). Diamond lapping films of grits 6 μm (0.0002-in), 3 μm (0.0001-in) were then used. As a final step, a diamond suspension in water of 0.05 μm (1.97 micro inches) grit was used to polish the surface. After polishing, samples were ultrasonically cleaned in water for 2 minutes and then

stored at 23°C (73°F) and 100% RH and then dried in a 30°C (86°F) oven before performing nanoindentation or microscopy.

4.2.2.2 Nanoindentation test

A typical nanoindentation test is composed of compressive loading and unloading responses (Figure 4.16). The unloading response of the material is assumed to be elastic, and thus the slope of the unloading graph can be used to calculate the elastic properties of the indented material. In this study, an MTS XP nanoindenter with an attached continuous stiffness measurement unit (CSM) was used (Figure 4.17). The tip used for the nanoindentation tests was a pyramid shape, diamond Berkovich tip with a nominal radius of 50 nm, an elastic modulus, E_{in}, of 1100 GPa (159,542 ksi), and a Poisson's ratio, v_{in}, of 0.07. The load of each indent was increased linearly to 2 mN (0.0004 lbs) in 10 seconds; the maximum load was kept for 2 seconds to allow the indenter to stabilize before taking the depth maesurement, and finally was decreased linearly in 10 seconds. The unloading curve, Figure 4.16, was used to calculate the Young's modulus of elasticity of the indented materials based on the method described by Oliver and Pharr (1992). In this method, the measured stiffness of the initial unloading response, $\frac{dP}{dh}$, is given by Equation 1.

$$\frac{dP}{dh} = \frac{2}{(\pi)^{1/2}} * A^{1/2} * E_r \tag{4.1}$$

Where P is the indentation load, h is the indentation elastic displacement, A is the projected area of the elastic contact, and E_r is a reduced modulus given by:

$$\frac{1}{E_r} = \frac{1-\nu^2}{E} + \frac{1-\nu_{in}^2}{E_{in}} \tag{4.2}$$

Where E and ν are the elastic modulus and the Poisson's ratio of the indented material and E_{in} and ν_{in} are the same constants for the indenter material. In this study, ν of the cementitious matrix was assumed to be 0.18 [Graybeal, 2005], while ν of steel fibers was assumed to be 0.30 [Gere, 2001]. Figure 16.b shows the indentation scheme followed in this study, where indents were performed in 2 perpendicular directions starting from the center of the fiber.

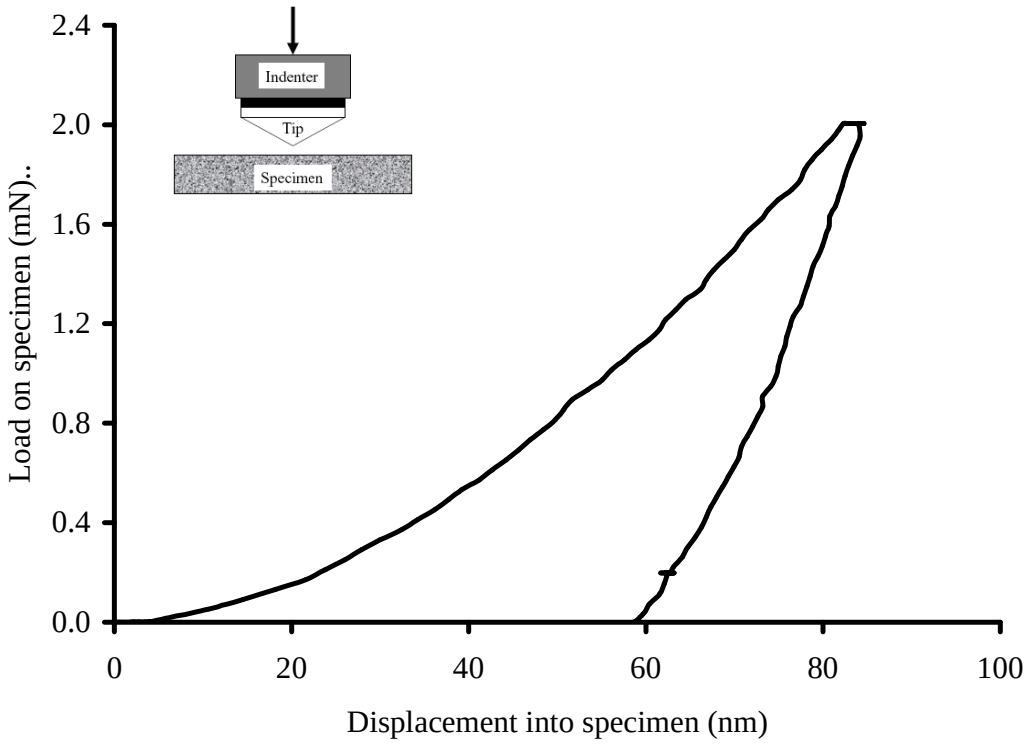

Figure 4.15: Typical load displacement curve for nanoindentation test

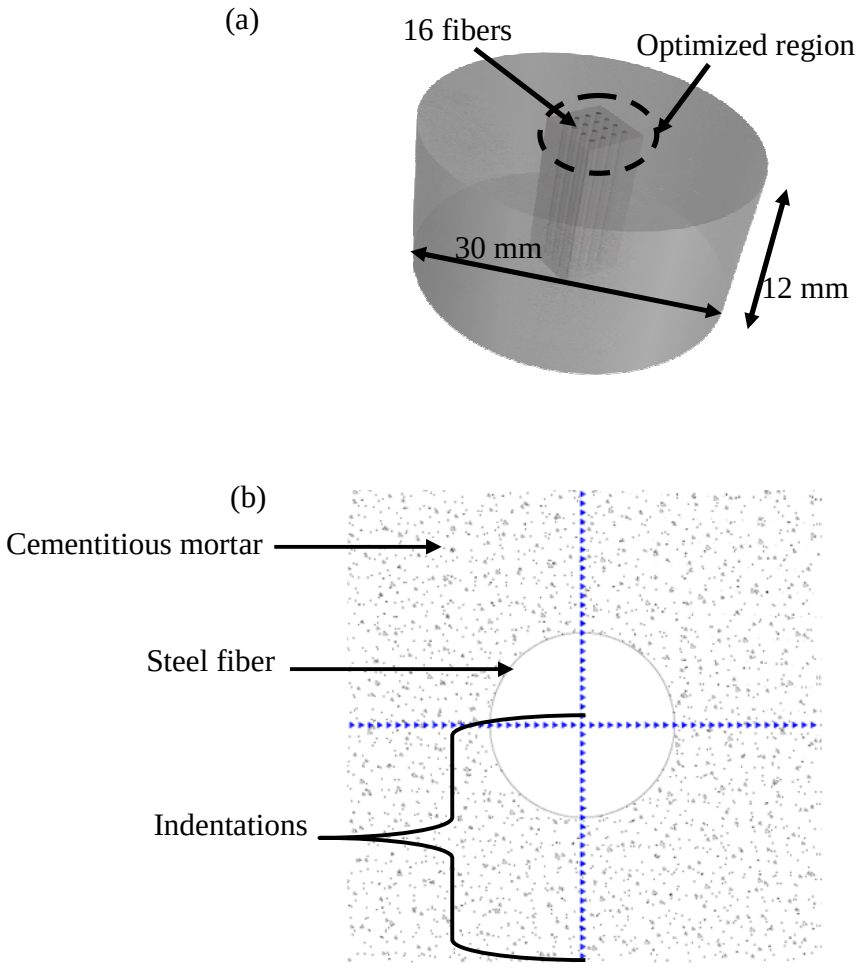

Figure 4.16: (a) UHPC sample used for nanoindentation and SEM and (b) nanoindentation scheme

Figure 4.17: Nanoindenter XP by MTS Systems

4.2.2.3 Scanning electron microscopy (SEM)

The indented surface of each specimen was then sputter coated with gold before SEM imaging was carried out. Images of the indented areas taken before the nanoindentation tests were used to identify where SEM imaging should be done. SEM was carried out using a LEO 1530 thermally-assisted field emission (TFE) scanning electron microscope at low pressure 10^{-7} Pa (1.45 ksi) (Figure 4.18). The accelerating voltage used was 10kV. Back-scattered electron mode was used in order to distinguish the surface characteristics with better clarity.

Figure 4.18: LEO 1530 Thermally-Assisted Field Emission (TFE) Scanning Electron Microscope (SEM)

4.3 References

Akita, H., Koide, H., Tomon, M., Sohn, D., "A practical method for uniaxial tension test of concrete", Materials and Structures Vol. 36, No. 260, July 2003, pp. 365-371.

Altoubat, S. A., and Lange, D. A., "Tensile Basic Creep: Measurements and Behavior at Early Age", ACI Materials Journal, Vol. 98, No. 5, September-October, 2001, pp. 386-393.

ASTM C190, "Standard Test Method for Tensile Strength of Hydraulic Cement Mortars," American Society for Testing and Materials Standard Practice C190, Philadelphia, Pennsylvania, 1990.

ASTM C293, "Standard Test Method for Flexural Strength of Concrete (Using Simple Beam With Center-Point Loading)," American Society for Testing and Materials Standard Practice C293, Philadelphia, Pennsylvania, 2008.

ASTM C39, “Standard Test Method for Compressive Strength of Cylindrical Concrete Specimens”, American Society for Testing and Materials Standard Practice C39, Philadelphia, Pennsylvania, 2004.

ASTM C469, “ASTM C 469, “Standard Test Method for Static Modulus of Elasticity and Poisson's Ratio of Concrete in Compression,” American Society for Testing and Materials Standard Practice C469, Philadelphia, Pennsylvania, 2002.

ASTM C496, “Standard Test Method for Splitting Tensile Strength of Cylindrical Concrete Specimens,” American Society for Testing and Materials Standard Practice C496, Philadelphia, Pennsylvania, 1990.

ASTM C512, “Standard Test Method for Creep of Concrete in Compression,” American Society for Testing and Materials Standard Practice C512, Philadelphia, Pennsylvania, 2002.

STM C78, “Standard Test Method for Flexural Strength of Concrete (Using Simple Beam with Third-Point Loading),” American Society for Testing and Materials Standard Practice C78, Philadelphia, Pennsylvania, 2008.

Bissonnette, B., “Le Fluage en Traction: un Aspect Important de la Problematique des Reparations minces en Beton”, DSc Thesis in Civil Engineering, Université LAVAL, Québec, Canada, December 1996.

Bissonnette, B., and Pigeon, M., “Tensile Creep at Early Ages of Ordinary, Silica Fume and Fiber Reinforced Concretes”, Cement and Concrete Research, Vol. 25, N0. 5, 1995, pp. 1075-1085.

Bissonnette, B., Pigeon, M., and Vaysburd, A.M., “Tensile Creep of Concrete: Study of Its Sensitivity to Basic Parameters”, ACI Materials Journal, Vol. 104, N0. 4, 2007, pp. 360-368.

Graybeal, B. A., "Characterization of the Behavior of Ultra-High Performance Concrete", Ph.D. Thesis, University of Maryland, 2005.

Gere, J.M., “Mechanics of Materials”, 5th Edition, Brooks/Cole, 2001.

Kovler, K., “A New Look at the Problem of Drying Creep of Concrete under Tension”, ASCE Journal of Materials in Civil Engineering, Vol. 11, No. 1, February, 1999, pp. 84-87.

Kovler, K., “Interdependence of Creep and Shrinkage for Concrete under Tension”, ASCE Journal of Materials in Civil Engineering, Vol. 7, No. 2, May, 1995, pp. 96-101.

Kovler, K., “Testing System for Determining the Mechanical Behavior of Early Age Concrete under Restrained and Free Uniaxial Shrinkage”, Journal of Materials and Structures, Vol. 27, 1994, pp. 324-330.

Kovler, K., Igarashi, S., and Bentur, A., “Tensile Creep Behavior of High Strength Concretes at Early Age”, Journal of Materials and Structures, Vol. 32, 1999, pp. 383-387.

Mehta, P.K. and Monteiro, P. J. M., “Concrete Microstructure, Properties, and Materials” 3rd Edition, McGraw-Hill, 2005.

Mondal, P., Shah, S.P., and Marks, L.D. “Nanoscale Characterization of Cementitious Materials”, ACI Materials Journal, Vol.105, No.2, 2008, pp. 174-179.

Oliver, W.C., and Pharr, G.M., “An Improved Technique for Determining Hardness and Elastic Modulus Using Load and Displacement Sensing Indentation Experiments”, Journal of Material Research, Vol.7, No.6, 1992, pp.1564-1583.

Rilem TC 162-TDF: “Test and Design Methods fir Steel Fibre Reinforced Concrete, Uniaxial Tension Test for Fibre Reinforced Concrete”, Materials and Structures, Vol.34, 2001, pp. 3-6.

Tao, Z., and Weizu, Q., “Tensile Creep due to Restraining Stresses in High-Strength Concrete at Early Ages”, Cement and Concrete Research, Vol. 36, 2006, pp. 584-591.

Todd J.D. “The Determination of Tensile Stress-Strain Curves for Concrete”, Proceedings, Institution of civil Engineers, Vol.4, No.2, Part 1, London, March 1955, pp. 210-211.

CHAPTER 5

EFFECT OF THERMAL TREATMENT ON THE TENSILE CREEP OF UHPC

5.1 Introduction

The aim of this study was to characterize and quantify the effect of the thermal treatment on tensile creep of UHPC. The experimental program, presented in Section 4.2.1, included testing of three UHPC mixtures under various curing conditions. All the mixtures designs were identical and were based on the UHPC manufacturer's recommendation; they all included steel fibers at 2% volume fraction. In addition, they were all mixed and cast following the procedure outlined in Chapter 3.

This chapter presents an analysis of the mechanical properties and time-dependent deformations obtained in the large-scale study in addition to the nano/microscale study for the three UHPC mixes considered. Results and analysis are grouped in six major sections. The first section presents an analysis of the effect of thermal treatment on the short-term mechanical properties of UHPC. The second section analyzes the influence of thermal treatment on tensile creep of UHPC. The third section analyzes the influence of thermal treatment on compressive creep of UHPC. The fourth section gives a comparison between tensile and compressive creep performance of UHPC. The fifth section presents results from the nano/microscale study. Finally, the sixth section presents the proposed tensile creep mechanisms based on the multi-scale study.

Table 5.1 summarizes the mixes, their main characteristics, and the main tests done, in addition to tensile and compressive strength tests, on each mix. The nomenclature used in this study was based on the type of UHPC used (i.e., Ductal® = D), fiber volume fraction (i.e., 2% volume fraction = 2f), maximum treatment temperature reached while curing (i.e. 23^{o}C, 60^{o}C or

90°C (73 °F, 140 °F or 194°F)), and the stress level maintained during the creep test (i.e. 40% means that the tensile stress ratio at the time of loading was 40%). For example, Mix "D-2f-90C-40" indicates that the Ductal premix was used with 2% by volume steel fiber content, thermally treated at 90°C (194°F), and loaded at 40% of its tensile strength at the time of loading. For the compressive creep test, the letter "C" is added after the letter "D" to differentiate between tensile and compressive creep mixes. Tensile and compressive creep specimens for a given curing condition were cast of the same batch. Also, the term that indicates the stress level was removed for the micro/nano-scale.

Table 5.1: Different UHPC mixes, curing and loading conditions

Tests performed	Mixture ID	Stress/strength at loading (%)	Curing temperature[1]	Fiber content
Tensile creep and free shrinkage	D-2f-90C-40	40	90°C (194°F)	2% by vol.
	D-2f-60C-40	40	60°C (140°F)	2% by vol.
	D-2f-23C-40	40	23°C (73°F)	2% by vol.
Compressive creep and free shrinkage	D-C-2f-90C-40	40	90°C (194°F)	2% by vol.
	D-C-2f-60C-40	40	60°C (140°F)	2% by vol.
	D-C-2f-23C-40	40	23°C (73°F)	2% by vol.
SEM and nanoindentation	D- 2f-90C	N/A	90°C (194°F)	2% by vol.
	D-2f-60C	N/A	60°C (140°F)	2% by vol.
	D-2f-23C	N/A	23°C (73°F)	2% by vol.

[1] All samples were cured between 95% and 100% RH

5.2 Research Significance

While some studies have examined tensile creep behavior in ordinary and high performance concrete [Umehara et al., 1994, Gutsch and Rostasy, 1994, Kovler, 1994, Bissonnette and Pigeon, 1995, Kovler, 1995, Kovler, 1999, Kovler, 1999, Altoubat, 2001, Tao and Weizu 2006, and Bissonnette et al., 2007], tensile creep of UHPC has not been characterized

in the published literature. Some previous studies have suggested that the short steel fibers typically used in UHPC mixes may serve as shear reinforcement similar to stirrups in bridge girders. However, the long-term behavior of inclined (shear) cracks induced by diagonal tension near girder supports in the absence of stirrups has not been investigated. That is, it is unknown whether UHPC girders without conventional stirrups will creep to failure, and it is unknown what reliability factor should be applied to the diagonal tension capacity of UHPC in bridge structures. In this chapter, the effect of different thermal treatment regimes on the tensile creep performance is studied on nano-, micro, and macro-scale levels. This investigation does not only present new data on creep and shrinkage of UHPC but also contributes to the understanding on the factors driving long-term tensile deformations in UHPC.

5.3 Thermal Treatment of UHPC

Several studies have shown that the application of thermal treatment to concrete, and specifically UHPC, can result in activation of silica fume (and perhaps other materials), resulting in a net reduction in the pore size which improves the cementitious matrix structure and performance [Richard and Cheyrezy, 1995, and Feylessoufi et al., 1997]. A study by Cheyrezy et al. [1995] using mercury intrusion porosimetry measured showed zero porosity, in the range 3.75nm to 300μm, in confined reactive powder concrete (RPC) specimens thermally treated between 150 ^{o}C (302 ^{o}F) and 200 ^{o}C (392 ^{o}F). Two other studies by Collepardi et al. [1997] and Richard and Cheyrezy [1995] showed reductions in both shrinkage and swelling in RPC where thermal treatment at 90 ^{o}C (194 ^{o}F) was applied. Heat treatment at 160 ^{o}C (320 ^{o}F) showed further improvements in RPC strength development when compared to RPC's that were heat-treated at 90 ^{o}C (194 ^{o}F) [Monosi et al., 2000]. Also, in a recent study by Graybeal [2005], the application of thermal treatment at 90^{o}C (194^{o}F) to UHPC for 48 hours significantly

improved almost all investigated material properties. On the other hand, Chen et al. [2009] argued that the heat-treatment at 105^{o}C (221^{o}F) or above can result in thermal damage by microcracking within the cementitious mortar. According to the same study, it was concluded that thermal damage resulted in a change in the stress-strain relationship from linear elastic with brittle failure to plastic with ductile failure due to more compliant solid skeleton and pore network collapse at temperatures above 105^{o}C (221^{o}F). Similarly, Lion et al., [2005] reported that microstructural degradation was observed for cement mortars upon applying thermal treatment at 150^{o}C (302^{o}F) or 250^{o}C (482^{o}F). Therefore, thermal curing has been shown to be both beneficial and detrimental to the structure and performance of cement-based materials, Furthermore, the influence of thermal curing on tensile creep of cement-based materials has not been considered in prior published research.

In construction practice, it is conventionally known that most steam curing beds in precast concrete plants are designed for temperatures not in excess of 70^{o}C (158^{o}F), to avoid delayed ettringite formation (DEF) in concrete [Taylor et al., 2001] . This common practice in the precast industry is a challenge to mass-producing UHPC structural elements where thermal treatment at 90^{o}C (194^{o}F) is required given that changing steam plants in casting plants may not by desired due to the associated costs.

In summary, the literature reviewed showed the importance of thermal treatment in developing UHPC structure and in tailoring performance. While numerous studies have shown improvements in strength, impermeability, and dimensional stability, some raise concerns regarding the potential for thermally-induced cracking. However, the question still exists whether thermal-treatment procedures which produce desired UHPC structure and performance

can be achieved practically. In this chapter, the effect of three curing regimes on tensile creep of UHPC are presented and discussed.

5.4 Ultra-High Performance Concrete Premix

The UHPC mixes investigated were prepared from the ultra-high performance premix, Ductal®, provided by Lafarge North America and ultra-high strength steel fibers, Dramix 13/0.20, provided by Bekaert. According to the manufacturer, the UHPC premix consisted mainly of Portland cement, silica fume, crushed quartz, and sand. The high strength steel fibers were 0.20 mm (0.008-in.) in diameter and 13.0 mm (0.51-in.) in length (aspect ratio = 65), and had a tensile strength of between 690 and 1000 MPa (96,600 and 140,000 psi) and a Young's modulus of Elasticity of 210,000 MPa (30,457 ksi), according to the manufacturer. Also, commercially available polycarboxylate high range water reducer (HRWR), Premia 150 provided by Lafarge was used. A typical UHPC mixture design is shown in Table 5.2.

Table 5.2 UHPC composition

Constituent	kg/m^3 (lb/ft^3)
UPHC Premix	2194 (137)
Water	109 (6.80)
HRWR	31 (1.94)
Steel fibers	156[1] (9.74)

[1] Dose recommended by the UHPC manufacturer (2% volume fraction)

5.5 Large Scale Study

5.5.1 Treatment Regimes

Three different curing regimes were selected for this study (Figures 5.1 through 5.3).

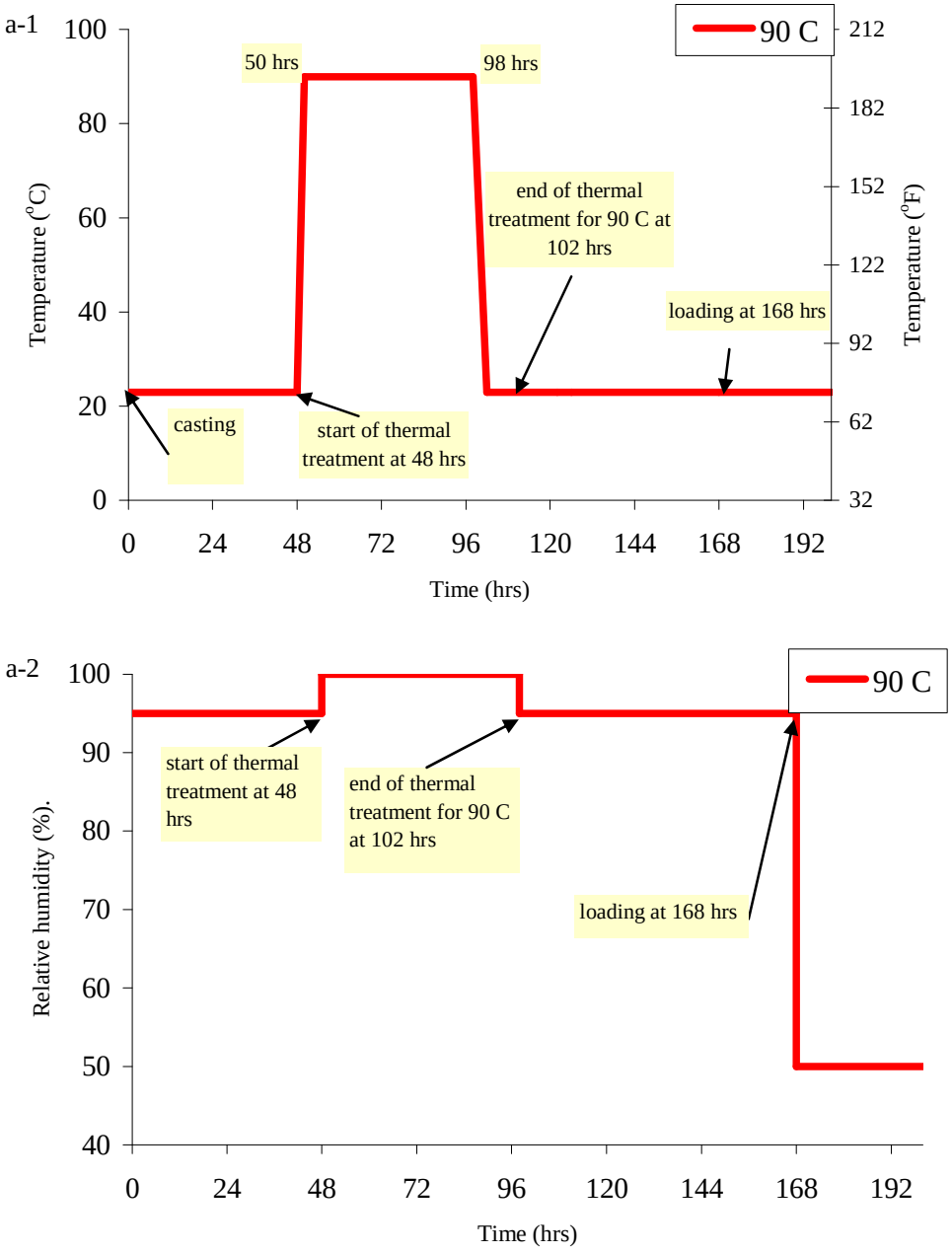

Figure 5.1 a: 90°C (194°F) curing regime

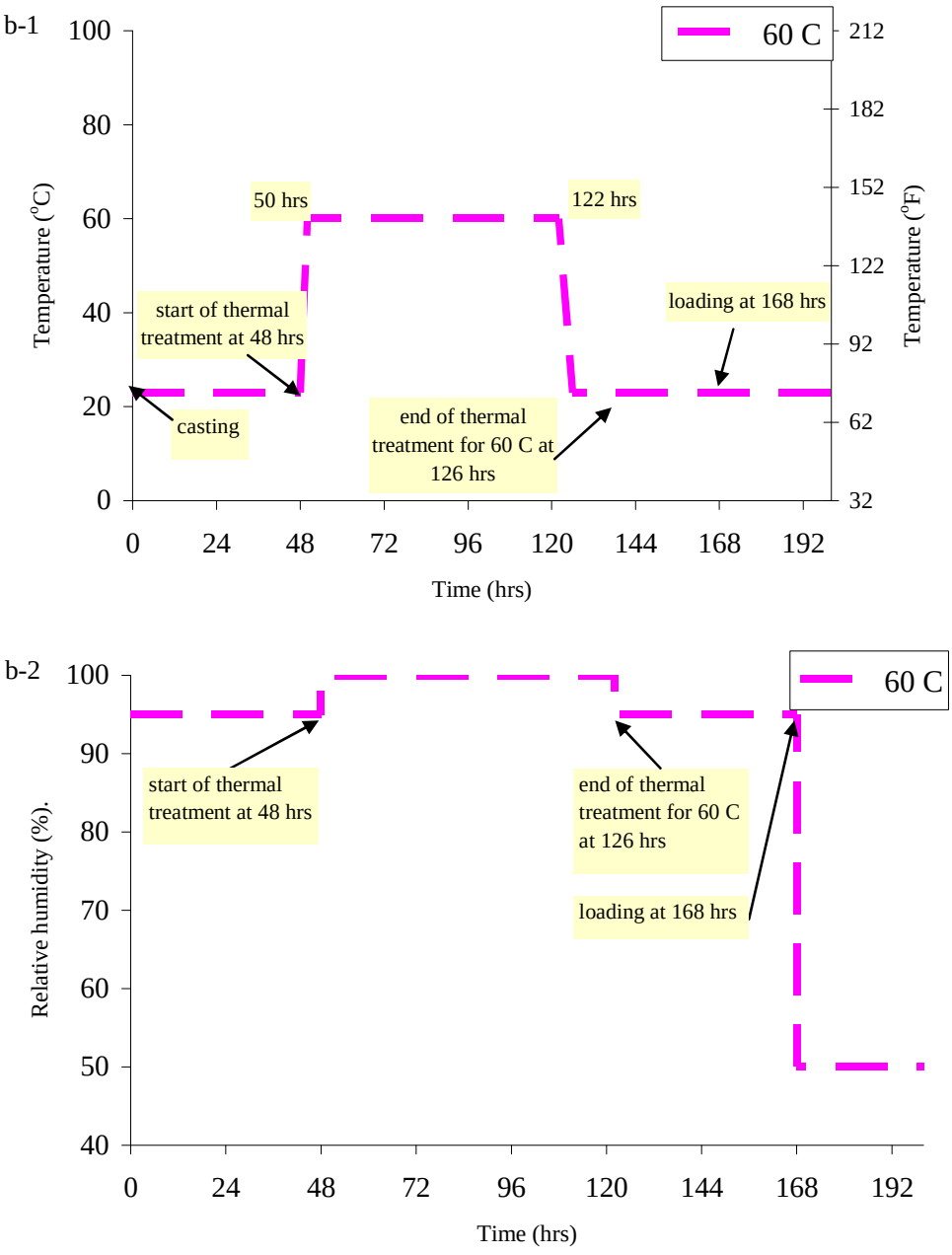

Figure 5.1 b: 60°C (140°F) curing regime

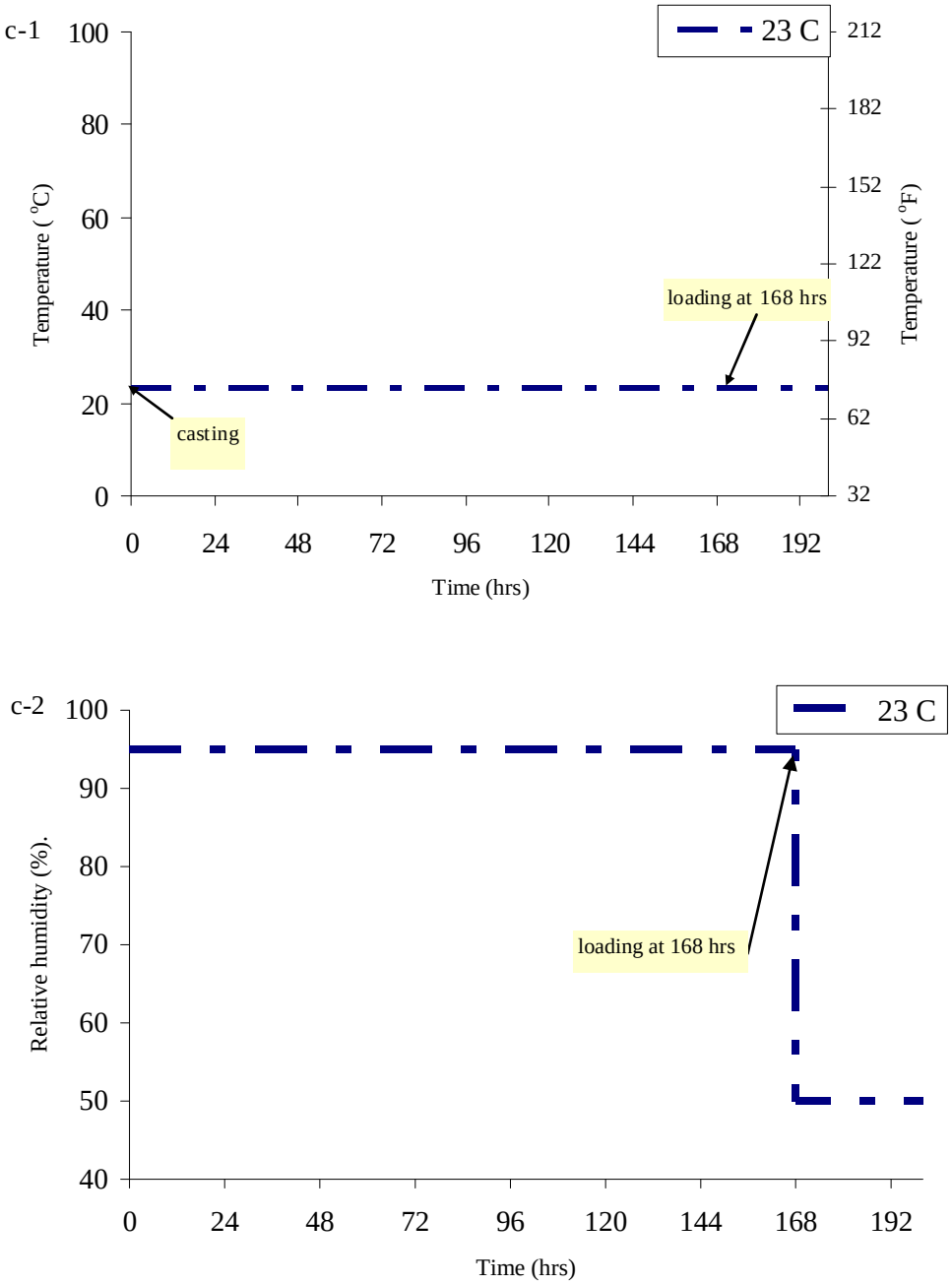

Figure 5.1 c: 23°C (73°F) curing regime

The 90°C regime followed UHPC manufacturer's recommended heat treatment at 90°C (194 °F) at 95% RH, starting at the age of 48 hours and continuing for 48 hours. The 60°C regime represented thermal curing conditions that can be achieved in most of US casting plants,

heat treatment applied at the age of 48 hours and continued for 72 hours at 60°C (140 °F) at 100% RH using steam curing. The third regime represented field curing at ambient temperature (i.e. 23°C (73°F)). Note that the total heat input applied during curing regime 2 (at 60°C) is equal to the manufacturer's recommended curing practice at 90°C.

5.5.2 Mechanical Properties

A summary of the compressive strength, tensile strength, modulus of elasticity in compression and tension, and Poisson's ratios in compression and tension is shown in Table 5.3. In addition, results from each test are separately presented and discussed in the following sections.

Table 5.3: Summary of 7-day mechanical properties of UHPC subjected to various curing regimes

Mixture ID	Compressive strength MPa (ksi)	Tensile strength MPa (ksi)		Modulus of Elasticity MPa (ksi)		Poisson's ratio	
		Splitting tension	Direct tension	E_c	E_t	υ_c	υ_t
D-2f-90C-40	169 (24.6)	22 (3.2)	10.3 (1.5)	47,950 (6,953)	57,470 (8,336)	0.14	0.20
D-2f-60C-40	148 (21.4)	19 (2.8)	9.7 (1.4)	50,870 (7,376)	58,060 (8,420)	0.16	0.18
D-2f-23C-40	116 (16.9)	16 (2.3)	7.5 (1.1)	44,900 (6,510)	56,810 (8,241)	0.14	0.16

5.5.2.1 Compressive strength

The compressive strength of UHPC was determined by testing 3 x 6-in (75x 150-mm) cylinders according to ASTM C 39. All compressive testing was performed in a SATEC MKIII 800 RD 3,558,580 kN (800 kip) capacity compression testing machine. Five specimens were

tested from each batch for each compressive strength measurement. All batches were tested at the ages of 7, 28, 90 and 365 days. Cylinder ends were machine finished.

Test results showed that the average 7-day compressive strengths of mixes D-2f-90C-40, D-2f-60C-40, and D-2f-23C-40 measured 169 (24.6), 148 (21.4), and 116 (16.9) MPa (ksi) respectively (Figure 5.2). Compared to the specimens with the 90^{o}C thermal treatment, that is a decrease of 12% and 31% in the 7-day compressive strength for the 60^{o}C (140^{o}F) and the 23 ^{o}C thermal treatment, respectively. The average 1-year compressive strengths of mixes D-2f-90C-40, D-2f-60C-40, and D-2f-23C-40 measured 176 (25.6), 153 (22.2), and 148 (21.5) MPa (ksi) respectively (Figure 5.2). This means that at the age of 1 year, the effect of eliminating thermal treatment was not as pronounced as at early ages. For example, a 16% relative reduction in compressive strength was measured at 1 year compared to a 31% decrease at 7 days. Figure 5.2 shows that with no thermal treatment mix D-2f-23C-40 continued to gain strength with time, particularly between 7 and 28 days, while no similar increase in the compressive strength was noticed for either of the thermally-treated mixes (i.e. D-2f-90C-40 and D-2f-60C-40). Results in Figure 5.2 show that 96%, 97%, and 78% of the 1 year compressive strength was achieved, respectively, after 7 days for mixes D-2f-90C-40, D-2f-60C-40, and D-2f-23C-40. The standard deviations at the earlier ages were higher than later ages, especially for thermally treated UHPC. It is proposed that this is probably due to some microstructural refinement or self-healing that occurred with time.

While these results follow the anticipated trends, they also provide an indirect quantitative measure of the effectiveness of thermal treatment regimes in refining the UHPC microstructure. It is presumably the decreased porosity and heterogeneity in the paste, imparted during thermal curing, that results in the greater early compressive strength. The development of

early high compressive strength is of particular importance to the precast prestressed girder industry where prestressing loads are typically desired to be applied as early as possible while minimizing prestressing loses due to creep and avoiding premature failure due to concentration of high compressive forces at the end of the prestressed girders.

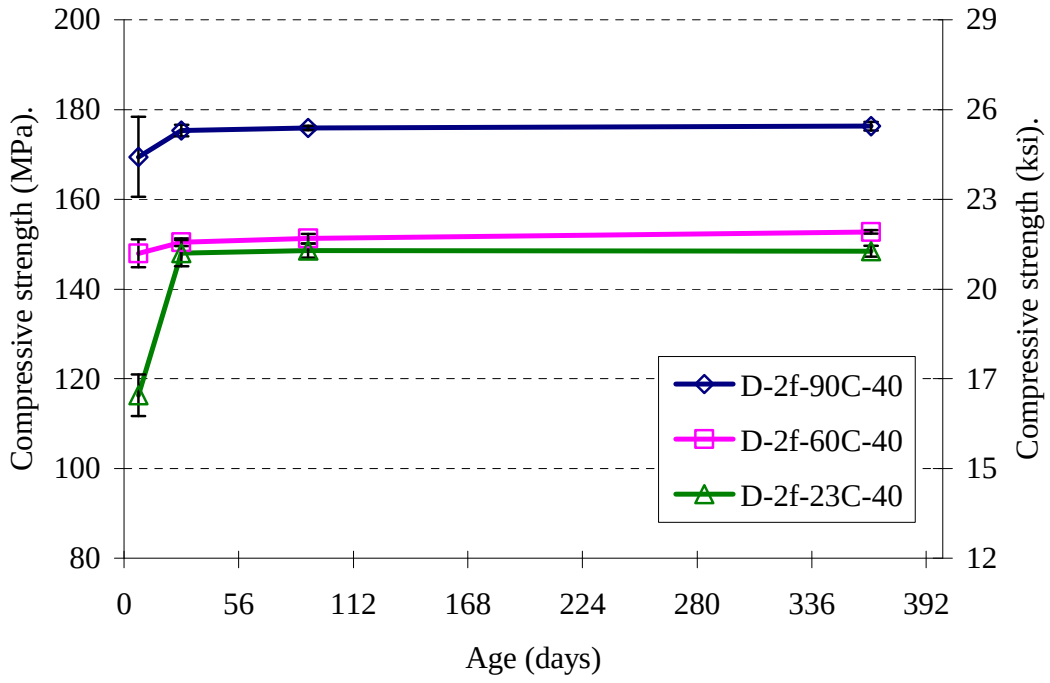

Figure 5.2 Compressive strength of different UHPC mixes

5.5.2.2 Tensile Strength

Two tensile strength tests, the splitting tension test and the direct tension test, were performed to characterize the tensile strength of UHPC. These were performed in addition to the modulus of rupture test (three-point bending) presented in Appendix A. The two tensile strength tests were performed with the aim of developing a correlation between them for UHPC. This is because of the relative ease in performing splitting tensile test compared to direct tension test. While it is strongly recommended by the author to perform direct tension tests, this correlation is

useful for design purposes when the true tensile strength of the material cannot be directly obtained from existing relationships for conventional concrete or due to the inability to perform direct tension tests.

5.5.2.2.1 Splitting tensile test [ASTM C496]

In the splitting tensile test, a compressive force is applied perpendicularly to the longitudinal axis of the cylinder. This force creates a nearly uniform tensile stress over the middle part of the vertical loading plane. As mentioned in Chapter 2, the tensile strength value calculated from the splitting tensile test is typically lower than the corresponding value obtained from a modulus of rupture test but also higher than values from the true tensile strength obtained from a direct tension tests [Mehta and Monteiro, 2005, and Graybeal, 2005].

Splitting tension tests were performed at the same ages as compression strength tests. All mixes were tested at the ages of 7, 28, 90 and 365 days using 75 x 150 mm (3x6-in) cylinders. Five split-tension specimens were tested from each mix.

Results showed that the average 7-day splitting tensile strength of mixtures D-2f-90C-40, D-2f-60C-40, and D-2f-23C-40 was 22 (3.2), 19 (2.8), and 16 (2.3) MPa (ksi), respectively (Figure 5.3). Compared to the 90°C cured specimens, the 60°C cylinders were 13% weaker and the 23°C cylinders were 27% weaker at 7-days. These relative decreases in measured 7-day tensile strength (compared to the recommended 90°C curing regime) are very close to those measured for compressive strength. The average 1-year splitting tensile strength for mixes D-2f-90C-40, D-2f-60C-40, and D-2f-23C-40 was 23 (3.3), 20 (2.8), and 17 (2.5) MPa (ksi), respectively. Results in Figure 5.3 show that 98%, 98%, and 91% of the 1 year split-tensile strength

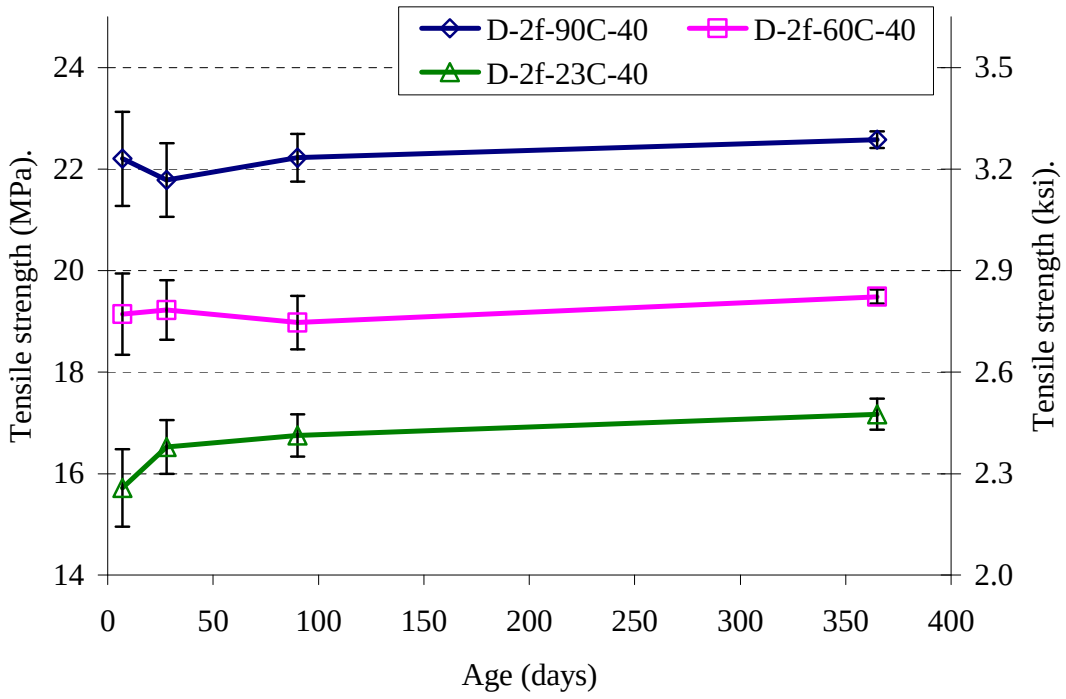

Figure 5.3: Tensile strength of different UHPC mixes obtained from splitting tension strength

was achieved, respectively, after 7 days for mixes D-2f-90C-40, D-2f-60C-40, and D-2f-23C-40. Similarly to the compressive strength results, this shows that the ambient cured samples showed the most relative strength gain over one year.

As it is typically the case in concrete, the splitting tension strength averaged about 12.7%, 12.8%, and 11.9% of the corresponding compressive strength values for mixes D-2f-90C-40, D-2f-60C-40, and D-2f-23C-40, respectively. The correlation between values obtained from the compressive strength and splitting tension test is plotted in Figure 5.4.

Comparing splitting tension strength results at 1 year to those at 7 days shows the relative insensitivity of the splitting tension test to the potential influence of varying curing regimes (and subsequent effects of the UHPC's microstructure) compared to the compressive strength test. It is believed that the primary underlying reason for this observation is the generation of localized high tensile stresses in the presence of local defects at the middle longitudinal section of the

specimens compared to the rest of the specimen. Although the splitting tension test assumes complete homogeneity of the material, which may not be the case in fiber-reinforced composites, the specimen is not sensitive to any defects or weaknesses unless they are located at highly stressed mid-plane section. In addition, the splitting tension test neglects the effect of the high compressive stresses generated at the top and bottom surfaces of the vertical plane, as well as neglecting lateral restraints provided by thin plywood bearing strips. Both should be overcome before the complete failure of the specimen. Therefore, the test should be regarded as an indirect measure of the actual tensile strength and often provides an overestimate.

5.5.2.2.2 Direct tension test

Direct tension tests were performed using a newly developed dog bone test specimen that is 235 mm (9.25-in) in length and has a reduced cross section of 50x50 mm (2x2-in) through the mid-length. The full details of the test setup are presented in Chapter 4. Two 1.2-in (30 mm) long electrical resistant strain gages were attached on two opposite sides of the specimen. These two strain gages were connected in a half bridge configuration in order to measure longitudinal strains during the tension test. In addition, two other perpendicular strain gages were attached on the same two opposite sides of the specimen as the longitudinal gages to measure transverse strains.

Three samples from each mix were tested at the age of 7 days. Tensile strength values obtained from the direct tension tests were used to calculate loads for tensile creep tests.

Test results showed that the average 7-day tensile strength of mixtures D-2f-90C-40, D-2f-60C-40, and D-2f-23C-40 were 10.3 (1.5), 9.7 (1.4), and 7.5 (1.1) MPa (ksi), respectively. Compared to the 90°C cured specimens, the 60°C cylinders were 6% weaker and the 23°C cylinders were 27% weaker at 7-days.

5.5.2.2.3 Comparing direct tension test to splitting tension Test

Results from splitting and direct tension tests were compared. The ratio between tensile strength obtained by the splitting tension test to the tensile strength obtained by the direct tension test ranged between 2.0 and 2.3 with an average value of about 2.14. Similar relationships were also found by Graybeal [2005] for UHPC. The relationship between the two tests is shown in Figure 5.6. Comparing these test results was of specific importance as it allows the prediction of direct tensile strength by conducting the relatively simpler standardized splitting tension test. However, the large magnitude of the differences between splitting and direct tension tests results obtained, with splitting tension test overestimating the actual tensile strength, emphasizes that splitting tension strength cannot be used for structural design purposes. It is believed that direct tension tests are more accurate than any splitting tension tests as they provide enough sensitivity to any defects throughout the tests specimen. Results obtained for both tests also showed that the standard deviation of the direct tension strength was generally larger than that of splitting tension strength. Also, at the age of 7 days, standard deviation for both tensile strengths was higher than the compressive strength. These differences in standard deviation values between different tests show that the direct tension test is the most sensitive test among the three tests to microstructural defects, while the splitting tension test is the least sensitive. Also, most of the compressive strength data were obtained from 5 specimens versus only 3 specimens for tension strength. It is then suggested that additional replicates be tested in tension for each case in future testing. Standard deviation for both tensile and compressive strengths was smaller at later ages compared to 7 days, further suggesting that microstructural refinement occurs during this period.

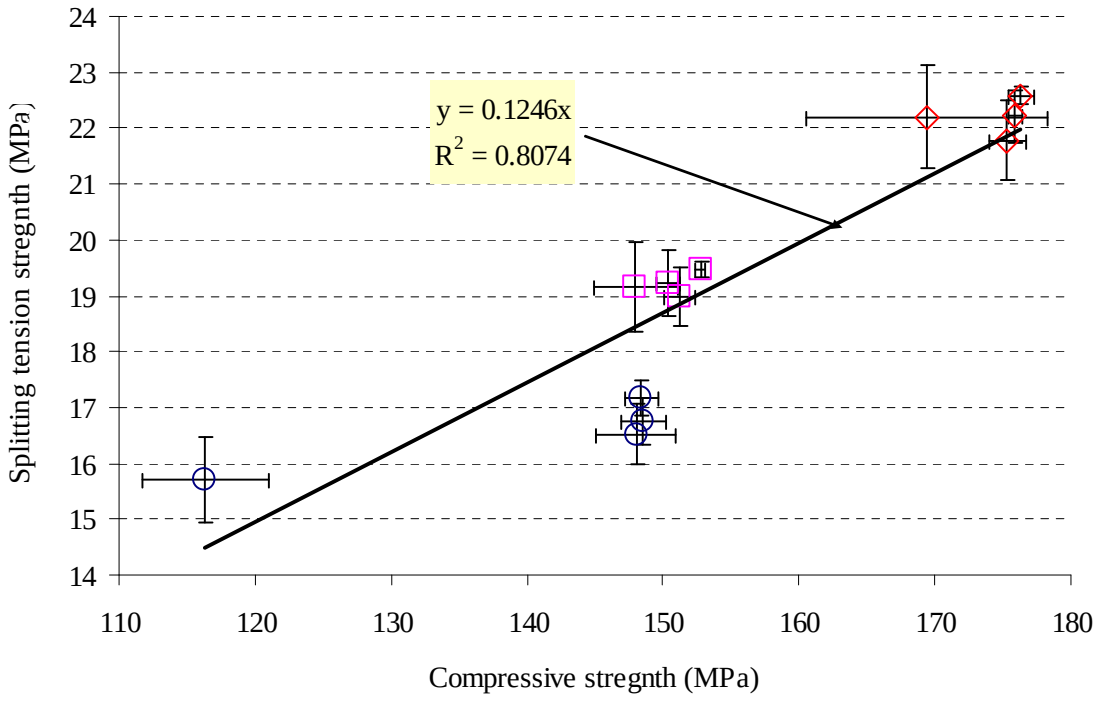

Figure 5.4: Correlation between compressive and splitting tension strengths

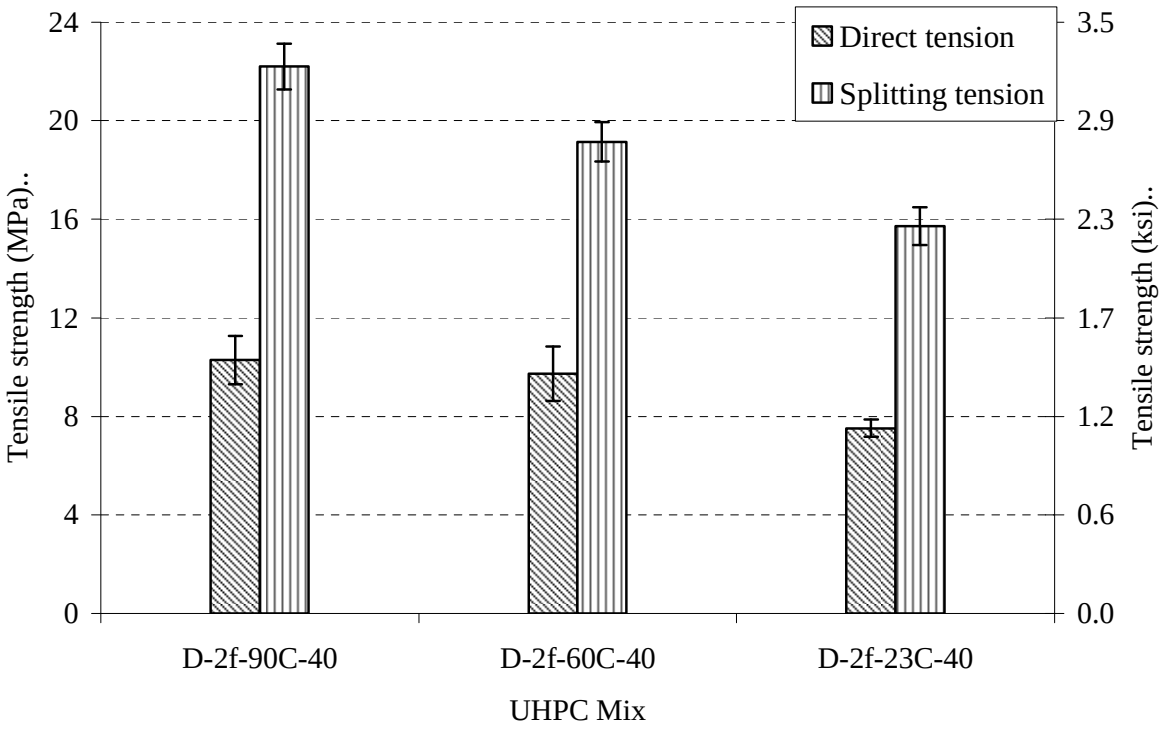

Figure 5.5: Direct tension and splitting tension test results for different UHPC mixes at 7 days

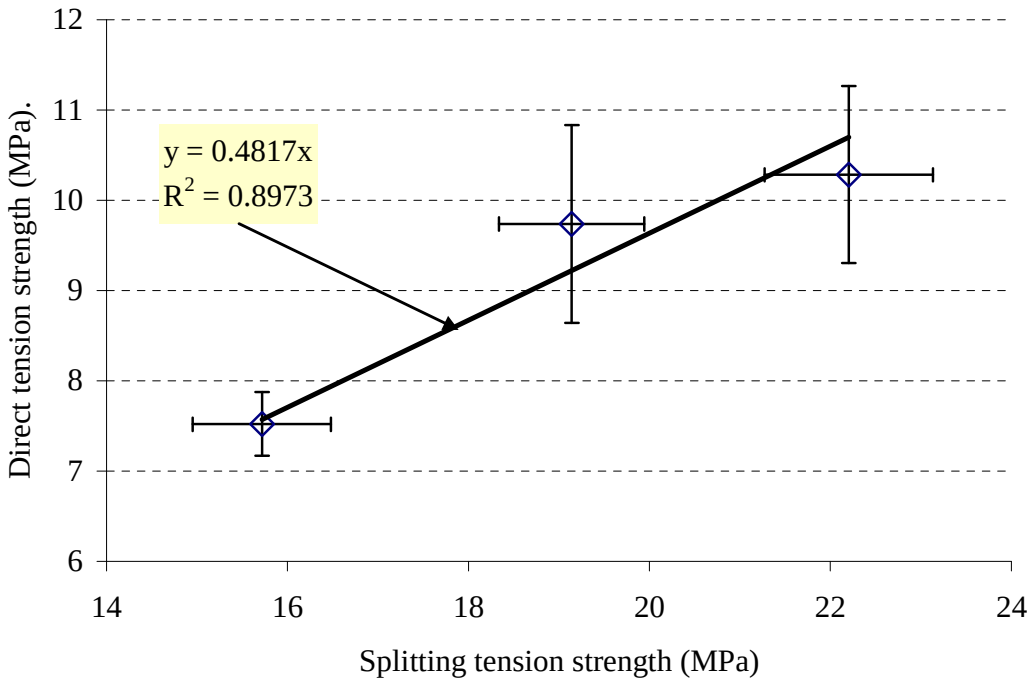

Figure 5.6: Comparison between splitting tension and direct tension strengths at 7 days

5.5.2.3 Modulus of Elasticity

The Young's modulus of elasticity and the Poisson's ratio were determined for each mix both in compression and tension using three specimens at the age of 7 days. In compression, the chord modulus of elasticity was measured using 4x8-in (100x200-mm) cylinders loaded in compression. The tests were run in an SATEC Baldwin 400 BTE 400 kip (1,800,000 kN) universal testing machine. More details about the test setup are presented in Chapter 4. The compressive and tensile stress-strain behaviors are shown in Figures 5.7 and 5.8. These two figures show that the stress-strain behavior of UHPC was linearly elastic up to 40% of the ultimate strength. The chord modulus in compression was calculated between 50 and the strain at 40% of the ultimate per ASTM C 469 standard. In tension, the chord modulus was calculated starting between about 20με and the strain at 40% of ultimate.

The average 7-day compression modulus of elasticity measured 47,950 (6,953), 50,870 (7,376), and 44,900 (6,510) MPa (ksi) for mixes D-2f-90C-40, D-2f-60C-40, and D-2f-23C-40, respectively (Figure 5.9). These modulus values are twice as much as normal strength concrete. These values of elastic modulus agree to a great extent with the values obtained by Graybeal [2005] for UHPC for similar mixes subjected to similar thermal treatment conditions prior to testing (i.e. average of 52,130 (7,560) MPa (ksi) for thermally treated UHPC at 90^{o}C and 39,033 (5,660) MPa (ksi) for non-thermally treated UHPC). Analysis of variance (ANOVA) was conducted and showed that the difference between the modulus of elasticity values for mixes D-2f-60C-40 and D-2f-23C-40 were significantly different while the difference between mixes D-2f-90C-40 and D-2f-60C-40 and mixes D-2f-90C-40 and D-2f-23C-40 are not significantly different.

Figure 5.10 shows the Poisson's ratios obtained for the three mixes considered, Poisson's ratio values in compression ranged from 0.15 to 0.16. These values are in the range for ordinary concretes [Mehta and Monteiro, 2005].

In tension, test results showed that the average 7-day modulus of elasticity was 57,470 (8,336), 58,050 (8,420), and 56,810 (8,241) MPa (ksi) for mixes D-2f-90C-40, D-2f-60C-40, and D-2f-23C-40, respectively (Figure 5.9). These values averaged 20% higher than the values obtained in compression. This is likely due to the difference in fiber distribution and orientation between the tension and compression specimens. In tension specimens, UHPC was cast from one end to the other, possibly causing the fibers to be more longitudinally aligned. This was not the case for compression test specimens where UHPC was poured from the top, resulting in a more random fiber orientation. Also, the shape and dimensional differences between the two sets of test specimens may have caused alignment in the narrower tension specimens.

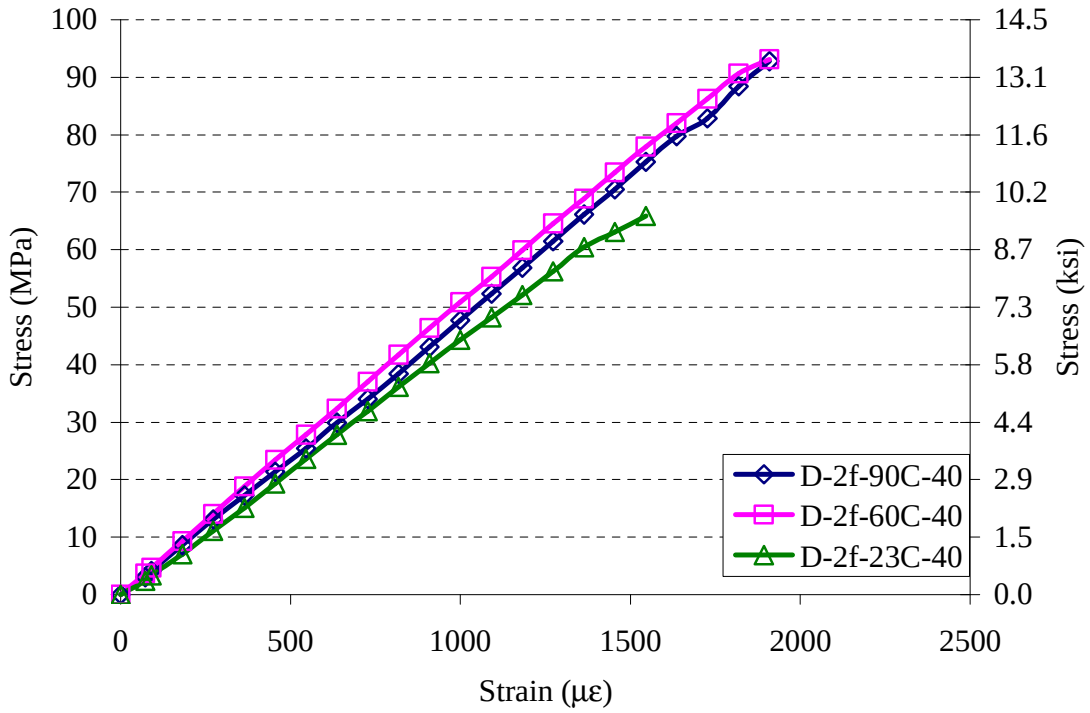

Figure 5.7: Compressive stress-strain behavior of different UHPC mixes

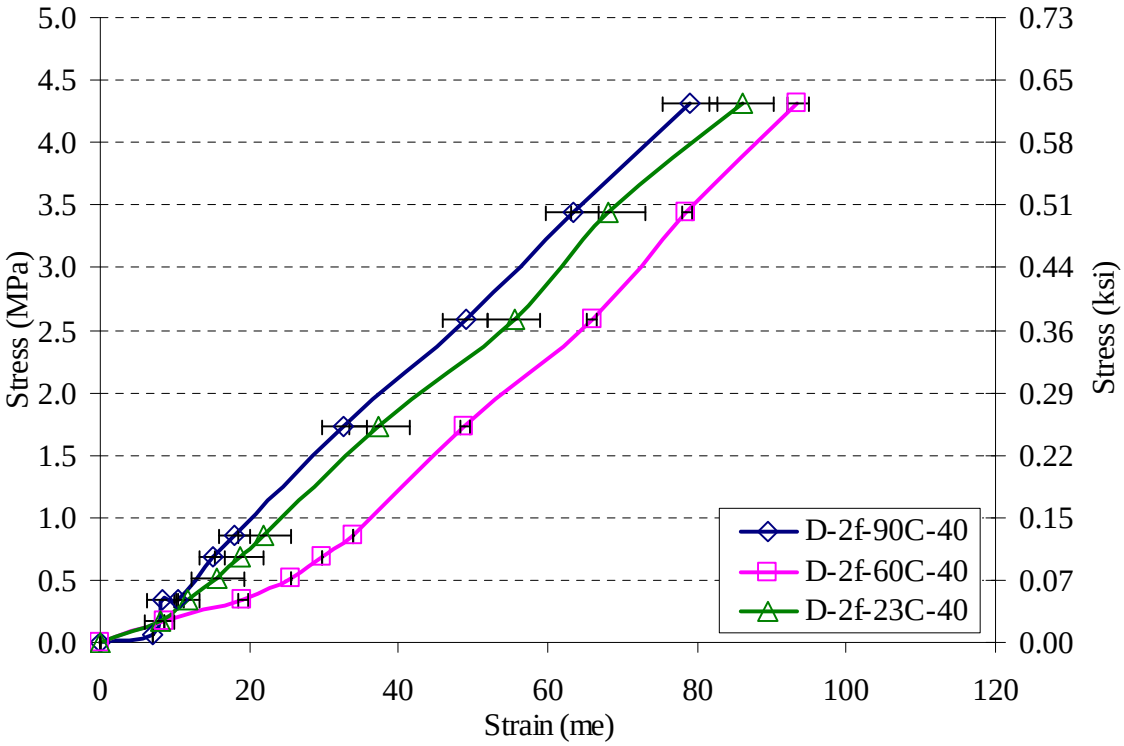

Figure 5.8: Tensile stress-strain behavior of different UHPC mixes

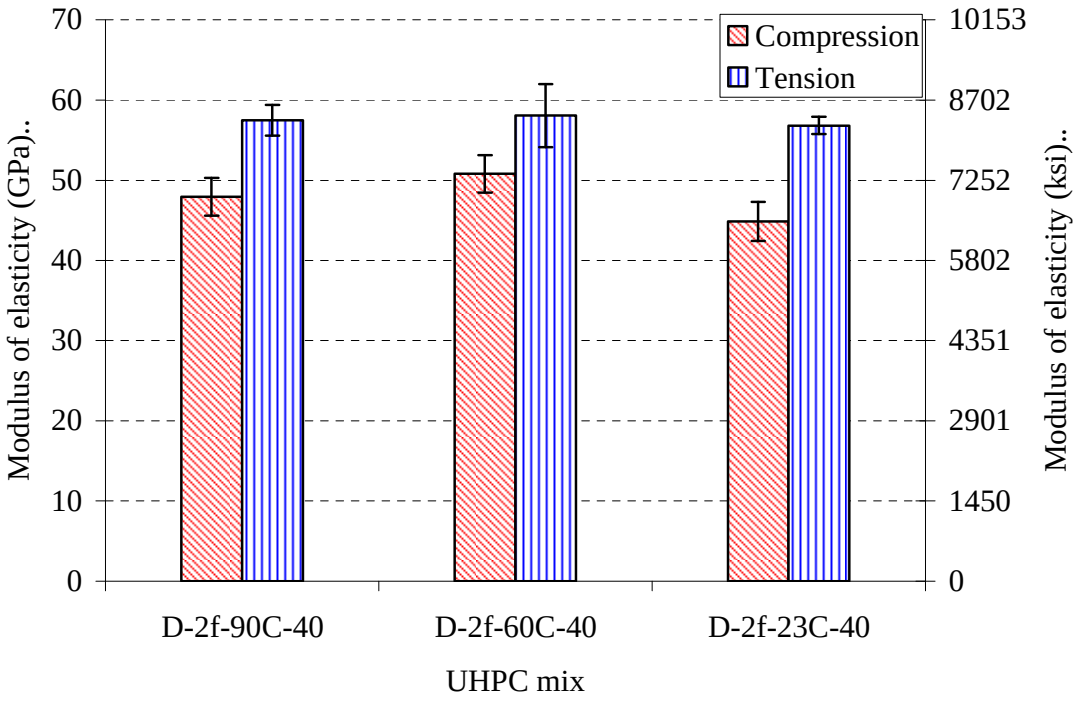

Figure 5.9: Compression and tension modulus of elasticity for different UHPC mixes

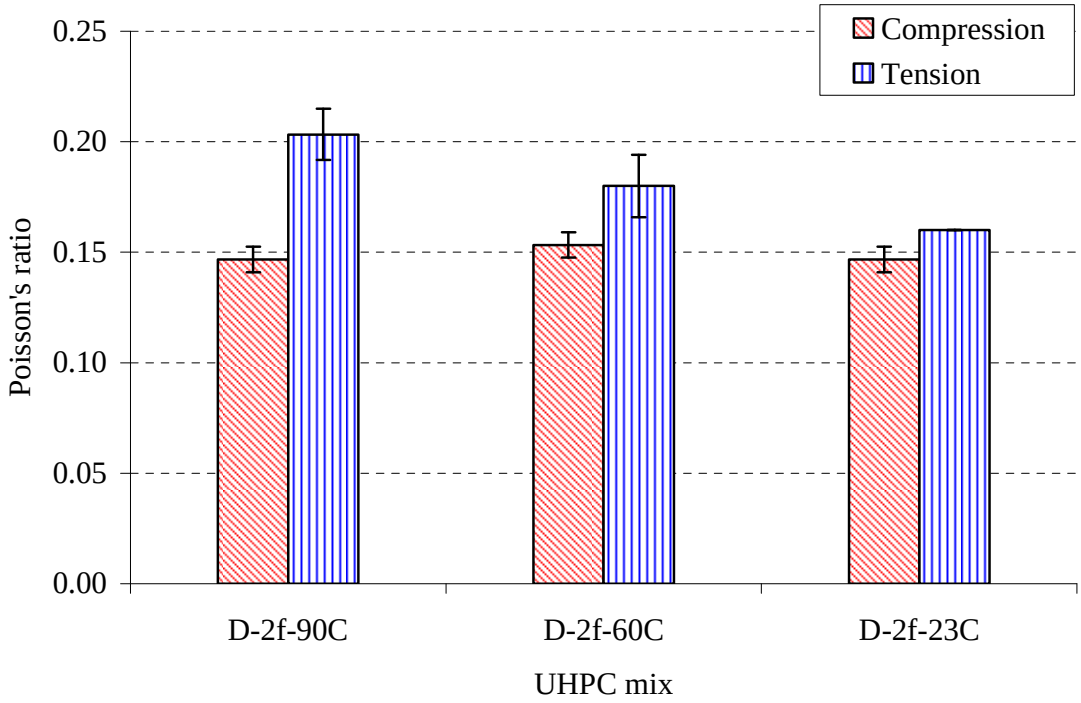

Figure 5.10: Compression and tension Poisson's ratio of different UHPC mixes

In addition, the elastic modulus of the fibers is likely a bigger contributor in tension than in compression. That is, fibers are more fully engaged, since cracks will occur at fairly low strains in tension in the matrix. The effect of fiber orientation on the relative tensile to compressive modulus of elasticity is considered in Chapter 6.

Figure 5.10 shows the Poisson's ratios obtained for the three mixes considered. Poisson's ratio values ranged from 0.15 to 0.16 in compression, with little variation between the different curing regimes. In tension, Poisson's ratio values varied from 0.16 to 0.20 and generally increased with the increasing temperature of thermal treatment. Overall, these values are typical for those found in ordinary concrete and high strength concrete, where Poisson's ratio typically measures between 0.15 and 0.20, with higher strength concrete typically having Poisson's ratio toward the lower end of this range [Mehta and Monteiro, 2005]. Here, it is proposed that randomly oriented fibers may also provide lateral restraint, contributing to relatively lower Poisson's ratio in the UHPC compression cylinders compared to the tensile strength specimens. Results discussed later in Chapter 6 for mix with no fibers gave an average Poisson's ratio of 0.155 and 0.19 in compression and tension, respectively. These values are on the higher side of the values reported for the three mixes reported in this chapter and are likely due to lack of fiber restraints. A summary of the mechanical properties of UHPC mixes investigated is shown in Table 5.3. The difference between the Poisson's ratio in compression and tension of non-fiber reinforced UHPC suggests that other factors may be responsible of this difference in addition to fiber orientation. These factors may include shape and size effects.

5.5.3 Tensile Creep of UHPC

5.5.3.1 Tensile creep samples

All specimens were cast according to procedures recommended by the UHPC manufacturer. First, the dry premix was mixed in an 85-liter capacity high shear mixer (Erich Model R 08 W), Figure 5.11, at 30-35 rpm for two minutes to break apart any clumps that might exist. This mixing speed was maintained over the entire mixing process. Water and half of the HRWR were mixed and then added slowly to the dry premix over a period of two minutes. These constituents, once combined, were mixed for one minute. The other half of the HRWR was then added over a period of 30 seconds, and mixing continued until the "turning point" was reached. The turning point is defined as the point at which the UHPC mix turns from clumps into a flowable, uniform paste. Finally, and once the turning point was reached, fibers were added over a two-minute period, and mixing continued for another one to two minutes to ensure good fiber dispersion.

Three tensile creep 75x75x483 mm (3x3x19-in) concrete prism specimens connected in series, and three companion free shrinkage specimens of the same dimensions were used for each testing case. After initial curing or initial curing plus thermal treatment, previously discussed mechanical tests were performed immediately before the start of creep tests at age of 7 days.

5.5.3.2 Tensile creep test

The tensile creep test setup and procedure used in the long-term study is discussed in detail in Chapter 4. At the age of 7 days, tensile creep tests were started on three replicate specimens from each mix. All samples were loaded at 40% of their measured direct tensile strength at 7 days. Conditions were kept at $23^{o}C \pm 2^{o}C$ ($73^{o}F$) and 50 ± 3% RH for the entire testing period. Tensile creep deformations were measured initially at 1, 2, 4, 6, and 24 hours after

loading. Subsequently, measurements were made daily for one week, weekly for a month, and monthly for a year. Two prisms identical to the creep specimens were stored adjacent to the creep specimens and were used to measure drying shrinkage. Strain data were collected at the same times as creep data. Specific creep was calculated by dividing the adjusted tensile creep strain by the initial applied stress. The adjusted tensile creep strain, also termed just creep strain, is equal to the algebraic sum of the measured total creep strains and the free shrinkage strains.

Figure 5.11: Erich shear mixer used for mixing UHPC mixes

5.5.3.3 Results and discussion

Figures 5.12 and 5.13 show the measured free shrinkage, adjusted creep strain, and specific tensile creep of UHPC where the influence of varying thermal treatment was examined for a period of one year. A summary of the key results is presented in Table 5.4.

Results from the long-term study show the significant influence of the curing conditions prior to loading on the tensile creep and shrinkage performance of UHPC. Compared to UHPC thermally-treated at 90°C for 48 hours, thermal treatment at 60°C for 72 hours prior to loading resulted in a 10% and 13% increase in the creep strain and the specific tensile creep, respectively. Also, eliminating thermal treatment resulted in a 107% and 172% increase in the creep strain and the specific tensile creep compared to UHPC thermally-treated at 90°C for 48 hours prior to loading.

Compared to UHPC thermally-treated at 90°C for 48 hours, free shrinkage results showed an increase of 28% and 260% in the free shrinkage strain with thermal treatment at 60°C for 72 hours and eliminating thermal treatment, respectively, after 1 year of drying

Table 5.4: Summary of tensile creep and shrinkage properties of UHPC at 1 year

Mix	Strains at 1 year		Specific tensile Creep at 1 year	% change of specific from D-2f-90C-40 at 1 year	
	Adjusted creep (με)	Free shrinkage (με)	με/MPa (με/ksi)	Tensile creep strain	Specific tensile creep
D-2f-90C-40	219	82	54 (372)	N/A	N/A
D-2f-60C-40	252	105	64 (443)	+15	+18
D-2f-23C-40	529	296	176 (1,216)	+141	+220

While the tensile creep of UHPC has not been previously investigated, the tensile creep behavior of UHPC from this study is compared to tensile creep data reported in the literature for other concrete types. In a study by Bissonnette and Pigeon [1995], six concrete mixes that varied in w/cm, silica fume content, curing period, and steel fiber content were subjected to tensile creep testing. Here, only the fiber-reinforced, unsealed mixes will be considered for comparison

with UHPC. Results from the Bissonnette and Pigeon study showed that the specific creep for steel-fiber reinforced concrete at 40 days ranged from 150 (1,035) to 190 (1,311) με/MPa (με/ksi) for concrete reinforced with macro [16 mm (0.63-in)], and micro [3 mm (0.12-in)] fibers respectively. In their study the water-to-cement ratio was 0.55 and the compressive strength at the time of loading ranged from 20 to 30 MPa (2.9-4.4 ksi). These values were obtained at stress levels that varied from about 28% to 34% at the time of loading while results from the current UHPC study were obtained at 40% stress level. The current results show that the specific creep for UHPC at 40 days is about 55 (382) με/MPa (με/ksi), 65 (451) με/MPa (με/ksi), and 125 (868) με/MPa (με/ksi) for mixes D-2f-90C-40, D-2f-60C-40,and D-2f-23C-40 respectively; that is, the specific tensile creep of non-thermally treated UHPC was 17% to 35% lower than fiber reinforced mixes tested by Bissonnette and Pigeon [1995]. Also, specific tensile creep of thermally treated UHPC was about 56% to 71% less than fiber reinforced mixes tested by Bissonnette and Pigeon [1995]. In another study by Bissonnette et al. [2007], specific creep of HPC concrete reinforced with 0.5% (volume fraction) of hooked fibers, a w/cm of 0.40, and loaded at 34% of its strength at 7 days was found to be about 135 (939) με/MPa (με/ksi) at 42 days of loading. That is, specific creep of UHPC mixes D-2f-90C-40, D-2f-60C-40, and D-2f-23C-40 was 60%, 52% and 8% lower compared to the mix tested by Bissonnette et al. [2007].

The significant reductions in tensile creep found for UHPC compared to other fiber-reinforced ordinary and high strength concretes mixes in the literature can be mainly attributed to the nano/microstructural improvements achieved in UHPC mixes through particle packing optimization in addition to thermal treatment (for those mixes which were cured in this manner). Larger differences in specific creep of non-thermally treated UHPC, mix D-2f-23C-40 and concretes tested in the literature were expected. The relative closeness of tensile creep results

between the current non-thermally treated UHPC and Bissonnette et al. [2007] can be in part attributed to the increased amount of fibers (i.e. 2% by volume) and silica fume content in UHPC relative to other concretes. The incorporation of fibers, especially straight or hooked fibers, in non-thermally treated concretes has been previously shown to increase tensile creep, due to the possible formation of a weak and porous interfacial zone around the fibers [Bissonnette and Pigeon, 1995, and Bissonnette et al., 2007]. In the current study, straight fibers were used at 4x the doze of hooked fibers used by Bissonnette et al. [2007]. The increase in tensile creep upon increasing the amount of silica fume found in the literature may be due to the formation of additional calcium silicate hydrate, C-S-H, which is the main creeping phase in a cementitious matrix. Also, silica fume particle are mainly spherical and thus, if unreacted or partially reacted, might facilitate viscoelastic deformations in the cementitious matrix. In addition, reduction in workability caused by incorporating silica fume might have caused decrease in workability that would increase the overall void ratio of concrete. While the specific influence of silica fume on creep will require further investigation, overall these prior observations suggest that deformations at the fiber-matrix interfacial zone could play an important role in the tensile creep performance of UHPC.

The effect of the fiber-paste interface on the tensile creep behavior of concrete was first suggested in a recent study Bissonnette et al. [2007]. In this study, the effect of fiber reinforcement on tensile creep, using 0.50% volume fraction of hooked fibers resulted in an increase of about 30 to 35% in tensile creep when compared to the non-reinforced mixes, while the same dosage of crimped fibers lead to a reduction of 30 to 35% in the tensile creep. However, doubling the dosage of crimped (wavy in shape) fibers resulted in increase in tensile creep. As a

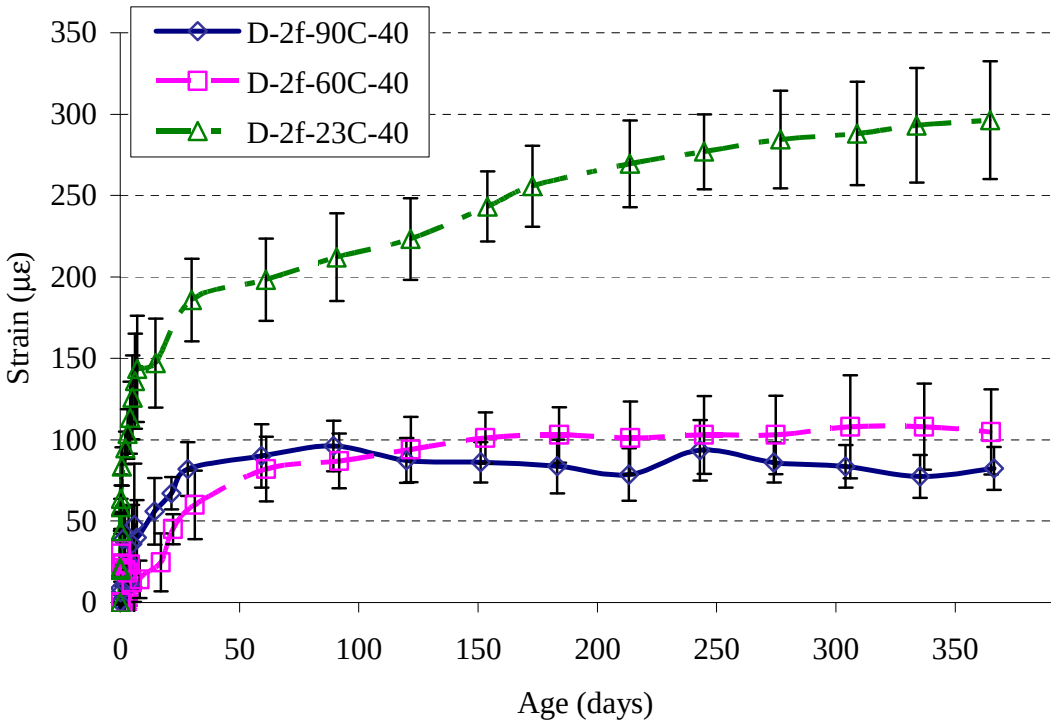

Figure 5:12: Effect of thermal treatment on free shrinkage strain of UHPC

result, the authors suggested that an important part of the creep deformations could be taking place in the more porous paste-fiber interfacial areas. This means that the influence of fiber reinforcement on tensile creep is a balance between their restraining effect and the viscoelastic properties of the surrounding cement paste, which can be negatively influenced by increased porosity and microcracking at the fiber/paste interface. The balance between these two counteracting effects may explain the initial reduction in tensile creep upon using 0.50% of crimped fibers and later the increase in tensile creep upon doubling the dosage of crimped fibers. On the other hand, it was noticed that the increase in tensile creep was more pronounced upon using hooked fibers compared to crimped fibers; this is probably because crimped fibers provided more friction and wedging in the fiber/matrix interface compared to hooked fibers.

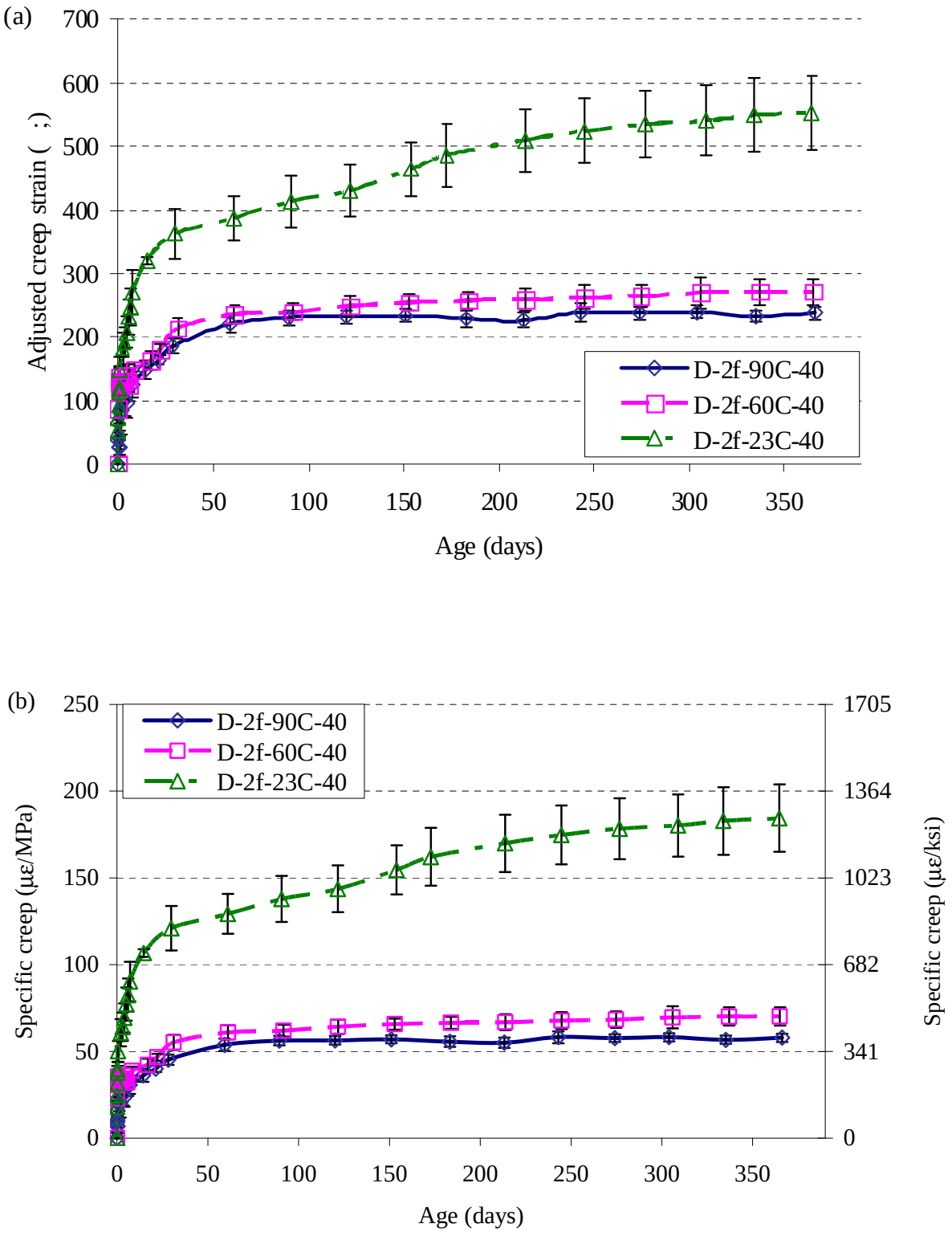

Figure 5:13: Effect of thermal treatment on: (a) adjusted creep strain and (b) specific tensile creep

However, no experimental or model-based evidence was provided to support this hypothesis by Bissonnette et al. [2007].

Based on the mean values reported in Tables 5.3 and 5.4, the effect of thermal treatment was more pronounced on the tensile creep deformation than in the tensile strength. For example, a 173% increase occurred in specific creep versus a 27% decrease in tensile strength upon eliminating thermal treatment. This observation underscores that tensile creep testing, rather than tensile strength values at the time of loading, should be used to predict long-term tensile performance. It is proposed that the ability of pre-existing cracks to coalesce and propagate during long-term creep testing rather than short-term strength test likely plays an important role in the difference between creep results and tensile strength results.

From a practical point of view, long-term tensile creep results obtained in this study along with the mechanical properties results detailed in previous sections suggest that the magnitude of thermal energy applied to UHPC is a more critical factor in developing the microstructure than the method in which this energy is applied, so long as the thermal treatment is applied beginning 2 days after casting in this case. This observation is of specific practical importance as it suggests that satisfactory UHPC mixes can be achieved at moderate thermal treatment temperatures that can be reached in most of the existing concrete precasting facilities. This observation emphasizes also the dependency of maturity on temperature and the dependency of tensile creep on the maturity level of concrete at the time of loading. The effect of relative maturity of the mixes investigated in the current study is discussed below.

Maturity is typically expressed using the equivalent age concept. Equivalent age is defined as the age at a constant standard temperature that results in the same relative strength that

actual temperature conditions produce. Equation 5.1 shows equivalent age when using Arrhenius dependency on temperature [Carino, 1984]:

$$t_e = \sum_i \exp\left\{\frac{-E}{R.\left(\frac{1}{T(\Delta t_i)} - \frac{1}{T_s}\right)}\right\}\Delta t_i \qquad (5.1)$$

where:

t_e : the equivalent age (days)

E : the apparent activation energy

R : gas constant, 8.3145 J/ g mol/ ^{o}K (1.9859 Btu/ lb mol/ ^{o}R)

T : temperature during the interval Δt_i (^{o}K)

Δt_i : period of time at temperature T

T_s : standard temperature taken as 23^{o}C (73^{o}F) in north America (296 ^{o}K).

UHPC typically contains high volumes of cementitious materials, low water-to-cementitious material ratio, and finer (rapid hardening) cement, all of which will result in acceleration of cement hydration. Fast hydration can lead to significant increase in temperature during the first hours after casting. Moreover, rise in temperature due to thermal treatment accelerates the hydration of the cementitious materials, thus generating more heat. As a result, an increase in the equivalent age (maturity) of UHPC is expected, especially in the case of thermally treated UHPC.

The dependence of creep on maturity has been known [Neville and Dilger, 1970]. However, the CEB-FIP creep model, [CEB/FIP, 1990 and CEB/FIP, 2001] is the only published creep model that explicitly provides expressions to incorporate the temperature history at the time of loading [Lopez, 2005].

$$t_e = t_{0,T}.\left(\frac{9}{2+t_{0,T}^{1.2}}+1\right)^{\alpha} \geq 0.5 \tag{5.2}$$

$$t_{0,T} = \sum_i \Delta t_i.\exp-\left\{\frac{4000}{273+T(\Delta t_i)}-13.65\right\} \tag{5.3}$$

where:

t_e: equivalent age (days) to be used in Equations 5.4 to 5.7

$t_{0,T}$: temperature adjusted age (days)

$T(\Delta t_i)$: temperature during the interval Δt_i (^{o}C)

Δt_i: period of time at temperature T (days)

α: parameter depending on the type of cement (-1 for slowly hardening cement, 0 for normal and rapid hardening cement, and 1 for rapid hardening high strength cement).

Several of the most used empirical models for creep include age of loading (rather than maturity) among their input variables, where it is commonly included as a multiplier to the ultimate creep value. The following expressions have been proposed to account for the influence of age on creep:

ACI-209 [1997]

$$F'(t') = \begin{cases} 1.25/(t'^{0.118}) \text{for moist curing} \\ 1.13/(t'^{0.094}) \text{for steam curing} \end{cases} \tag{5.4}$$

AASHTO-LRFD [2004]

$$F'(t') = 1.25/(t'^{0.118}) \text{for moist curing} \tag{5.5}$$

CEB-FIP [2001]

$$F'(t') = 1.25/(1+t'^{0.20}) \quad (5.6)$$

Sakata [1993]

$$F'(t') = \frac{1}{\left[\ln(t')\right]^{0.67}} \quad (5.7)$$

where:

F′(t′): age-of-concrete-at-loading multiplier

t′: age of concrete at loading (days)

Figure 5.1 shows that the complete temperature history prior to loading of the three UHPC considered in this study. The internal temperature of concrete was assumed to be the same as the temperature in the curing environment; this assumption is reasonable given the limited size of the sample and precision in controlling the environmental temperature. Table 5.5 presents the equivalent age as calculated from the temperature history of each mixture and stage using Equations 5.2 and 5.3 and assuming rapid hardening cement.

Results in Table 5.5 and Figure 5.14 show a clear inverse relationship between the maturity at the time of loading and the ultimate tensile creep achieved. Also, results in Figure 5.14 show that the sensitivity of tensile creep to maturity decreased as thermal treatment was varied from 60^{o}C (140^{o}F) to 90^{o}C (194^{o}F). This reduction in sensitivity is evident as a pronounced reduction in slope between the two thermally-treated systems compared to the slope between the non-thermally treated UHPC and UHPC thermally treated at 60^{o}C (140^{o}F). This observation has an important practical impact as it allows for modifying the method of thermal treatment by decreasing the maximum temperature and increasing the treatment time to achieve satisfactory long-term tensile performance.

In summary, thermal treatment of UHPC whether at 90°C (194°F) for 48 hours or 60°C (140°F) for 72 hours had a comparable but significant impact on the short-term mechanical properties of UHPC; namely, tensile and compressive strengths and moduli of elasticity were

Table 5.5: Maturity adjusted ages of UHPC at the time of testing (7 days)

Mix	Temperature adjusted age at 7 days (days)	Equivalent age at 7 days (days)
D-2f-90C-40	33.94	38.26
D-2f-60C-40	20.12	24.80
D-2f-23C-40	8.02	13.11

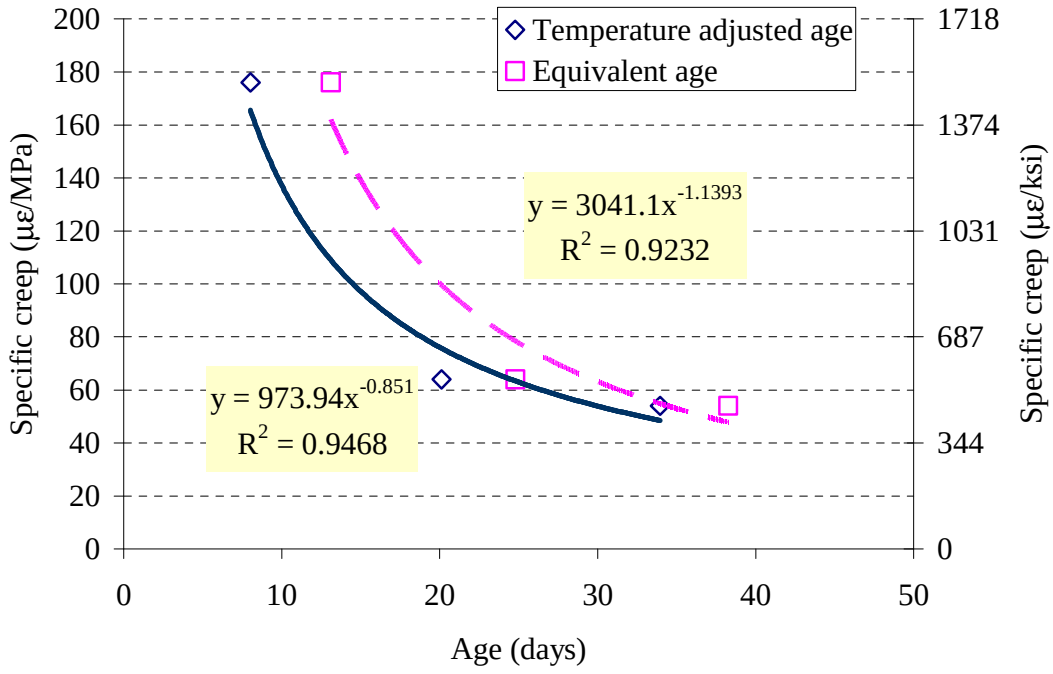

Figure 5:14: Correlations between the ultimate tensile creep after 1 year and the maturity level of UHPC at the time of loading

higher than for specimens with no thermal treatment. More pronounced effects were observed, however, in the long-term tensile creep reductions due to increased maturity of thermally treated UHPC at the time of loading compared to non-thermally treated UHPC. Results showed that both short-term mechanical properties and long-term tensile creep behavior of UHPC thermally treated at 60^{o}C (140^{o}F) for 72 hours matched to a great extent UHPC treated at 90^{o}C (194^{o}F) for 48 hours. This result has an important practical impact as the lower 60^{o}C temperature will facilitate using current precast facilities to produce UHPC without modification.

5.5.4 Compressive Creep of UHPC

Very few published studies considered compressive creep of UHPC [Graybeal, 2005 and Burkart and Muller, 2008]. To confirm these prior results, to examine the influence of curing regimes on compressive creep, and to allow comparisons between tensile and compressive creep behaviors of UHPC, this investigation included compressive creep testing. In the following sections, results of the compressive study are presented first, and then a comparison between the tensile and compressive creep performances of UHPC is made. The proposed mechanisms for tensile creep of UHPC are presented in section 5.7.

5.5.4.1 Compressive creep samples and test

Compressive creep of each UHPC mix shown in Table 5.1 was measured on three 100x380 mm (4x15-in) cylinders according to ASTM C 512 specifications. The size of the specimens used in this study is different from the ASTM C 512 standard (150x300 mm (6x12-in)). This modification was necessary due to the strength of UHPC which dictated reducing the cross section of the test specimens. Three additional non-loaded companion specimens were used to measure free shrinkage. Both compressive creep and shrinkage specimens were poured

horizontally from one end to the other resulting in a similar fiber alignment like tensile creep specimens. All cylinders were instrumented with four sets of steel inserts located diametrically opposite on the surface of each specimen. Each set of inserts had a 10-in (254-mm) long gauge length for measuring deformation with a detachable mechanical gauge (DEMEC gauge). Specific creep was calculated by dividing the adjusted compressive creep strain by the initial applied stress. The adjusted compressive creep strain was calculated by subtracting the shrinkage strain from the measured creep strains and the free shrinkage strains.

Each mix was cured and/or thermally treated as the tensile creep specimens were; compression and tensile specimens were cast from the same batch. Before the creep tests started, compressive strength and modulus of elasticity tests were performed for each mix. Compressive creep tests started at the same ages as tensile creep tests (i.e. at the age of 7 days). The cylinders used in compressive creep here had the same surface area-to-volume ratio, 1, as the cylinders used by Graybeal [2005] (i.e., 100x200 mm (4 x 8-in) cylinders which had a 150 mm (6-in) gage length). Graybeal [2005] also used a DEMEC gage to measure deformations.

5.5.4.2 Results and discussion

Figures 5.15 and 5.16 show the measured free shrinkage, adjusted creep strain, and specific compressive creep where the influence of varying thermal treatment was examined for a period of one year. A summary of the key results is presented in Table 5:6.

Results from the long-term study showed a significant influence of the curing conditions prior to loading on the shrinkage and compressive creep performance. Compared to UHPC thermally-treated at 90^{o}C for 48 hours, thermal treatment at 60^{o}C for 72 hours prior to loading resulted in a 10% and 24% increase in the creep strain and the specific compressive creep, respectively. Also, eliminating thermal treatment resulted in a 81% and 163% increase in the

creep strain and the specific compressive creep compared to UHPC thermally-treated at 90^{o}C for 48 hours prior to loading. These percentage increases in specific compressive creep upon altering the thermal treatment regime or eliminating thermal treatment were much larger than decreases in compressive strength resulting from either modification. That is, thermal treatment of fiber reinforced UHPC at 60^{o}C for 72 hours prior to loading resulted in a 12% decrease in compressive strength while eliminating thermal treatment of UHPC resulted in a 31% decrease in compressive strength compared to UHPC thermally-treated at 90^{o}C for 48 hours prior to loading.

In addition, free shrinkage results showed an increase of 28% and 266% in the free shrinkage strain after 1 year of drying with thermal treatment at 60^{o}C for 72 hours and eliminating thermal treatment compared to UHPC thermally-treated at 90^{o}C for 48 hours.

In a study by Graybeal [2005, Appendix B], a mix very similar to D-C-2f-90C-40 was investigated at a 41% stress level but loaded at 4 days, rather than at 7 days as in the current study. After one year, the mix studied by Graybeal [2005] resulted in 5.7 με/MPa (39 με/ksi) specific compressive creep. The UHPC mix studied by Graybeal [2005] showed ~70% increase in creep compared to mix D-C-2f-90C-40 of the current study after 1 year. This difference may be in part attributed to the difference in the loading ages between the two experiments (i.e. 4 days in the case of the previous study by Graybeal [2005] versus 7 days in the current study). The equivalent age of the UHPC mix by Graybeal [2005] at the time of loading was about 31.14 days versus 38.26 days for D-C-2f-90C-40 in the current study, which is a 22% increase in the relative maturity of the current UHPC mix compared to the previously studied mix. Also, differences in casting procedures between the current and the previous studies may

Table 5.6: Summary of compressive creep and shrinkage properties of UHPC at 1 year

Mix	Strains at 1 year		Specific compressive creep at 1 year	% change from D-2f-90C-40 at 1 year	
	Adjusted creep (με)	Free shrinkage (με)	με/MPa (με/ksi)	Compressive creep strain	Specific compressive creep
D-2f-90C-40	223	65	3.3 (22.6)	N/A	N/A
D-2f-60C-40	244	83	4.1 (28.5)	+10	+24
D-2f-23C-40	404	238	8.7 (59.8)	+81	+163

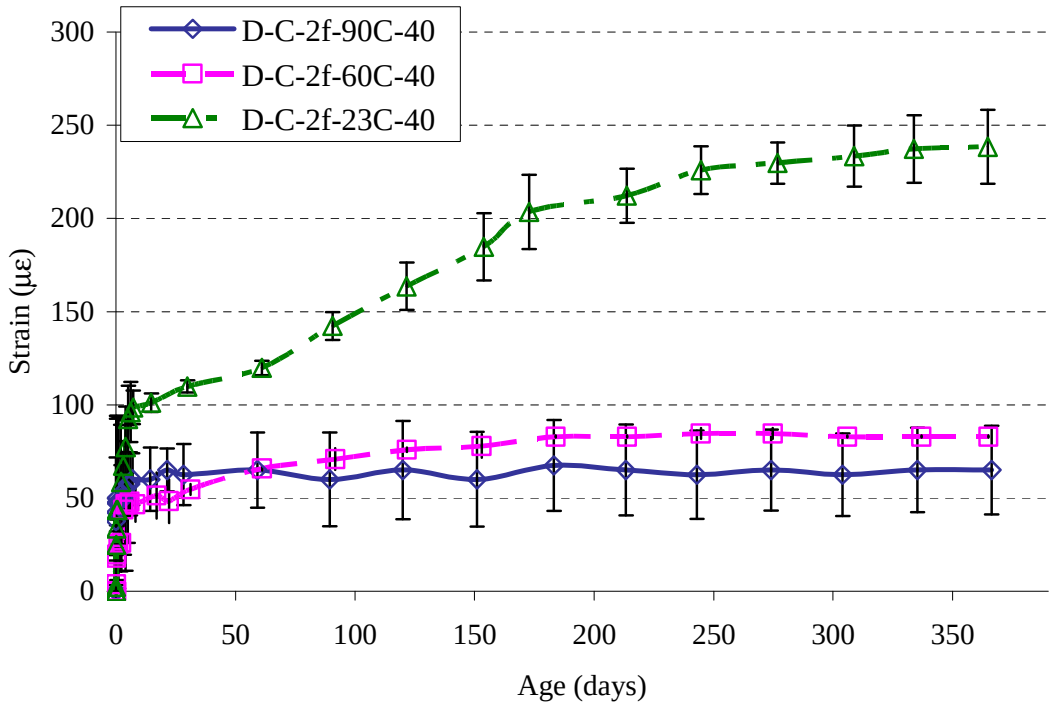

Figure 5.15: Effect of thermal treatment on free shrinkage strain of UHPC

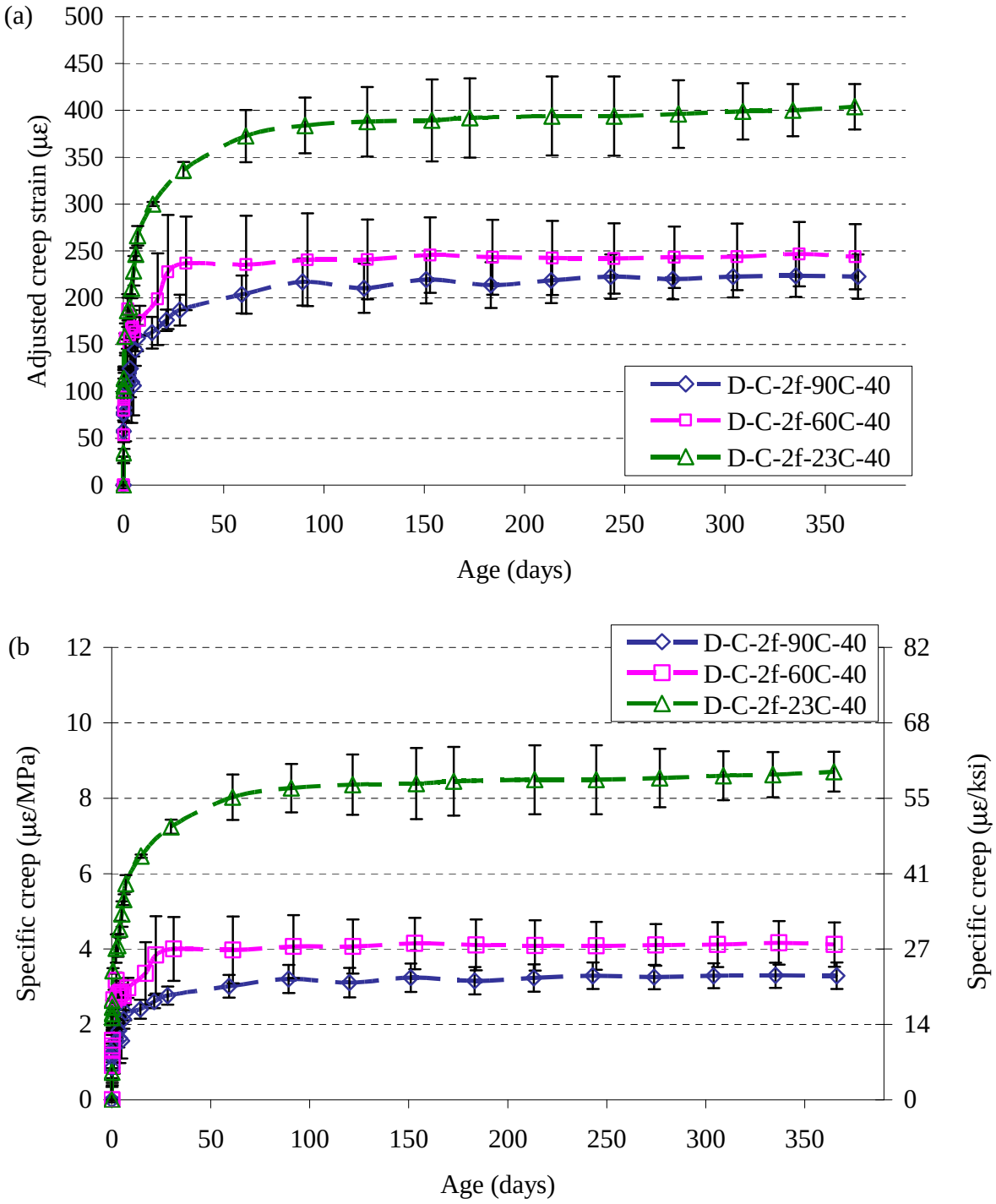

Figure 5.16: Effect of thermal treatment on: (a) adjusted creep strain and (b) specific compressive creep

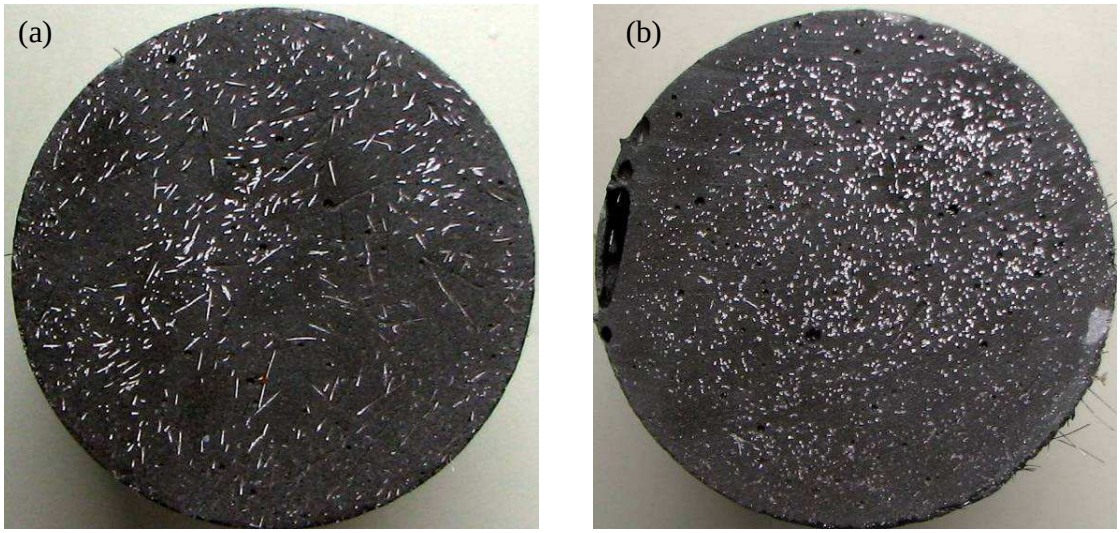

Figure 5.17: Cross sectional image at mid-height of (a) 100 x 200 mm cylinder poured vertically from the top and (b) 100 x 380 mm cylinder poured horizontally from one end to the other

have contributed to these differences. In the current study, the molds were horizontal, and the UHPC was poured into the molds from one end to the other which allowed fiber alignment in the longitudinal (loading) direction and which simulated the field methods used to cast UHPC bridge girders. This was not the case in the study by Graybeal [2005] where the cylinder molds were oriented vertically, and the UHPC was poured from the top until molds were full. This vertical placement procedure would result in more random fiber orientation which, on one hand, may increase the Poisson's ratio of the material but would decrease the amount of longitudinally-oriented fibers. The decreased amount of fibers aligned parallel to the load could then result in increased longitudinal deformations. The difference between a 100 x 200 mm (4 x 8-in) specimen cast from the top and a 100x380 mm (4x15-in) specimen cast from one end to the other is shown in Figure 5.17. The image at the right clearly shows an increase in fibers aligned longitudinally in the case of the 100x380 mm (4x15-in) specimens used in the current study, while this was not the case in 100 x 200 mm (4 x 8-in) used by Graybeal [2005].

The results presented here for the compressive creep of UHPC and the effect of the thermal treatment in reducing creep correlate well with the discussion of the tensile creep results, Section 5.5.3.3. However, a comparison between tensile and compressive creep of UHPC is given in the following section.

.

5.5.4 Comparison between Tensile and Compressive Creep of UHPC

The main objective in comparing tensile and compressive creep results for the three UHPC mixtures was to better understand the mechanisms affecting tensile creep of UHPC. It was necessary to adjust the tensile creep results reported in Section 5.5.3 to account for the shape and size differences between specimens used in the tensile and compressive creep studies. This adjustment was possible due to the fact that the specimens used in the short-term study for tensile creep had the same size and shape of those used in the long-term compressive creep study discussed in Section 5.5.4. This allowed adjusting the long-term tensile creep and shrinkage results based on the specific creep and shrinkage strain results after 7 days obtained for mix D-2f-90C-40 in both studies (long-term and short-term tensile creep studies). That is, results from the long-term tensile creep and shrinkage D-2f-90C-40, D-2f-60C-40, and D-2f-23C-40 were multiplied by specific creep and shrinkage strain short-term-to-long-term ratio. Adjusted long-term tensile creep and shrinkage will be referred to as “adjusted tensile creep” and “adjusted shrinkage”.

The short-term-to-long-term ratio for mix D-2f-90C-40 was 1.05 and 1.00 for specific creep and for free shrinkage, respectively. Based on these results, no adjustment was done to the long-term shrinkage data. Figure 5.18 shows the adjusted long-term specific tensile creep. This small difference between the short and the long term specimens is in part due to the shape and size effects. Figure 5.19 shows a comparison between tensile and compressive creep behaviors

of all UHPC mixes investigated. In this figure, and except for mix D-2f-90C-40, tensile creep is still showing an increase after 1 year while compressive creep reached an asymptotic value.

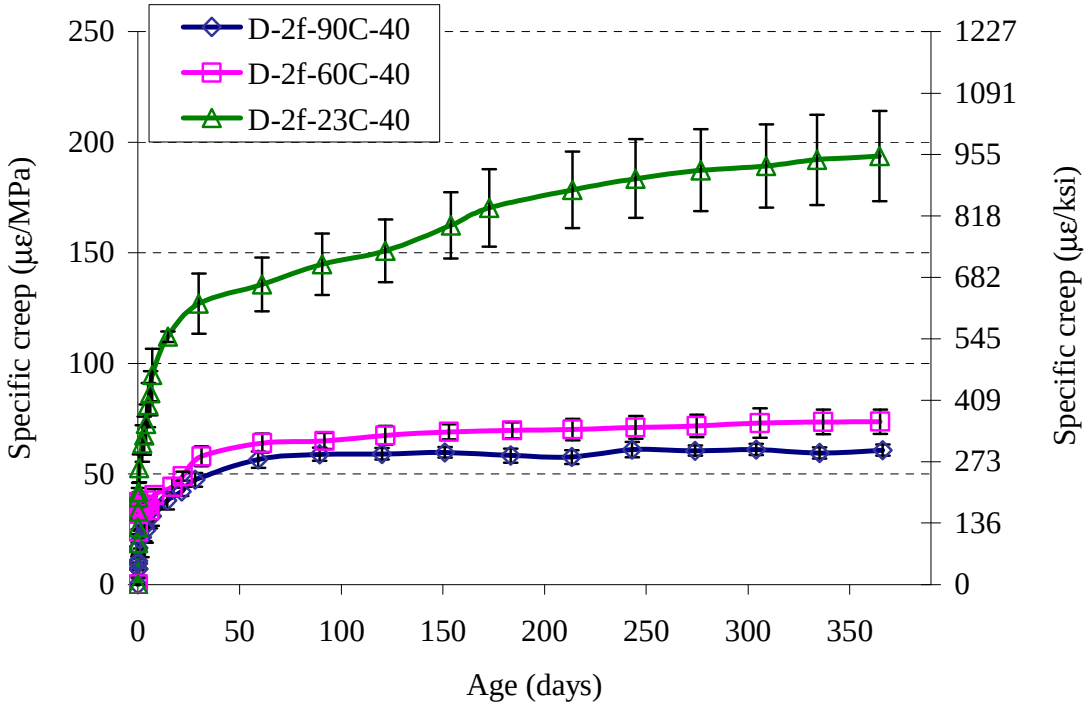

Figure 5.18: Adjusted specific tensile creep

Comparing adjusted tensile creep results in Figure 5.18 to compressive creep results in Figure 5.16 show that the tensile creep of mixes D-2f-90C-40, D-2f-60C-40, D-2f-23C-40 was about 17, 16, and 18 times the measured compressive creep, respectively. The large differences between tensile creep and compressive creep emphasizes that both phenomena occur fundamentally different from each other and that tensile creep tests should be performed if the tensile capacity of UHPC is to be utilized in structural design of bridge girders. It is well known that the influence of defects, such as pores and microcracks, in brittle materials like concrete is more pronounced in tension than in compression [Mehta and Monteiro, 2005].

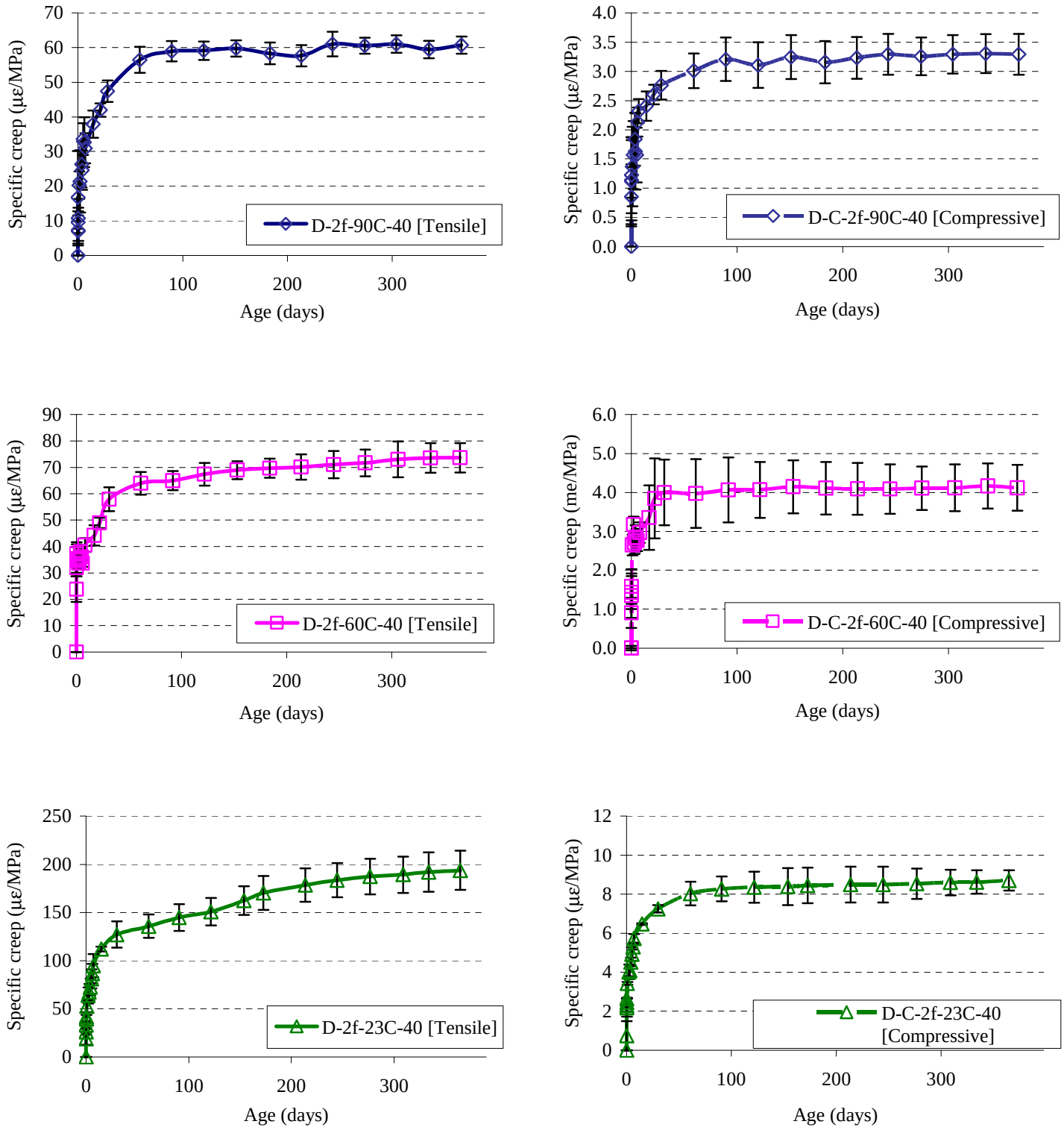

Figure 5.19: Comparison between compressive and adjusted tensile creep of UHPC

Therefore, the order of magnitude increase in tensile creep compared to compressive creep suggests that these defects, which are likely to be present in increased proportions at an interface such as that between the fibers and paste in UHPC, have an important effect on the tensile creep performance of UHPC. This hypothesis is further discussed at the end of this chapter in the light of the multi-scale study performed.

5.6 Nano/Microscale Study

To better characterize the influence of the fiber-cementitious matrix interfacial characteristics in thermally treated and non-thermally treated UHPC mixes, a nano/microstructural investigation was undertaken. The main objective of the nano/microscale study was to characterize the structure and properties at the fiber-matrix interface. Nanoindentation and scanning electron microscopy (SEM) were used in this study.

5.6.1 Samples

Nano/microscale UHPC samples were cast in 30 mm (1.2-in) diameter cylinders with depth of ~12 mm (1/2-in) (Figure 5.20). All samples were cast and cured following similar procedures identical to the large-scale study described above with the exception of the method of fiber addition. After casting non-fiber reinforced UHPC into the molds, 16 steel fibers pre-fixed on a plastic sheet in a square configuration were pushed vertically into the middle 5 x 5 mm (0.2 x0.2-in) region of the specimen to create a 2% fiber volume fraction in this region similar to that of the creep specimens. After curing or curing and thermal treatment, fast setting epoxy was poured on the top surface of the specimens to cover the top ends of fibers and also to provide more support to fibers during polishing. Bottom surfaces of the samples were then prepared by

successive dry polishing as outlined by Mondal et al. [2008]. Complete details about samples' preparation are provided in Section 4.2.2.

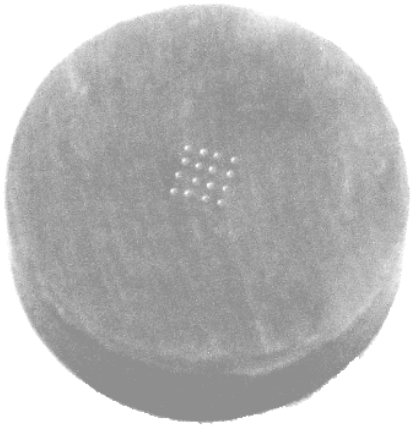

Figure 5.20: Nano/microscale UHPC sample (top surface view)

5.6.2 Nanoindentation Testing

A typical nanoindentation test is composed of compressive loading and unloading responses (Figure 4.16). The unloading response of the material is assumed to be elastic, and thus the slope of the unloading graph can be used to calculate the elastic properties of the indented material. The tip used for the nanoindentation tests was a pyramid shape, diamond Berkovich tip with a nominal radius of 50 nm, an elastic modulus, E_{in}, of 1100 GPa (159,542 ksi), and a Poisson's ratio, v_{in}, of 0.07. Figure 5.21 shows a typical indentation impression of the tip used in this study. Figure 5.22 generally shows the indentation scheme followed in this study.

Nanoindentation tests were done in two phases. In Phase I, a coarser, load controlled indentation scheme was used, and in Phase II, a finer, displacement controlled indentation scheme was used. The major differences between the two phases are shown in Table 5.7.

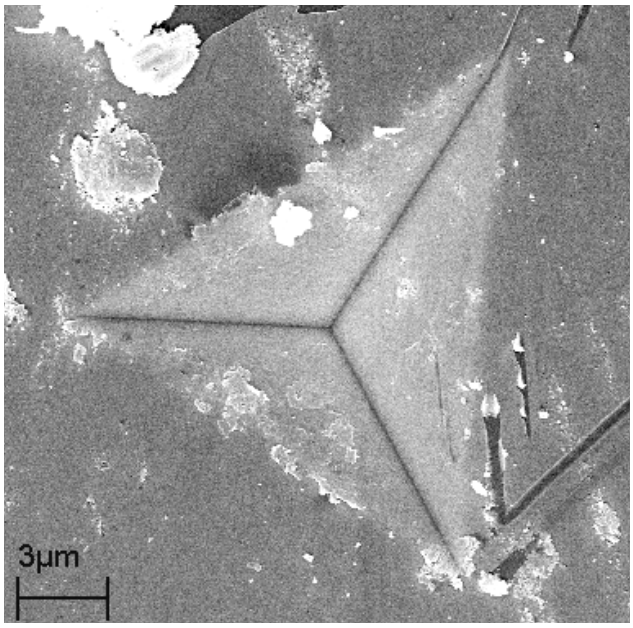

Figure 5.21: Pyramid shape nanoindentation impression on steel fiber [diamond Berkovich tip]

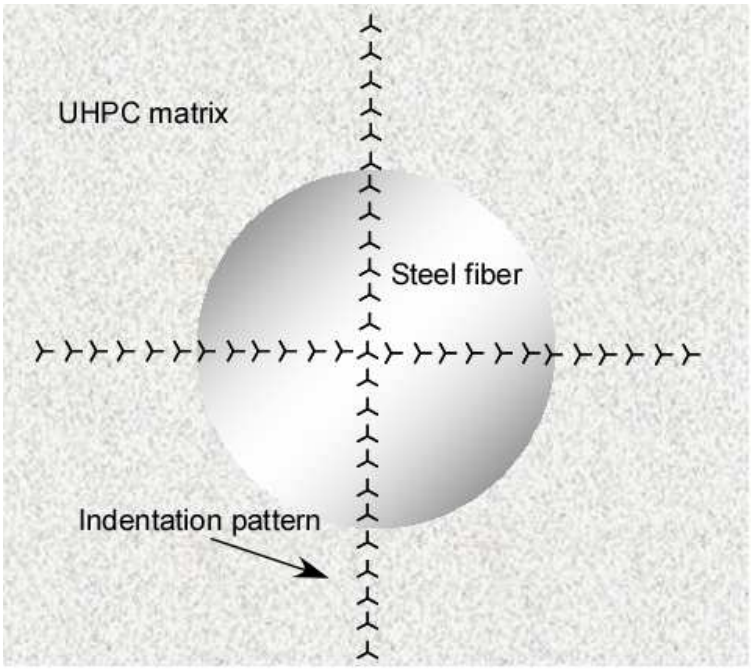

Figure 5.22: Nanoindentation pattern for a single fiber location in UHPC (not drawn to scale)

Results from each phase of the nano/microscale study are presented in separate sections. After performing the Phase I tests, it was necessary to refine the nanoindentation test in order to increase the resolution by decreasing the spacing between the indents from 10 μm (393 micro-inch) to 2 μm (79 micro-inch), to better capture the properties of the fiber/paste interfacial region, relative to the bulk paste. As such, the indentation test in Phase II was displacement controlled rather than load controlled as in Phase I in order to keep a spacing-to-indentation depth ratio of 20 to assure that no overlap would occur between successive indents.

Table 5.7: Major differences between the two nanoindentation phases

Item	Phase I (coarser indentation)	Phase II (finer indentation)
Test control	Load control	Displacement control
Spacing between indents	10 μm (393 micro inch)	2 μm (79 micro inch)
Maximum displacement	N/A	0.1 μm (3.93 micro inch)
Maximum load	2 mN (0.0004 lbs)	N/A
Target number of indents in matrix	15	50
Loading time	10 seconds	10 seconds
Unloading time	10 seconds	10 seconds
Time at peak load	2 seconds	2 seconds
Number of specimens/case	1	4
Curing temperatures considered	90^{o}C and 23^{o}C	90^{o}C, 60^{o}C and 23^{o}C

5.6.3 Scanning Electron Microscopy

After sputter coating with gold, SEM imaging was performed on the indented samples. SEM was carried out using a LEO 1530 thermally-assisted field emission (TFE) scanning electron microscope at low pressure 10^{-7} Pa (1.45 ksi). The accelerating voltage was 10kV. Characterization was performed in secondary electron mode to better distinguish the surface features.

5.6.4 Results and Discussion

In this section results from each phase of nanoindentation tests and SEM are presented and discussed.

5.6.4.1 Phase I: Course nanoindentation test

Figure 5.23 shows results from Phase I nanoindentation performed on thermally treated and non-thermally treated samples. In this figure, all measurements of elastic modulus are normalized by the modulus for the steel fibers (E/E_f), and the normalized modular ratio is plotted versus the distance from the edge of the fiber; as a result, the fiber elastic modulus is 1 for both thermally treated and non-thermally treated cases and the moduli within the pastes can be compared relative to one another and to the fiber. As the fiber modulus was an order of magnitude higher than the matrix modulus, it was rather easy to distinguish between indents in the fiber and in the matrix in the raw data. Both E and E_f were calculated from the unloading indentation curves.

Nanoindentation results showed an average reduction of 63% in the bulk matrix modulus in the UHPC with no thermal treatment as compared to the bulk matrix modulus for the thermally treated UHPC. The compressive modulus test [ASTM C 469] was also performed on the two mixes. Results from this test showed only about 7% reduction in the compressive modulus of the fiber-reinforced UHPC with no thermal treatment compared to that of the 90°C specimen (Table 5.3). The difference in the modulus drop between the nano- and the macroscale tests may be partially due to the fact that the compressive modulus test [ASTM C 469] accounted for all material phases (fiber, cementitious matrix, and fiber-cementitious matrix interface), where the material behaves as a composite. This is not the case in the nanoindentation test where each phase was characterized separately. In addition, differences in the casting methodology between macro-

and nanoscale samples may have contributed in some part in the inconsistency between the macro and nano scale results.

In addition, the modulus of the cementitious mortar for the non-thermally treated case reached a minimum value of $E/E_f = 0.04$ at ~10 μm away from the fiber, while the corresponding modulus in this region for the thermally treated case was stable at an E/E_f of 0.1. Also, an increase in E/E_f was measured at ~30 μm (for Mix D-2f-23C) and at ~40 μm (for Mix D-2f-90C) from the fiber (Figure 5.23). No explanation for this phenomenon can be presented; further validation and additional investigation is needed, but there is a possibility that particles in this region tens of microns from the fiber may have a higher packing factor than the bulk matrix. Also, these jumps in the modulus values might have been outliers that were not verified due to low test resolution.

The presence of a porous zone around the fiber in the non-thermally treated case was then confirmed via SEM scans carried out at the same indentation locations. SEM also showed no such porous zone for the thermal treatment case (Figures 5.24 and 5.25).

For the non-thermally treated case, Figure 5.25 shows a thin film of cementitious paste, with apparently lower density, around fibers. In some regions, this apparently lower density paste contacts a thin void, which is adjacent to the bulk matrix. This porous and weaker region might have been due to the formation of water films around fibers during casting and vibrating. It is worth noting that this void might have been affected by sample preparation especially when coarser grit paper discs were used to expose fibers. However, in the case of non-thermally treated UHPC, this more porous interface was not evident.

The problem of water films around fibers may be greater in UHPC bridge girder construction. This is due the fact that UHPC is likely to be poured from one end to the other to

align fiber in the horizontal direction. Aligning most of the fibers in the horizontal direction may cause water accumulation under the fibers due to their relatively large aspect ratio and size compared to other UHPC constituents. That is, fibers are 200 μm (7,874 micro inches) in diameter while the biggest particle size in a UHPC premix is significantly smaller [Personal communication with Paul Acker].

The decrease in modulus, measured by nanoindentation, for the non-thermally treated specimen occurred approximately in the same region (with regard to distance from the fiber) as the elongated voids evident in SEM. This suggests that the increased porosity in the interfacial region is present and is not entirely an artifact of sample preparation.

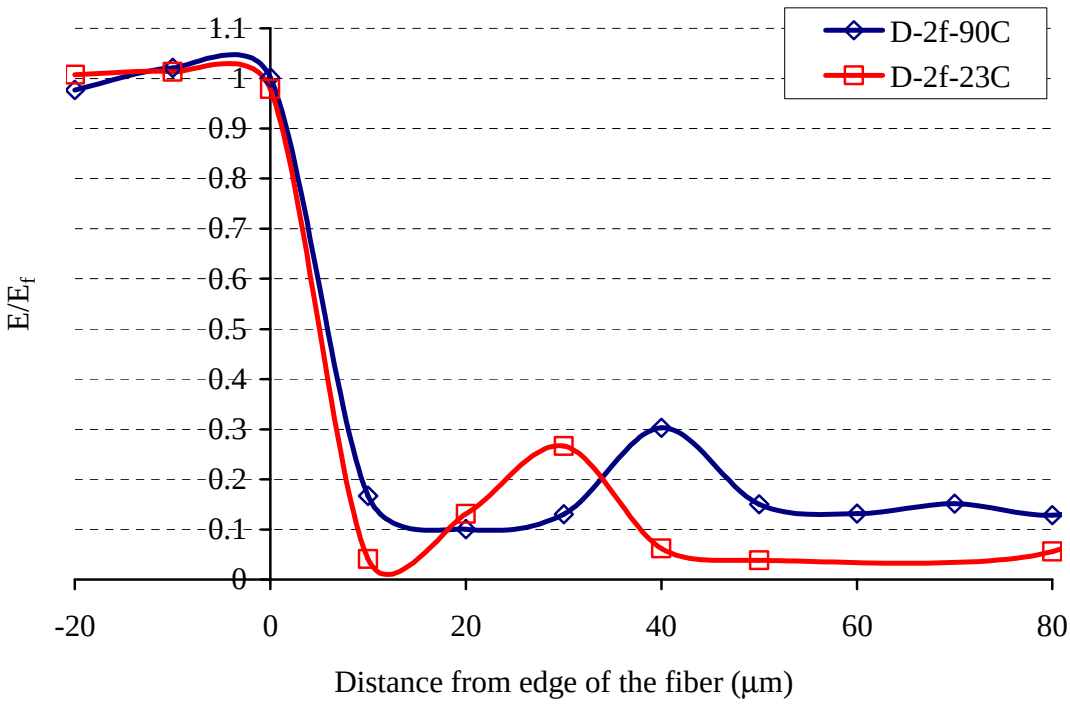

Figure 5.23: Phase I nanoindentation test results

The formation of water films around fibers, in turn, would result in a higher local water-to-cementitious materials ratio around fibers. Due to the mismatch in mechanical properties between the paste and the steel fiber; an apparent zone of weakness develops in the interfacial zone compared to the bulk cementitious matrix. Similar weak interfacial transition zones were also monitored around fine aggregates 1.18-2.36 mm (0.05-0.09-in) in size via nanoindentation and microscopy by Mondal et al. [2008]. The fibers used here are of smaller diameter (0.20mm (0.080-in)), but a similar effect may be occurring.

In the case of thermally treated samples, it was evident from Figure 5.24 that thermal treatment has resulted in an improvement in the fiber-cementitious matrix interface. The appearance of the cementitious matrix at the fiber interface is quite similar - if not the same - as the bulk paste. With thermal treatment, the interfacial region appears to be dense with no apparent interfacial voids or cracks, such as those evident without thermal treatment. Similar results were also obtained for thermally-treated UHPC by Sorelli et al. [2008]. It is proposed that this increased densification in the paste and lack of voids or cracking may be attributed to the thermal treatment. Thermal treatment could promote further reaction of the cementitious paste, leading to a reduction in the porosity around fibers and thus decreasing the overall relative weakness in the interfacial zone.

(a)

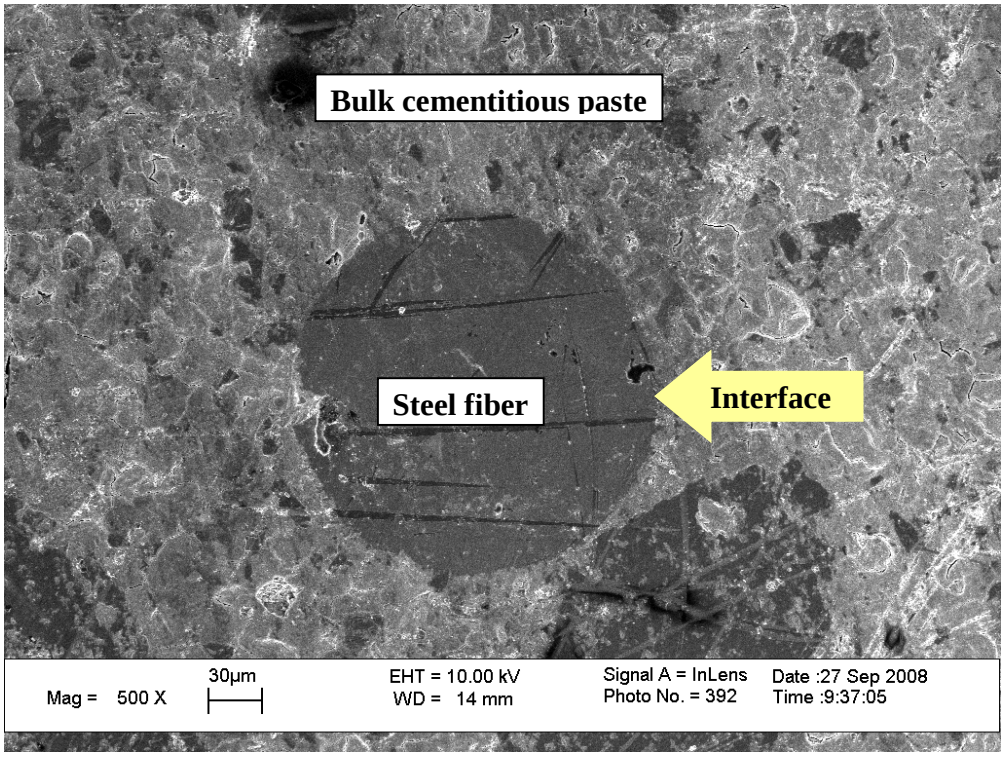

(b)

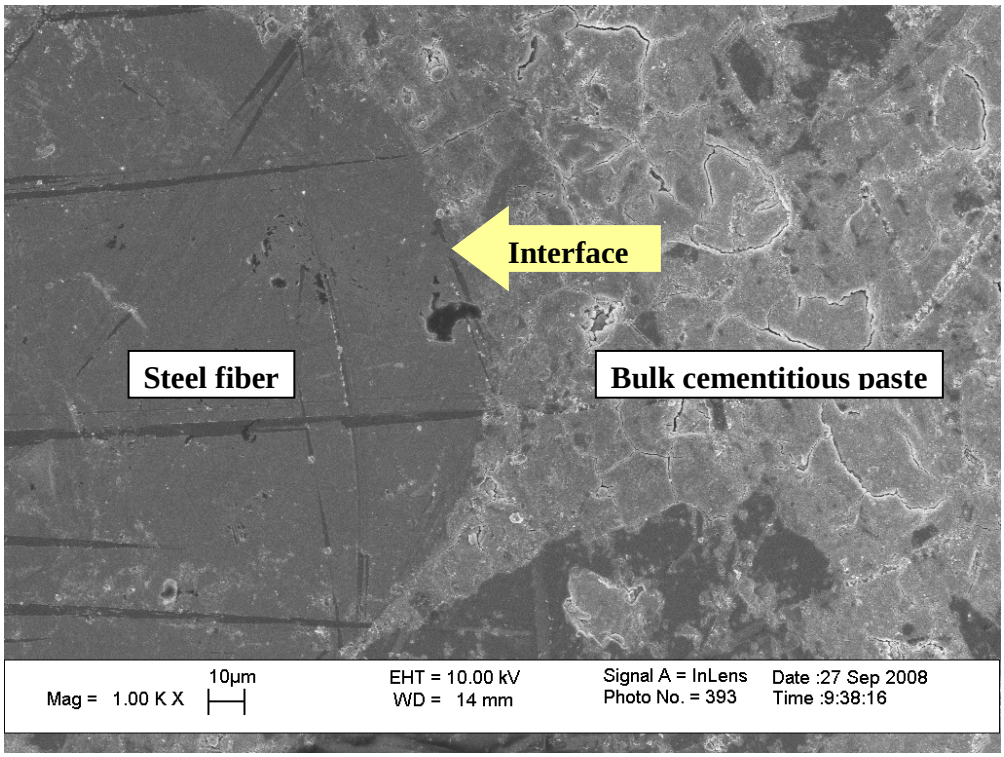

Figure 5.24: SEM images for mix D-2f-90C (a) 500 X magnification and (b) 1000 X magnification

(a)

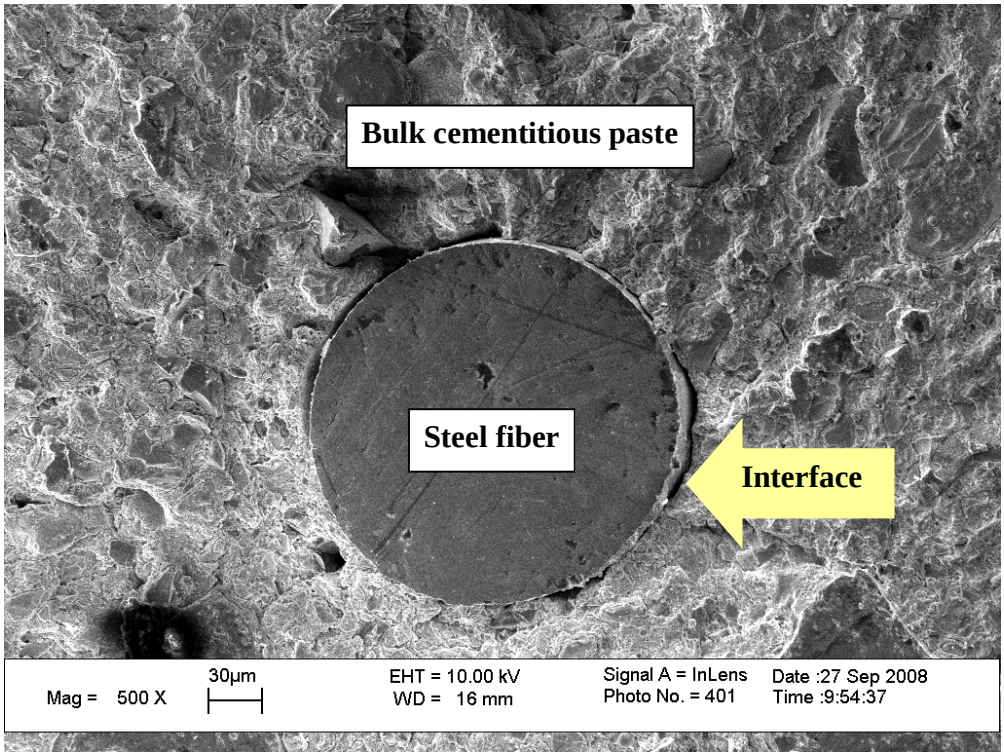

(b)

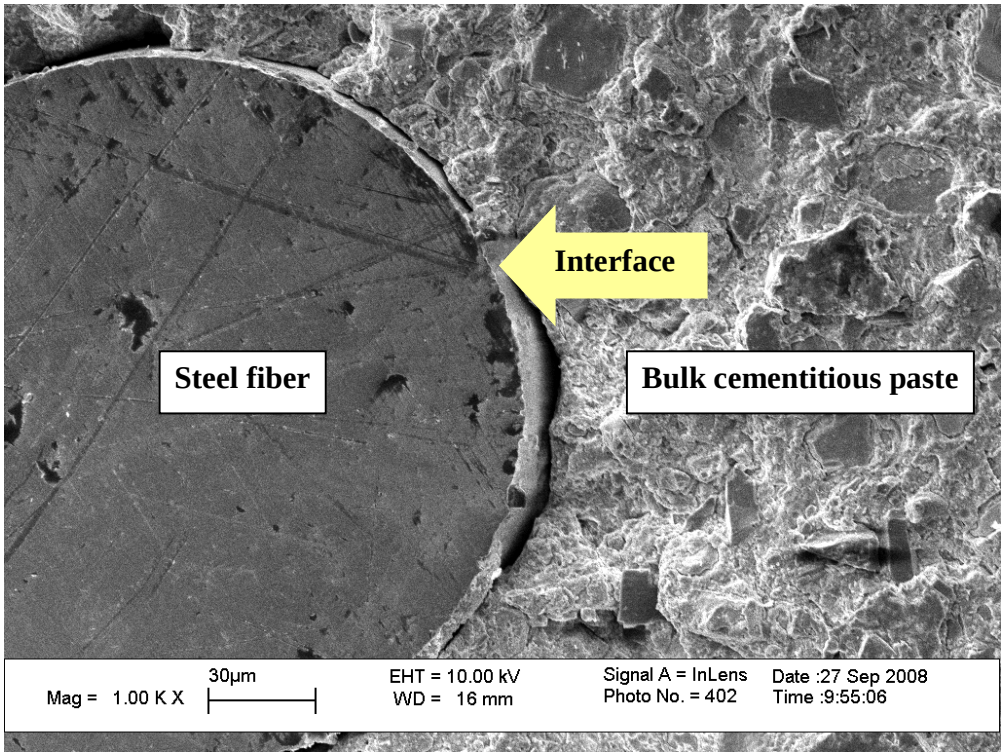

Figure 5.25: SEM images for mix D-2f-23C (a) 500 X magnification and (b) 1000 X magnification

5.6.4.2 Phase II: Fine nanoindentation test

Specimen preparations for both the coarser and finer nanoindentation tests were exactly the same. Figure 5.26 shows an SEM image of the indentation pattern at the fiber-matrix interfacial zone of a non-thermally-treated specimen. It is clear from this figure that it was easier to track the indents' impressions on the steel fiber compared to the matrix in the case of the displacement-controlled experiment. This figure also shows a crack formed at the fiber/paste interface surrounded by a zone of unreacted cementitious particles with a width that ranged between 2 and 3 μm (79- and 118-micoinch).

Prior to performing the nanoindentation test, successive calibrations of the indents' locations were performed. Figure 5.27 shows the variation in the modulus of elasticity versus the distance from the fiber edge for each of the three curing conditions considered. All the modulus values were calculated from the unloading indentation curves.

The modulus of elasticity for mix D-2f-90C ranged between 38.7 GPa (5,613 ksi) and 57.2 GPa (8,296 ksi) with an overall average of 47.6 GPa (6,904 ksi). This average modulus of elasticity of mix D-2f-90C is just ~1% less than the static compressive modulus of elasticity for mix D-2f-90C-40 (Table 5.3), suggesting good agreement between the modulus determined by nanoindentation and standard testing. The average modulus of elasticity obtained here is in good agreement with values obtained by Sorelli et al. [2009] where the average modulus value for UHPC thermally treated at 90^{o}C (194^{o}F) was 49.4 GPa (7,225 ksi). The modulus of elasticity for mix D-2f-60C ranged between 40.2 GPa (5,825 ksi) and 50.4 GPa (7,304 ksi) with an overall average of 45.6 GPa (6,608 ksi). This average modulus of elasticity of mix D-2f-60C is about 10% less than the static compressive modulus of elasticity for mix D-2f-90C-40 (Table 5.3). This difference between static compressive modulus of elasticity and the modulus obtained from

nanoindentation needs further research to investigate whether this difference is resulting from variation in UHPC properties. That is, the modulus of elasticity of the cementitious matrix for mix D-2f-90C was about 6% higher than that for mix D-2f-60C. ANOVA revealed significant difference between the modulus of elasticity of both mixes. In addition, relatively low variability in modulus results for each mix, particularly near the fiber interface, suggests that defects at the interface are not prevalent for these two mixes. The closeness of the modulus results from the nanoindentation study is in good agreement with the closeness of the creep results obtained for these two mixes (Figures 5.13 and 5.16).

In contrast, relatively larger variations in the modulus of elasticity values are shown in Figure 5.27 for mix D-2f-23C. The over all average modulus value was 23 GPa (3,365 ksi). The modulus values are at a local minimum adjacent to the fiber and generally increase within the 20 μm closest to the fiber, but the values remain relatively inconsistent across the 70 μm distance interrogated. It is proposed that this variation is related to defects present in the microstructure in the interfacial zone.

Localized high porosity or debonding around the fibers is evident from results in Figures 5.27 and 5.28 where it can be seen that an average modulus of elasticity of zero was measured in the 4 μm (157 micro inches) adjacent to the fibers. As the distance from the fiber edge increased beyond 4 μm (157 micro inch), the modulus of elasticity values increased constantly to reach a value of 26.9 GPa (3,902 ksi) at a distance of about 10 μm (394 micro inch) from the fiber edge (Figure 5.27). As result, the porous interface can be defined in this case by the 10 μm (394 micro inches) wide annulus around the fibers. The modulus value measure at 10 μm (394 micro inch) was maintained for about another 50 μm (1,969 micro inch) away from the fiber (i.e. up to a distance of 60 μm (2,362 micro inch)), and then modulus values started to increase to a value of

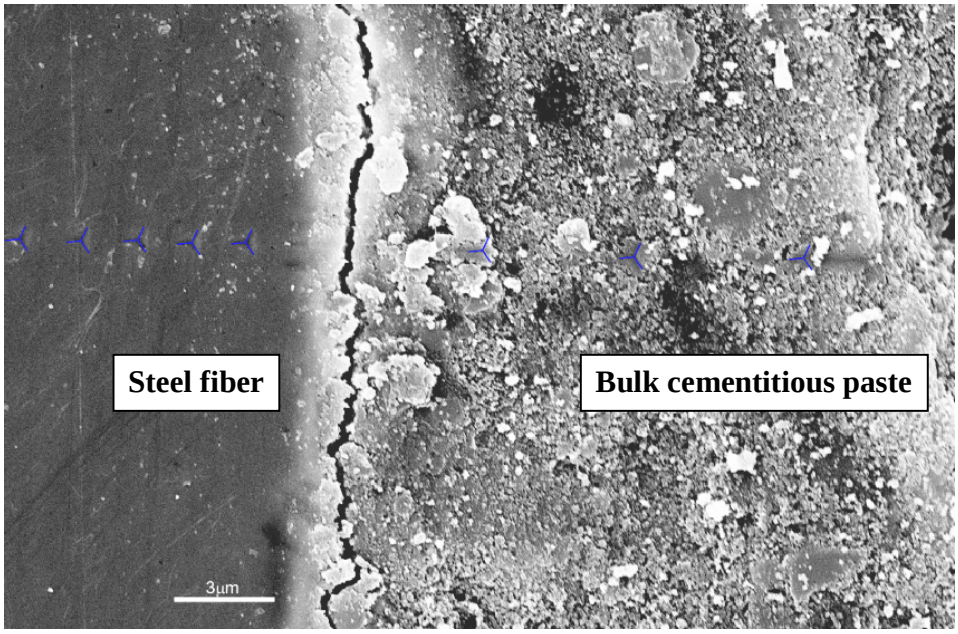

Figure 5.26: Fine indentation pattern at the fiber-matrix interfacial zone of a non-thermally treated specimen

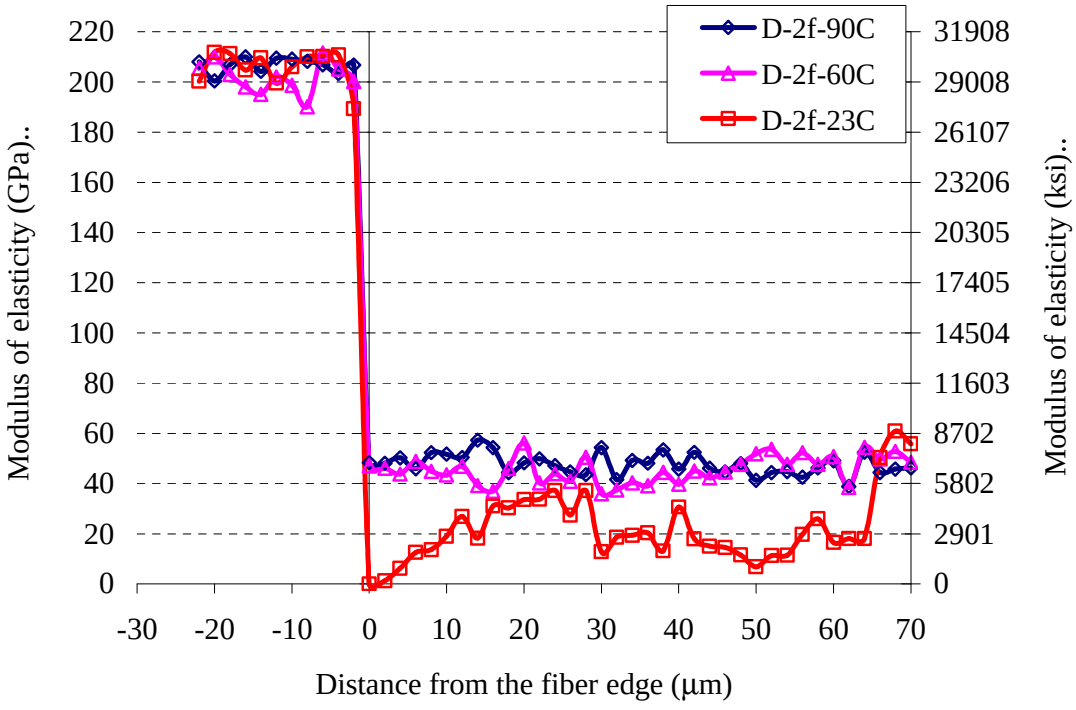

Figure 5.27: Phase II nanoindentation test results

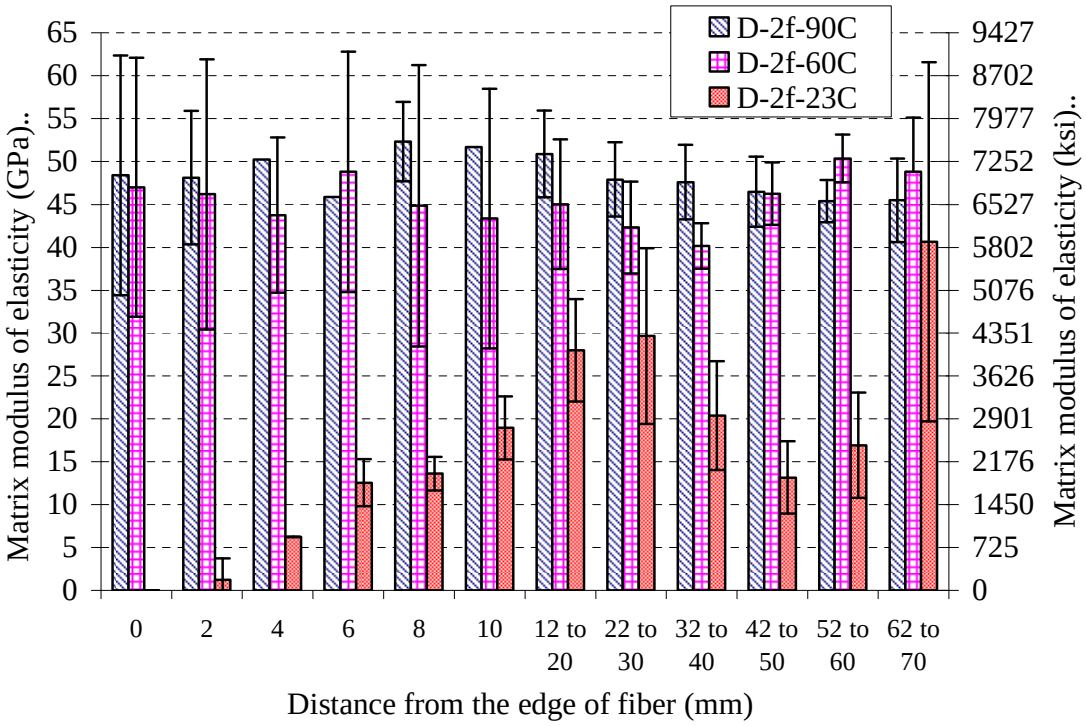

Figure 5.28: Average modulus of elasticity test results for Phase II nanoindentation

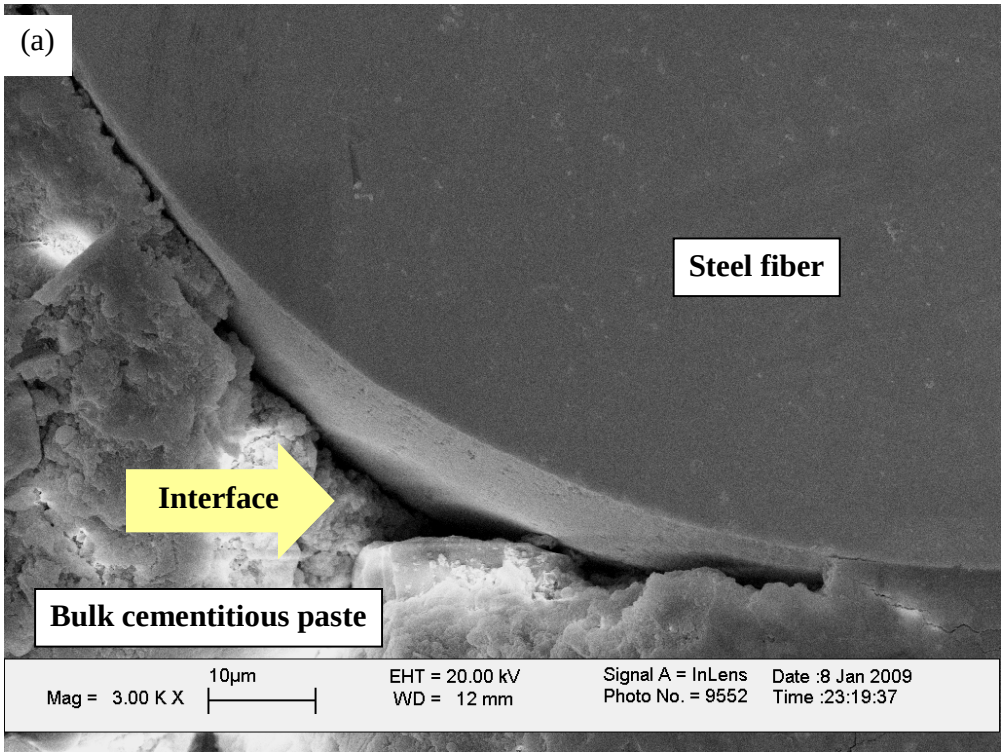

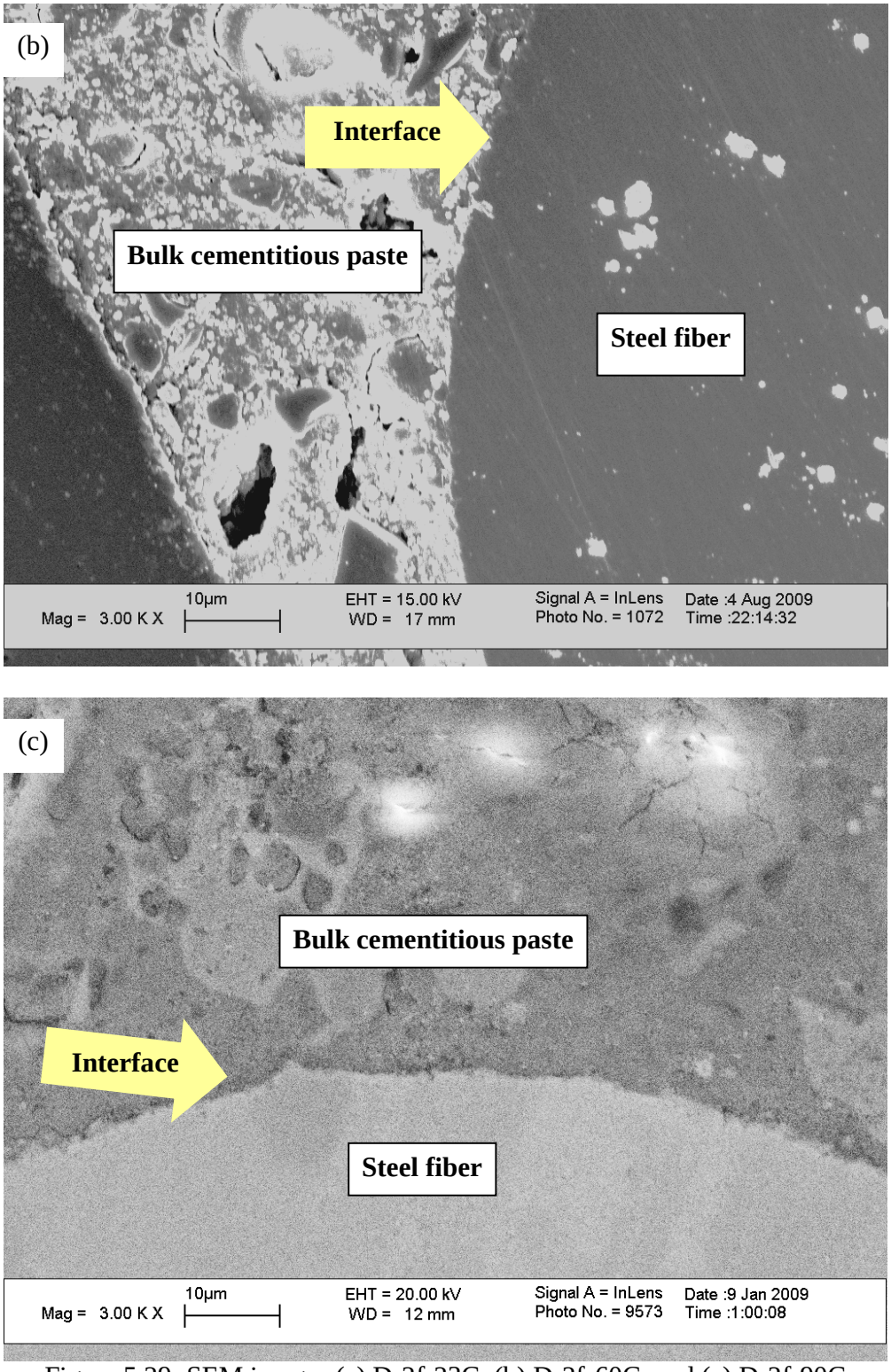

Figure 5.29: SEM images (a) D-2f-23C, (b) D-2f-60C, and (c) D-2f-90C

about 55 GPa (7,977 ksi) at a distance of 70 μm (2,756 micro inch) from the fiber edge. No indentations were done beyond 70 μm (2,756 micro inches) due to the equipment limitations on the maximum number of indents allowed at a time.

To make clearer the spatial trends in modulus values, results for all mixes were grouped according to the distance from fiber edge and the average values were plotted in Figure 5.28.

As in Phase I, the presence of a porous zone around the fiber in the non-thermally treated case was then confirmed via SEM scans carried out at the same locations as the indentations. SEM also showed no such porous zone for the thermally treated cases (Figure 5.29). For non-thermally treated UHPC, the size of the porous zone, 10 μm (394 micro inches) found from nanoindentation tests is in good agreement with SEM images (Figure 5.29 (a).

In summary, while the fiber-matrix interface was better captured in the fine nanoindentation test, nanoindentation/SEM results in both coarse and fine tests show clear differences in the interfacial zone around the fibers between thermally treated and non-thermally treated UHPC. Given that in both cases samples were prepared and tested following exactly the same procedure, the clear differences in behavior and structure can be attributed to the differences in curing.

5.6.5 Challenges with the Nanoindentation Test

There are some challenges that are associated with nanoindentation testing that warrant discussion. The first challenge was that fibers were introduced vertically to the UHPC premix after casting. This methodology might create packing problems around the fibers if not compacted (vibrated long enough) to allow premix consolidation around the fibers (Figure 5.30). Another challenge with nanoindentation of cementitious-based materials is optimum surface

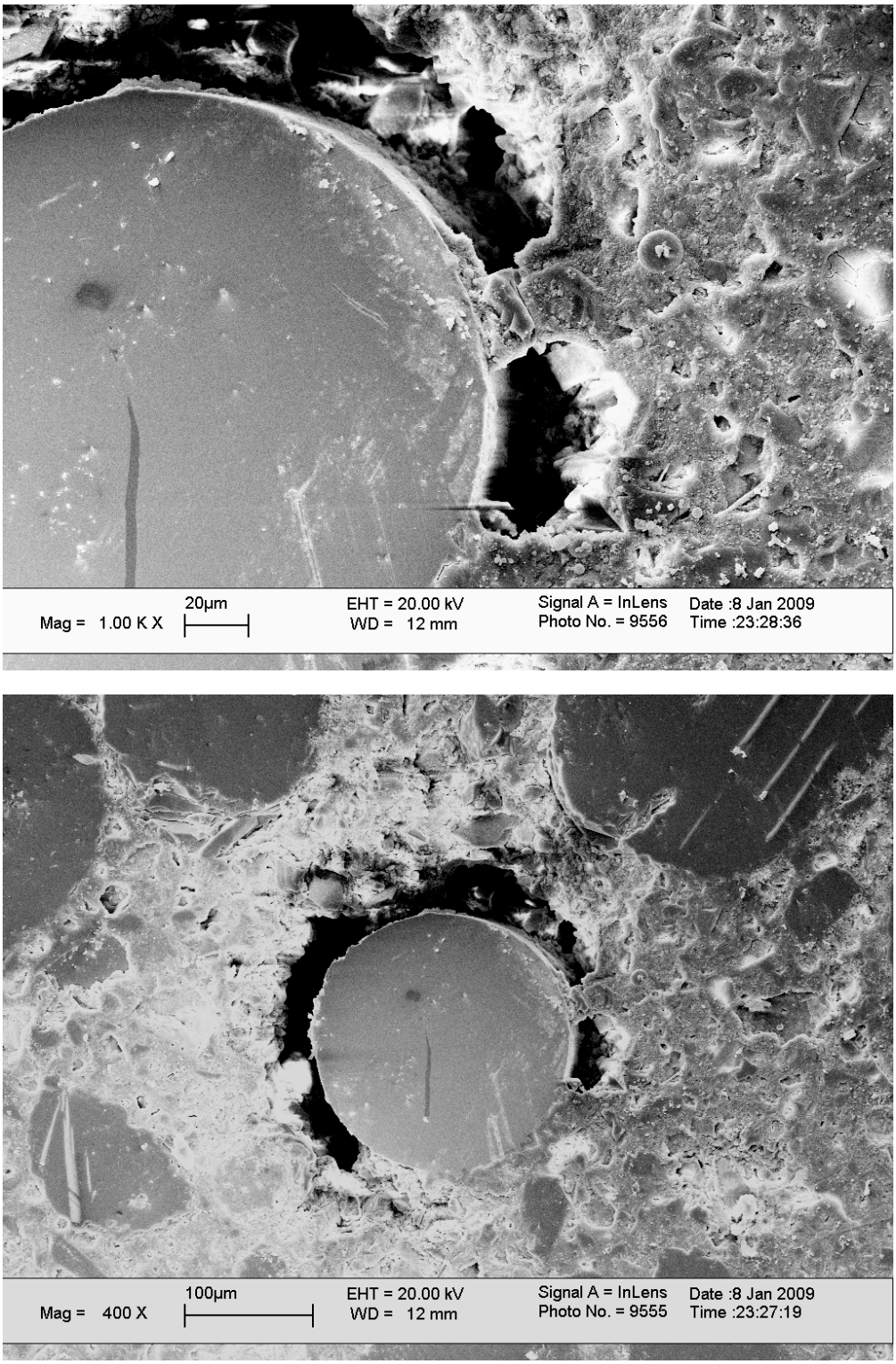

Figure 5.30: Voids around fibers due to lack of compaction in a non-thermally treated UHPC sample

preparation. In the current study, a preparation regime suggested by Mondal et al. [2008] was adopted. However, some surface cracking was noticed under electron microscopy that may be due to shrinkage or excessive dry surface polishing. While no extensive packing or cracking problems were observed in most of the nanoindentation specimens, these issues might cause some noise in the results at the nanoscale.

5.7 Proposed Tensile Creep Mechanisms

The multi-scale investigation presented in this chapter forms the foundation of the following discussion regarding the possible tensile creep mechanisms in fiber-reinforced UHPC. This discussion is also based on the well-established mechanisms of compressive creep which are discussed in Appendix C.

No single creep mechanism theory can be used solely to comprehensively explain creep in concrete since none of these theories was capable of accounting for all the factors affecting creep. As such, utilizing two or more of these theories might be more beneficent in explaining concrete deformations under loading and drying conditions.

Based on the current multi-scale study, it is proposed that the tensile creep phenomenon in fiber-reinforced UHPC is mainly controlled by three major mechanisms: (1) microcracking effect, (2) viscous flow, and (3) microprestress. In addition, in it possible that seepage may also contribute to tensile creep, although it is considered to be a lesser contributing mechanism compared to the others.

5.7.1 Microcracking Effect

The current multi-scale investigation suggests that microcracking is the major factor affecting tensile creep of UHPC. The importance of this factor can be seen both by comparing

the tensile creep behavior of thermally treated and defect free UHPC to that of the non-thermally treated UHPC and also by comparing the tensile to the compressive creep behavior of all mixes investigated.

The nanoscale investigation showed that steel fibers in non-thermally treated UHPC were surrounded by a porous interface that may contain pre-existing cracks. The weak bond between fibers and the cementitious matrix in non-thermally treated UHPC would result in limited stress transfer to fibers. Tensile cracks are likely to propagate and grow interconnected under tension stress due to stress concentrations occurring at the crack tips [Neville and Dilger, 1970]. Each of these cracks is likely to keep propagating until arrestment by a fiber present in the crack path(s). Once microcrack growth is locally arrested by a fibers a decrease in the tensile creep rate can be expected.

It is then proposed that in non-thermally treated UHPC the failure of fibers to adequately arrest microcracks - due to the weak bond at the interface - resulted in the continuous increase in tensile creep after one year; in comparison, compressive creep, where stress concentrations at the crack tip would be expected to be less than in the case of tensile creep, reached almost an asymptotic value after 150 days.

Further evidence for this hypothesis is provided by various finding throughout this investigation. In the short term tensile creep study [Chapter 3], the magnitude and rate of tensile creep was found to be dependant on the level of stress applied, relative to the material strength. Also, in the long-term study, a 25% increase in the tensile-to-compressive creep ratio (i.e., 20 versus 16) was found for non-thermally treated UHPC compared to thermally treated UHPC.

The microcracking effect on creep was introduced by Neville and Dilger [1970] for compressive creep of concrete and was adopted later by Bissonnette et al. [2007] to explain

tensile creep. However, no microstructural evidence was provided in these prior studies. Here, nanoindentation data and SEM images show the presence of a more porous and more poorly bonded fiber/matrix interfacial region in the non-thermally cured samples. Both short and long term tensile creep studies showed that the non-thermally cured mixes experienced greater creep, particularly in tension.

5.7.2 Viscous Flow Effect

The theory of viscous flow in creep ascribes a major part of creep mechanism in concrete to viscous flow, whereby particles move over one another when loaded [Thomas, 1937]. This mechanism can have more pronounced effect on creep in tension than compression [Brooks and Neville, 1977]. The reason for that is upon loading in tension while allowing concrete to dry, the adsorbed water layers to CSH particle are disturbed by two counteracting forces which are (1) the adsorption of water in the pores due to pores' opening in tension and (2) the evaporation that is taking place at the same time. These counteracting actions would facilitate sliding or flow of gel particles against each other. The increased relative motion between gel particles would result in an overall increase in tensile creep more than in compressive creep where both compressive stress and evaporation tend to expel water from the pores to the environment and, thus, decreasing viscous flow. A similar effect was proposed by Bissonnette et al. [2007] but was not proven due to the lack of compressive creep data.

5.7.3 Microprestress Effect

Microprestress can also play a role in increasing specific tensile creep much more than its compressive counterpart. The microprestress theory, [Bazant et al., 1997], states that creep in concrete may result from interatomic bond breaks in overstressed locations. At these

overstressed locations, the adsorbed water diffuses to the capillary pores and accelerates the bond-breaking process in the C-S-H structure. This progressive process of bond breaking and diffusion are likely to form new overstressed locations that will also undergo creep as well. This effect is accompanied by a shift in adsorbed water to capillary pores in compression, and from them in tension. This effect would continue until a state of uniform stress is achieved. One may expect that achieving a state of uniform stress might be quicker in compression than tension. This is because compaction of concrete would eventually lead to a more uniform distribution of stresses allover concrete particles in compression. This is not necessarily the case in tension, since the pulling apart of the sample is not limited in the same way. This difference between the compression and tension cases suggest that the microprestress effect could continue for longer, leading to higher specific creep in tension than in compression.

5.7.4 Seepage Effect

The seepage theory states that creep in concrete is due to the loss of water from the C-S-H, which is a common phenomenon in rigid gels [Weiser, 1938]. Upon applying load, the vapor pressure of the physically adsorbed water increases, and thus expelled from the C-S-H surface to the capillary pores to restore equilibrium with external conditions [Neville, 1955; and ACI Committee 209, 2005], this will, in turn, result in volume changes. Upon loading concrete, the water in the cement paste starts to be squeezed out which increases the stress in aggregates and decreases stress in the cement paste. Later, and as water is expelled from the C-S-H surface, it becomes increasingly difficult to remove thus, reducing the rate of creep.

The seepage theory can explain the mechanism of tensile creep in concrete. Tensile stress causes a decrease in vapor pressure transforming capillary free water into adsorbed water. This

would restore pressure equilibrium within cement paste microstructure and would cause expansion [Lopez, 2005].

Depending on whether compressive or tensile loading has a larger effect on the size change (i.e., reduction in compression or expansion in tension), seepage theory could in part explain the difference between creep in compression and tension. The only way to prove this is through conducting creep tests on sealed specimens which was outside the scope of this work.

However, the seepage effect may be of less importance in UHPC due to very low water-to-cement ratio (i.e., less than 0.20)

5.7.5 Other Effects

Other theories currently used to explain compressive creep of concrete, such as the mechanical deformation theory [Freyssinet, 1951] or the plasticity theories [Vogt, 1935], have not proven experimentally to apply to concrete or other cement-based materials. In addition, the solidification theory [Bazant and Prasannan, 1989] cannot be applied to tensile creep like in compressive creep since the formation of new hydration products is not likely to occur under tensile loading.

Differences between tensile and compressive mechanical properties particularly Poisson's ratios, Table 5.3, suggests that other mechanisms may also be playing an important role in the tensile creep phenomenon of UHPC. The fact that the Poisson's ratios in tension were generally higher than compression can explain some of the observed results. That is, pores are likely to open in tension and thus facilitate flow to a greater extent than in the case of compression where particles or surfaces are likely to get closer to each other, thus impeding flow.

This means that, a full explanation of the tensile creep phenomenon in concrete needs further investigation.

5.8 Conclusions

The current study is the first comprehensive multi-scale investigation of tensile creep of UHPC. Based on this experimental investigation, an improved understanding of the influence of thermal treatment on the tensile creep behavior of UHPC is gained and the following conclusions can be drawn:

(1) Tensile creep of UHPC was found to be more sensitive to thermal treatment compared to tensile strength. With variations in thermal treatment resulting in quite similar tensile strengths but quite different tensile creep behavior, results from the long-term investigation show that tensile creep testing – rather than tensile strength values at the time of loading – should be used to predict long-term tensile performance of fiber-reinforced UHPC.

(2) Direct tensile tests should be used to determine tensile strength of UHPC. If split cylinder tests are used, the tensile strength should be estimated as one-half the tensile strength given by the split tensile test.

(3) The following relations between mechanical properties of UHPC are proposed based on the this experimental study:

- $f'_{dt} = 7.64 \times \ln(f'_c) - 28.7$
- $f'_{dt} = 0.48 \times f'_{st}$

where: f'_{dt} is the direct tensile strength in MPa, f'_{st} is the splitting tensile strength in MPa, and f'_c is the compressive strength in MPa.

(4) Large scale tensile creep tests showed that thermal treatment of UHPC at 90oC (194oF) for 48 hours or at 60°C (140oF) for 72 hours prior to loading decreased specific tensile creep by about 63% and 57%, respectively, when compared to non-thermally treated UHPC.

(5) The closeness of the results obtained for the two thermally treated UHPC mixes investigated suggests the possibility of achieving satisfactory microstructural refinement if the same temperature energy is input to UHPC despite of the maximum temperature applied.

(6) Results from this study suggest that the tensile creep phenomenon in UHPC occurs differently than compressive creep. This result emphasizes the importance of further study of the tensile creep behavior of UHPC, particularly for applications where satisfactory long-term tensile performance is required.

(7) For the first time, the presence of a porous fiber-cementitious matrix interface was demonstrated by nanoindentation and scanning electron microscopy, for the case of the non-thermally treated UHPC only. The width of the interface measured was about 10 μm (394 micro inches). No porous interface was found in thermally treated UHPC, in either the 90oC or 60oC curing regimes.

(8) It is proposed based on this multi-scale study that tensile creep of fiber-reinforced UHPC is primarily controlled by microcracking, which is likely to initiate in the more porous fiber-matrix interface, as well as viscous flow, and microprestress. Further research is still need to fully describe the factors affecting the tensile creep phenomenon in concrete.

(9) It is proposed that unless the fiber-cementitious matrix interface in UHPC is refined via thermal treatment and adequate compaction to minimize or eliminate its porosity, fibers cannot be accounted for as shear reinforcement in lieu of stirrups in bridge girders.

5.9 References

AASHTO-LRFD, AASHTO LRFD Bridge Design Specifications. Third Edition, Washington: American Association of State Highway and Transportation Officials, 2004.

ACI Committee 209, "Factors Affecting Shrinkage and Creep of Hardened Concrete", American Concrete Institute: Farmington Hills, MI. 2005, pp. 209-1R-05.

ACI Committee 209, "Prediction of Creep, Shrinkage, and Temperature Effects in Concrete Structures", in ACI Manual of Concrete Practice. American Concrete Institute: Farmington Hills, MI. 1997, pp. 209R.1-209R.47.

Altoubat, S. A., and Lange, D. A., “Tensile Basic Creep: Measurements and Behavior at Early Age”, ACI Materials Journal, Vol. 98, No. 5, September-October, 2001, pp. 386-393.

ASTM C512, “Standard Test Method for Creep of Concrete in Compression,” American Society for Testing and Materials Standard Practice C512, Philadelphia, Pennsylvania, 2002.

Bažant, Z. P., Hauggaaed, A. B., Baweja, S., and Ulm, F. J., “Microprestress-Solidification Theory for Concrete Creep. I: Aging and Drying effects.” Journal of Engineering Mechanics, Vol. 123. No. 11, 1997, pp. 1188–1194.

Bažant, Z.P. and Prasannan, S., "Solidification Theory for Concrete Creep .1. Formulation". Journal of Engineering Mechanics-ASCE, Vol. 115, No. 8, 1989. pp. 1691- 1703.

Bissonnette, B., and Pigeon, M., “Tensile Creep at Early Ages of Ordinary, Silica Fume and Fiber Reinforced Concretes”, Cement and Concrete Research, Vol. 25, N0. 5, 1995, pp. 1075-1085.

Bissonnette, B., Pigeon, M., and Vaysburd, A.M., “Tensile Creep of Concrete: Study of Its Sensitivity to Basic Parameters”, ACI Materials Journal, Vol. 104, N0. 4, 2007, pp. 360-368.

Brooks, J. J., and Neville, A. M., “A Comparison of Creep, Elasticity and Strength of Concrete in Tension and in Compression,” Magazine of Concrete Research, Vol. 29, No. 100, 1977, pp. 131-141.

Burkart, I., and Muller, H.S., “Creep and Shrinkage Characteristics of Ultra-High Strength Concrete (UHPC), Proceedings of the Second International Symposium on Ultra-High Performance Concrete, Kassel, Germany, March 5-7, 2008, pp. 469-476.

Carino, N.J., "The Maturity Method: Theory and Applications". Cement, Concrete and Aggregates, Vol. 6, No. 2, 1984, pp. 61-73.

Chen, X., Davy, C.A., Skoczylas, F., and Shao, J.F., “Effect of Heat-treatment and Hydrostatic Loading upon the Poro-elastic Properties of a Mortar”, Cement and Concrete Research, Vol. 39, No.3 , 2009, pp. 195-205.

Cheyrezy, M., Maret, V., and Frouin, L., “Microstructural Analysis of RPC (Reactive Powder Concretes”, Cement and Concrete Research, Vol. 24, No. 7, October 1995, pp. 1491-1500.

Collepardi, S., Coppola, L., Troli, R., and Collepardi M., “Mechanical properties of modified Reactive powder Concrete”, ACI international Conference on “Superplasticizers and Other Chemical Admixtures in Concrete”, SP 173, October 1997.

Comite Euro-Internacional du Beton (CEB) and Federation Internationale de la Precontrainte (FIP), Evaluation of the Time Dependent Behavior of Concrete. Lancaster: The Construction Press, 1990.

Comite Euro-Internacional du Beton (CEB) and Federation Internationale de la Precontrainte (FIP), CEB Code Final Draft Section 3 Materials prEN 1992-1, 2001, pp. 25-31.

Feylessoufi, A., Crepin, M., Dion, P., Bergaya, F., Van Damme, H., and Richard, P., “Controlled Rate Thermal Treatment of Reactive Powder Concretes”, Advanced Cement Based materials, Vol. 6, No. 1, 1997, pp. 21-27.

Freyssinet, E., “The Deformation of Concrete”, Magazine of Concrete Research (London), No. 8, Dec. 1951, pp. 49-56.

Graybeal, B. A., "Characterization of the Behavior of Ultra-High Performance Concrete", Ph.D. Thesis, University of Maryland, 2005.

Gutsch, A., Rostasy, F.S., “Young concrete under High Tensile Stresses, Creep, Relaxation and Cracking”, in: R. Springenschmid (Ed.), Thermal Cracking in Concrete at Early Age, E & FN Spon, London, RILEM, 1994, pp.111 –118.

Kovler, K., “A New Look at the Problem of Drying Creep of Concrete under Tension”, ASCE Journal of Materials in Civil Engineering, Vol. 11, No. 1, February, 1999, pp. 84-87.

Kovler, K., “Interdependence of Creep and Shrinkage for Concrete under Tension”, ASCE Journal of Materials in Civil Engineering, Vol. 7, No. 2, May, 1995, pp. 96-101.

Kovler, K., “Testing System for Determining the Mechanical Behavior of Early Age Concrete under Restrained and Free Uniaxial Shrinkage”, Journal of Materials and Structures, Vol. 27, 1994, pp. 324-330.

Kovler, K., Igarashi, S., and Bentur, A., “Tensile Creep Behavior of High Strength Concretes at Early Age”, Journal of Materials and Structures, Vol. 32, 1999, pp. 383-387.

Lion, M., Skoczylas, F., Lafhaj, Z., and Sersar, M., “Experimental Study on a Mortar. Temperature Effects on Porosity and Permeability. Residual Properties or Direct Measurements Under Temperature”, Cement and Concrete Research, Vol. 35, No. 10 , 2005, pp. 1937-1942.

Lopez, M. “Creep and Shrinkage of High Performance Lightweight Concrete: A Multi-Scale Investigation”, Ph.D. Thesis, Georgia Institute of Technology, 2005.

Mehta, P.K. and Monteiro, P. J. M., “Concrete Microstructure, Properties, and Materials” 3rd ed: McGraw-Hill, 2005.

Mondal, P., Shah, S.P., and Marks, L.D., “Nanoscale Characterization of Cementitious Materials”, ACI Materials Journal, Vol. 105, N0. 2, 2008, pp.174-179.

Monosi, S., Pignoloni, G., Collepardi, S., Troli, R., and Collepardi M., “Modified Reactive Powder Concrete with Artificial Aggregate”, ACI International Conference on “Superplasticizers and Other Chemical Admixtures in Concrete”, SP 175, October 2000.

Neville, A.M. and W.H. Dilger, Creep of Concrete: plain, reinforced, and prestressed. Amsterdam, New York,: North-Holland Pub. Co., American Elsevier, 1970, xix, 622.

Neville, A.M., "Theories of Creep in Concrete", ACI Journal, Vol. 52, No. 9, 1955, pp. 47-60.

Richard, P., and Cheyrezy, M., “Reactive Powder Concretes with High Ductility and 200-800 MPa Compressive Strength”, ACI International Conference on “Concrete Technology Past, Present and Future”, SP 144, 1995.

Sakata, K. "Prediction of Creep and Shrinkage, Creep and Shrinkage of Concrete", in Fifth International RILEM Symposium. Barcelona, Spain: RILEM, 1993, pp. 649-654.

Sorelli, L., Constantinides, G., Ulm, F.J., and Toutlemonde, F., “The Nano-mechanical Signature of Ultra High Performance Concrete by Statistical Nanoindentation Techniques”, Cement and Concrete Research, Vol. 38, No. 12, 2008, pp. 1447–1456.

Tao, Z., and Weizu, Q., “Tensile Creep due to Restraining Stresses in High-Strength Concrete at Early Ages”, Cement and Concrete Research, Vol. 36, 2006, pp. 584-591.

Taylor, H.F.W., Famy, C, Scrivener K.L., “Delayed Ettringite Formation”, Cement and Concrete Research, Vol. 31, No. 5, 2001, 683-693.

Thomas, F.G. "Creep of Concrete under Load". London: International Association of Testing Materials, 1937.pp. 292-294.

Umehara, H., Uehara, T., Iisaka, T., and Sugiyama, A., “Effect of Creep in Concrete at Early Ages on Thermal Stress”, in: R. Springenschmid (Ed.), Thermal Cracking in Concrete at Early Age, E & FN Spon, London, RILEM, 1994, pp.79– 86.

Vogt, F., “On the Flow and Extensibility of Concrete”, Stockholm, 1935, pp. 24.

Weiser, H.B., Inorganic Collide Chemistry”, V.III-The Colloidal Salts, Chaman and Hall, New York, 1938.

CHAPTER 6

EFFECT OF FIBER CONTENT AND STRESS LEVEL ON THE TENSILE CREEP OF UHPC

6.1 Introduction

The aim of this study was to characterize and quantify the effect of steel fiber content and tensile stress level (stress-to-direct tensile strength ratio) on the tensile creep of UHPC. The outline and goals of the complete experimental program are presented in Section 4.2.1. Some UHPC mixes in this study were altered by varying the fiber content from the 2% by volume dose recommended by the UHPC manufacturer for optimized particle packing. Fiber contents considered for this study included 0%, 1%, and 2% by volume. All mixes were mixed and cast following the same procedure outlined in Chapter 3 (Section 3.3.3).

This chapter presents an analysis of the mechanical and time-dependent properties obtained in the large-scale study. Results and analyses are grouped in two major sections. The first section presents an analysis of the effect of varying the fiber content on the mechanical and time-dependant properties of UHPC. The second section analyzes the influence of varying the applied stress level on the tensile creep of UHPC.

Table 6.1 presents a summary of the mixes considered, nomenclature, their main characteristics, and the tests performed on each.

The nomenclature used in this study was based on the type of UHPC used (i.e., Ductal® = D), fiber volume fraction (i.e., 2% volume fraction = 2f), maximum treatment temperature reached while curing (i.e. 23°C, 60°C or 90°C (73 °F, 140 °F or 194°F)), and the stress level maintained during the creep test (i.e. 40% means that the stress level at the time of loading was 40%). For example, Mix “D-2f-90C-40” indicates that the Ductal premix was used with 2% steel

fiber content, thermally treated at 90°C (194°F), and loaded at 40% of its tensile strength at the time of loading. For the compressive creep test, the letter "C" is added after the letter "D" to differentiate between tensile and compressive creep mixes. It is to be noted that tensile and compressive creep specimens for a certain curing condition were cast of the same batch. Also, the term that indicates the stress level was removed for the micro/nano-scale. The only difference in nomenclature here is adding the letter "P" for the mix where creep specimens were pre-cracked. The purpose of pre-cracking specimens from a certain mix was to investigate whether introduced cracks would creep to failure in tension or not under sustained load.

Table 6.1: Different UHPC mixes, curing, and loading conditions

Tests performed	Mixture ID	Stress/strength at loading (%)	Curing temperature[1]	Fiber content	Notes
Tensile creep and free shrinkage	D-2f-90C-40	40	90°C (194°F)	2% by vol.	Discussed in Chapter 5
	D-2f-23C-40	40	23°C (72°F)	2% by vol.	
	D-1f-90C-40	40	90°C (194°F)	1% by vol.	
	D-0f-90C-40	40	90°C (194°F)	0% by vol.	
	D-0f-23C-40	40	23°C (73°F)	0% by vol.	
	D-2f-90C-60	60	90°C (194°F)	2% by vol.	
	D-2f-90C-80	80	90°C (194°F)	2% by vol.	Failed after 2 minutes
	D-2f-90C-40-P	40	90°C (194°F)	2% by vol.	
Compressive creep and free shrinkage	D-C-2f-90C-40	40	90°C (194°F)	2% by vol.	Discussed in Chapter 5
	D-C-2f-23C-40	40	23°C (72°F)	2% by vol.	
	D-C-1f-90C-40	40	90°C (194°F)	1% by vol.	
	D-C-0f-90C-40	40	90°C (194°F)	0% by vol.	
	D-C-0f-23C-40	40	23°C (73°F)	0% by vol.	

[1] All samples were cured at 100% RH

6.2 Research Significance

Tensile creep of UHPC has not been characterized in the published literature. Because of the potential of UHPC to reduce maintenance costs associated with the conventionally reinforced concrete girders and steel girders, UHPC is being considered for use in precast prestressed concrete highway bridge girders. UHPC girder construction differs from that of girder produced from conventional structural concrete in that there may be reduced requirements for transverse shear reinforcement due to the higher tensile and shears strengths of the material. This means that the UHPC's tensile capacity may be used to resist shear-induced diagonal tensile forces may eliminate the need for stirrups. Before specifying such girders without shear reinforcement, the long-term tensile performance of the material has to be fully characterized because there is no steel reinforcement backup to the concrete's tensile/shear capacity.

In this chapter, the effect of steel fiber content, tensile stress level, and tensile overloading on the tensile creep of UHPC is investigated. This investigation complements the study presented in Chapter 5, presents new data on creep and shrinkage of UHPC, and contributes to the understanding of the factors driving long-term tensile deformations in UHPC.

6.3 Effect of Fiber Content

Several studies have shown that incorporating fibers in concrete can improve tensile and flexural strength, impact resistance and toughness, control cracking, and increase post-cracking ductility [Lankard, 1975; Swamy and Barr, 1989; and Banthia et al. 1999]. Fiber contents in concrete typically range from about 0.3 to 2.0% by volume. The toughening mechanisms provided by incorporating fibers in concrete are explained in detail in Chapter 2. In summary, three different stages can be defined from the beginning of tensile loading of fiber reinforced

concrete until failure. In stage one, microcracks form randomly throughout the entire volume of concrete, although there may be a preference for their initiation at sites of stress concentration, such as at the interfaces between dissimilar materials. During stage two, the newly formed microcracks join together (and with pre-existing microcracks) to form localized macrocracks which negatively affect the mechanical behavior. In stage three, one or more macrocracks become wider and propagate causing the overall failure [Namaan and Homrich, 1989 and Rossi, 2001].

In spite of the various improvements resulting from incorporating fibers in concrete mentioned above, recent studies have shown that using short steel fibers may increase tensile creep compared to the same mix without fibers. This increase in tensile creep with fiber reinforcement is believed to be due to an increase in the void ratio or the formation of porous interface around fibers [Bissonnette and Pigeon, 1995 and Bissonnette et al., 2007].

In this chapter, the effect of varying the fiber content in UHPC is investigated. The UHPC mix design used in the study is presented in section 5.4. Three fiber contents were selected for this study (0%, 1%, and 2% by volume). Five UHPC mixes were considered at two curing regimes, 23°C (73^{o}F) and 90°C (194^{o}F) (Table 6.1).

6.3.1 Mechanical Properties

A summary of all mechanical properties is shown in Table 6.2. In addition, results from each test is separately presented and discussed in the following sections.

Table 6.2: Summary of mechanical properties of UHPC mixes at the age of 7 days

Mixture ID	Compressive Strength MPa (ksi)	Tensile strength MPa (ksi) [Direct Tension]	Modulus of Elasticity MPa (ksi)		Poisson's ratio	
			E_c	E_t	υ_c	υ_t
D-2f-90C-40	169 (24.6)	10.30 (1.50)	47,950 (6,953)	57,470 (8,336)	0.14	0.20
D-1f-90C-40	188 (27.0)	7.55 (1.10)	46,488 (6,743)	55,530 (8,054)	0.14	0.19
D-0f-90C-40	159 (23.0)	7.25 (1.05)	45,294 (6,570)	50,729 (7,358)	0.16	0.20
D-2f-23C-40	116 (16.9)	7.50 (1.10)	44,900 (6,510)	56,810 (8,241)	0.14	0.16
D-0f-23C-40	90 (13.0)	4.80 (0.70)	42,900 (6,220)	47,540 (6,893)	0.15	0.18

6.3.1.1 Compressive strength

The compressive strength of UHPC was determined by testing 3 x 6-in (75x 150-mm) cylinders according to ASTM C 39. Five specimens were tested from each batch for each measurement. All batches were tested at the ages of 7 and 28 days.

Test results showed that the average 7-day compressive strength of mixes D-2f-90C-40, D-1f-90C-40, and D-0f-90C-40 was 169 (24.6), 188 (27), and 159 (23) MPa (ksi) respectively. When comparing the specified 2% fiber volume to unreinforced thermally treated UHPC, this is decrease of 6% upon eliminating fiber reinforcement. Compressive strengths of non-thermally treated UHPC, mixes D-2f-23C-40, and D-0f-23C-40 were 116 (16.9) and 90 (13) MPa (ksi), respectively (Figure 6.1). This is 22% reduction in the 7-day compressive strength upon eliminating fiber reinforcement. That is, as the fiber content was reduced, more loads would be carried directly by the cementitious matrix causing reduction in strength. In addition, reductions in the compressive strength upon eliminating fibers could have resulted, partly, from variations

in the particle packing of UHPC premix due to changing fiber content and, thus, increasing the void ratio of the matrix. However, there may be additional effects related to the fiber/paste bonding and improvements in mixture consolidation, as suggested by the higher compressive strength values for the 1% fiber volume fraction thermally treated case. Overall, the variations in compressive strength with varying fiber dosage rates are smaller than the reductions which resulted from eliminating thermal treatment (Chapter 5), demonstrating that the effect of thermal treatment on the compressive strength is larger than the influence of fiber content within the range of 0-2%.

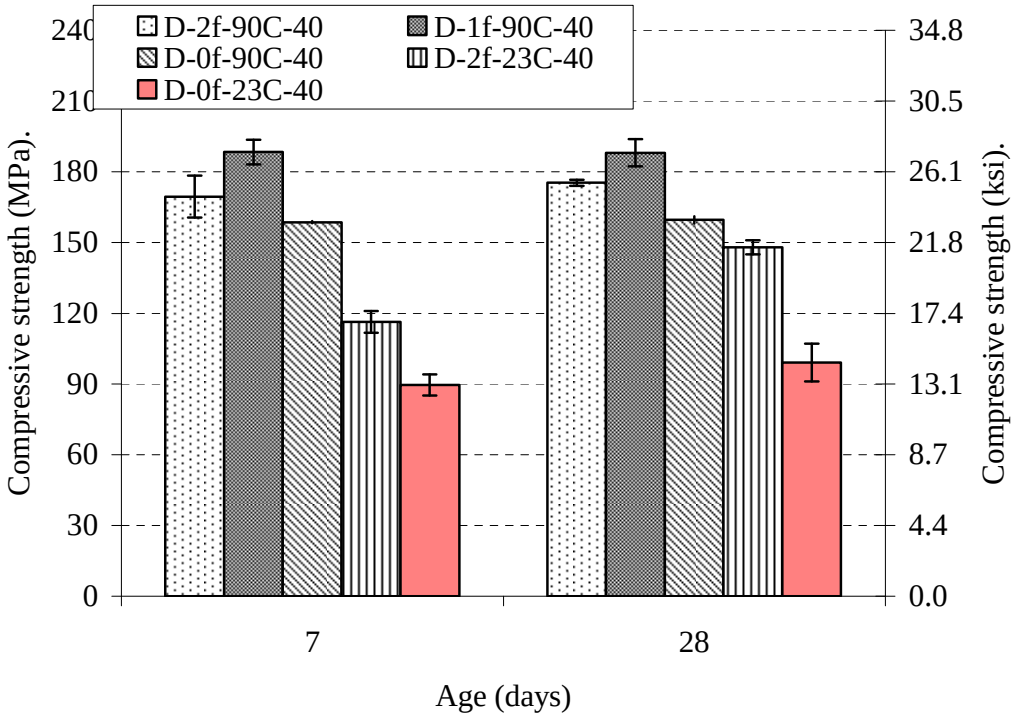

Figure 6.1 Compressive strength of different UHPC mixes

Figure 6.1 shows that thermally treated UHPC did not significantly increase strength between 7 and 28 days. In contrast, 28-day strength for the non-thermally treated UHPC mixes

D-2f-23C-40 and D-0f-23C-40 increased by 27% and 10% compared to their 7-day strength values. These results indicate the effectiveness of thermal treatment regimes in refining the UHPC microstructure and in promoting early compressive strength development, which is critical to the precast prestressed girder industry.

6.3.1.2 Tensile strength

Direct tension tests were performed using dog bone-shaped test specimens 235 mm (9.25-in) in length with a cross section of 50x50 mm (2x2-in). The full details of the test setup are presented in Chapter 4. Two 1.2-in (30 mm) long electrical resistance strain gages were attached longitudinally and two transversely on opposite sides of the specimen to determine the elastic modulus and Poisson's ratio. All batches were tested at the age of 7 days.

Direct tension test results for thermally treated UHPC showed a decrease of 26% and 27% in the tensile strength upon decreasing the fiber content to 1% or 0%, respectively. That is, the tensile strength of the 1% and unreinforced thermally treated cases were indistinguishable. These results suggest that fibers at 2% volumetric content were close enough to carry loads and cross tensile cracks while this was not the case when the fiber content was reduced to 1%. These results further suggest that the measured increase in compressive strength when reducing the fiber content to 1% were likely due to improved consolidation (i.e., reduced porosity) of the mixture, rather than true improvements in packing efficiency. A similar reduction (35%) in tensile strength was measured for the unreinforced non-thermally treated case compared to the reinforced case. It is to be mentioned that fibers were aligned more with the loading direction in tensile strength tests compared to compressive strength tests. That is, longitudinally aligned fibers in tension would cross tensile cracks while transversally aligned fibers would cross tensile cracks in compression.

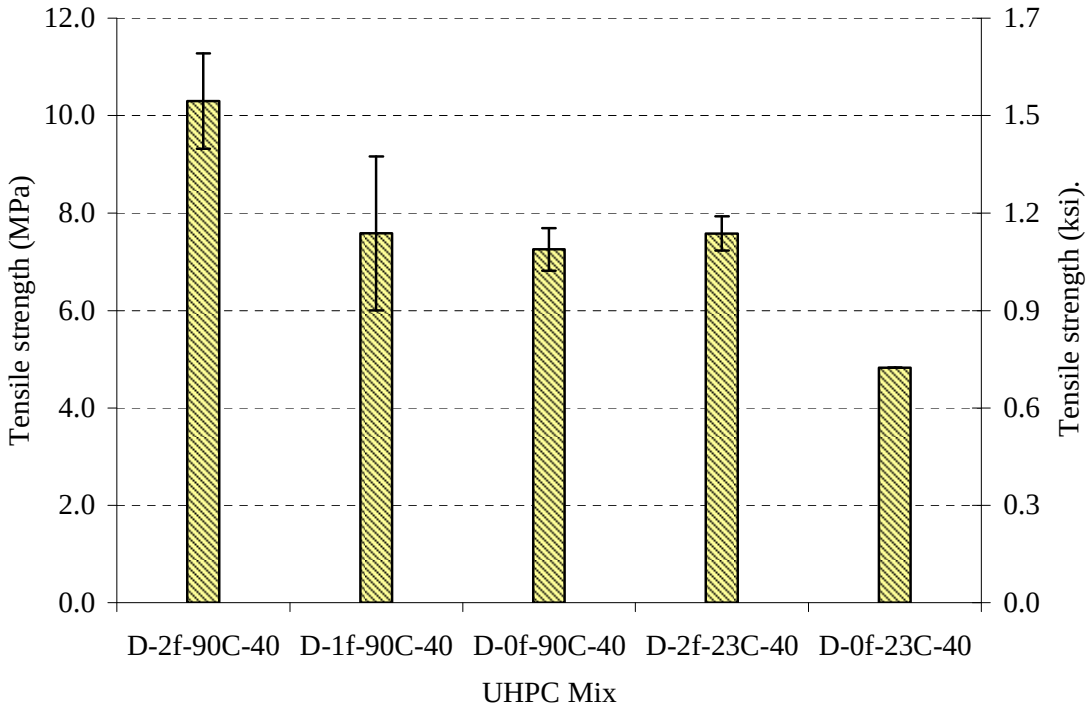

Figure 6.2: Direct tension test results for different UHPC mixes

This direct relation found between the fiber content and the tensile strength is due to the efficiency of steel fibers in restraining cracking and thus increasing the ultimate tensile strength. Also, reductions in the tensile strength upon reducing or eliminating fibers could have been affected by the lack of optimized particle packing of the UHPC resulting from altering the reference design mix (i.e., 2% fibers). It is to be noted that tensile failure happened as soon as the first crack appeared for non-fiber reinforced UHPC. This was not the case in fiber-reinforced UHPC where the load capacity decreased gradually as fibers continued to pull out of the matrix to the point of complete failure. This observation suggests that incorporating fibers in UHPC for bridge girders is essential if no shear reinforcement is used.

6.3.1.3 Modulus of elasticity

The Young's modulus of elasticity and the Poisson's ratio were determined for each mix both in compression and tension at the age of 7 days. In compression, the chord modulus of elasticity was measured using 4x8-in (100x200-mm) cylinders loaded in compression. More details about the test setup are presented in Chapter 4. Tensile and compressive moduli were calculated as explained in chapter 5.

In compression, the elastic modulus decreased 3% and 6% upon decreasing the fiber content to 1% and 0%, respectively. Results also showed a decrease of 5% upon eliminating fibers for non-thermally treated UHPC (Figure 6.3). Analysis of Variance (ANOVA) was conducted and showed the difference in moduli upon varying the amount of fibers was insignificant within each curing regime. In addition, results in Table 6.2 showed that the Poisson's ratios in compression obtained for the three mixes considered ranged from 0.14 to 0.16. These values were within the range for ordinary concretes [Mehta and Monteiro, 2005].

In tension, elastic modulus decreased 3% and 12% upon decreasing the fiber content to 1% and 0%, respectively. Results also showed a decrease of 16% upon eliminating fibers for non-thermally treated UHPC (Figure 6.3). These E_t values averaged 19% higher than the E_c values obtained in compression; this is likely due to the fact that fibers were longitudinally aligned in the dog bone specimens while they were more randomly dispersed in the compression test cylinders. The Young's modulus of elasticity of fibers used was 210,000 MPa (30,457 ksi). This hypothesis can be partially explained by the fact that the difference in Poisson's ratios for non-fiber reinforced UHPC was half of that for fiber reinforced mixes.

It is to be mentioned that the increase in the modulus values with fibers in compression was in good agreement with the rule of mixture predictions while this was not the case in tension

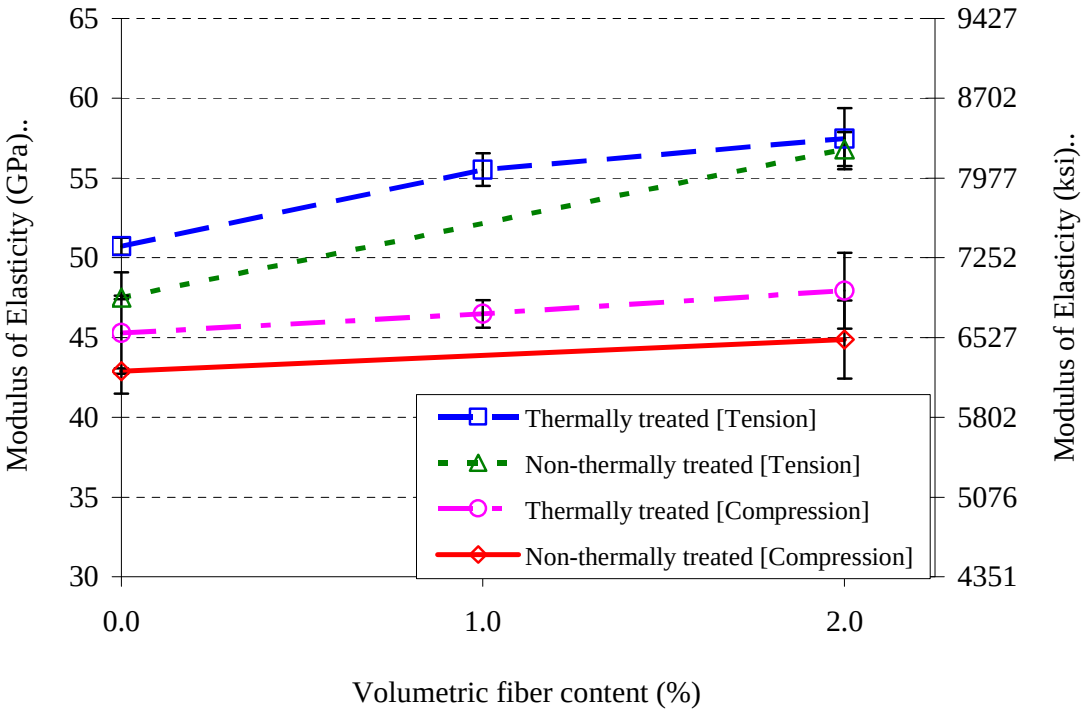

Figure 6.3: The effect of fiber content of the compressive and tensile modulus of elasticity for different UHPC mixes

where the rule of mixture prediction would underestimate the effect of fibers. Further research is still needed to explain this observation.

By comparing modulus of elasticity reductions resulting from fiber elimination in tension and compression (i.e., 6% in compression versus 12% in tension), it is evident that the influence of fiber reinforcement is more pronounced in tension than compression since more fibers were aligned in the longitudinal direction in tension than compression. This observation again emphasizes the importance of fibers in resisting the shear induced diagonal tension in bridge girders if no conventional shear reinforcement (i.e., stirrups) is used. Also, results in Table 6.2 showed reductions in the Poisson's ratio upon increasing the amount of fibers for both thermally treated and non-thermally treated UHPC. These reductions ranged between 5% and 11% in

tension and 7% and 13% in compression. This shows a relatively bigger effect of fibers in compression than tension due to more random fiber orientation.

In summary, mechanical properties measured underscores the importance of the fiber content and fiber orientation in determining strength and stiffness properties of UHPC.

6.3.2 Tensile Creep

6.3.2.1 Tensile creep samples

Three tensile creep 75x75x483 mm (3x3x19-in) concrete prism specimens connected in series and three companion free shrinkage specimens were used for each testing case. After initial curing or initial curing plus thermal treatment, previously discussed mechanical tests were performed before the start of creep tests at age of 7 days.

6.3.2.2 Tensile creep test

The tensile creep test setup and procedure used in the long-term study is discussed in detail in Chapter 4. Test conditions were kept at 23 ± 2 ^{o}C and 50 ± 3% RH for the entire creep testing period. Tensile creep deformations were measured initially at 1, 2, 4, 6, and 24 hours after loading. Subsequently, measurements were made daily for week, weekly for a month, and monthly for the rest of the testing period. Specific creep was calculated by dividing the adjusted tensile creep strain by the initial applied stress. The adjusted tensile creep strain is equal to the sum of the measured creep strains and the free shrinkage strains.

6.3.2.3 Results and discussion

Figure 6.4 shows the measured free shrinkage strains where the influence of varying the fiber content was examined for a period of 90 days. A summary of the key results is presented in

Table 6.3. The following discussion mainly focuses on the differences found in the specific creep values for thermally treated and non-thermally treated UHPC (Figure 6.5).

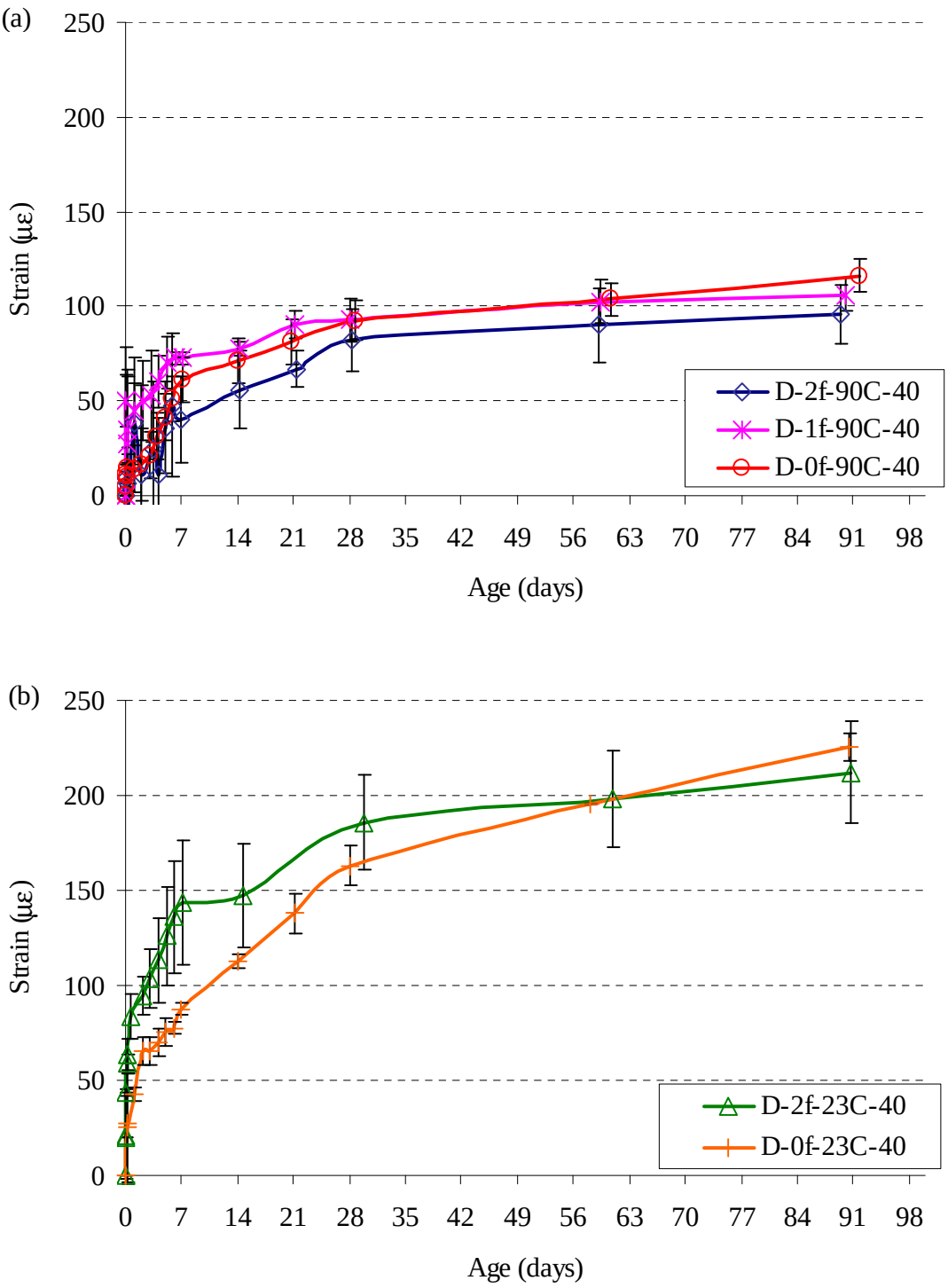

Figure 6.4: Free shrinkage of: (a) thermally treated UHPC and (b) non-thermally treated UHPC

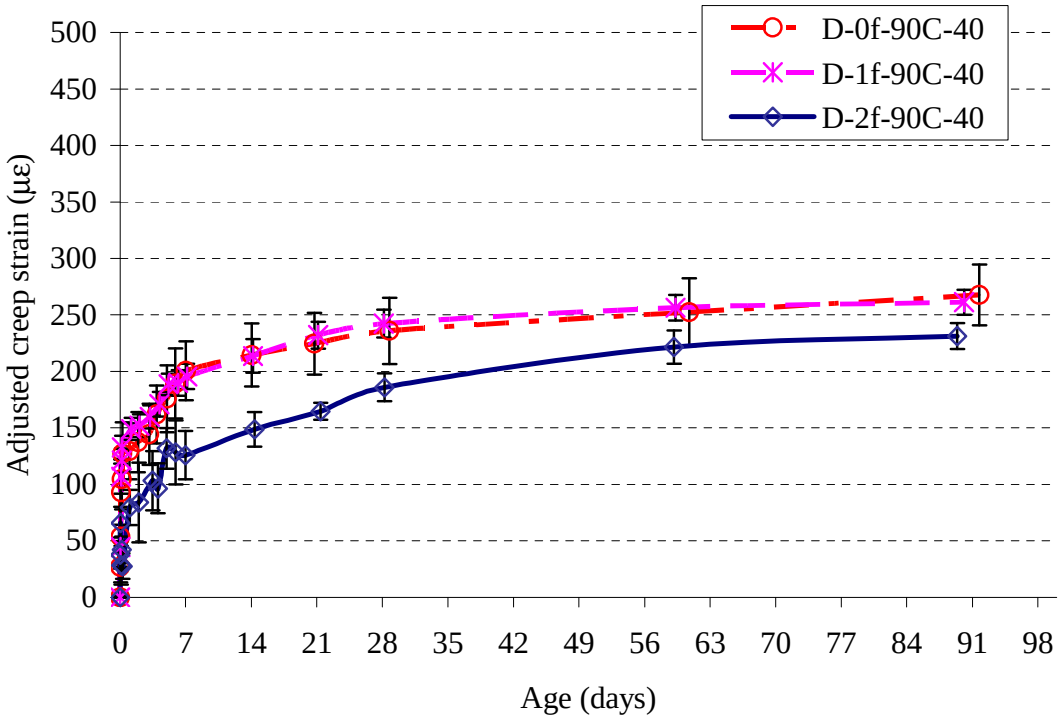
D-0f-90C-40
D-1f-90C-40
D-2f-90C-40
Adjusted creep strain (με)
Age (days)
0
50
100
150
200
250
300
350
400
450
500
0
7
14
21
28
35
42
49
56
63
70
77
84
91
98

(b)

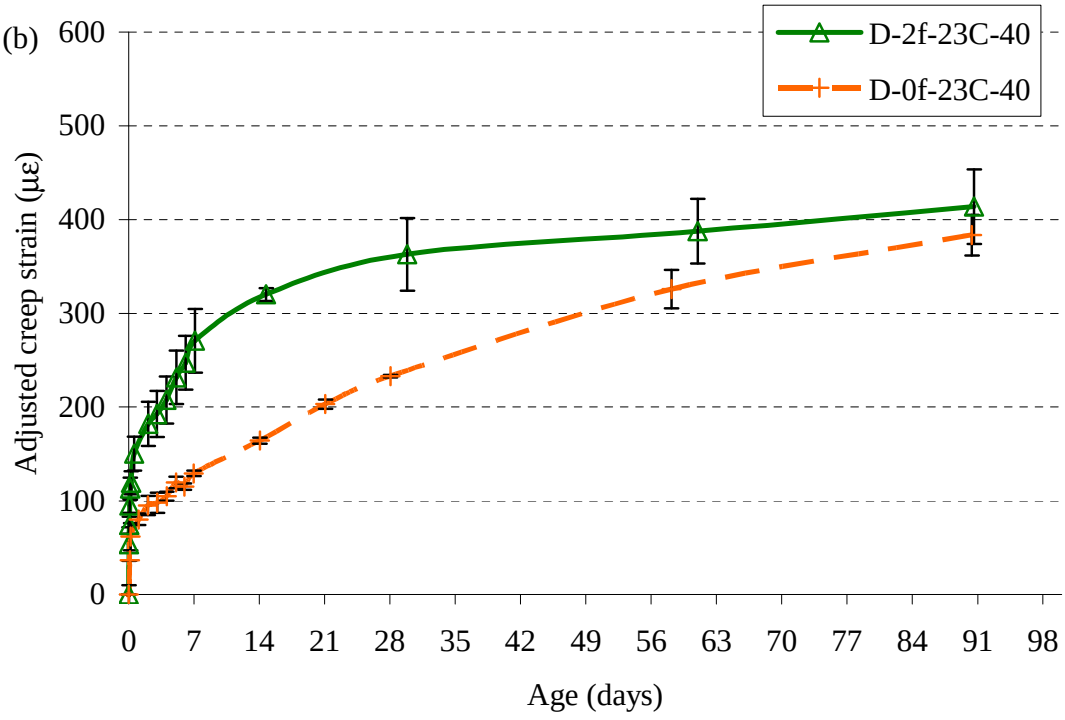
D-2f-23C-40
D-0f-23C-40
Adjusted creep strain (με)
Age (days)
0
100
200
300
400
500
600
0
7
14
21
28
35
42
49
56
63
70
77
84
91
98

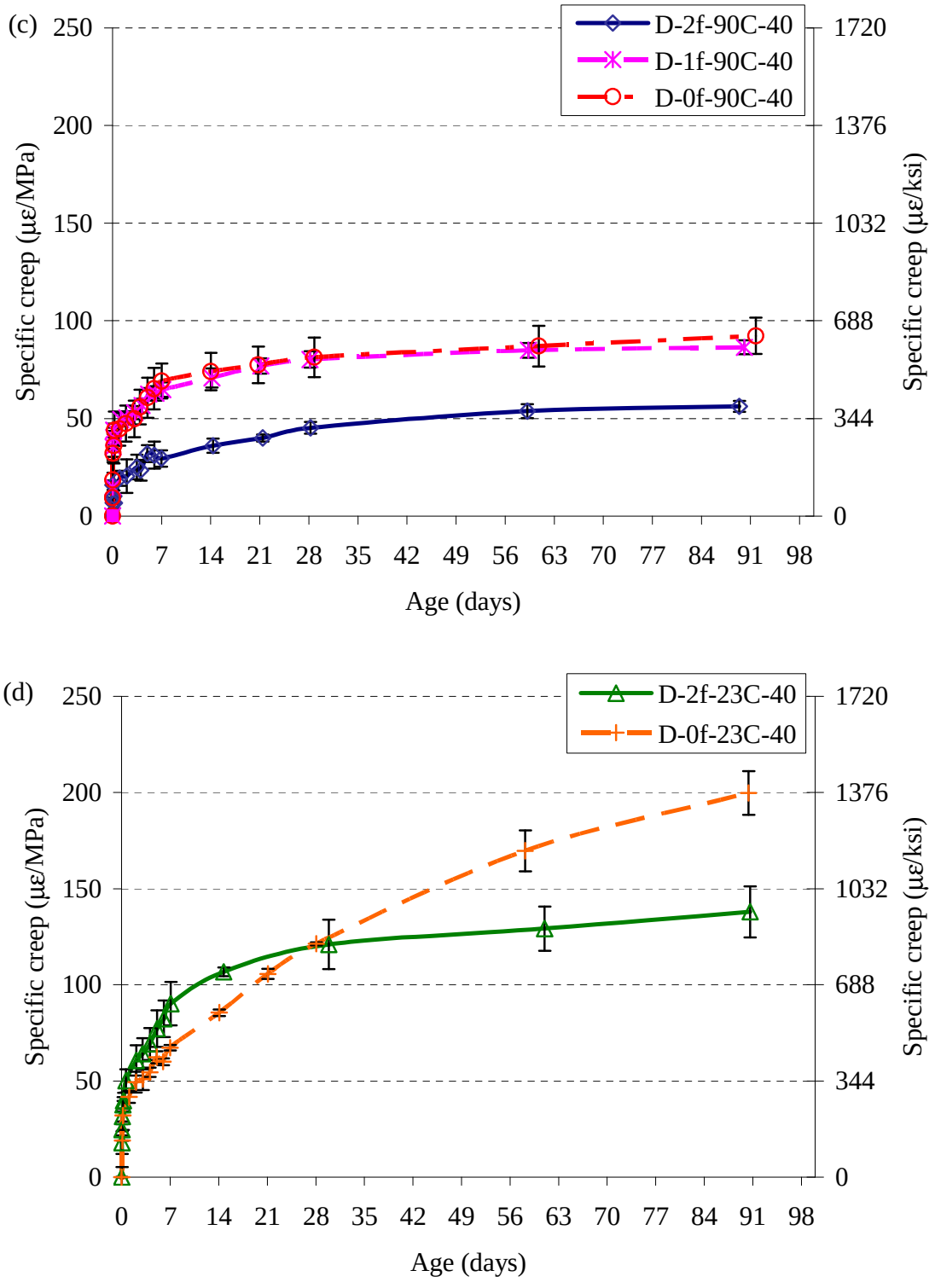

Figure 6.5: Effect of fiber content on tensile creep of UHPC (a) adjusted creep strain for thermally treated UHPC, (b) adjusted creep strain for non-thermally treated UHPC, (c) specific creep of thermally treated UHPC, and (d) specific creep of non-thermally treated UHPC

Table 6.3: Summary of tensile creep and shrinkage properties of UHPC at 90 days

Mix	Strains at 90 days		Specific tensile Creep at 90 days	% change of specific from D-2f-90C-40 at 90 days	
	Adjusted creep (με)	Free shrinkage (με)	με/MPa (με/ksi)	Tensile creep strain	Specific tensile creep
D-2f-90C-40	231	96	56 (385)	N/A	N/A
D-1f-90C-40	261	106	86 (593)	+13	+53
D-0f-90C-40	268	116	92 (637)	+16	+64
D-2f-23C-40	414	212	137 (940)	+79	+145
D-0f-23C-40	383	226	200 (1,370)	+65	+257

Free shrinkage results of thermally treated UHPC at 90 days showed an increase of 10% and 21% in the free shrinkage strain upon decreasing the fiber content to 1% and 0%, respectively. For non-thermally treated UHPC, results showed an increase of 7% in the free shrinkage strain upon eliminating fibers.

Results in Figure 6.5 showed a significant influence of fiber content on the specific tensile creep. For thermally treated UHPC, Figure 6.5 (b), specific tensile creep increased 53% and 64% when the fiber content was decreased to 1% and 0%, respectively. For non-thermally treated UHPC, Figure 6.5 (d), an increase of 46% in the specific tensile creep was measured upon eliminating fibers. This showed that the efficiency of fibers in resisting creep was more pronounced in thermally treated UHPC compared to non-thermally treated UHPC. It may be suggested that this difference in fiber efficiency can be attributed to the presence of a stronger fiber-matrix interface in thermally treated UHPC mixes [Section 5.7]. In addition, it is noteworthy that, upon eliminating fibers, the relative increase in tensile creep was about double

the relative decrease in the tensile strength, for both thermally treated and non-thermally treated UHPC.

The effect of fibers on tensile deformation of concrete is a balance between the restraints they induce due to their higher modulus compared to the matrix and the creation of a more porous fiber-cementitious matrix interface. The influence of fiber-matrix interfacial structure and bonding has been previously recognized for normal and high strength concretes [Bissonnette & Pigeon, 1995, Bissonnette et al., 2007, Stengel, 2008, and Stengel, 2009].

The decrease in tensile creep with the use of fibers is opposite to the trends reported in the literature [Bissonnette & Pigeon, 1995 and Bissonnette et al. 2007]. For example, previous research, on high strength concrete reinforced with crimped and hooked fibers [Bissonnette et al., 2007], ascribed greater tensile creep in the fiber reinforced samples to increased porosity at the fiber/matrix interface. It is proposed that the thermal curing used in UHPC but not in normal or high performance concretes contributes importantly to this variation in behavior. In previous studies, concretes were subjected to ordinary curing, and, as a result, any defects present at the fiber-matrix interface (as evident in Chapter 5) would increase tensile creep. In the current study, the potential influence of greater porosity at this interface was mitigated via thermal treatment. Also, the continuous increase in tensile creep of UHPC without fibers both in thermally treated and non-thermally treated UHPC can be attributed to failure of arresting propagating microcracks due to absence of fibers. In addition, and unlike previous studies, the efficiency of fibers in controlling microcrack growth in UHPC can be attributed to the relatively large length of steel fibers. This is, in a previous study by Bissonnette et al. [2007], the fiber length-to-maximum size of aggregates ratio was 3 while in UHPC, straight steel fibers 13 mm (0.5-in) in length were used while the maximum size of particles in a UHPC premix was about 0.6 mm

(0.02-in) [Sorelli et al., 2009], this is a fiber length-to-maximum size of aggregates ratio of 22. This relatively large size of fibers in UHPC would result in more fiber efficiency in restraining deformations compared to previous studies. Results from the current study agree with what was suggested by Bissonnette et al. [2007], that the use of straight-shape fibers in higher amounts than1% would result in improving cracking resistance of cement-based materials and, thus, in reducing tensile creep deformations.

The tensile creep of non-thermally treated UHPC exceeded that of other corresponding UHPC mixes at the age of 28 days. It is evident through comparing tensile creep results for mixes D-2f-90C-40, D-2f-23C-40, and D-0f-23C-40 that the effect of fiber content (i.e., mix D-2f-23C-40 versus mix D-0f-23C-40) on tensile creep is less significant than thermal treatment (i.e., mix D-2f-90C-40 versus mix D-2f-23C-40).

A tensile creep specimen from mix D-0f-23C-40 was found broken at the age of 94 days of loading. There is no current explanation for this failure. However, there are some givens that suggest that the failure was accidental.

Generally, two main types of bonds – tensile and shear – are recognized to occur between fibers and cementitious matrix in fiber-reinforced cement composites [Bartos, 1981]. Shear bonding transfers stresses parallel to the longitudinal axis of a fiber, while tensile bonding transfers stresses in the perpendicular direction of a fiber. In a specific composite and under specific loading configuration, one type of bond can be of much greater importance than the other, but typically both types are present and interrelated due to the Poisson's effect.

Shear bond strength plays an important rule in determining the nature of the failure mode in tension [Wang et al., 1988, Alwan et al., 1991, and Li and Mobasher, 1998]. This is because in addition to providing fiber pullout resistance, shear bond strength in fiber reinforced

cementitious composite transfers stresses from the matrix into the fiber before cracking. After cracking, shear bonding is responsible for transfer of load to uncracked parts of the matrix until failure is reached when all fibers pull out of the matrix. Two types of shear bonds are capable of transferring stresses acting along the interface: these are the elastic shear bond and the frictional shear bond. When the elastic or frictional shear bond at the fiber-matrix interface exceeds the shear strength of the matrix, a shear failure of the matrix occurs. In the presence of an elastic shear bond at the fiber-matrix interface and the shear stress does not exceed the strength of the bond the longitudinal displacements of the fiber and matrix at the interface remain compatible. On the other hand, frictional shear bond resists displacements along the interface parallel to the length of the fiber but permits a relative slip along the interface.

The tensile bond resists deformations due to forces acting perpendicular to the interface (the longitudinal axis of a fiber). It is well-recognized that tensile bond strength has a direct influence on the strength of cementitious composites reinforced with random discontinuous fibers as in UHPC. In such cases, a weak fiber-matrix interface would reduce the fibers' contribution to strength and stiffness.

Part of the contribution of the tensile bond in strengthening a cementitious fiber composite is through resisting radial deformations (contractions in case of tension) due to the Poisson's effect. When the tensile stress acting at the interface exceeds the strength of the tensile bond, an instantaneous and complete debonding occurs. As in shear bonding, if the magnitude of the tensile bond strength is higher than either composite phases surrounding it, cracking and failure would occur in either or both phases instead of at the interface. A precise determination of the tensile bond strength in fiber composites remains difficult to measure experimentally;

single fiber pull-out tests remain the most commonly used methods for assessing tensile bond strength, but is prone to high variability [Bartos, 1981].

Recently, Stengel [2009] described a method to improve tensile bond strength between straight steel fibers and UHPC, a material system similar to that under study here. Stengel examined roughening of the steel fiber surface with abrasive papers and found that the fiber-matrix bond measured by assuming constant bond stress over the whole embedded length was improved up to 200%, as measured by pull-out tests. This improvement was attributed to the increased stress transfer area resulting from increased fiber roughness [Stengel, 2009]. While providing a reasonable option for improving the fiber-matrix bond, practical issues stemming from fiber roughening – including potential decreases in workability – should be investigated. Therefore, it is the author's opinion that thermal treatment is currently the most suitable solution for obtaining good tensile bond.

In summary, it is proposed that steel fiber reinforcement at a rate of 2% by volume with thermal treatment would result the desired UHPC microstructure and mechanical performance. Improvements in the initial microstructure, particularly at the fiber/matrix interface, will improve the fibers' efficiency in reducing long-term tensile and free shrinkage deformations.

6.3.3 Compressive Creep

Compressive creep of UHPC has been the subject of very few prior studies [Graybeal, 2005 and Burkart and Muller, 2008]. The current compressive creep study helps to understand the mechanisms underlying tensile creep. Results of the compressive study are presented here followed by a comparison between the tensile and compressive creep performances of UHPC.

6.3.3.1 Compressive creep samples and test

Compressive creep of each UHPC mix shown in Table 6.1 was measured on three 100x380 mm (4x15-in) cylinders similar to ASTM C 512 specifications. The size of the specimens used in this study is different from the ASTM C 512 standard (150x300 mm (6x12-in)). This modification was necessary due to the ultra-high strength of UHPC which dictated reducing the cross section of the test specimens. Three additional non-loaded companion specimens were used to measure free shrinkage. All cylinders were instrumented with four sets of steel inserts located diametrically opposite on the surface of the specimen. Each set was a 10-in (254-mm) long gauge line for measuring deformation with a detachable mechanical gauge (DEMEC gage). Each mix was cured or cured and thermally treated the same as tensile creep specimens since they were cast from the same mix. Before creep tests started, compressive strength and modulus of elasticity tests were performed for each mix. Compressive creep tests were started at the same times as tensile creep tests, at the age of 7 days. Specific creep was calculated by dividing the adjusted compressive creep strain by the initial applied stress. The adjusted compressive creep strain was calculated by subtracting the shrinkage strain from the measured creep strains and the free shrinkage strains.

6.3.3.2 Results and discussion

Figure 6.6 shows the measured free shrinkage strains where the influence of varying the fiber content was examined for a period of 90 days. A summary of the key results is presented in Table 6.4.

Free shrinkage at 90 days of thermally treated UHPC increased by 38% upon decreasing the fiber content to 1% or 0%. For non-thermally treated UHPC, results showed an increase of 20% in the free shrinkage strain upon eliminating fibers.

Similarly, a significant influence of fiber content was demonstrated in the compressive creep data (Figure 6.7) For thermally treated UHPC, Figure 6.7 (b), an increase of 13% and 31% in the specific tensile creep was measured upon decreasing the fiber content to 1% or 0%, respectively. For non-thermally treated UHPC, Figure 6.7 (d), an increase of 27% in the specific compressive creep was found upon eliminating fibers from the mix. These results agree with tensile creep results that showed that the efficiency of fibers in resisting creep is generally more pronounced in thermally treated UHPC compared to non-thermally treated UHPC; it was proposed that this is due to increasing strength of the fiber-matrix interface in thermally-treated UHPC. It is to be noted that the relative increase in compressive creep upon eliminating fibers were larger than the decrease in the compressive strength for both thermally treated and non-thermally treated UHPC at 7 days.

Table 6.4: Summary of compressive creep and shrinkage properties of UHPC at 90 days

Mix	Strains at 90 days		Specific compressive creep at 90 days	% change from D-2f-90C-40 at 90 days	
	Adjusted creep (με)	Free shrinkage (με)	με/MPa (με/ksi)	Compressive creep strain	Specific compressive creep
D-2f-90C-40	217	60	3.2 (22.0)	N/A	N/A
D-1f-90C-40	269	83	3.6 (24.9)	+24	+13
D-0f-90C-40	184	83	4.2 (28.9)	+26	+31
D-2f-23C-40	385	142	8.7 (51.5)	+77	+140
D-0f-23C-40	379	171	10.6 (73.1)	+75	+230

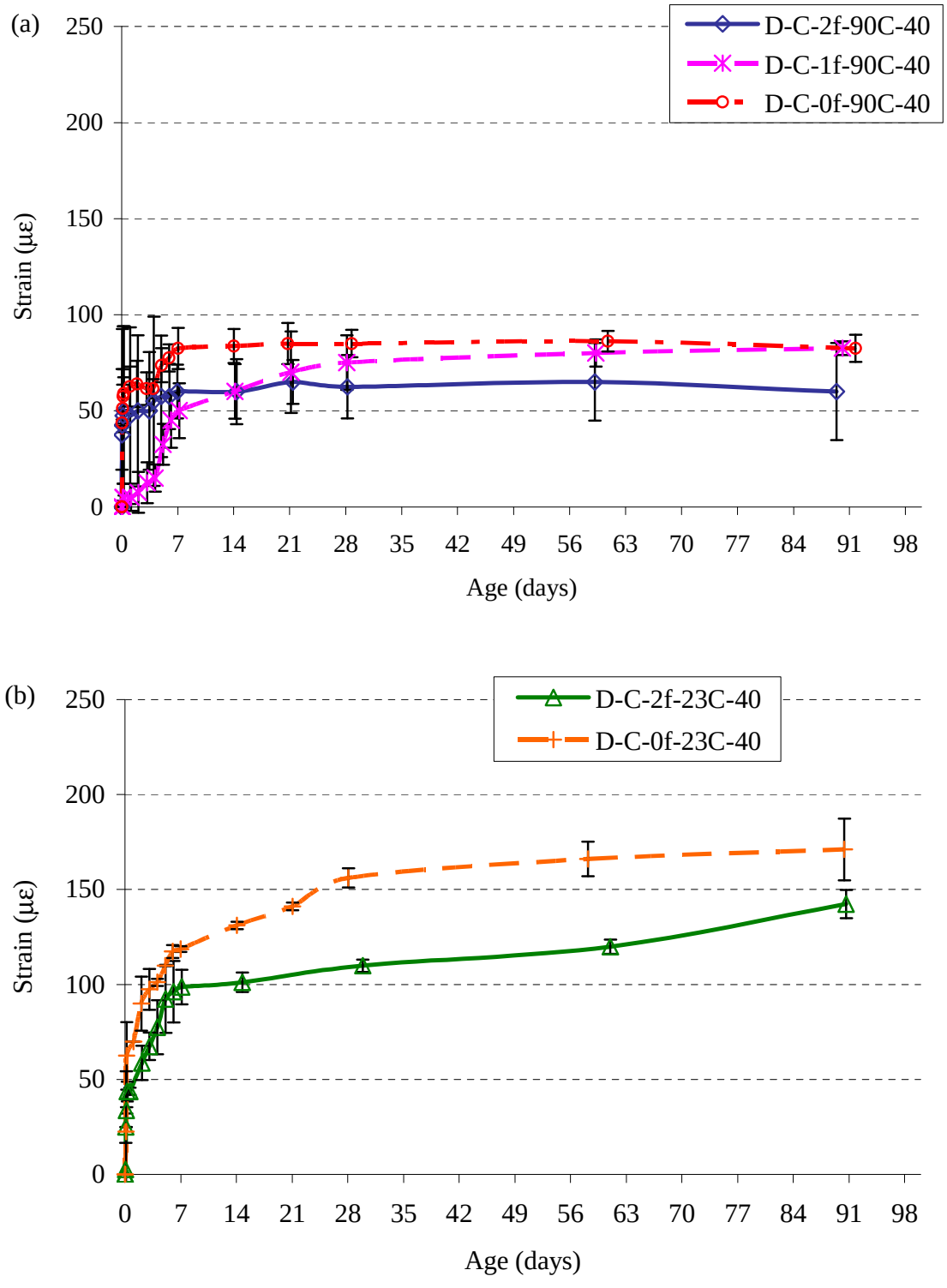

Figure 6.6: Free shrinkage of: (a) thermally treated UHPC and (b) non-thermally treated UHPC

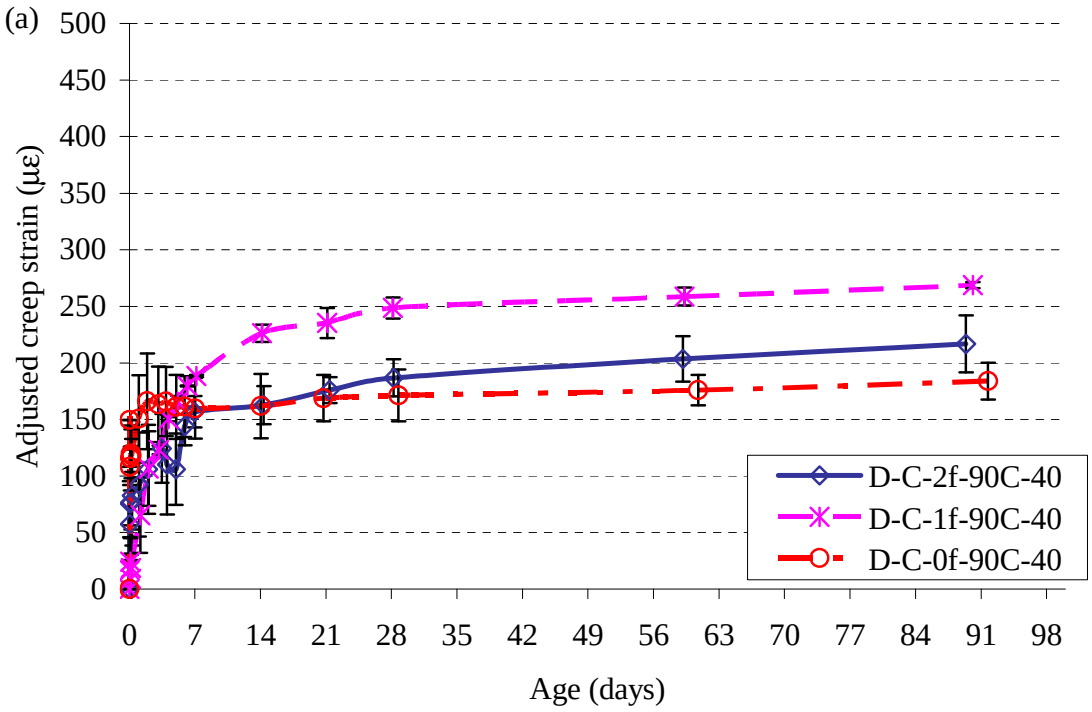
(a)
Adjusted creep strain (με)
500
450
400
350
300
250
200
150
100
50
0
0
7
14
21
28
35
42
49
56
63
70
77
84
91
98
Age (days)
D-C-2f-90C-40
D-C-1f-90C-40
D-C-0f-90C-40

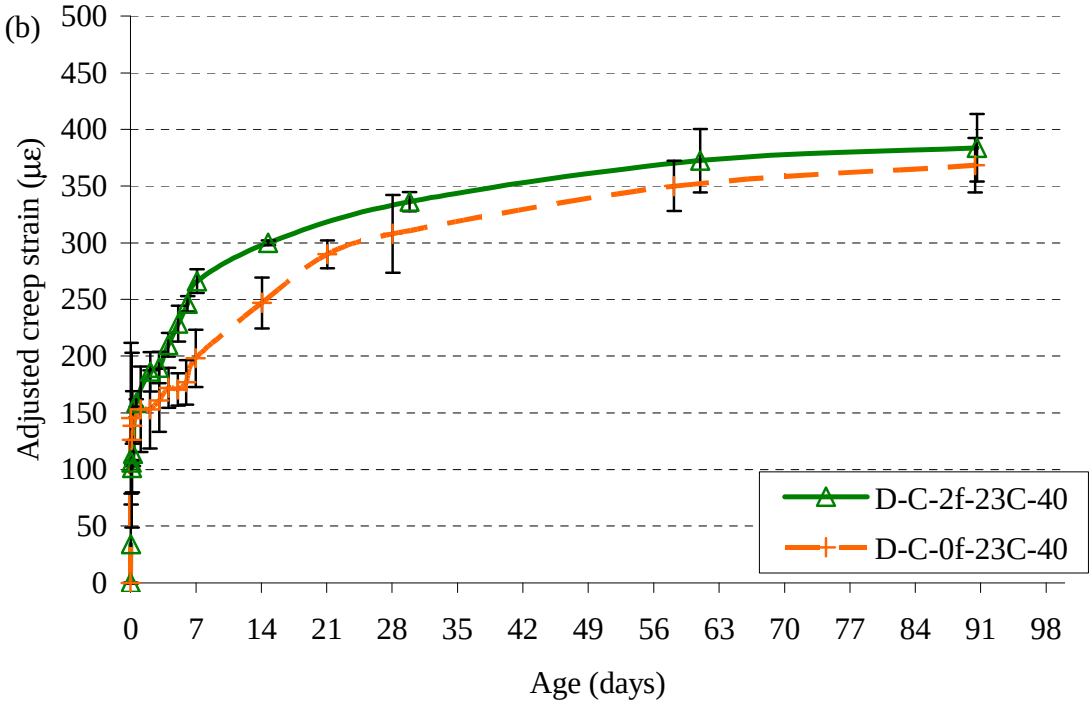
(b)
Adjusted creep strain (με)
500
450
400
350
300
250
200
150
100
50
0
0
7
14
21
28
35
42
49
56
63
70
77
84
91
98
Age (days)
D-C-2f-23C-40
D-C-0f-23C-40

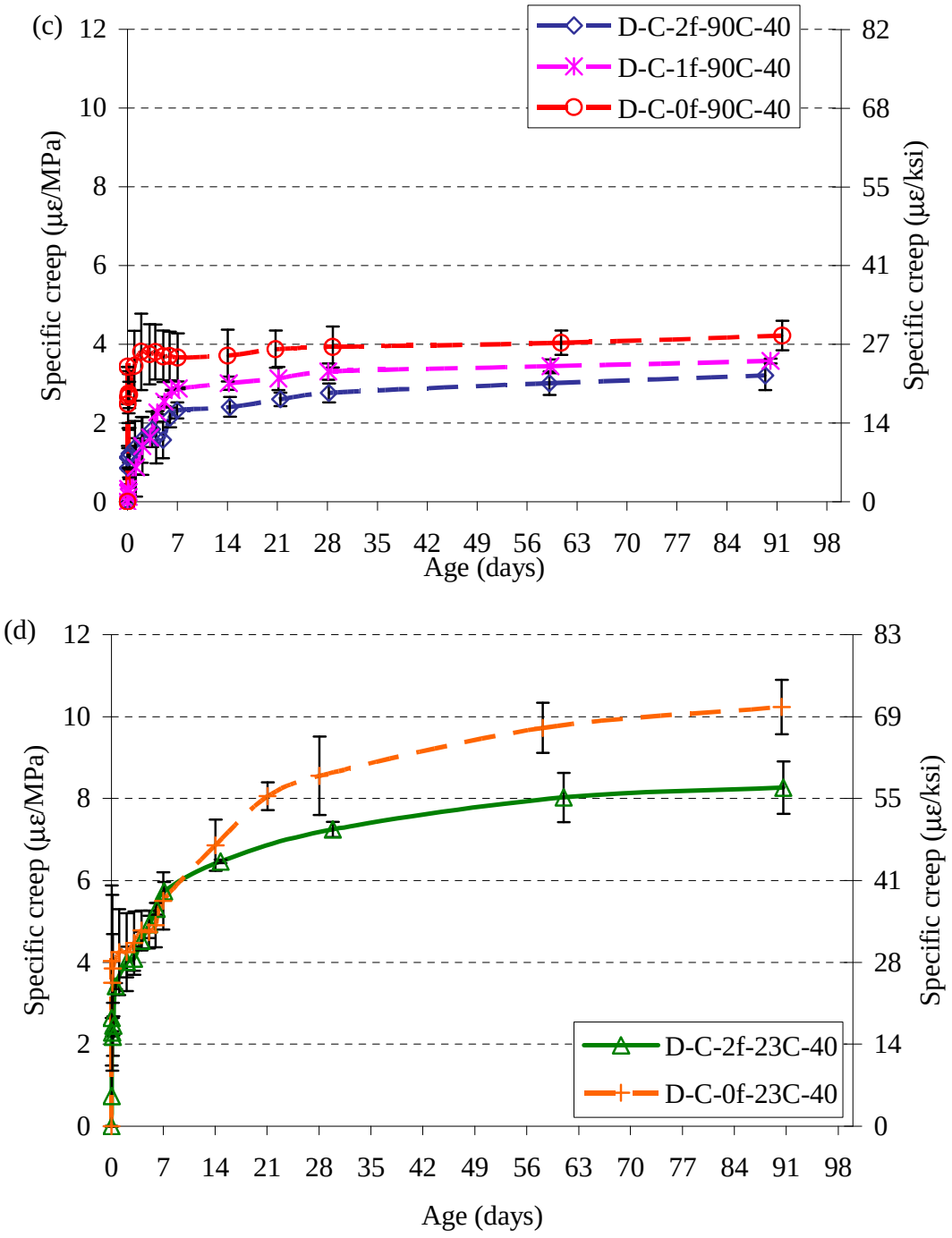

Figure 6.7: Effect of fiber content on compressive creep of UHPC (a) adjusted creep strain for thermally treated UHPC, (b) adjusted creep strain for non-thermally treated UHPC, (c) specific creep of thermally treated UHPC, and (d) specific creep of non-thermally treated UHPC

Also, the presence of fibers in a high dose (i.e., 2%) may make them function as barriers against water seepage to the environment or at least reduce the rate of seepage especially if preferably aligned perpendicular to the seepage direction (i.e., fibers aligned longitudinally while seepage is likely to happen radially). In addition, since most of the fibers were aligned in the loading (longitudinal) direction, it is likely that more of the loads were carried by fibers as their volume content increased. The increase in the load carried by fibers resulted in reduced load on the cementitious matrix, thus reducing creep deformations.

The influence of fibers on the compressive creep and shrinkage of concrete has been the subject of some prior theoretical and experimental studies where the effect of various fiber properties was investigated [Mangat and Azari, 1985, Zhang and Li, 2001, and Zhang, 2003]. Major assumptions of these studies were: (1) cylindrical fibers, (2) perfect initial fiber-matrix interface, (3) fiber alignment in the loading direction, (4) fibers affected only the flowing part of creep not the delayed elastic part, (5) no overlap between fibers' effect zones in the matrix, and (6) shear bond strength between fibers and cementitious matrix to be directly proportional to the net pressure exerted on the fiber by the matrix through the coefficient of friction. The net value of the radial compressive pressure exerted on a fiber, *P*, can be calculated by considering the virtual lateral strains occurring in the matrix, *u*, given by Equation 6.1:

$$u = u_m - u_1 - u_f \tag{6.1}$$

where: u_m is the unrestrained radial shrinkage of the matrix, u_1 is the lateral deformation of the matrix resulting from sustained loads, and u_f is the lateral strain of the fiber under pressure *P*. This pressure, *P*, is directly proportional to the fiber-matrix shear bond shear strength, τ (Equation 6.2) (Figure 6.8):

$$\tau = \mu P \tag{6.1}$$

where: μ is the coefficient of friction between steel fibers and cementitious matrix.

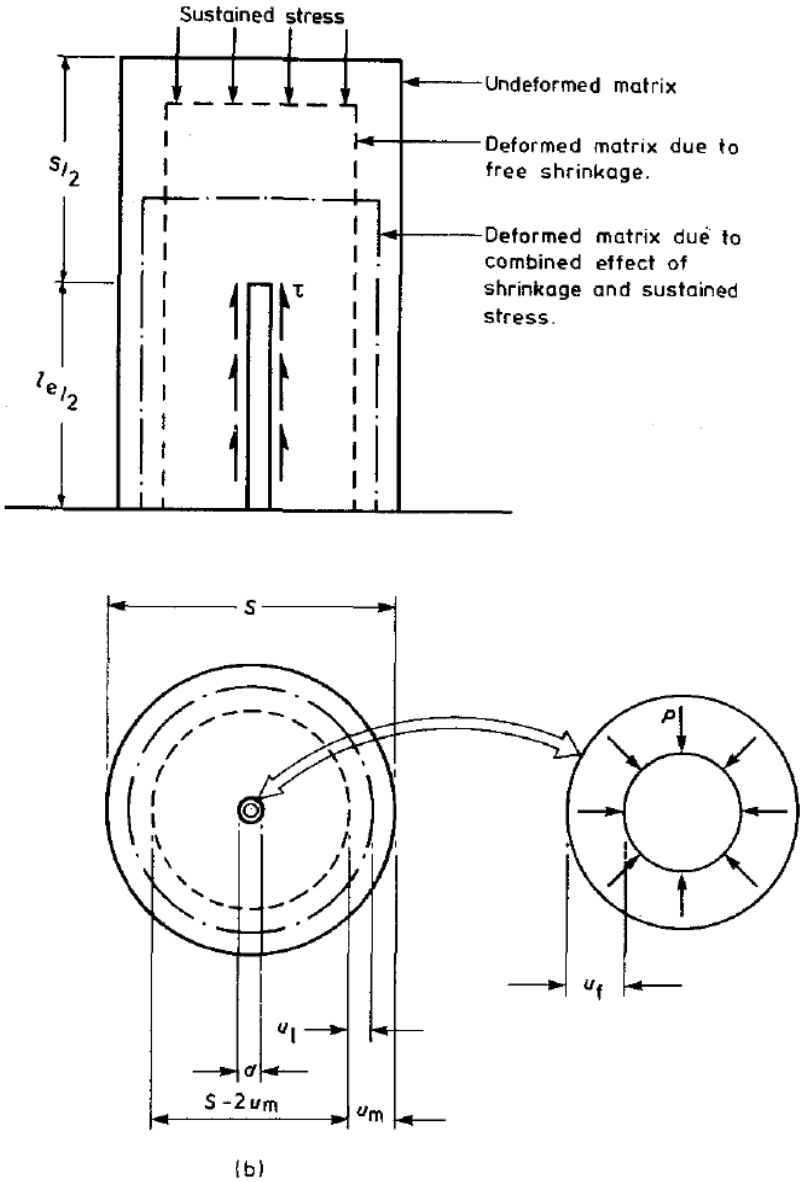

Figure 6.8: Creep model for fiber reinforced concrete [Mangat and Azari, 1985]

Experimental results of the study by Mangat and Azari [1985] showed that incorporating steel fibers reduced the overall composite compressive creep up to a stress level of 30% due to an over all increase in restraints provided by fibers through the fiber-matrix interface. At stress

level of 0.55, the matrix lateral deformation, $u_{1,}$ became large enough to reduce P and thus reduced fibers' efficiency in resisting creep deformations. Also, since τ was assumed to only affect the flowing part of creep, the effect of τ was proven to increase with time as a result of the increase in the viscous flow portion of creep and also due to the increases in shrinkage with time [Chern and Young, 1989]. Similar effects of fibers on drying shrinkage have been also reported in the literature [Zhang and Li, 2001]. In all previous studies, both creep and shrinkage were inversely proportional to the fiber-to-matrix moduli ratio and aspect ratio of fibers up to 50 after which this effect becomes less significant. That is, since concrete microcracks due to tensile creep, it is likely that the matrix modulus would reduce with time [Bissonnette et al. 2007], resulting in bigger effect of fibers in tension relative to compression. On the other hand, increase of fiber content beyond a certain threshold may result in less effectiveness in restraining long-term deformation due to possible overlapping between the restrained zones of the matrix surrounding each fiber [Mangat and Azari, 1985].

Models developed based on these assumptions, although idealized, can provide a good explanation of why incorporating steel fibers in UHPC reduced compressive creep.

6.3.4 Comparison between Tensile and Compressive Creep of UHPC

Figures 6.9 through 6.13 show a comparison between the specific creep in tension and compression for different investigated mixes. As for specific creep, the tensile creep results were calibrated using short-term results as explained in Chapter 5 in order to account for the shape and size differences between specimens used in the tensile and compressive creep studies. No adjustment was done to the long-term shrinkage data. Figure 6.14 shows the adjusted long-term specific tensile creep for thermally treated and non-thermally treated UHPC.

Comparing tensile creep results in Figure 6.14 to compressive creep results in Figure 6.7 show that the tensile creep of mixes D-2f-90C-40, D-1f-90C-40, D-0f-90C-40, D-2f-23C-40, D-0f-23C-40 was about 18, 25, 23, 17, and 20 times the measured compressive creep, respectively. As discussed in chapter 5, results emphasize that compressive and tensile creep phenomena are fundamentally different. That is, tensile creep differs from compressive creep in the magnitude of the effects of microcracking, viscous flow and microprestress as explained in section 5.7.

As for the relative effect of fibers on both tensile and compressive creep behaviors, it can be seen that the effect of eliminating fibers in tension was more pronounced than in compression (i.e., 64% increase in tension versus 31% increase in compression compared to the 2% fiber volume companion specimens). This is opposite to what was expected from the previously discussed model when it is known that the fiber-matrix bond in compression is stronger than it is in tension [Mangat and Azari, 1985]. However, it is well established that microcracking occurs in the cementitious matrix in tensile creep more than compressive creep [Ward and Cook, 1969, Cook, 1972, Gagne' et al., 1996, Bissonnette et al. 2007, and Chapter 5 of this study]. This is, cementitious matrices suffer damage during the tensile creep process especially in drying conditions. This microstructural damage of concrete would result in transferring a bigger portion of the load carried by the damaged parts of the matrix to the undamaged parts though fibers as tensile microcracking progresses. This load transfer mechanism between different matrix parts through fibers would result in a bigger contribution of fibers in resisting tensile deformations compared to compressive deformations where microcracking is less likely to occur at stress levels as low as 40%. Variations of specific creep in tension and compression with different fiber contents are plotted in Figure 6.15.

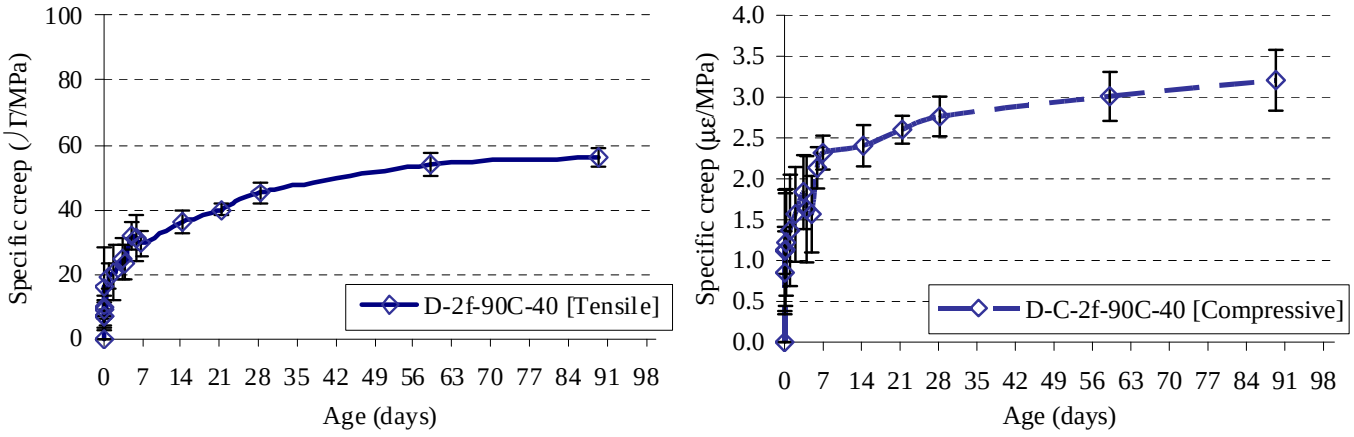

Figure 6.9: Comparison between tensile and compressive creep for mix D-2f-90C-40

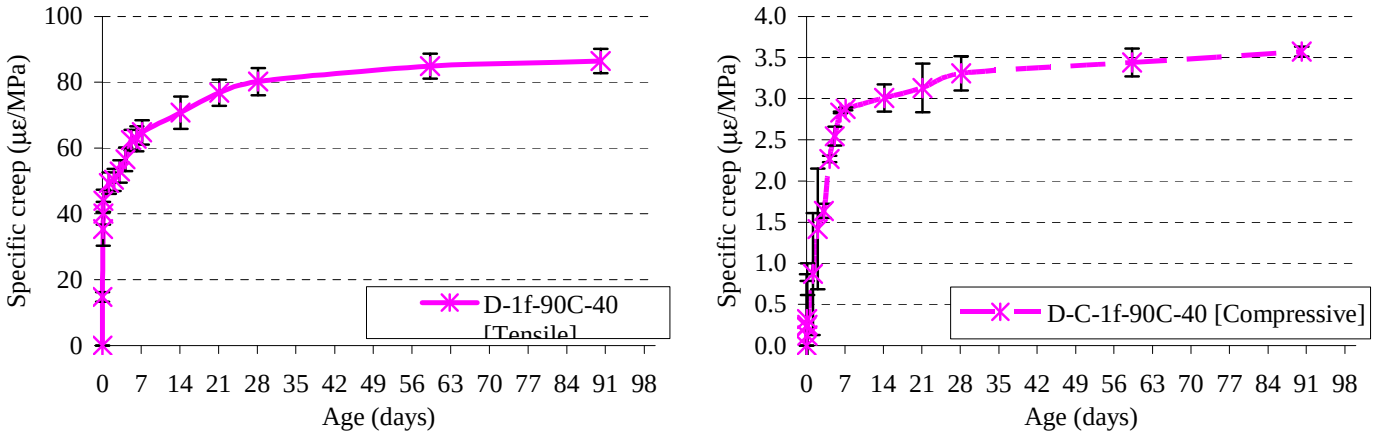

Figure 6.10: Comparison between tensile and compressive creep for mix D-1f-90C-40

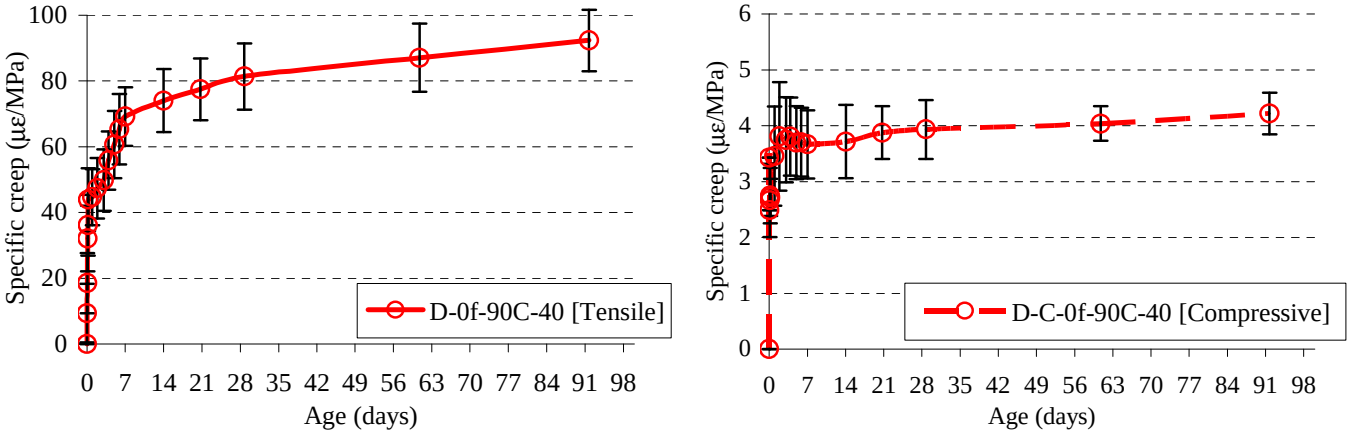

Figure 6.11: Comparison between tensile and compressive creep for mix D-0f-90C-40

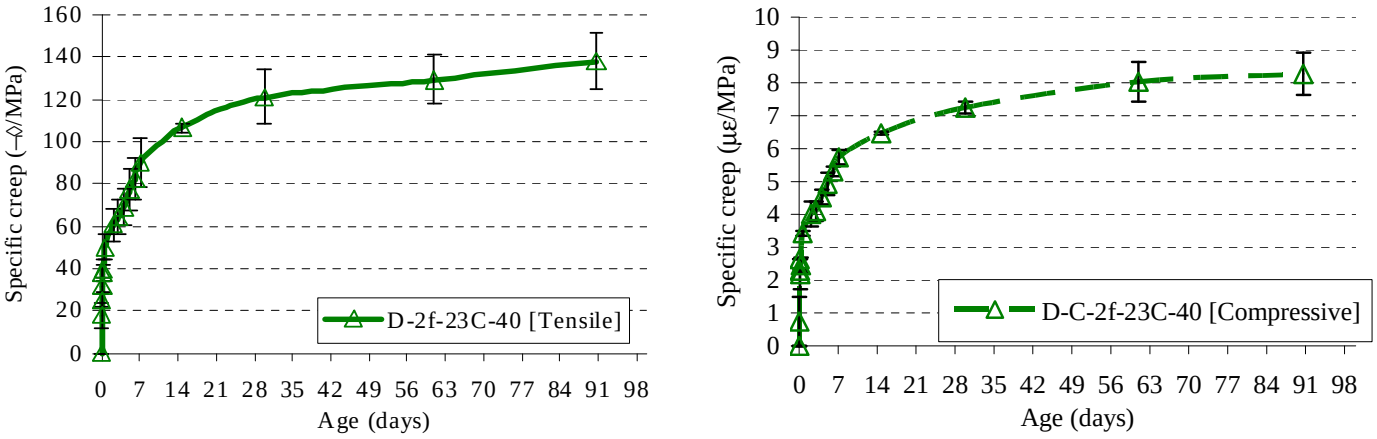

Figure 6.12: Comparison between tensile and compressive creep for mix D-2f-23C-40

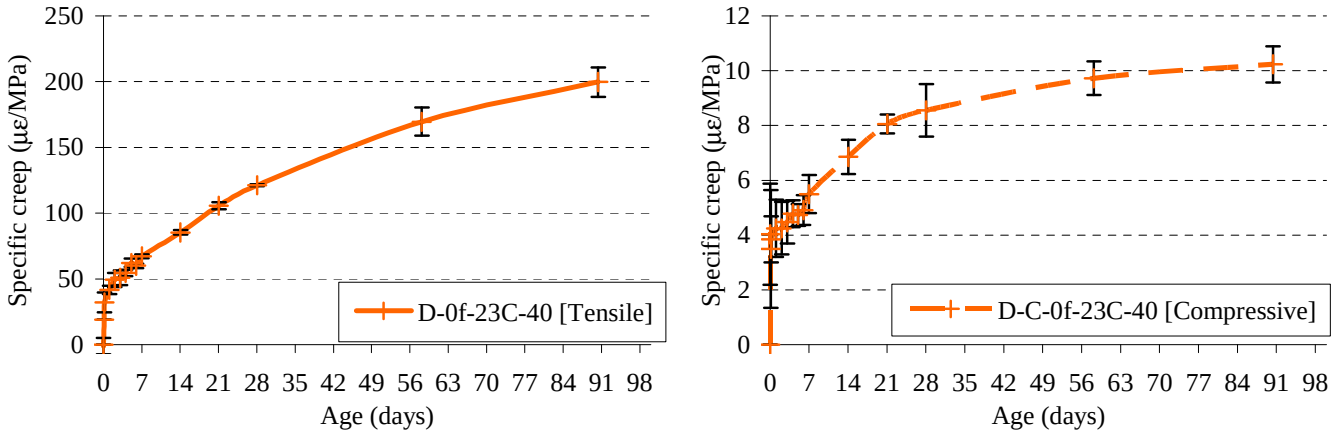

Figure 6.13: Comparison between tensile and compressive creep for mix D-0f-23C-40

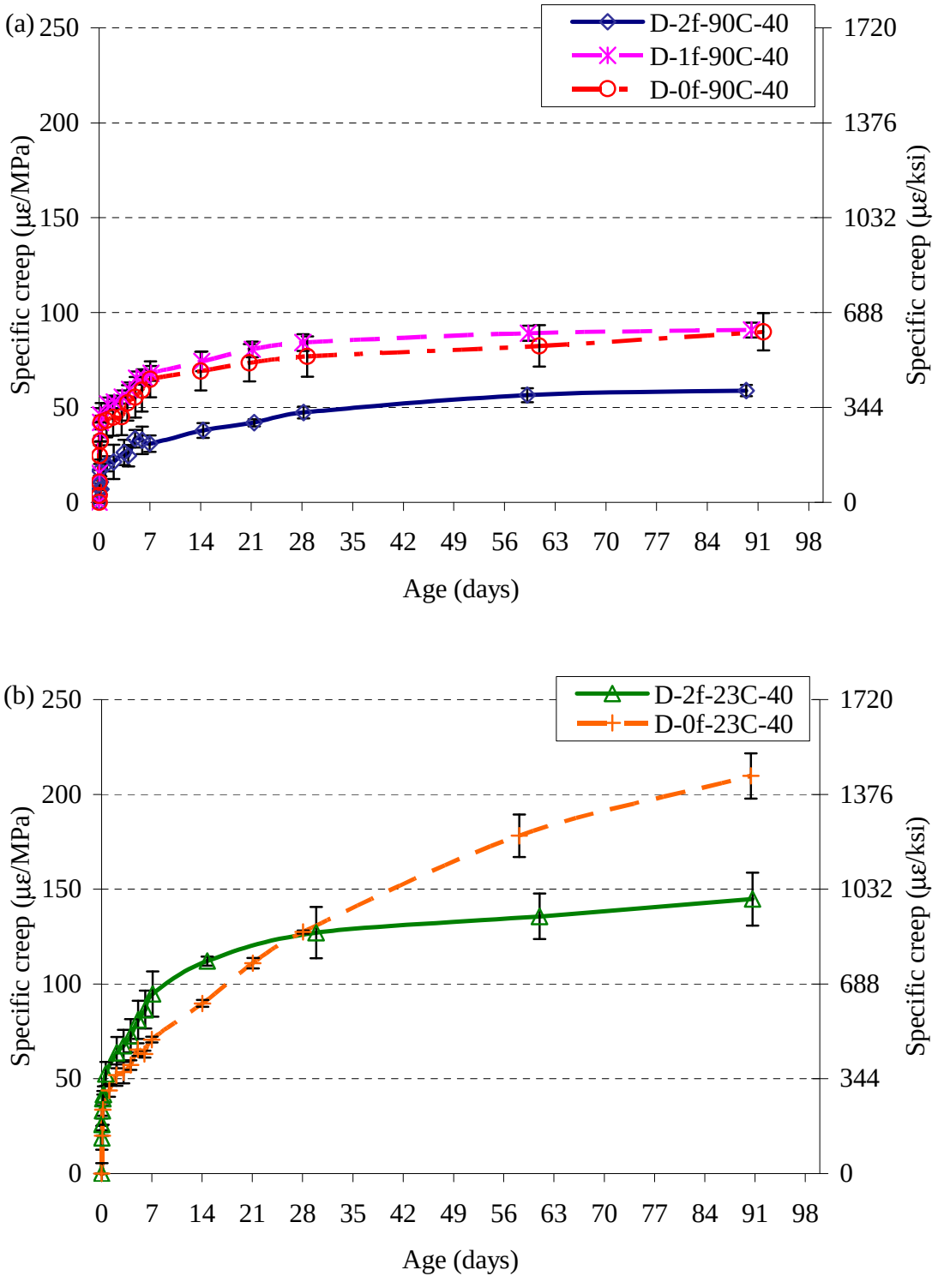

Figure 6.14: Adjusted specific tensile creep (a) thermally treated UHPC and (b) non-thermally treated UHPC

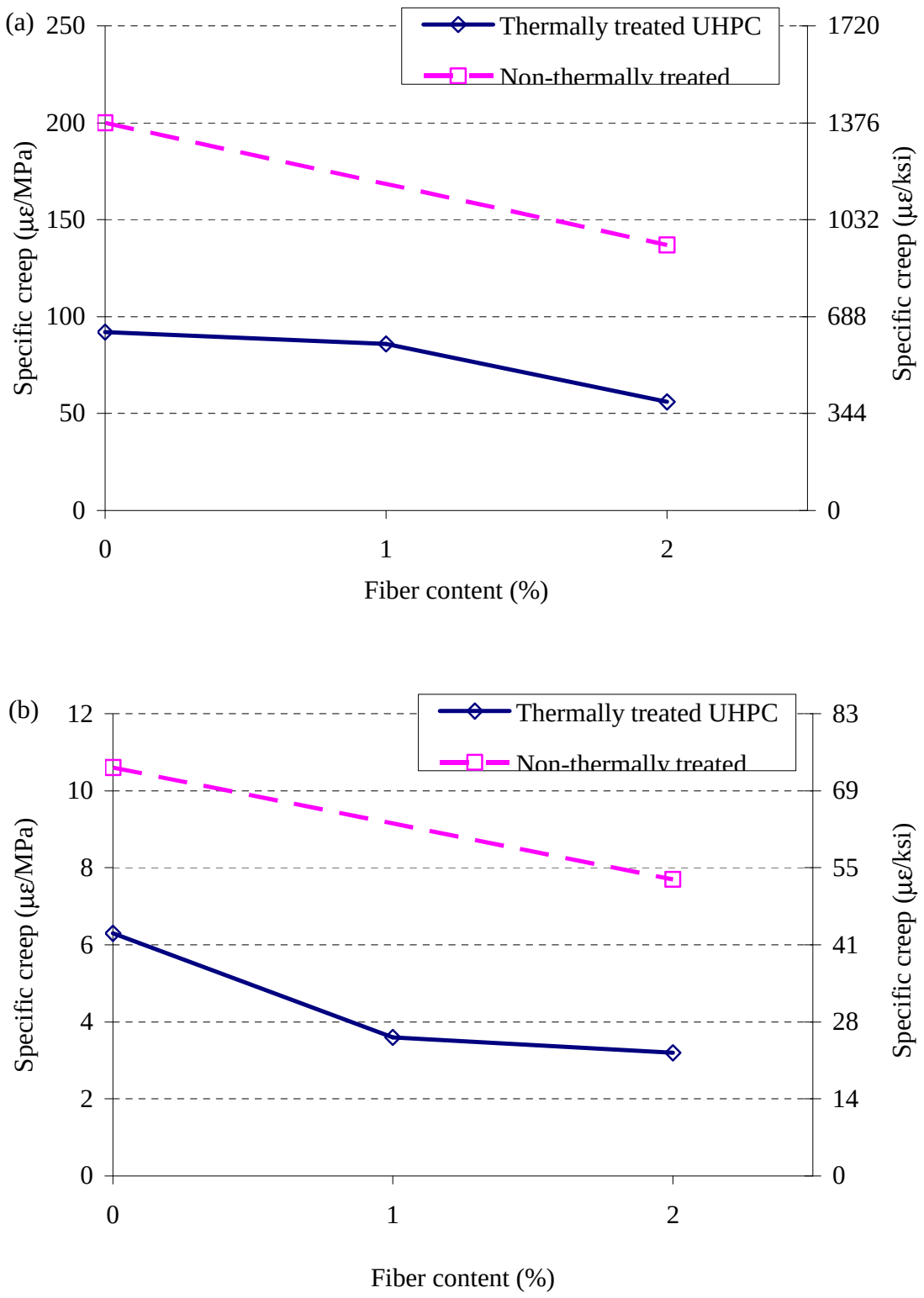

Figure 6.15: Effect of fiber content on the specific creep (a) tensile and (b) compressive

6.4 Effect of Load Level

In order to determine the appropriate working stress levels of UHPC for bridge girder applications, tensile creep tests at stress levels higher than 40% were conducted. Four stress levels were selected for this study: 40%, 60%, 70% and 80% (i.e., mixes D-2f-90C-40, D-2f-90C-60, and D-2f-90C-80), in addition to pre-cracked specimens (i.e., mix D-2f-90C-40-P) to address the effect of accidental overloading prior to long-term loading (Table 6.1). Original D-2f-90C-80 mixes were used for the 70% loading. All UHPC mixes considered for this study were thermally treated at 90^{o}C (194^{o}F). Tensile creep tests for mixes D-2f-90C-40 and D-2f-90C-60 were continued for ninety days of loading. Tensile creep for mix D-2f-90C-40-P was continued for 1 year. No long-term results were obtained for 70% and 80% stress levels as specimens crept to failure within few minutes after loading.

Mix D-2f-90C-80 represents loading up to 80% of the ultimate load which is equivalent to about 90% of the cracking load. Results from this mix help put an upper bound on the useable tensile stress of UHPC for structural design. That is, results from this mix would show whether UHPC would creep to cracking and then to failure at this high stress level or not.

Mix D-2f-90C-40-P represents overloading a girder up to cracking due to an accidental event after which the girder would be operating at lower stress level (i.e., 40% of ultimate in this case). Results from this mix would answer the question of whether existing diagonal tensile cracks in UHPC girders would creep to failure or not under operating (lower) tensile stresses.

6.4.1 Mix D-2f-90C-80

The measured direct tensile strength for mix D-2f-90C-80 was 10.6 MPa (1.53 ksi) with standard deviation of 0.1 MPa (0.014 ksi). The cracking stress measured was 9.3 MPa (1.35 ksi) (88% of ultimate strength) with zero standard deviation. The D-2f-90C-80 specimens loaded up

to 80% of their ultimate tensile strength crept to failure within the two minutes after the full load was applied (Figure 6.16). It was not possible to collect tensile creep readings for this mix within this short period of time. Figure 6.17 shows that the tensile creep failure happened close the tip of threaded inserts likely due to stress concentrations at this plane. The actual failure stress was calculated based on the net UHPC cross section at the plane of failure.

The actual stress on the failure plane was 8.9 MPa (1.29 ksi) which is equivalent to 95% of the cracking stress and 84% of the ultimate strength. This result shows that there is a potential for initiation or occurrence of similar failures at high loads in bridge girders wherever reinforcing bars are discontinued. Similar failures can also initiate or occur due to stress concentrations if large voids are present and no reinforcement is provided.

No cracks were found in the two non-failed specimens showed in figure 6.16. The failed specimen was then replaced by another available specimen of the same batch in attempt to repeat the test at 70% of the ultimate tensile strength instead of 80%. In this case, a single crack in the middle specimen, which is the specimen that replaced the damaged one, started developing after about 35 minutes of loading. This crack kept growing until failure occurred after about 55 minutes of loading.

Results from these two experiments emphasize the insufficiency of tensile strength tests to predict long-term tensile performance of UHPC. More importantly, they show that tensile design load of UHPC has to be below 70% of the ultimate strength obtained from direct tension tests to avoid tensile creep leading to failure.

Figure 6.16: Failure of mix D-2f-90C-80 within two minutes after loading

Figure 6.17: Failure plane close threaded inserts' tip of mix D-2f-90C-80

6.4.2 Mechanical Properties

A summary of all mechanical properties is given in Table 6.5. Results from each test is separately presented and discussed in the following sections. Although, Table 6.5 shows some variation in the tensile strength results between different mixes, ANOVA revealed no significant difference between the tensile strength of the three mixes. Further statistical analyses were performed in order to estimate upper and lower limits for the tensile strength for thermally treated UHPC reinforced with 2% fibers. All tensile strength results from the three mixes shown in Table 6.5 were considered since no testing error is recognized. Statistical analysis revealed that the average direct tensile strength falls between 9.6 MPa (1,398 psi) and 10.6 MPa (1,539 psi) with 95% confidence. That is, a conservative value of 9.65 MPa (1,400 psi) for the ultimate direct tensile strength can be used for design purposes.

Table 6.5: Summary of mechanical properties of UHPC mixes at the age of 7 days

Mixture ID	Compressive strength MPa (ksi)	Tensile strength MPa (ksi) [Direct Tension]	Modulus of Elasticity MPa (ksi)		Poisson's ratio	
			E_c	E_t	υ_c	υ_t
D-2f-90C-40	169 (24.6)	10.30 (1.50)	47,950 (6,953)	57,470 (8,336)	0.14	0.20
D-2f-90C-40-P	159 (23.1)	9.30 (1.35)	48,380 (7,015)	56,600 8,210	0.15	0.20
D-2f-90C-60	160 (23.3)	9.60 (1.40)	48,140 (6,980)	56,530 (8,200)	0.14	0.20

6.4.3 Mix D-2f-90C-40-P

Figure 6.18 shows the setup used for pre-cracking UHPC tensile creep specimens. Pre-cracking was done using an upper and lower knife-edge steel bars at the middle of each

specimen. Loading continued till at least one crack extended from the top to the bottom of each specimen on two opposite faces. The average maximum load needed for cracking the 75x75 mm (3x3-in) specimens was 7,350 (16,200 lbs) with a standard deviation 410 kg (900 lbs). Crack width during the tensile creep test for the pre-cracked mix was measured using a concrete crack microscope, Elcometer 900 (Figure 6.19). The concrete crack microscope had a magnification of 50X, range of 2.5 mm (0.1-in), and resolution of 0.02 mm (0.001-in). Two crack opening measurements were taken on each side where tensile creep measurements were taken. The initial average crack width was 0.076mm (0.003-in), 0.559mm (0.022-in), and 0.114mm (0.005-in) for the three creep specimens.

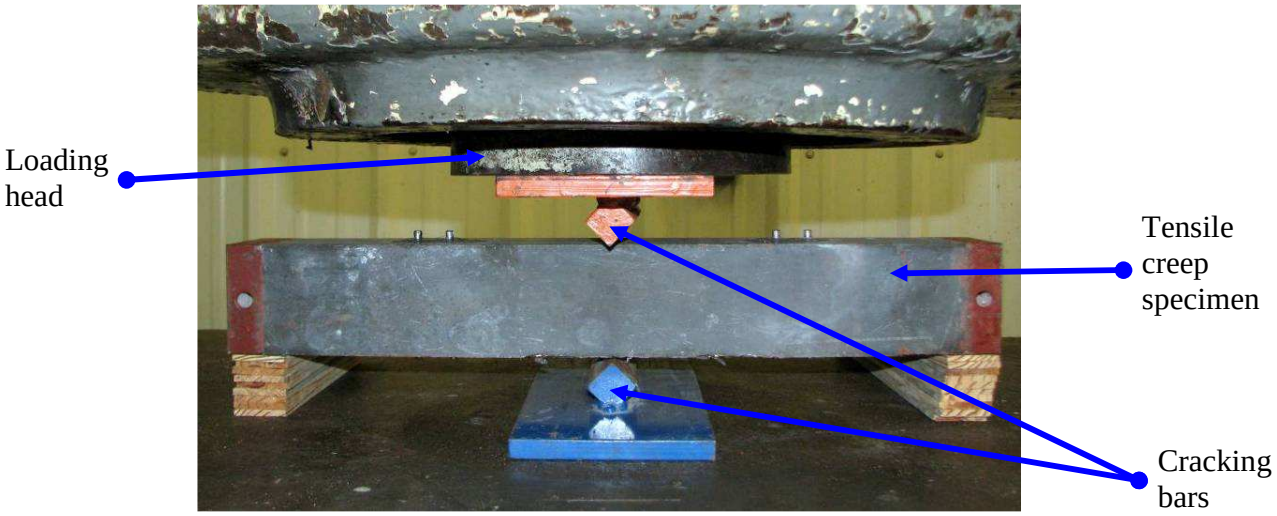

Figure 6.18: Pre-cracking setup for mix D-2f-90C-40-P

Free shrinkage and specific tensile creep results for this mix are shown in Figure 6.20. Tensile creep for mix D-2f-90C-40-P was calculated by subtracting the width of the crack on each of the two faces of each creep specimen at all ages.

Comparing tensile creep results for mixes D-2f-90C-40 (Figure 6.5) and D-2f-90C-40-P (Figure 6.20) show that the specific tensile creep at 1 year of loading of mix D-2f-90C-40-P was

about 11% higher than mix D-2f-90C-40. Like in mix D-2f-90C-40, tensile creep of mix D-2f-90C-40-P reached an asymptotic value at 90 days. The maximum specific tensile creep for mix D-2f-90C-40-P was 64 με/MPa (440 με/ksi).

Figure 6.21 shows the cracks' deformations measured on all specimens upon applying 40% of the ultimate tensile strength on the tensile creep specimens. Right after loading, all cracks opened by an average of 0.016mm (0.00066-in), all cracks kept deforming for the first 6 hours after loading where a the maximum crack deformation measured was 0.033mm (0.0013-in). No further crack deformation was measured for the rest of the testing period. That is, pre-cracked specimens did not creep to failure within a period of one year under 40% of the ultimate tensile strength. This result means that 40% of the ultimate strength did not fail the fiber-matrix bond and cause complete fiber pull-out.

In the light of results from mixes D-2f-90C-80 and mix D-2f-90C-40-P, it can be seen that the tensile creep phenomenon is stress-dependant. That is, under 70% and 80% of the ultimate tensile strength (mix D-2f-90C-80), thermally treated UHPC crept to failure at different times. The time to failure was inversely proportional to the amount of stress applied. On the other hand, pre-cracked UHPC specimens were able to carry 40% of the ultimate load for 1 year without failure occurring.

This result is of specific important for UHPC bridge girder design as it suggests that 40% of the ultimate strength of thermally treated UHPC can be used in structural design. Even in the case of accidental overloading of girders that would cause cracking, it is not expected that those cracks would creep to failure if a cracked UHPC girder would be operating within the design conditions.

(a)

(b)

Figure 6.19: Pre-cracked specimens (a) concrete crack microscope (Elcometer 900) and (b) taking crack opening reading using the Elcometer 900 microscope

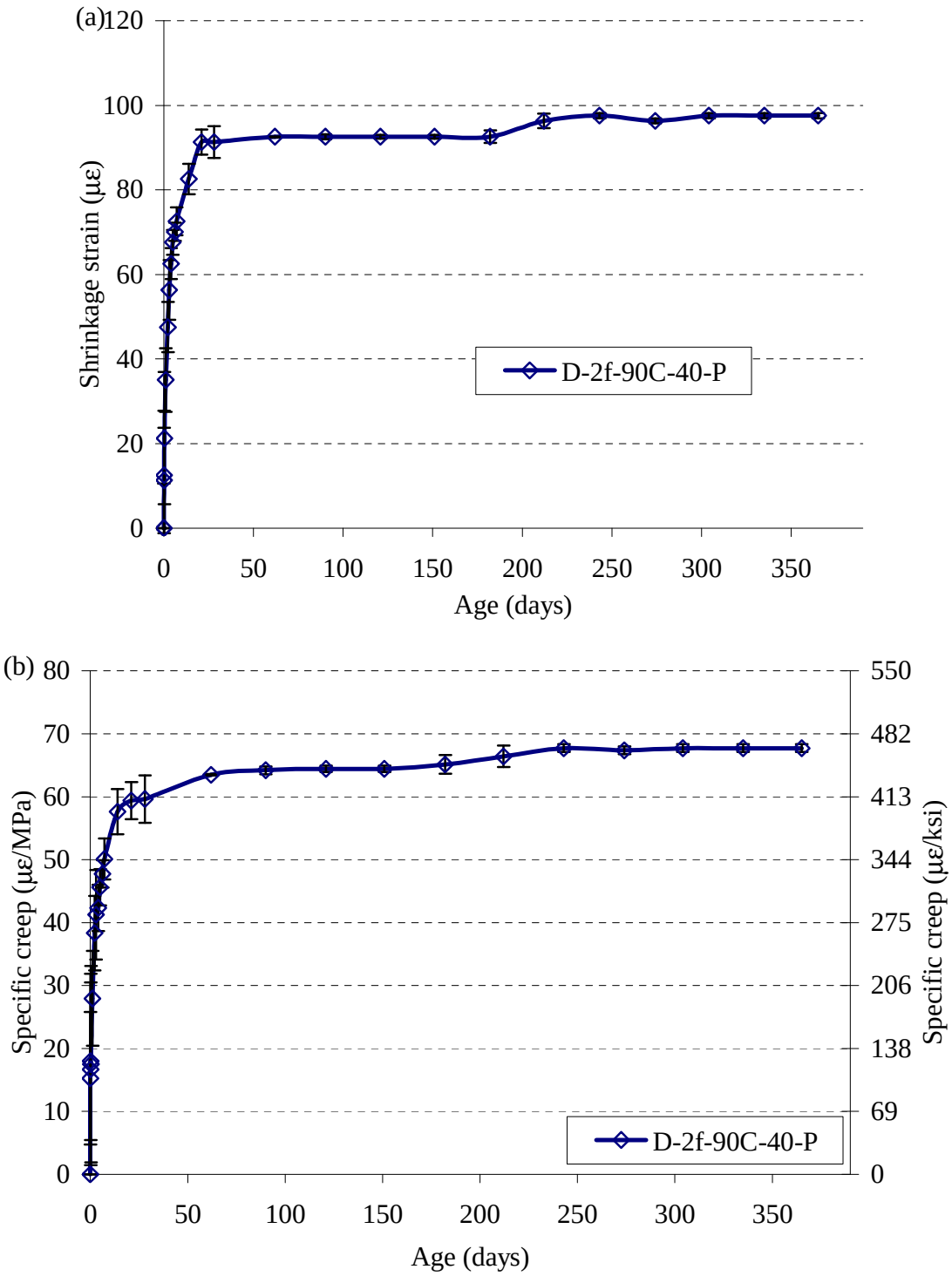

Figure 6.20: Mix D-2f-90C-40-P (a) free shrinkage and (b) specific tensile creep

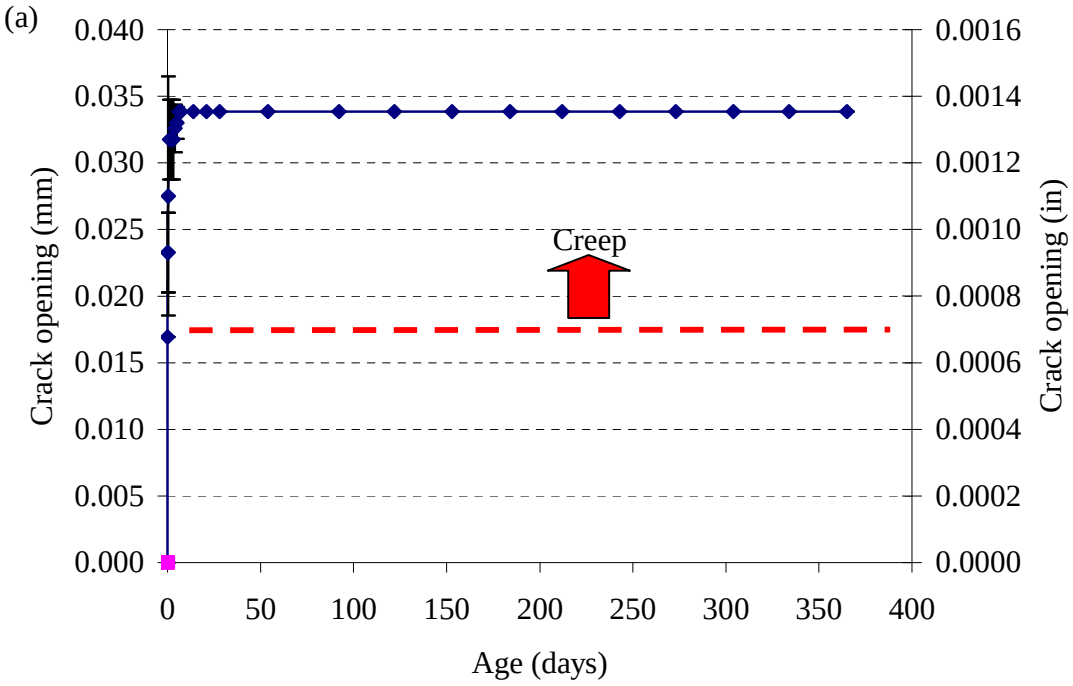

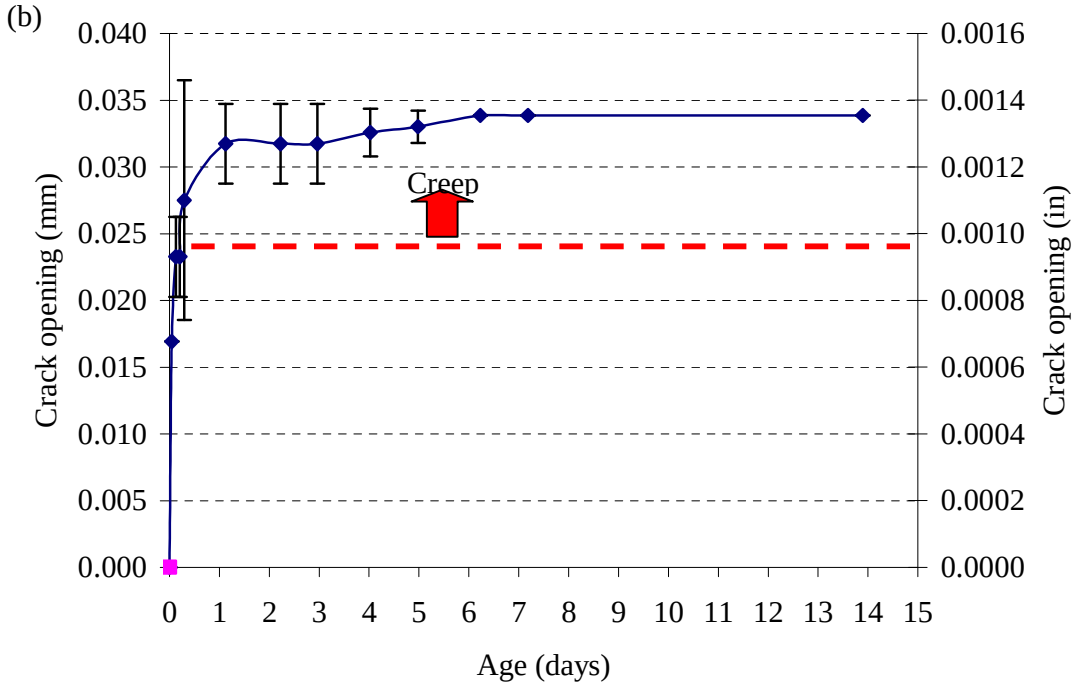

Figure 6.21: Average crack deformation after pre-cracking: (a) period of 1 year and (b) period of 14 days

6.4.4 Mix D-2f-90C-60

Figure 6.22 shows surface attachments used to measure tensile deformations for mix D-2f-90C-60. These attachments replaced the inserts used for most of the other mixes to eliminate excessive stress concentrations at higher stress levels. These surface attachments were only used for mixes D-2f-90C-60 and D-2f-90C-80. Surface attachments were glued to the surface using fast setting/ high strength epoxy and cyanoacrylate super glue.

Free shrinkage and tensile creep results for this mix are shown in Figures 6.23 and 6.24, respectively. The average free shrinkage strain measured for mix D-2f-90C-60 was 109 με at 90 days. Results in Figure 6.24 shows that the specific tensile creep of mix D-2f-90C-60 at 90 days was only 2% higher than mix D-2f-90C-40. This insignificant difference between the specific tensile creep at stress level of 40% and 60% suggests that no excessive cracking or overall damage occurred up to 60% of the ultimate tensile strength.

Also, it was of interest to perform statistical analysis on the shrinkage data of mixes D-2f-90C-40, D-2f-90C-60, and D-2f-90C-40-P. ANOVA revealed no significant difference between the free shrinkage strains of the three mixes at 90 days. Further statistical analysis was performed in order to estimate upper and lower limits for the shrinkage strain thermally treated UHPC reinforced with 2% fibers at 90 days. All data results from the three mixes were considered since no testing error is recognized. Statistical analysis revealed that the average shrinkage strain falls between 65 με and 135 με with 95% confidence.

In the light of results obtained for mixes D-2f-90C-60 and D-2f-90C-80, the stress-to-strength proportional limit where creep strains are proportional to the stress applied can be estimated to fall between 60% and 70%. Similar conclusion was drawn by Staquet and Espion

Figure 6.22: Surface attachment used to measure deformations for mix D-2f-90C-60

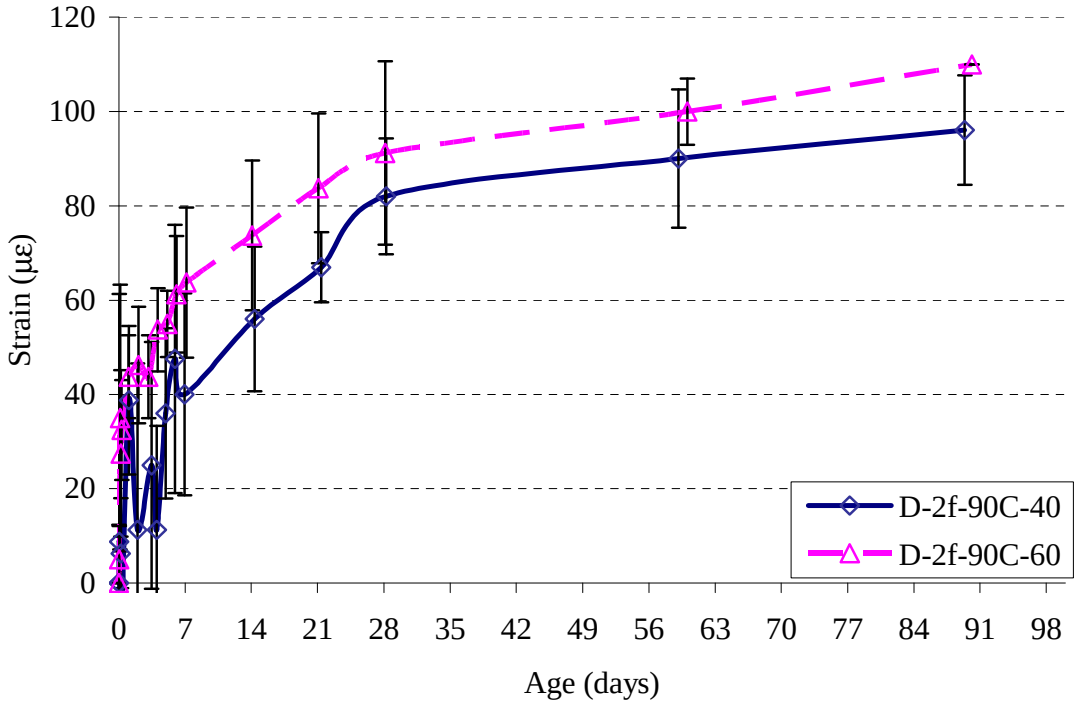

Figure 6.23: Comparison between the free shrinkage of mixes D-2f-90C-40 and D-2f-90C-60

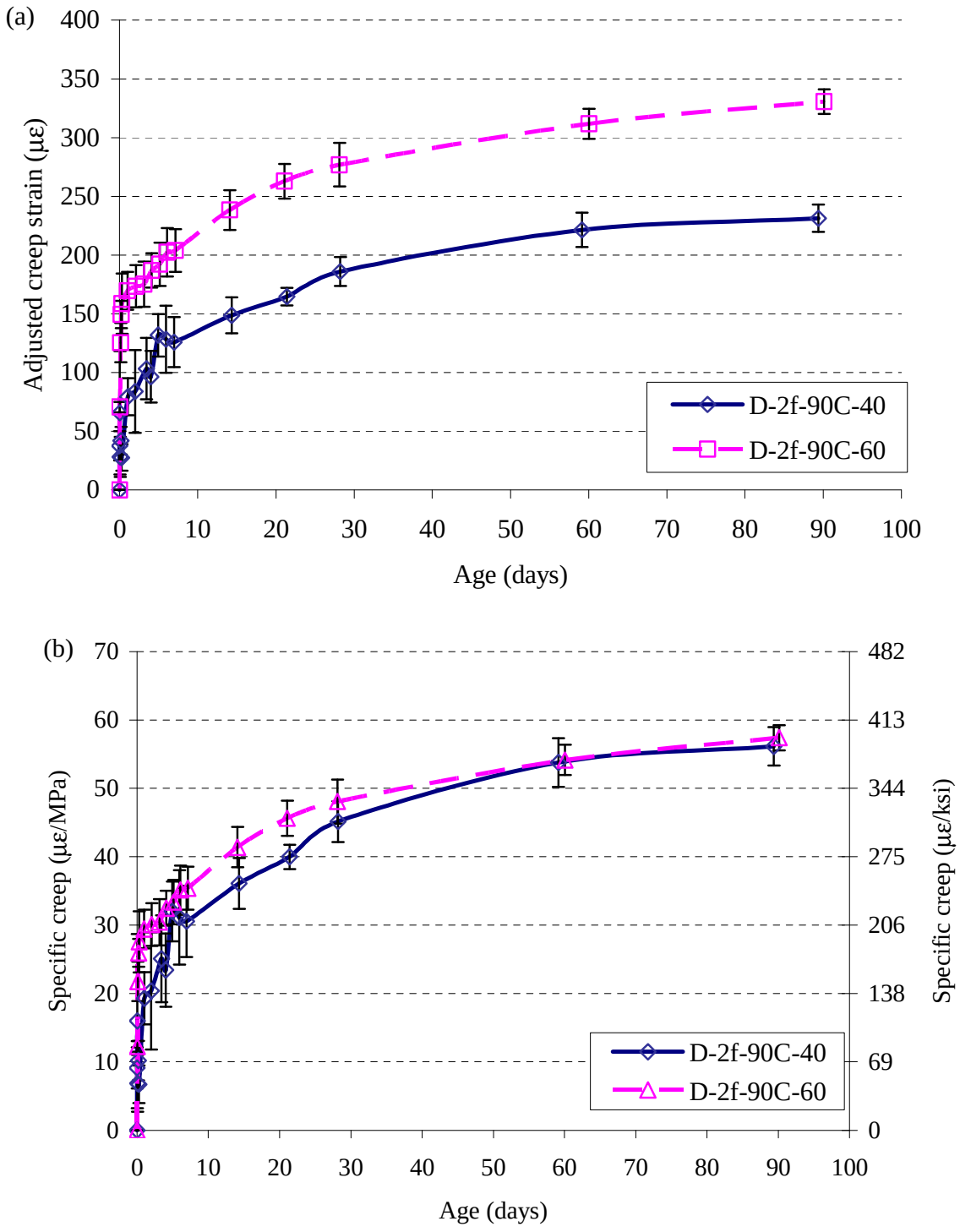

Figure 6.24: Comparison between tensile creep of mixes D-2f-90C-40 and D-2f-90C-60: (a) adjusted creep strain and (b) specific tensile creep

[2003] for HPC where the proportional limit was found to be 70% and also by Bissonnette et al. [2007].

Tensile creep test for mix D-2f-90C-60 is still running to insure that this hypothesis is still valid up to an age of at least 1-year.

Results presented for mix D-2f-90C-60 also suggest the possibility of using 60% of the ultimate tensile strength for structural design of girders. This suggestion is still to be confirmed experimentally by running tensile creep tests on pre-cracked specimens at 60% of the ultimate tensile strength.

6.5 Conclusions

The effect of varying fiber content and loading level on the tensile creep of UHPC was investigated. Based on this experimental investigation, the following conclusions can be drawn:

(1) Tensile creep of UHPC was found to be more sensitive to thermal treatment than was tensile strength. Variations in fiber content resulted in quite similar tensile strengths but quite different tensile creep behaviors. Results from the long-term investigation showed that tensile creep testing, rather than tensile strength values, should be used to predict long-term tensile performance of fiber-reinforced UHPC.

(2) In the case of variable fiber content, tensile creep test results showed an increase in specific tensile creep of UHPC upon decreasing the fiber content. For thermally treated UHPC, decreasing the fiber content from 2% to 1% by volume increased tensile creep by 53%, while eliminating fibers increased tensile creep by 64% compared to the 2% volume mix. Eliminating fibers for non-thermally treated UHPC increased tensile creep by 46%.

(3) Measured increases in tensile and compressive creep upon reducing the fiber content for thermally treated and non-thermally treated UHPC suggests that fibers carry part of the sustained load and, thus, reduce tensile stress in the matrix.

(4) The effect of fibers in reducing tensile creep of UHPC was more pronounced than in reducing compressive creep. It is suggested that this difference in the relative influence of fibers is due to microcracking in tension that results in engaging fibers in the load transfer process from cracked to uncracked parts of the cementitious matrix of UHPC.

(5) The effect of fibers in reducing tensile creep of UHPC contradicts with some of the previous literature where tensile creep increased upon using fibers in normal and high strength concretes. This discrepancy is due to the development of defect-free fiber-matrix interface in UHPC in addition to the large fiber-to-aggregate size ratio in UHPC.

(6) The effect of fibers in reducing compressive creep of UHPC agreed with published literature for normal strength concrete.

(7) The effect of fibers in reducing tensile creep was more pronounced in thermally treated UHPC compared to non-thermally treated UHPC due to stronger fiber-matrix bond associated with thermal-treatment. Results of the nano/micro-scale study in Chapter 5 suggest that this difference in relative influence of fibers is due to stronger fiber-matrix interface in thermally treated UHPC

(8) UHPC pre-cracked and tested for tensile creep did not creep to failure in a period of 1 year under stress equivalent to 40% of the ultimate direct tensile strength.

(9) UHPC tested for tensile creep at 40% and 60% of the ultimate strength showed almost the same specific creep after 90 days of loading indicating no excessive damage happening up to 60% of the strength.

(10) No tensile creep failure occurred at 60% of the strength during the testing period. Tensile creep failure occurred at both 70% and 80% of the ultimate load. Time to failure was inversely proportional to the stress level.

(11) Results from this study suggest that the maximum design stress for bridge girders should not exceed 60% of the ultimate direct tensile strength.

(12) Tensile creep tests should be performed on pre-cracked specimens at 60% of the ultimate strength to insure safe design.

(13) Results from this study suggest that the tensile creep phenomenon in UHPC occurs differently than compressive creep. This result emphasizes the importance of further study of the tensile creep behavior of UHPC, particularly for applications where satisfactory long-term tensile performance is required.

6.6 References

Alwan, J.M., Naaman, A.E., and Hansen, W. "Pull-out Work of Steel Fibers from Cementitious Composites: Analytical Investigation", Cement and Concrete Composites, Vol.13, 1991, pp. 247-255.

ASTM C512, "Standard Test Method for Creep of Concrete in Compression," American Society for Testing and Materials Standard Practice C512, Philadelphia, Pennsylvania, 2002.

Banthia, N., MacDonald, C., and Tatnall, P., "Structural Applications of Fiber Reinforced Concrete", ACI International SP 182, 1999.

Bartos, P., "Review Paper: Bond in Fibre Reinforced Cements and Concretes", The International Journal of Cement Composites, Vol.13, No.3, August 1981, pp. 159-177.

Bissonnette, B., and Pigeon, M., "Tensile Creep at Early Ages of Ordinary, Silica Fume and Fiber Reinforced Concretes", Cement and Concrete Research, Vol. 25, N0. 5, 1995, pp. 1075-1085.

Bissonnette, B., Pigeon, M., and Vaysburd, A.M., "Tensile Creep of Concrete: Study of Its Sensitivity to Basic Parameters", ACI Materials Journal, Vol. 104, N0. 4, 2007, pp. 360-368.

Burkart, I., and Muller, H.S., "Creep and Shrinkage Characteristics of Ultra-High Strength Concrete (UHPC), Proceedings of the Second International Symposium on Ultra-High Performance Concrete, Kassel, Germany, March 5-7, 2008, pp. 469-476.

Chern, J.C., and Young, C.H., “Compressive Creep and Shrinkage of Steel Fibre Reinforced Concrete”, international Journal of Cement Composites, Vol. 11, No. 4, 1989, pp. 205-214.

Cook, D.J., “Some Aspects of the Mechanism of Tensile Creep in Concrete,” ACI Journal, Proceedings Vol. 69, No. 10, 1972, pp. 645-649.

Graybeal, B.A., "Characterization of the Behavior of Ultra-High Performance Concrete", Ph.D. Thesis, University of Maryland, 2005.

Lankard, D.R., “Fiber Concrete Applications”, (Fibre Reinforced Cement and Concrete), The Construction Press LTD, England, 1975.

Li, C.Y., and Mobasher, B., **“**Finite Element Simulations of Fiber Pullout Toughening in Fiber Reinforced Cement Based Composites”, Advanced Cement Based materials, Vol. 7, 1998, pp. 123-132.

Mangat, P.S., and Azari, M.M., “A Theory of Steel Fibre Reinforced Cement Matrices under Compression”, Journal of Materials Science, Vol. 20, 1985, pp. 1119-1133.

Neville, A.M., Dilger, W., and Brooks, J.J., “Creep of Plain and Structural Concrete”, Construction Press, London, UK, 1983.

Sorelli, L., Constantinides G., Ulm, F.J., and Toutlemonde, F., “The Nano-mechanical Signature of Ultra High Performance Concrete by Statistical Nanoindentation Techniques”, Vol. 38, No. 12, 2008, pp. 1447-1456.

Staquet, S. and Espion, B., "Effects of Heat Treatment on Creep Functions of HPC Loaded at Very Early Age", Advances in Cement and Concrete, Copper Mountain, Colorado: Engineering Conferences International, 2003, pp. 471-479.

Stengel, T., “Effect of Surface roughness on the Steel Fibre Bonding in Ultra High Performance Concrete”, Proceedings of the NICOM3 Conference, 2009, pp. 371-376

Stengel, T., “Optimisation of Steel Fibre Bonding High Performance Concrete” Proceedings of the 7th International RILEM Symposium on Fibre Reinforced Concrete: Design and Application BEFIB, 2008.

Swamy. R. N., and Barr, B., “Fibre Reinforced Cements and Concretes: Recent Developments”, Elsevier Science Publishing Co., Inc, 1989.

Wang, Y., Li, V.C., Backer, S., ““Modeling of Fibre Pull-out from a Cement Matrix”, The International Journal of Cement Composites and lightweight Concrete, Vol.10, No.3, August 1988, pp. 143-149.

Ward, M. A., and Cook, D. J., “The Mechanism of Tensile Creep in Concrete,” Magazine of Concrete Research, Vol. 21, No. 68, 1969, pp. 151-158.

Zhang, J., “Modeling of Influence of Fibers on Creep of Fiber Reinforced Cementitious Composite”, Composites Science and Technology, Vol. 63, No. 13, 2003, pp. 1877-1884.

Zhang, J., and Li, V., “Influences of Fibers on Drying Shrinkage of Fiber-Reinforced Cementitious Composite, Journal of Engineering Mechanics, Vol. 127, No. 1, 2001, pp. 37-44.

CHAPTER 7
CONCLUSIONS AND RECOMMENDATIONS

The current study is the first to characterize the tensile creep performance of UHPC on the macro-, micro-, and nano-scales (Figures 7.1 and 7.2). A summary of the main conclusions and recommendations drawn are presented below.

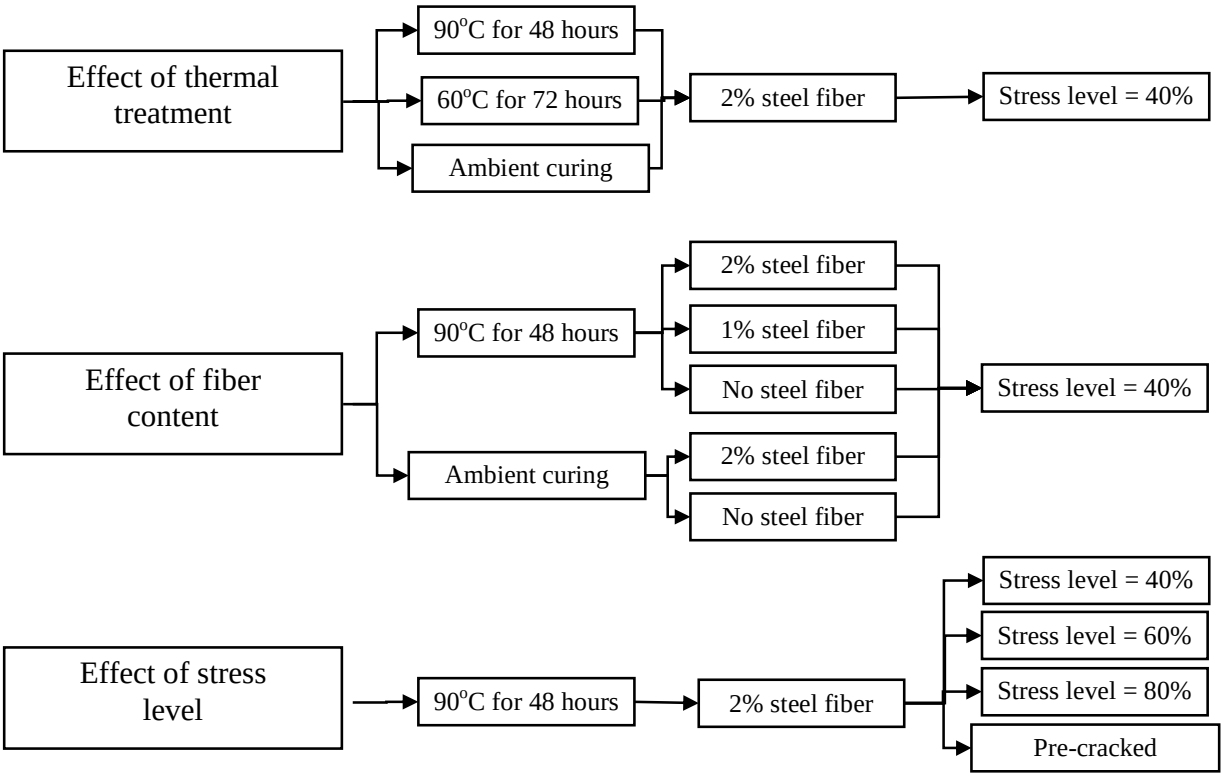

Figure 7.1: Large-scale research program

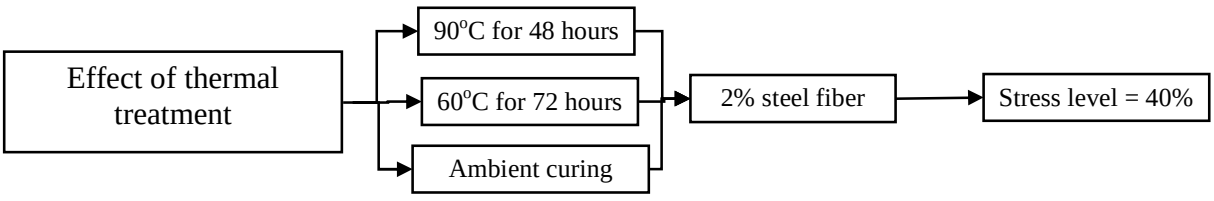

Figure 7.2: Nano/micro-scale research program

7.1 Conclusions

7.1.1 Short-Term Study

Short-duration, 14-day, tensile creep tests were used to preliminary investigate the sensitivity of the tensile creep and free and autogenous shrinkage phenomena to variations in thermal treatment (i.e., 23^{o}C (73^{o}F) and (90^{o}C (194^{o}F)), incorporating short steel fibers (i.e., no fibers and 2% fibers by volume), and stress level at time of loading (i.e., 40% and 60%).

Results from this preliminary investigation showed that while variations in 7-day tensile strength among the different conditions examined measured just a maximum of 8%, tensile creep behavior varied by up to ~70% when the influence of curing conditions and fiber reinforcement were compared. These results emphasized the importance of conducting tensile creep testing to predict the long-term tensile performance of UHPC.

Autogenous shrinkage results showed that 87% of the total autogenous shrinkage occurred during the thermal treatment due to accelerated rate of early hydration at higher temperature. The use of 2% steel fibers by volume decreased autogenous shrinkage during thermal treatment after 14 days by 42%, compared to unreinforced UHPC.

Thermal treatment of UHPC at 90^{o}C (194^{o}F) for 48 hours decreased both the tensile creep coefficient and specific tensile creep at 7 days of loading by 73% and 77%. It is proposed that reduction in tensile creep with thermal treatment is due to the enhancements at the fiber-matrix interface during thermal treatment. In contrast to findings of increased tensile creep reported the literature for steel fiber-reinforced NSC and HPC (relative to unreinforced materials), reinforcement with short straight steel fibers decreased the tensile creep of UHPC. The 14-day tensile creep coefficient and specific tensile creep increased by 44% and 11% upon increasing the stress level from 40% to 60%.

According to this preliminary investigation, tensile creep of UHPC was found to depend on variations in thermal treatment, fiber content, and applied stress; with thermal treatment being the most significant factor that affects tensile creep. This research suggests that the combined effect of thermal treatment and incorporation of short steel fibers act to limit tensile creep and shrinkage in UHPC. A more extensive, long-term tensile creep multi-scale study was carried out based on the results of this preliminary investigation.

7.1.2 Tensile Creep Test Setup and Direct Tension Test

7.1.2.1 Tensile creep test setup

Prior to conducting the long-term study it was necessary to design and manufacture a new test setup to carry out the tensile creep tests for UHPC. After reviewing test set-ups described in the literature, it was desired to develop a new tensile creep test setup that would be best suited for testing the variations in UHPC behavior under examination in this study. The main desired features include: (1) Reductions in both the space requirements and costs associated with running multiple tests at the same time while meeting existing creep testing standards, (2) More efficient load transfer mechanisms that minimizes or eliminates friction losses, and (3) Strain reading technique that would represent the creep experienced throughout the specimens adequately. Therefore several modifications have been developed to adjust previous setups reviewed in the literature to achieve these main goals. These modifications are briefly outlined here.

In order to maintain a low cost and reduce the space required to run multiple creep tests at the same time, six identical frames were manufactured using commercially available structural steel tubing and fittings. Frames were spaced at (0.75 mm) 30-in from each other. Each frame is capable of testing three 480 mm (19-in) specimens connected in series to meet the minimum

number of specimens required by ASTM C 512 for every testing case without the need for multiple frames per case.

The load transfer and magnification system has been significantly modified from previous setups in order to achieve high loads required to test UHPC with adequate efficiency. This was achieved by increasing the load magnification factor to 10 and by introducing side guides and track rollers to the systems that would keep the loads planar with the specimens while eliminating possible friction losses while loading. This modification allows for loading up to 6,800 kg (15,000 lb) and has been successfully used up to 4,940 kg (10,800 lb) without requiring excessive amounts of dead load.

The method for measuring tensile deformations throughout the test has been changed from a surface-based technique that featured a single measurement on two opposite sides to a technique that utilized brass inserts on four points on the surface of each specimen. This technique provides more data per measurement time. And, because the data is from embedded measurement points rather than a surface measurement, they are expected to be more representative of the creep experienced throughout the specimen.

These fundamental changes introduced to previous setups makes the current setup unique as it features:

- Increased load capacity (i.e. 6,800 kg (15,000 lbs)) that allowed testing ultra-high strength concretes, including UHPC, for the first time,
- Increased number of specimens tested per case to conform to existing standards while offsetting fabrication and test running costs,
- Increased number of deformation readings per specimen that are more representative of the actual creep deformations compared to most of the previous setups, and

- Modified load application method, using dead loads rather than pneumatic jacks, thus easily maintaining constant tensile load throughout the test period.

7.1.2.2 Direct tension test

Prior to performing tensile creep testing, it was necessary to measure tensile strength of the various specimen types as accurately as possible so that the applied stress level could be controlled for each case. Because indirect tension testing can provide results of varying accuracy, a direct tensile strength test was preferred. Testing was done using a dog-bone type specimen, where the specimen shape is designed to mitigate stress concentrations. The dog-bone test configurations are the most accurate method to obtain the true tensile strength of UHPC, because: (1) sections in a dog-bone test configuration are uniformly loaded, (2) tensile Young's modulus of elasticity and Poisson's ratio can be determined using dog-bone configuration, (3) the dog-bone specimen configuration offsets most of the problems related with adhesively bonding specimens' ends to loading plates or loading heads in constant cross section configurations, and (4) the use of a reduced cross section is a practical alternative to the use of notched specimens. In addition, and particularly for the present study, casting dog-bone specimens (i.e., from one side to the other along the longitudinal axis) is similar to casting prestressed bridge girders where fiber alignment occurs. Also, this casting method is similar to casting the tensile creep specimens. As a result, the alignment of fibers in the tension specimens replicates the stress behavior of the creep specimens and large girders.

7.1.3 Long-Term Study

The following conclusions can be drawn from this experimental investigation outlined in Figures 7.1 and 7.2.

7.1.3.1 Effect of thermal treatment

- Tensile creep of UHPC was found to be more sensitive to thermal treatment compared to tensile strength. With variations in thermal treatment resulting in quite similar tensile strengths but quite different tensile creep behavior, results showed that tensile creep testing – rather than tensile strength values at the time of loading - should be used to predict long-term tensile performance of fiber-reinforced UHPC. These results agree with results obtained from the short-term study.
- It was concluded that only direct tension tests gave a reliable estimate of the tensile strength required for analysis of bridge girders. Thermally treated UHPC with 2% fibers showed a conservative ultimate direct tensile strength of 9.65 MPa (1,400 psi) with 95% confidence. This ultimate tensile strength is about 5 times greater than that of normal strength, 40 MPa (6,000 psi) concrete.
- The following relations between mechanical properties of UHPC are proposed based on the this experimental study:
  - $f'_{dt} = 7.64 \times \ln(f'_c) - 28.7$
  - $f'_{dt} = 0.48 \times f'_{st}$

  where: f'_{dt} is the direct tensile strength in MPa, f'_{st} is the splitting tensile strength in MPa, and f'_c is the compressive strength in MPa.
- Both large-scale tensile creep tests and nano-scale tests showed similarities in material properties and long-term tensile creep behavior between the two thermally treated UHPC mixes (i.e., D-2f-90C-40 and D-2f-60C-40).
- Large scale tensile creep tests showed that thermal treatment at 90^{o}C (194^{o}F) for 48 hours or at 60^{o}C (140^{o}F) for 72 hours prior to loading decreased tensile creep by 63% and 57%,

respectively, compared to non-thermally treated UHPC. The closeness of the results obtained for the two thermal treatment regimes suggests the possibility of achieving satisfactory microstructural refinement at the same thermal energy input despite reducing the maximum temperature applied. This hypothesis was proved by nanoindentation testing and scanning electron microscopy.

- Comparing tensile to compressive creep behaviors showed fundamental differences between the two phenomena with tensile creep being an order of magnitude higher than compressive creep which suggests significant differences in the underlying mechanisms between the two phenomena.
- Nanoindentation testing and scanning electron microscopy provided the first experimental evidence of a more porous fiber-cementitious matrix interface for non-thermally treated UHPC only. The width of the more porous interface measured was about 10 μm (394 micro inches). No porous interface was found in UHPC thermally treated either at 90^{o}C (194^{o}F) for 48 hours or at 60^{o}C (140^{o}F) for 72 hours.
- Increases in tensile and compressive creep of non-thermally treated UHPC are proposed to be mainly due to the presence of the weak fiber-matrix interface.

7.1.3.2 Effect of fiber content

The effect of varying fiber content on the tensile creep of UHPC was investigated. Based upon this experimental investigation, the following conclusions can be drawn:

- Similar to the case of varying thermal treatment, tensile creep of UHPC was found to be more sensitive than tensile strength to variations in fiber content. Tensile creep generally increased with reduction in fiber volume fraction or with elimination of fibers.

- For thermally treated UHPC, tensile creep increased by 53% and 64% upon decreasing the fiber volumetric content from 2% to 1% and eliminating fibers, respectively. For non-thermally treated UHPC, tensile creep increased by 46% upon eliminating fibers. Measured increases in tensile creep upon reducing the fiber content suggests that fibers carry part of the sustained load and thus reduce stress in the UHPC matrix, resulting in reductions in creep.
- The effect of fibers in reducing tensile creep was more pronounced in thermally treated UHPC compared to non-thermally treated UHPC. It is proposed that this is due to stronger fiber-matrix bond associated with thermal treatment.
- The effect of fibers in reducing tensile creep was more pronounced than compressive creep. It is suggested that this difference in the relative influence of fibers is due to microcracking in tension that results in engaging fibers in the load transfer process from cracked to uncracked part of the cementitious matrix.

7.1.3.3 Effect of stress level

The effect of varying stress level (i.e., stress-to-strength ratios of 0.40, 0.60, 0.70, and 0.80) on the tensile creep of UHPC was investigated. All samples were thermally treated and fiber reinforced. Based on this experimental investigation, the following observations and conclusions can be drawn:

- Pre-cracked UHPC did not experience failure during 1 year under 40% stress level in tension. Also, no tensile creep failure occurred at 60% stress level for a testing period of 90 days.
- UHPC stressed to 40% and 60% of their strength exhibited almost the same specific creep after 90 days of loading. These results indicated that UHPC loaded up to a stress level of 60% did not reach the tertiary stage of creep (i.e., creep at increasing rate) where excessive damage would occur leading to failure.

- Tensile creep failure occurred at both 70% and 80% stress levels. Time to creep failure was inversely proportional to the stress-to-strength ratio.
- When evaluating UHPC for structural applications, it is recommended that tensile creep tests be performed on pre-cracked specimens at 60% of the ultimate strength to ensure safe design.

In summary, tensile creep and shrinkage results from the long-term, large-scale study were in good agreement with the short-term study. This multi-scale study suggests that tensile creep of fiber-reinforced UHPC is controlled by microcracking, which is likely to initiate in the more porous fiber-matrix interface as shown in the nano/micro-scale study, as well as viscous flow and microprestress effects. The role of seepage in tensile creep of UHPC needs further investigation. This study also suggests that fibers should not be used as shear reinforcement in lieu of stirrups unless a truly defect-free fiber-matrix interface can be achieved.

7.2 Recommendations

7.2.1 Recommendation for Future Research

Results and conclusions drawn from the current study suggest some potential important topics for future research. These are summarized below.

- Concrete has been always assumed to act as an isotropic material for structural design purposes. Depending on the method of casting fiber-reinforced UHPC, anisotropy can be induced due to anisotropic fiber dispersion. It is recommended that the isotropy of the material using different casting procedures be further studied. The aim would be to guarantee satisfactory long-term performance and to develop suitable design and casting guidelines that can be standardized later.

- Results from this study showed that reinforcing UHPC with randomly dispersed straight steel fibers is vital for achieving satisfying long-term structural performance in bridge girders due to the brittle nature of the UHPC premix. Using fibers in cementitious materials can be problematic if a good fiber-matrix interface is not created while casting and curing. It is recommended that fibers of different types, such as crimped or hooked fibers be tested to investigate if the trends observed here are maintained for different fibers.
- Also, it is recommended to test fibers with roughened surfaces for the same purpose to investigate if fibers' roughness would improve the fiber-matrix interface bond.
- Full-scale testing of UHPC bridge girders should be conducted prior to using the material for bridges. Full-scale testing will help answer some of the questions not addressed in previous research, such as the UHPC girder-normal strength/HPC deck shear interface behavior, the possible girder failure mechanisms in shear, and the dependency of flexural performance on fiber orientation.
- Fundamental questions remain regarding the mechanistic differences between tensile and compressive creep of UHPC. Further multi-scale studies are needed to better understand the contributions of nanoscale features, including molecular rearrangements of the cementitious gel, on creep in tension and compression.
- The current multi-scale study characterized the mechanical properties of the fiber-matrix interface and in the bulk paste of UHPC at different curing conditions through nanoindentation. It is recommended that properties measured in the current study be used in the future to develop three-phase (i.e., fiber, matrix, and interface) numerical creep models for UHPC. Such models improve the understanding of the localized effects of fiber reinforcement and their effect on the creep of the cementitious matrix. This approach is

useful in predicting creep behavior for UHPC with varying fiber type, geometry, alignment, as well as variations in matrix composition and thermal treatment which may not only affect the bulk paste properties but also the interfacial structure and properties.

- It has been shown in previous research that three-dimensional maps of x-ray absorptivity for geomaterials can provide precise identification of material internal features as well as the microstructural response under different loading conditions. Because the amount of x-ray absorbed by a material depends on the density and the atomic mass of the material, microtomography is quite useful for evaluation of heterogeneous materials. With recent advances in the resolution of microtomography, this is a potentially very useful technique to investigate the effect of materials constituents, environmental conditions, and load level on the tensile creep performance of cementitious materials. Results from this study will help developing guidelines that aim at optimizing mix designs and fiber-orientation for the desired mechanical properties. In addition, two and three-dimensional maps obtained from μCT can be used to perform virtual viscoelastic experiments using softwares such as OOF2 developed at the National Institute for Standards and Technology (NIST) and ABAQUS. Microstructural FE analysis will mainly allow for quantifying local strains, assessing the effect of constituents' volume fractions and orientations, quantifying relative deformation of different phases, and developing internal stress and deformation distribution.
- Further improvements in tensile creep testing can be achieved with improvements to sample loading mechanism. UHPC was successfully loaded up to a stress level of 60% in the current study using newly designed tensile creep test setup. It is believed that higher stress levels can be achieved by using hollow/double-sided threaded inserts. That is, threaded rods with

internal and external threads. This modification will increase anchorage between threaded inserts and concrete and maximize the net concrete cross section.

- Another way to overcome the stress concentration problem at the threaded rods-concrete interface is to use dog bone tensile creep specimens with a reduced cross section away from the inserts. However, it is to be noted that most of the previous long-term tensile creep studies used straight prismatic specimens similar to the ones used in the current study.

7.2.2 Recommendations for Bridge Design

- In the light of the current study, thermally treated UHPC at temperature above 60^{o}C (140^{o}F) with 2% fiber volume fraction is recommended for use in highway bridge girders due to the superior short and long-term properties obtained for UHPC compared to normal or high-performance concretes. However, thermal treatment at 90°C (194^{o}F) is recommended based on this research.
- For highway bridge girder applications, it is recommended to take advantage of the UHPC long and short-term properties both in tension and compression. This can be achieved via optimized bridge girder design.
- It is further recommended that direct tensile tests be used to determine tensile strength of UHPC. If split cylinder tests are used, the tensile strength should be estimated as one-half the tensile strength given by the split tensile test.

APPENDIX A
MODULUS OF RUPTURE OF UHPC
[CUSTOMARY UNITS]

A one-speed shear mixer of about 2.0 ft^3 volumetric capacity was used for all mixes (Figure A.1).

Figure A.1: Batching Ductal® premix in a 2.0 ft^3 shear mixer

Once mixing was complete, 2x2x2-in (50x50x50 mm) cubes and 3x6-in (75x150 mm) cylinders for compressive strength and 2x2x9-in (50x50x225 mm), 2x2x16-in (50x50x400 mm), and 2x2x23-in (50x50x575 mm) beams for 3-point bending test were filled during vibration using a vibrating table. In this study thermal treatment at 90^{o}C (194^{o}F) for 48 hours and ambient curing were considered.

A.1 Compressive Strength

Cubes and cylinders were tested according to the ASTM C109, and ASTM C39 respectively except that the load rate used was increased to 145 psi (1 MPa)/min to be consistent

with the Ductal® Batching and Testing Procedures and the procedures found in the literature. Five specimens were tested at ages of 2, 4, 7 and 28 days using a Satec compression testing machine, model MKIII 800RD with an 800-kip capacity. Compressive strength results are shown in Table A.1 and Figures A.2 and A.3.

Table A.1: Compressive strength results

Age	3x6" Cylinders					2x2x2" Cubes				
	f_c(psi)		SD(psi)		Thermal/ ASTM	Curing regime		f_c(psi)		Thermal/ ASTM
	ASTM	Thermal	ASTM	Thermal		ASTM	Thermal	ASTM	Thermal	
2	10945.3		1667.8			13003.2		906.9		
4	13112.8	22631.4	752.5	1821.0	1.7	17024.4	29809.1	1341.6	2598.4	1.8
7	14523.5	22643.8	800.0	3591.6	1.6	18389.0	30159.9	1860.0	1582.9	1.6
28	18356.8	22127.9	893.5	1598.0	1.2	23440.0	29986.9	2018.6	2015.3	1.3

A.2 Modulus of Rupture

Figure A.4 shows the 3-point bending test setup used to determine the tensile properties of UHPC. This test involves the three-point flexural loading of small-scale concrete prisms. During the test, the load on and the deflection of the prism are monitored. These data were then used to determine the modulus of rupture.

Midspan defections were measured using either a digital dial gage with an accuracy of 0.0001" for the 2-days ambient cured series (Series A-2), or using a digital deflectometer connected an electronic data acquisition system for all other series. This later setup is able to record and save loads and deflections through out automatically.

The nomenclature used in this study was based on the curing conditions (i.e. A = ambient curing and T = Thermal treatment) and age of loading (i.e. 2= tested at age of 2 days). For example, Series "T-28" indicates that specimens of this series were thermally treated at 194^{o}F (90^{o}C), and testes at 28 days.

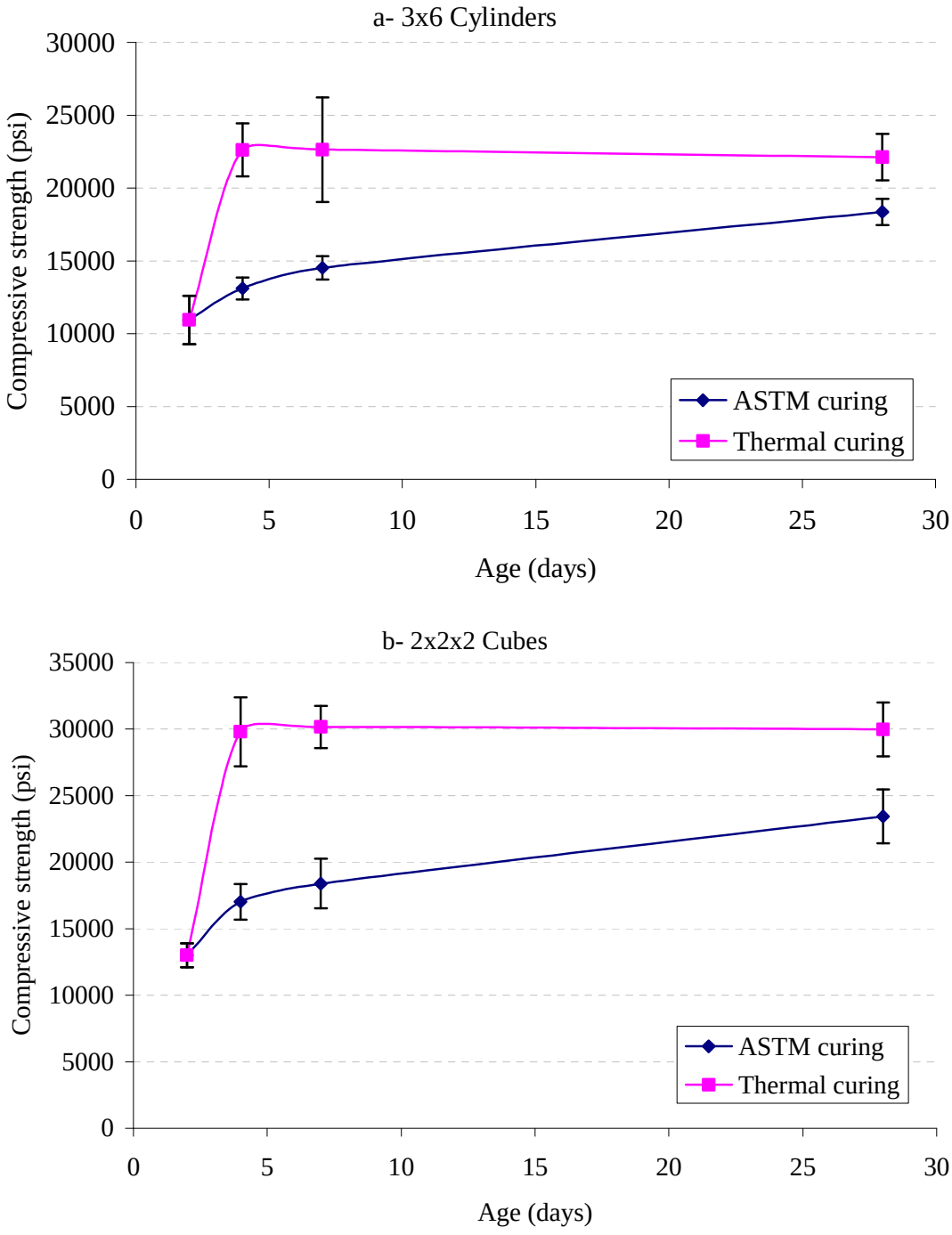

Figure A.2: Compressive strength results a- cylinders, b- cubes

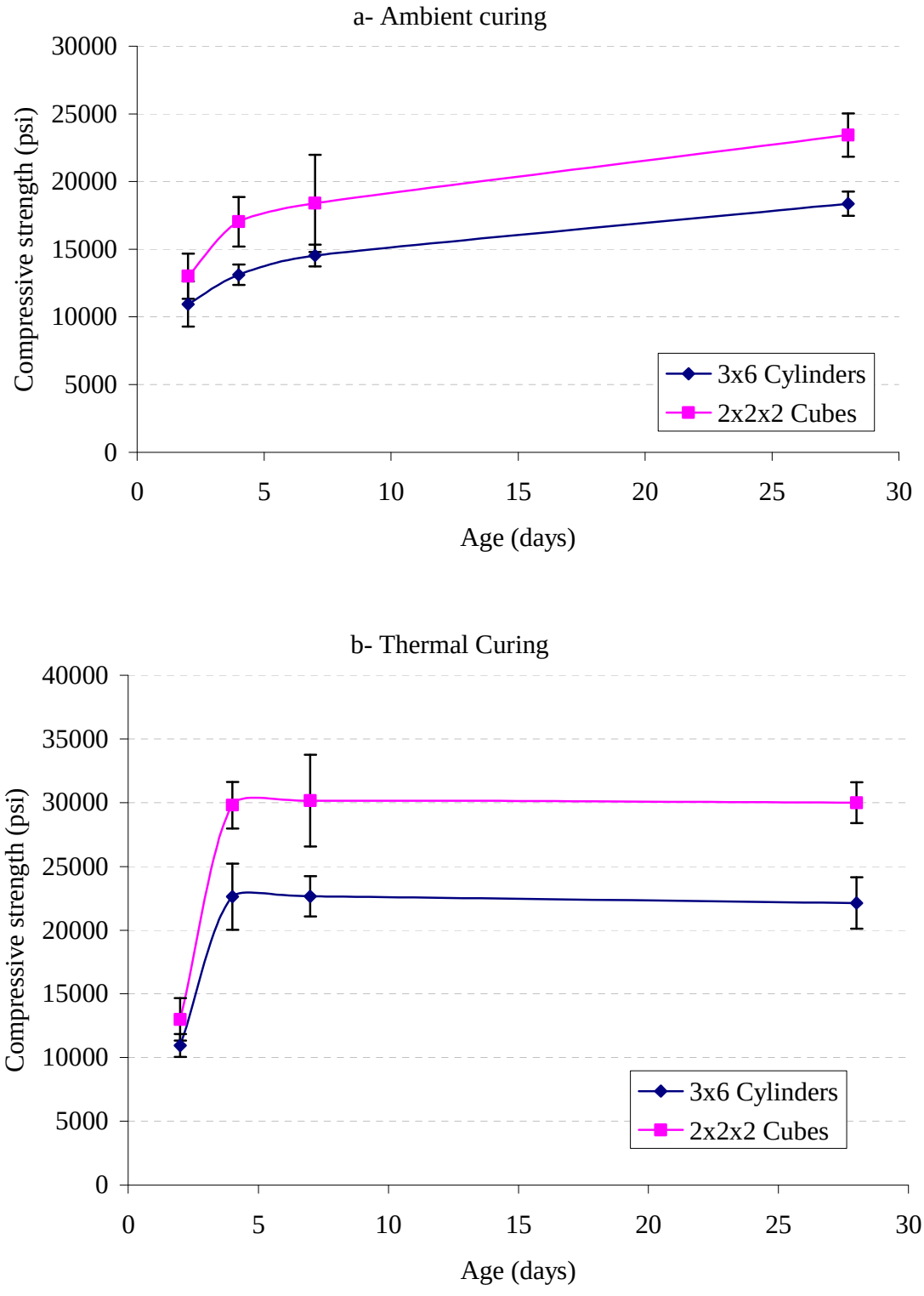

Figure A.3: Comparison between cylinders and cubes results a- Ambient curing, b- Thermal curing

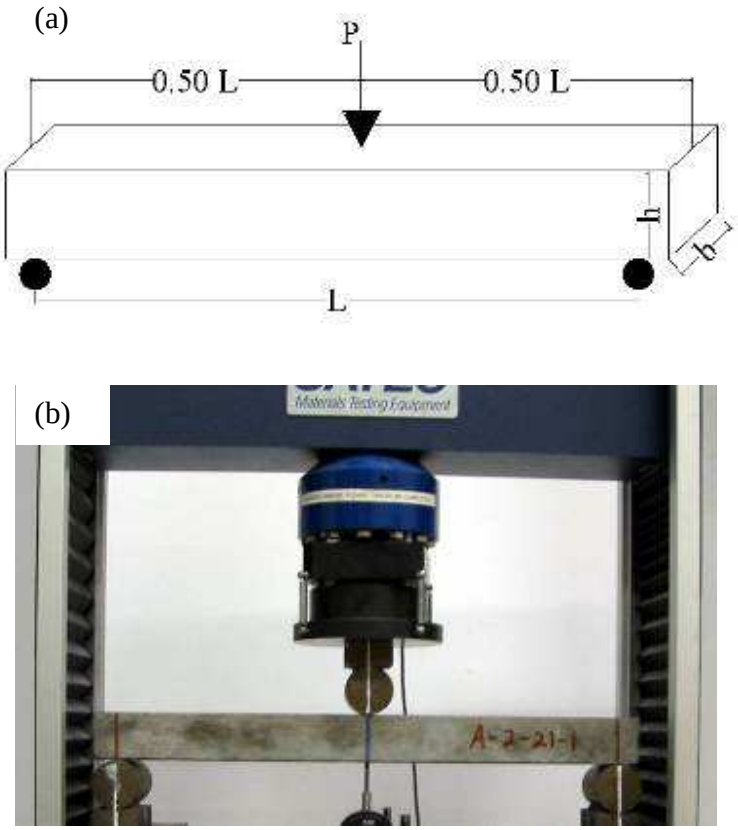

Figure A.4: (a) Schematic diagram of 3-bending test setup; (b) 3-point bending test with a deflectometer at mid-span

In order to determine the aspect ratio (L/h) effect on the tensile behavior and properties on UHPC, also, as larger shear span to prism depth ratio would much more accurately represent the flexural response of UHPC, the span (L) was varied from 7", 14", and 21", while the cross section dimensions (2x2 in) were kept constant for all specimens. During casting of each prism, special care was taken to ensure that the UHPC flowed from one end of the prism to the other, thus ensuring a fiber distribution and alignment system that was similar to that which would occur in the large-scale casting of a beam or plate type flexural member. At least three specimens of each span length were testes at each age for each curing regime using a Satec load frame. The deflection rate was set so that the expected first crack deflection would occur approximately 1

minute into the test. This rate varied depending on the prism cross-section and loading configuration. The test was stopped after a load dropped down at least to half of the maximum value.

The first cracking noticed for all specimens was tensile stress cracking on the bottom of the specimen. Thus, first cracking—recorded by the data acquisition system and physically observed on the specimen was usually quite clear. Figure A.5 shows the load-deflection response curves for all series tested. Figures show that the prism response is linear until first cracking when a clearly defined decrease in load carrying capacity occurs. Soon thereafter the load again begins to increase transferring the load to adjacent fibers. The saw-tooth pattern visible in the response is indicative of additional individual cracks resulting from continuous fibers pull out on the tension face, which is thought to be the dominant failure mechanism of almost all the tested specimens. It was also noticed that in most of cases shorter spans, (i.e. 7-in spans and some 14-in spans) showed typical shear failure cracks prior to failure.

As mentioned before, prism flexure testing of three different loading configurations for each curing regime at each age was intended to identify the benefits and detriments of varying the beam span (L). From a qualitative standpoint, the results of both the A-2-14, and A-2-21 were more consistent than other series. While from a quantitative standpoint, as the span to depth ratio of the beam decreases, the modulus of rupture general decreased, the best configuration to predict the tensile strength obtained by splitting tension test was the 21-in configuration (Figure A.6).

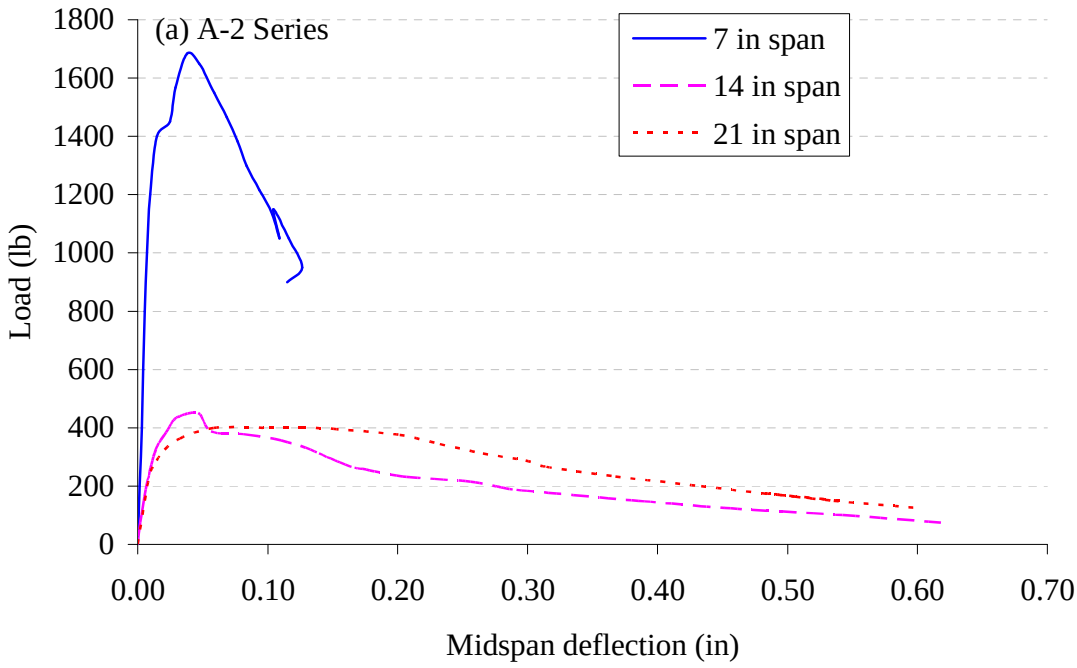
(a) A-2 Series
7 in span
14 in span
21 in span
Load (lb)
1800
1600
1400
1200
1000
800
600
400
200
0
0.00
0.10
0.20
0.30
0.40
0.50
0.60
0.70
Midspan deflection (in)

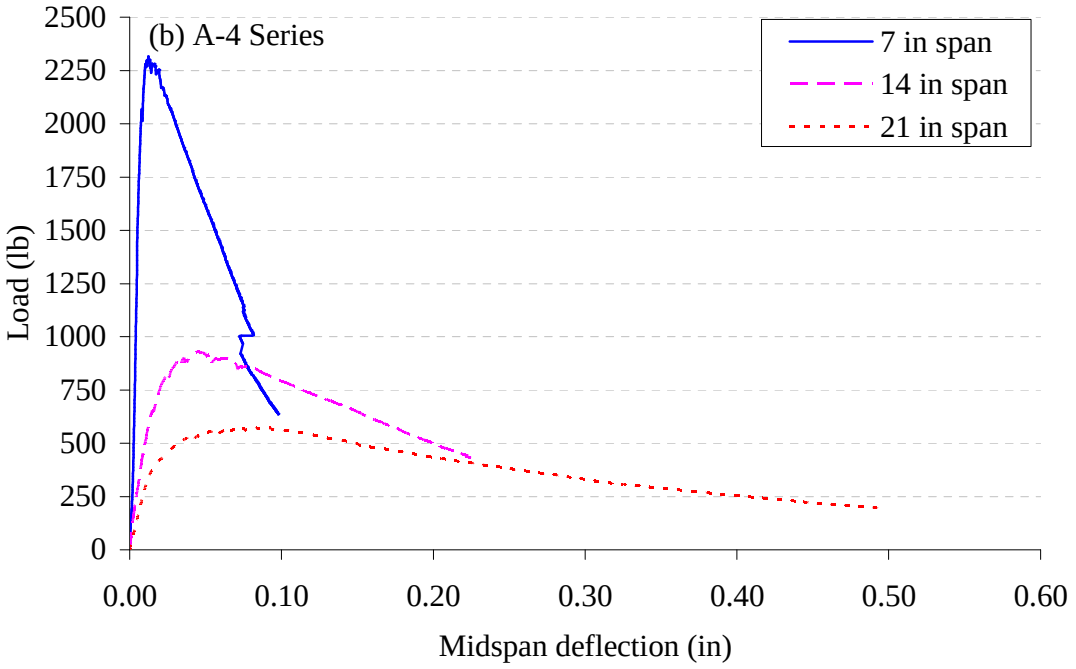
(b) A-4 Series
7 in span
14 in span
21 in span
Load (lb)
2500
2250
2000
1750
1500
1250
1000
750
500
250
0
0.00
0.10
0.20
0.30
0.40
0.50
0.60
Midspan deflection (in)

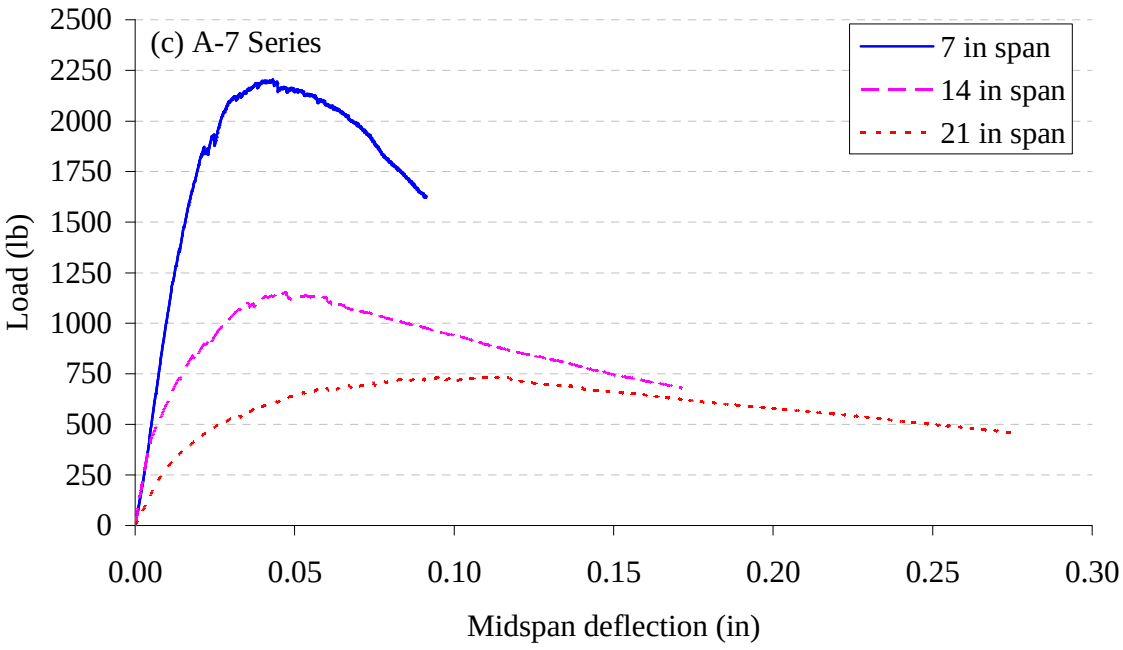
(c) A-7 Series
7 in span
14 in span
21 in span
Load (lb)
2500
2250
2000
1750
1500
1250
1000
750
500
250
0
0.00
0.05
0.10
0.15
0.20
0.25
0.30
Midspan deflection (in)

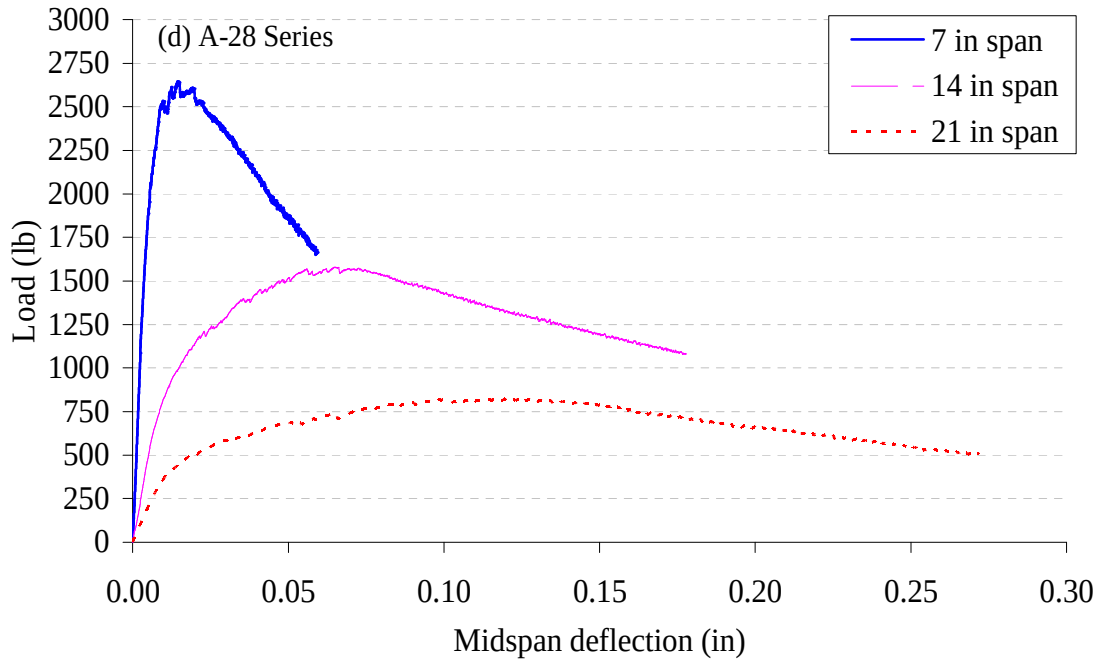
(d) A-28 Series
7 in span
14 in span
21 in span
Load (lb)
3000
2750
2500
2250
2000
1750
1500
1250
1000
750
500
250
0
0.00
0.05
0.10
0.15
0.20
0.25
0.30
Midspan deflection (in)

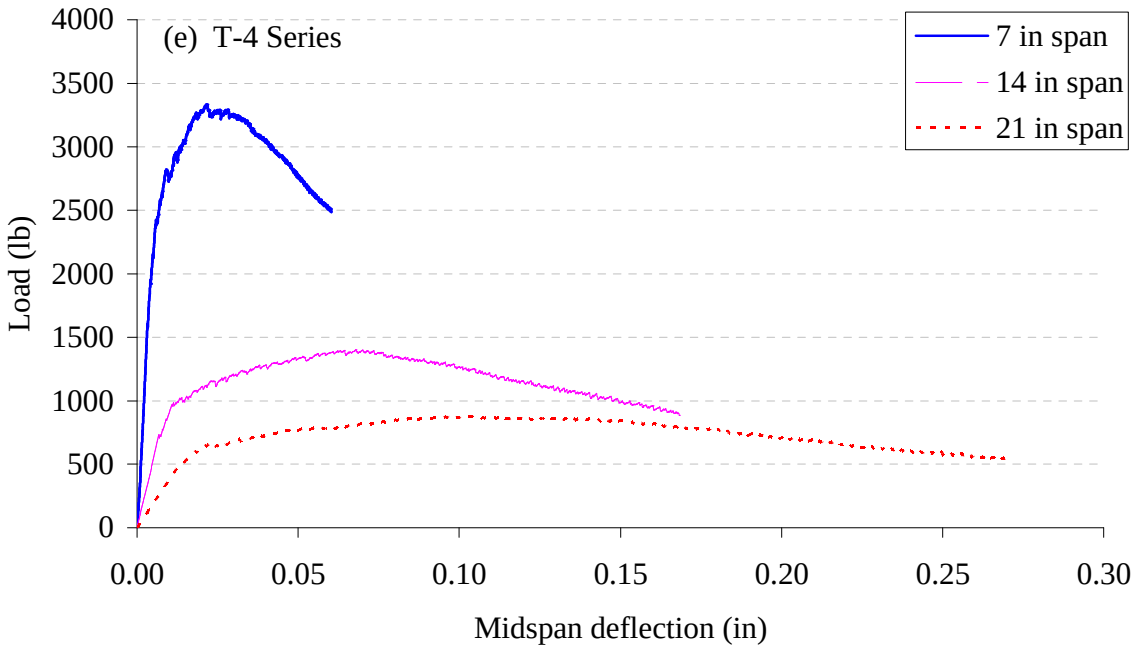
(e) T-4 Series
7 in span
14 in span
21 in span
Load (lb)
4000
3500
3000
2500
2000
1500
1000
500
0
0.00
0.05
0.10
0.15
0.20
0.25
0.30
Midspan deflection (in)

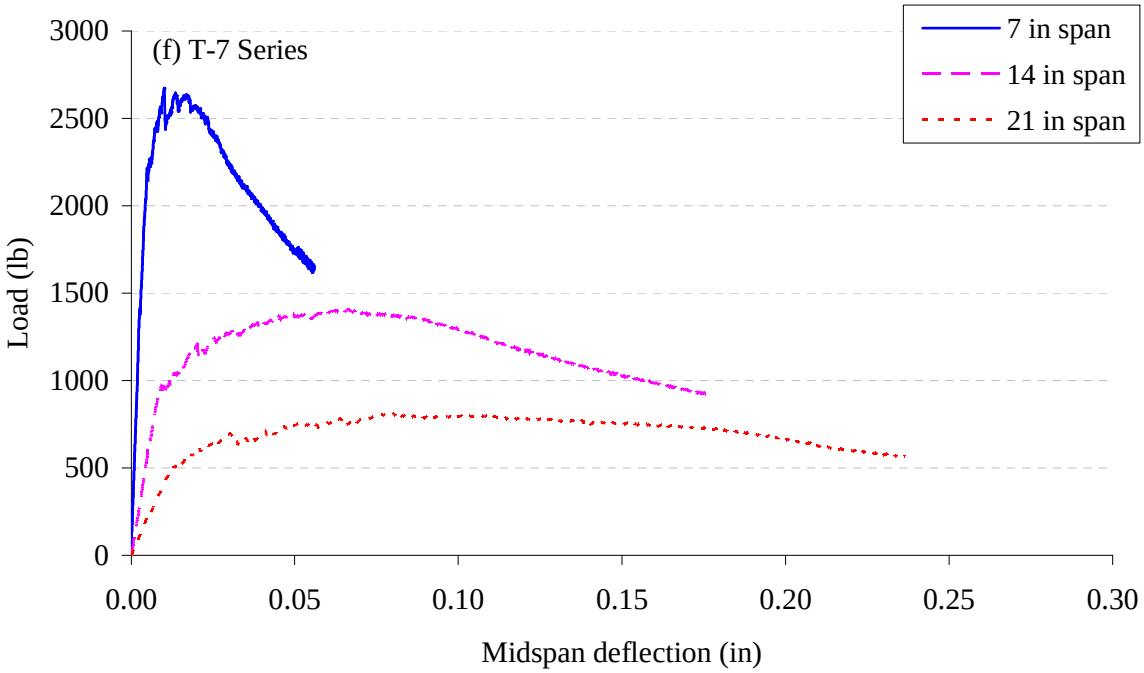
(f) T-7 Series
7 in span
14 in span
21 in span
Load (lb)
3000
2500
2000
1500
1000
500
0
0.00
0.05
0.10
0.15
0.20
0.25
0.30
Midspan deflection (in)

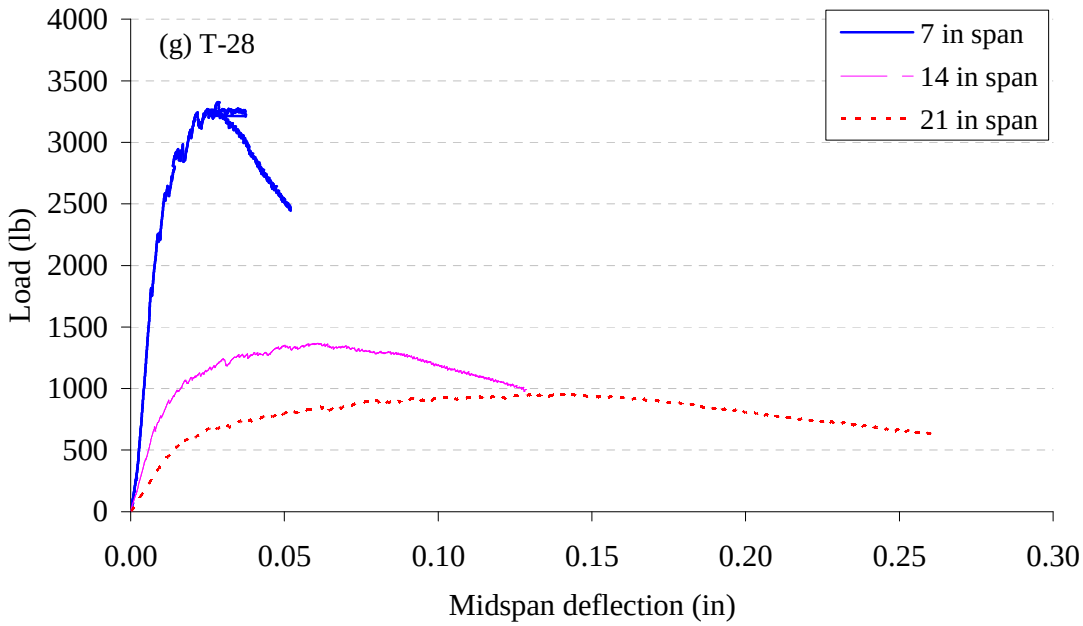

Figure A.5: Average load-deflection behavior of different UHPC series

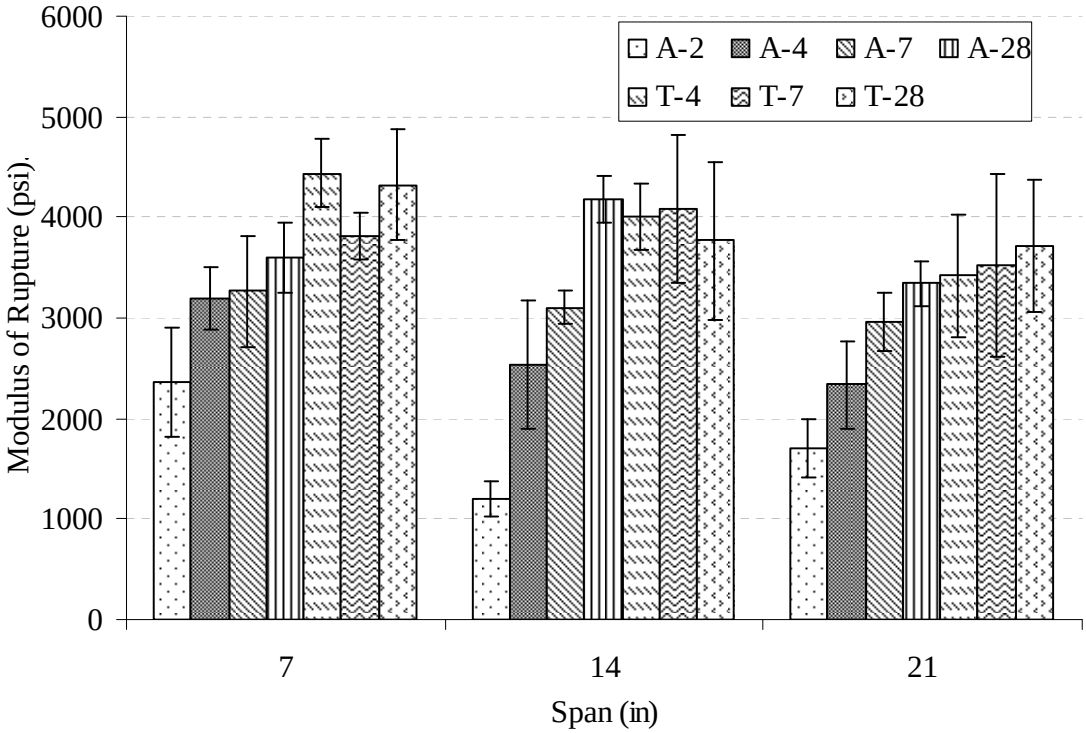

Figure A.6: Modulus of rupture of different UHPC series

Figure A.6 shows a summary of the modulus of rupture values obtained for all UHPC series tested. It can be noticed that the modulus of rupture kept increasing with age for all ambient-cured series (i.e. A-2, A-4, A-7, A-28), while this was not the case of for T-4, T-7, and T-28 series. For all spans, the A-2 series had the minimum average modulus of rupture. The absolute average minimum and maximum modulus of rupture recorded was for series A-2 @ span of 14-in (i.e. 1198 psi (8.25 MPa)) and series T-4 @ span of 7-in (i.e. 4440 psi (30.60 MPa)).

APPENDIX B
COMPRESSIVE CREEP OF UHPC

Review of the published literature reviews only one study that characterizes the compressive creep of steel fiber-reinforced UHPC [Graybeal, 2005]. In this study, long-term compressive creep test were conducted on ultra-high performance concretes, cast from Ductal, with 16.53 – 27.27 ksi compressive strengths. When comparing the creep coefficient, C_{cu}, values of this study (Table B.1) to the values of creep coefficients reported by Dilger and Wang (2000) for High Performance Concrete (HPC) (i.e. 1.8 – 2.4), and Normal Strength Concrete (NSC) (i.e. 2.0 – 4.0), the creep coefficient of UHPC is from 0.13 x to 0.43 x of the creep coefficient of HPC, and from 0.07 x to 0.39 x of the creep coefficient of NSC. These lower creep coefficient values of UHPC are likely due to the lower water-to-cementitious materials ratio which results in lower permeability and also due to the use of silica fume [Wolsiefer, J., 1984 and Dilger and Wang, 2000]. Dilger and Wang [2000] attributed these lower C_{cu} values mainly to lower drying creep in HPC.

It is to be noticed also from Table B.1, that the C_{cu} values decreased upon increasing the curing temperature. The rise in curing temperature would likely accelerate the rate of hydration of the cementitious materials at early ages, increase maturity, and reduce creep.

Finally, the low creep values of UHPC reported in this study might be also attributed to the use of steel fibers. Chern and Young [1989] studied basic creep of steel fiber-reinforced concrete at 1% and 2% (volumetric fraction). It was concluded from this study that steel fiber reinforcing resulted in a significant decrease in basic creep, and that basic creep decreased progressively upon increasing the fiber content, and that creep reduction was higher as the fiber

content increased from 0% to 1% than from 1% to 2%. This decrease in basic creep was explained by the ability of fibers to restrain the flow of the cement matrices.

Table B.1: UHPC long-term creep results [Graybeal, 2005]

Curing regime	Age of loading (days)	Control strength MPa (ksi)	Stress/ strength	Creep coeff. C_{cu}	Specific creep δ_{cu} με/MPa (με/ksi)
Steam *(90°C & 95% RH) for 48 h after casting*	4	188 (27.27)	0.41	0.29	5.66 (39)
Air *(Ambient Conditions)*	28	114 (16.53)	0.67	0.78	21.17 (146)
Tempered Steam *(60°C & 95% RH) for 48 h after casting*	4	177 (25.65)	0.43	0.66	14.21 (98)
Delayed Steam *(90°C & 95% RH) for 48 h starting at 15 days*	21	168 (24.42)	0.46	0.31	6.38 (44)

References

ASTM C512, "Standard Test Method for Creep of Concrete in Compression," American Society for Testing and Materials Standard Practice C512, Philadelphia, Pennsylvania, 2002.

Chern, J.-C., and Young, C.-H., "Compressive Creep and Shrinkage of Steel Fibre Reinforced Concrete", The International Journal of Cement and Cement Composites and Light weight Concrete, Vol. 11, No. 4, 1989, November 1989, pp. 205-214.

Dilger, W.H., and Wang, C., "Creep and Shrinkage of High-Performance Concrete", in The Adam Neville Symposium: Creep and Shrinkage – Structural Design Effects, SP-194. Atlanta: American Concrete Institute, 2000, pp. 361-379.

Graybeal, B. A., "Characterization of the Behavior of Ultra-High Performance Concrete", Ph.D. Thesis, University of Maryland, 2005.

Wolsiefer, J., "Ultra High-Strength Field Pleaceable Concrete with Silica Fume Admixture". Concrete International, Vol. 6, No. 4, 1984, pp. 25-31.

Zhang, J., "Modeling of the Influence of Fibers on Creep of Fiber Reinforced Cementitious Composite", Composites Science and Technology, Vol. 63. 2003, pp. 1887-1884.

APPENDIX C
COMPRESSIVE CREEP OF CONCRETE

ACI Committee 209 [2005] defines creep strain in concrete as the time dependent increase in strain under sustained constant load taking place after the initial strain at loading. A typical creep curve is given in Figure C.1. When a specimen is unloaded, the instantaneous recovery is approximately the same as the instantaneous strain on first application of the load; but creep recovery is by no means complete, and thus a considerable amount of the total creep is irreversible. Under typical service conditions, concrete is also most likely drying while under load. And it has been found that under such conditions creep deformation are greater than if the concrete is dried prior to loading. Different dimensional changes in concrete under loading and drying conditions are shown in Figure C.2. When free shrinkage (ε_{sh}) (determined while the specimen is unloaded, but subjected to the same drying conditions) and basic creep (ε_{bc}) (determined while specimen is loaded, but not drying) are added together, their sum is less then the total strain (ε_{tot}) determined during simultaneous loading and drying. The excess deformation is called drying creep (ε_{dc}). Total creep strain (ε_{tot}) is the sum of ε_{bc} and ε_{dc}. It is common practice, however, to ignore this distinction, and creep is usually considered as the deformation under load in excess of free shrinkage (Figure C.1).

Two terms are generally used to describe creep, the first is the creep coefficient defined as the ratio of the creep strain to the initial strain (dimensionless) and the second is specific creep defined as the creep strain per unit stress (strain/stress).

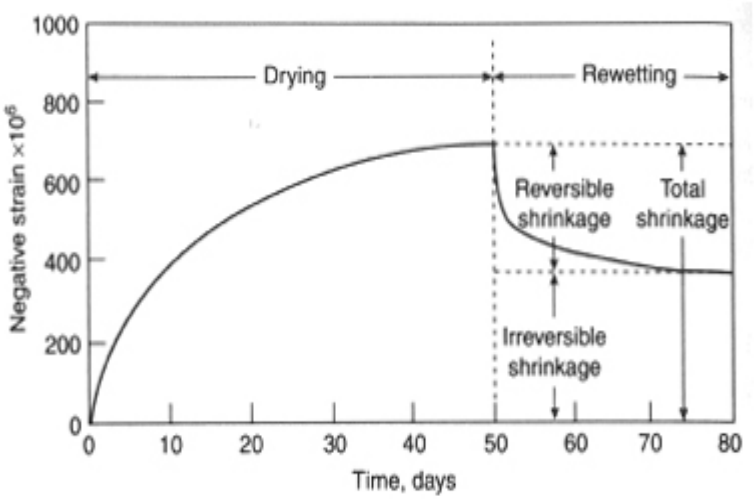

Figure C.1: Creep and drying shrinkage [Mindess and Young, 1981]

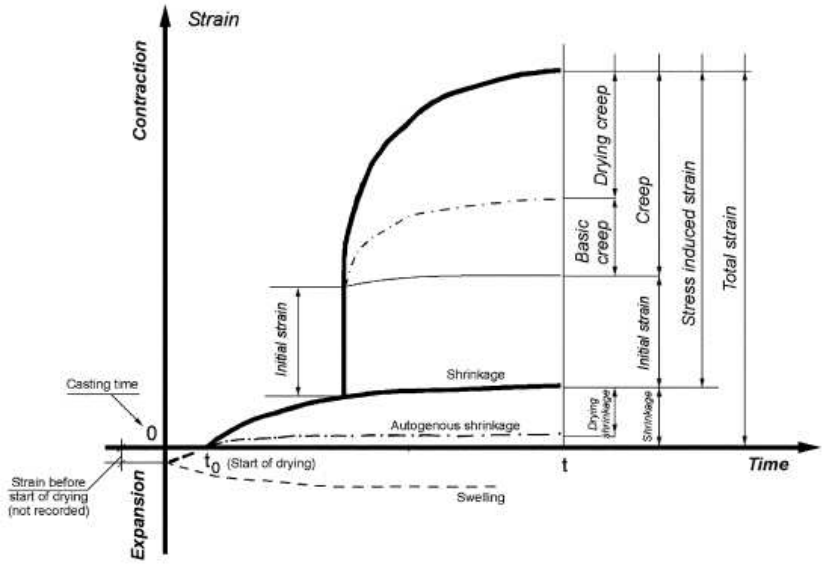

Figure C.2: Deformations of concrete under simultaneous loading and drying [ACI 209-1R-05]

C.1 Basic Creep

Basic creep is defined as the time-dependent increase in strain under sustained constant stress in which moisture losses or gains are prevented (i.e., sealed specimen) [ACI 209, 2005]. Experimentally, it is calculated as the difference between the total creep strain measured, (ε_{tot}) and the elastic strain under no drying condition. (i.e. when drying creep (ε_{dc}) = 0). Due to the age-dependent decrease in the actual elastic strains, as the modulus of elasticity of the material

increases as the hydration process advances with age, it is not easy to determine basic creep in concrete in practice [Troxell et al, [1958]; Neville, [1983]; and Neville, [1996]]. However, and for practical applications, it is only critical to accurately measure the total creep; as in most conditions, concrete elements subjected to load are also allowed to dry simultaneously [Lopez, 2005].

C.2 Drying Creep

Drying creep is the additional creep (in excess of basic creep and drying shrinkage) occurring in a specimen exposed to a drying environment [ACI Committee 209, 2005]. Drying creep is not a material property, as it not only depends on mixture characteristics, but also on environmental parameters (relative humidity and temperature) and member dimensions [Lopez, 2005]. Drying creep strain (ε_{dc}) can only be calculated through measuring total strain, ε_{tot}, and subtracting the elastic strain, basic creep (ε_{bc}), and shrinkage (autogenous and drying) (ε_{sh}) (i.e. $\varepsilon_{dc} = \varepsilon_{tot} - \varepsilon_{bc} - \varepsilon_{sh}$).

C.3 Mechanisms of Compressive Creep

Numerous theories have been advanced to explain compressive creep in concrete since the beginning of the twentieth century when creep in concrete was first measured by Hatt [1907], and, thus, the following discussion is focused on the most widely accepted theories.

C.3.1 Mechanical Deformation Theory

This theory attributes the behavior of concrete under load to internal stresses that result from changes that occur in the material's capillary structure under load. On the removal of the load, the resulting changes in the pressure differences between the water and the air phases within the capillary structure create forces which tend to return the capillaries to their original

shape, but the time for full recovery is infinite just as the limiting creep value is achieved only in an infinite time. According to Freyssinet [1951], one part of the creep is due to the tendency of the system towards maximum stability, while the other part is due to elastic deformation deferred by the wetness of concrete. This part of creep is believed by Freyssinet to be completely reversible. However, no experimental data supported this theory [Neville, 1955].

C.3.2 Plastic Theories

This theory suggests that the creep in concrete is similar to that in metals which takes a nature of crystalline flow (resulting from slipping along planes within the crystal lattice) [Vogt, 1935]. However, plastic flow in metals is a nonelastic deformation that occurs when a certain stress (yield stress) is exceeded. Vogt [1935], and Jensen and Richart [1938] observed creep at stresses as low as one percent of the ultimate strength. And, thus, it was suggested that the creep of concrete at low stress levels is in the form of viscous flow, and only near the ultimate load does the deformation take the form of slipping [Glanville, 1939].

C.3.3 Viscous Theory

This theory assumes that the major creep mechanism in concrete is due to viscous flow where particles move over each other when loaded. According to this theory concrete is to be divided into two phases: (1) cementitious material (viscous loaded), and (2) non-flowable inert aggregate. These two phases share carrying the applied load according to their relative stiffness [Thomas, 1937]. Due to the resistance of the aggregate, load transfer gradually from the cementitious “viscous” phase to the aggregates. Now, as the creep in the paste is proportional to the applied stress in that phase, the rate of creep will decrease as the load transferred from the paste to the aggregate is increasing. This theory, while being able to successfully represent the

stress dependency of creep, fails to predict any creep recovery upon unloading [Ali and Kesler, 1964]. In addition, a viscous flow would require a constant volume condition of the concrete, and as this case is not experimentally evident. Thus, viscous flow cannot be responsible for all creep in concrete [Neville, 1955].

C.3 4 Seepage Theory

The seepage theory states that creep in concrete is due to the loss of water from the C-S-H, which is a common phenomenon in rigid gels [Weiser, 1938]. Upon applying load, the vapor pressure of the physically adsorbed water increases, and thus expelled from the C-S-H surface to the capillary pores to restore equilibrium with external conditions [Neville, 1955; and ACI Committee 209, 2005], this will in turns result in volume changes. As explained earlier in the viscous theories section, upon loading the concrete, the water in the cement paste starts to be squeezed out which increases the stress in aggregates and decreases stress in the cement paste. Later, and as water is expelled from the C-S-H surface, it becomes increasingly difficult to remove and thus reducing the rate of creep.

The seepage theory can explain both basic and drying creep. In addition, it can also explain the mechanism of tensile creep. Tensile stress causes a decrease in vapor pressure transforming capillary free water into adsorbed water. This would restore pressure equilibrium within cement paste microstructure and would cause expansion [Lopez, 2005].

A major problem of the seepage theory might be the creep reversibility. That is, a full creep recovery would be expected upon unloading as the vapor pressure at the C-S-H surface would decrease and, thus, adsorbed water should be restored. This scenario is not evident experimentally [Han, 1996]. One possible explanation of this inconsistency may be the formation

of new bonds in C-S-H which are strong enough to prevent total recovery of creep upon unloading [Neville, 1955].

C.3.5 Microcracking Effect Theory

Several studies explained the non-linear stress-strain relation of concrete in compression by the presence of an interfacial transition zone (ITZ) between the coarse aggregates and the cement paste [Hsu, 1956; Mehta and Monteiro, 2005]. The ITZ in concrete is generally is characterized by higher porosity, larger and aligned calcium hydroxide crystals, and concentration of pre-existing microcracks. According to Mehta and Monteiro [2005], the presence of the ITZ in concrete is not only responsible of the stress-stain nonlinearity but also of its brittle nature in tension, higher strength in compression when compared to tension, and higher permeability of concrete in general when compared to the permeability of the cement paste. So, Neville and Dilger [1970] suggested that the major effect of creep is that it propagates cracks formed in the ITZ during initial loading, drying or thermal shrinkage. The propagation of the preexisting microcracks with loading the concrete can then well explain not only the presence of residual strains in concrete upon unloading due to the development of permanent strains in cracks upon loading, but also the increase in creep values noticed upon increasing the stress/strength ratio [Lopez, 2005].

C.3.6 Solidification Theory

Bazant and Prasannan [1989] suggested that the decrease in the creep rate with time is due to the formation of new hydration products in the micropores of the cement paste. The increasing volume of these “newly formed” hydration products is believed to be capable of carrying loads and thus decreasing the stress causing creep. The two main deficiencies associated

with this theory are: (1) this theory fails to explain the role of water and the increase in creep under drying conditions, and (2) this theory ignores the fact that no significant increase in the hydration products volume was observed experimentally after one month while the volume of loaded concrete keeps changing for several years.

C.3.7 Microprestress (Solidification Theory)

This theory could be considered and extension of the “Solidification Theory” discussed before [Bazant et al., 1997]. This theory stated that in addition to the aging effect described in the solidification theory, creep in concrete may also result from interatomic bond breaks in overstressed locations. At these overstressed locations, the adsorbed water diffuses to the capillary pores and accelerates the bond-breaking process in the C-S-H structure. This progressive process of bond breaking and diffusion are likely to form new overstressed locations that will also undergo creep as well. An eventual exhaustion of overstress sites causes the creep rate to decline as well. It is to be pointed out here that both this theory and the “Seepage Theory” mainly relate creep in concrete to the movement of water from the C-S-H surface to the capillary pores.

So, it can be seen from the previous discussion that the creep phenomenon in concrete is still poorly understood even after all these previously mentioned theories came to existence. The reason is that none of these theories was capable of accounting for all the factors that affect creep. Utilizing two or more of these theories might be more efficient in explaining concrete deformations under loading and drying conditions.

C.4 Factors Affecting Creep of Concrete

C.4.1 Materials and Mix Proportions

Although many studies have tried to relate creep and drying shrinkage in concrete only to the amount of cement and the degree of hydration of the cement paste, no direct proportionality exist because of the restrains against deformation provided by the aggregates [Mehta and Monteiro, 2005].

Neville [1964] suggested that the creep of concrete (C_c) and creep of the cement paste (C_p) can be related to the sum of both the aggregate (g) and unhydrated cement (μ) contents by the following equation:

$$\text{Log}\,(C_p/C_c) = \alpha \log\,(1/(1- g - \mu)) \qquad \text{(C.1)}$$

In well-cured concrete, and by neglecting the small fraction of unhydrated cement (μ), the expression can be rewritten as:

$$C_c/C_p = (1 - g)^{\alpha} \qquad \text{(C.2)}$$

In addition, the aggregate gradation, size, shape, texture and more importantly modulus of elasticity have also been suggested as important factors influencing creep.

The effect of aggregate properties on creep has been studied by Troxell et al. [1958]. Creep and shrinkage of concretes with same mix proportions but different aggregates were characterized for over a period of 23 years. The results (Table C.1) show that creep of concrete increased 2.5 times when an aggregate with a high elastic modulus (i.e. quartz or limestone) was substituted by an aggregate with low elastic modulus (i.e. gravel or sandstone).

Table C.1: Creep deformations of concretes of different aggregates types [Troxell et al., 1958]

Type of aggregate	Elastic strain	Creep strain
Quartz	220×10^{-6}	600×10^{-6}
Limestone	220×10^{-6}	800×10^{-6}
Gravel	280×10^{-6}	1070×10^{-6}
Sandstone	280×10^{-6}	1500×10^{-6}

As for cement type, several experimental studies have shown that normal changes in cement fineness or composition may significantly affect drying shrinkage of pastes and mortars but not concrete [Mehta and Monteiro, 2005]. On the other hand, if the type of cement influences the strength of concrete at the time of application of load, the creep of concrete will obviously be affected. For example, when loaded at early ages, concretes containing ordinary portland cement generally show higher creep than the corresponding concrete containing high-early-strength cement [Jones et al. 1959]. In addition, an increase in the overall cement paste volume means a decrease in the aggregate fraction (g) and thus a corresponding increase in the moisture-dependent deformations in concrete [Jones 1959]. Also, at a given cement content, creep is expected to increase upon increasing the water/cement ratio due to the decrease in strength and the elastic modulus that accompanies increasing the water content.

In addition, chemical admixtures like calcium chloride, water-reducing, and set-retarding admixtures, and pozzolans, tend to increase the volume of fine pores in the cement hydration product, and thus, concretes containing admixtures that cause pore refinement usually exhibit higher drying shrinkage and creep [Mehta and Monteiro, 2005].

C.4.2 Time and Humidity

As diffusion of the adsorbed water and the water held by capillary tension in small pores (under 50 nm) of hydrated cement paste to large capillary voids within the system or to the

atmosphere is a time-dependent process that takes place over long periods, Troxell et al. [1958] found that only 20 to 25 % of the 10-year creep was realized in 2 weeks, 50 to 60 % in 3 months, and 75 to 80 percent in 1 year.

Also, an increase in the atmospheric humidity is expected to slow down the moisture flow from the interior to the outer surfaces of concrete. For a given condition of exposure, the effects of relative humidity on drying shrinkage strain and creep coefficient are illustrated in Table C.2 [CEB/FIB, 1976].

Table C.2: Effect of relative humidity on shrinkage and creep [CEB, 1976]

Relative humidity (%)	Drying shrinkage strain (με)	Creep coefficient
100 %	Assumed to be 0	Assumed to be 1
80 %	200	2
45 %	400	3

C.4.3 Geometry of Concrete Element

At a constant relative humidity, both the size and the shape of a concrete element affect both creep and drying shrinkage. The size and shape parameters are normally represented by single quantity called the *"effective or theoretical thickness"*, which is defined as the area of the section divided by the semi perimeter in contact with the atmosphere. The relations between theoretical thickness and the drying shrinkage and creep coefficient show an inverse relation between them due to higher resistance to water transport from the interior to the exterior of a concrete section upon increasing the theoretical thickness.

C.4.4 Fiber Reinforcement

Review of published literature shows that only few researchers have focused on studying the effect of fiber-reinforcement on the creep behavior of concrete, [Mangat and Azari, 1986],

[Chern and Young, 1989], and [Zhang, 2003]], and. In the study by Mangat and Azari [1986], uniaxial compressive creep tests were carried out on concrete, mortar, and paste for a period of 150 days. Steel fibers (about 1-in long and 0.02-in n diameter) were used at volume fractions up to 3%. The results from this study showed general reduction in creep for concrete, mortar, and paste upon incorporating fibers in the mix. Concrete and mortar reduction in creep were almost identical in all cases investigated, while the creep reduction in the paste was much greater than both the concrete and the mortar. This is likely due to the better efficiency of fibers in bridging between particles in the case of paste as compared to the cases of concrete and mortar. In addition, it was shown in the same study that the relationship between creep of steel fiber-reinforced concrete in compression can be represented by hyperbolic and logarithmic relations used for plain concretes. Chern and Young [1989] studied compressive creep of steel fiber-reinforced concretes . Fibers used in this study were carbon steel fibers 19 mm (3/4) long with an effective diameter of 0.43 mm (0.017-in) at 1 and 2% volume fraction. Results from this study showed that as the fiber volume fraction in increased, both drying shrinkage and basic creep decreased. In addition, increasing the temperature at which the test specimens were kept from 23^{o}C to 35^{o}C while resulted in increasing the creep rate on non-reinforced concrete, had less pronounced effect on the fiber reinforced concrete. In a recent study by Zhang [2003], an analytical model was developed to study the influence of steel fiber incorporation on the creep phenomena in cement based composites. In developing this model, the author focused on the shear stresses that develop between fibers and concrete matrix as the fundamental source of restraint against creep. Model predictions were then calibrated using creep data in the literature, and results showed good agreement with the model predictions. It has been shown in this study that the creep behavior of fiber-reinforced concrete is a function of both the fibers and the matrix

properties, elastic moduli ratio of fiber and matrix, fiber orientation, fiber aspect ratio, and fiber content V_f That is, with the same fiber content and fiber geometry, the higher the moduli ratio between fiber and matrix, the smaller the composite creep strain and high elastic modulus fibers were more effective than those with low elastic modulus in restraining long-term deformation. Also composite compressive creep decreased nonlinearly with the increase in fiber aspect ratio. However, the influence of matrix microcracking on compressive creep was not accounted for in this model.

C.4.5 Additional Factors

Other additional factors that may affect creep include curing history, temperature of exposure, and magnitude of applied load due to their known effects on the porosity, microcracking, and strength of the concrete [Mehta and Monteiro, 2005].

C.5 References

ACI Committee 209, "Factors Affecting Shrinkage and Creep of Hardened Concrete", American Concrete Institute: Farmington Hills, MI. 2005, pp. 209-1R-05.

Ali, I. and C.E. Kesler. "Mechanisms of creep in concrete". in American Concrete Institute -- Symposium on Creep of Concrete, 1964: American Concrete Institute, Detroit, MI, United States, 1964.p. 35-63.

Bažant, Z. P., Hauggaaed, A. B., Baweja, S., and Ulm, F. J., "Microprestress-Solidification Theory for Concrete Creep. I: Aging and Drying effects." Journal of Engineering Mechanics, Vol. 123. No. 11, 1997, pp. 1188–1194.

Bažant, Z.P. and Prasannan, S., "Solidification Theory for Concrete Creep .1. Formulation". Journal of Engineering Mechanics-ASCE, Vol. 115, No. 8, 1989. pp. 1691- 1703.

Chern, J.-C., and Young, C.-H., "Compressive Creep and Shrinkage of Steel Fibre Reinforced Concrete", The International Journal of Cement and Cement Composites and Light weight Concrete, Vol. 11, No. 4, 1989, November 1989, pp. 205-214.

Freyssinet, E., "The Deformation of Concrete", Magazine of Concrete Research (London), No. 8, Dec. 1951, pp. 49-56.

Glanville, W.H., and Thomas, F.G., "Further Investigations on the Creep or Flow of Concrete under Load", Building Research Technical Paper, No. 21, London, 1939.

Hatt, W.K., "Effect of Time Element in Loading Concrete". ASTM Proceedings: 1907, pp. 421.

Hsu, T.T.C., Inelastic Behavior T-Loading. Cornell University: Ithaca. 1956, p. 6.

International Recommendations for the Design and Construction of Concrete Structures, CEB/FIB, 1976.

Lopez, M. “Creep and Shrinkage of High Performance Lightweight Concrete: A Multi-Scale Investigation”, Ph.D. Thesis, Georgia Institute of Technology, 2005.

Mangat, P.S., and Azari, M.M., “Compressive Creep Behaviour of Steel Fibre Reinforced Cement Composites”, Materials and Structures, Vol. 19, No. 113, September 1986, pp. 361-370.

Mehta, P.K. and Monteiro, P. J. M., “Concrete Microstructure, Properties, and Materials” 3rd ed: McGraw-Hill, 2005.

Mindess, S., and Young, J. F., "Concrete", Prentice-Hall Inc., Englewood Cliffs, New Jersey, 1981.

Neville, A.M., "Theories of Creep in Concrete", ACI Journal, Vol. 52, No. 9, 1955, pp. 47-60.

Neville, A.M., “Creep of Concrete as a function of Its Cement Paste Content”, Magazine of Concrete Research London, Vol. 16, No. 46, 1964, pp. 21-30.

Neville, A.M., “Properties of concrete.”, 4th and final ed: J. Wiley, 1996.

Neville, A.M. and W.H. Dilger, Creep of concrete: plain, Reinforced, and Prestressed. Amsterdam, New York,: North-Holland Pub. Co., American Elsevier, 1970.

Neville, A.M., Dilger, W.H., and Brooks, J.J., “Creep of plain and structural concrete: Construction Press”, 1983.

Thomas, F.G. "Creep of Concrete under Load". London: International Association of Testing Materials, 1937.pp. 292-294.

Troxell, G.E., Raphael, J.M., and Davis, R.E.. "Long-term Creep and Shrinkage Tests of Plain and Reinforced Concrete". in Cement and Concrete. Los Angeles: ASTM Proceedings, 1958, pp. 1101-1120.

Vogt, F., “On the Flow and Extensibility of Concrete”, Stockholm, 1935, pp. 24.

Weiser, H.B., :Inorganic Collide Chemistry”, V.III-The Colloidal Salts, Chaman and Hall, New York, 1938.

Zhang, J., “Modeling of the Influence of Fibers on Creep of Fiber Reinforced Cementitious Composite”, Composites Science and Technology, Vol. 63. 2003, pp. 1887-1884.

Jensen, R.S. and F.E. Richart, "Short-Time Creep Test of Concrete in Compression". ASTM Proceedings, 38: 1938. p. 410-417.

Han, N., Time dependent behaviour of high strength concrete. 1996.

Jones, T.R., Hirsch, T.J., and Stephenson, H.K., Texas Transportation Institute Report E52, 1959.